Functionalized Discotic Molecules for Optoelectronic Applications: Synthesis and Characterization

A Thesis Submitted for the Degree of
DOCTOR OF PHILOSOPHY

by

Shilpa Setia

Department of Chemical Sciences
Indian Institute of Science Education and Research (IISER) Mohali
Sector 81, Knowledge City, S. A. S. Nagar, Mohali, 140306.
Punjab, India.

February 2016

DEDICATED TO

My Beloved Parents, Grandparents

&

My Brother

DECLARATION

The work presented in this thesis entitled "***Functionalized Discotic Molecules for Optoelectronic Applications: Synthesis and Characterization***" has been carried out by me under the supervision of **Dr. Santanu Kumar Pal** in the Department of Chemical Sciences, Indian Institute of Science Education and Research (IISER) Mohali, Mohali.

This work has not been submitted in part or full for a degree, diploma or a fellowship to any other university or institute.

Whenever contributions of others are involved, every effort is made to indicate this clearly with due acknowledgements of collaborative work and discussions. This thesis is a bona fide record of original work done by me and all sources listed within have been detailed in the bibliography.

Shilpa Setia

Date:

Place:

In my capacity as the supervisor of the candidate's thesis work, I certify that the above statements by the candidate are true to the best of my knowledge.

Dr. Santanu Kumar Pal

Associate Professor

Department of Chemical Sciences

Indian Institute of Science Education and Research Mohali

Date:

Place:

ACKNOWLEDGEMENTS

It would not have been possible to write this doctoral thesis without the help and support of numerous people around me including my teachers, family, friends and colleagues. At the end of my doctoral research, it is a pleasant task to express my gratitude to all those who contributed in many ways to make this thesis possible and made it memorable for me.

It is difficult to overstate my gratitude to my Ph.D. supervisor ***Dr. Santanu Kumar Pal*** *for giving me this wonderful opportunity to explore the exciting field of Discotic Liquid Crystals and for his suggestions and meticulous scrutiny of the thesis work. His words of encouragement and constant surveillance on the progress of the study motivated and helped me throughout my work. I am highly thankful to my supervisor for the time he spent in explaining me various aspects of our field. Without his guidance; this work would never have been possible. I am highly indebted for his amicable understanding attitude.*

I also thank ***Prof. Ramesh Kapoor*** *and* ***Dr. Angshuman Roy Choudhury****, members of my doctoral committee for fruitful discussions during the yearly assessment of my work.*

I would like to acknowledge our director, ***Prof. N. Sathyamurthy****, for providing the space and all the research and infrastructural facilities. I am thankful to HOD, Department of Chemical Sciences* ***Prof. K. S. Viswanathan*** *for permitting the use of various departmental facilities. I am grateful to all the faculties of IISER for their teaching and constant encouragement.*

I acknowledge IISER Mohali for central NMR, HRMS, SAXS & WAXS and Raman facilities. I also acknowledge the training received from ***Dr. Kavita Dorai*** *to operate the NMR instrument. I would like to thank Department of Chemical Sciences for various departmental facilities like UV-vis, FTIR spectrophotometers, TGA, DSC, Microwave Reactor etc.*

I want to acknowledge ***Dr. P. Balanarayan*** *and* ***Dr. Satya Prakash Singh*** *for doing all the theoretical calculations. I also want to thank* ***Shruti Arya*** *and* ***Dr. Samrat Mukhopadhyay*** *for their help in fluorescence experiments. I am also thankful to* ***Priyanka Dogra*** *and* ***Dr. Samrat Mukhopadhyay*** *&****. Mritunjay, Suman, Mohammad Balal*** *and* ***Dr. Goutam Sheet*** *for their help in AFM studies. I would like to acknowledge* ***Ritu Rai*** *and* ***Dr. Vivek Bagchi*** *for their help in electrochemical studies.*

*I would like to thank **Satyam** and **Maheswararao** for helping in various aspects of my thesis work.*

*My sincere thanks to **Sumyra Sidiq**, my lab-mate cum friend, for her support and encouragement at various stages of my work during my Ph.D. It was a very pleasant experience to work with her and learn. She is the best lab-mate one can ever get. I am also thankful to my other current and former lab-mates **Joydip, Aneeshma, Dibyendu, Indu Bala, Golam, Indu Verma, Harpreet, Vidhika, Supreet, Manmohan, Monika, Akash, Srijit** and **Sudhakar** for their help and cooperation and for making the working atmosphere in the lab extremely enjoyable and cheerful. I am delighted to have **Joydip**, **Aneeshma** and **Prithwish** as my juniors.*

*I wish to thank my dear friends **Sumyra**, **Shruti**, **Satyam**, **Chinmoy, Gurpreet, Maheswararao** and **Nayyar*** for their cheerful companionship *and for their timely encouragement. A special vote of thanks to my dear friends **Sujita**, **Vishesh**, **Shalini** and **Ashutosh** for their companionship and concern.*

*I also thank all the staff members of stores, purchase office, administrative office, account section, library and computing facility of IISER Mohali for their help and co-operation during the course of time. I also wish to thank **Mr. Satvinder**, **Mr. Bahadur**, **Mr. Mangat**, **Mr. Prahlad** and **Mr. Ganesh**, lab assistants of chemistry teaching lab, for their timely help. I am thankful to **Mr. Balbir Singh** and **Mr. Triveni Shanker Verma** for recording NMR and HRMS spectras. I would also like to thank **Mr. Inderjit Singh** for taking the SEM images.*

*I am highly thankful to **Prof. Kamal Nain Singh** and **Prof. Paramjit Singh**, my M.Sc. project supervisor for giving me the flavor of research.*

*I deeply express my gratitude to my parents, **Palvinder Setia** & **Parveen Setia** and my brother**, Pankaj Setia** for their never-ending support and inspirations throughout my life. Their constant motivation and believe in me, made me travel this longer. I sincerely acknowledge **all my family members** for their love, support, encouragement and care throughout my life for my welfare.*

*I am thankful to **CSIR**, **India** for research fellowship for five years and **IISER Mohali** for financial support to carry out the experimental work, giving me the fellowship on time and also for providing all the research facilities that enabled me to complete my Ph.D.*

Contents

CHAPTER 1

Introduction: Discotic Liquid Crystals for Optoelectronic Applications

Organic semiconductors i.e., organic materials exhibiting semiconductor properties are receiving considerable attention nowadays for the development of electronic electronics such as organic light-emitting diodes (OLEDs), field effect transistors and display applications due to their easy fabrication, mechanical flexibility and low cost. Organic semiconductors can be single molecules, oligomers or polymers and can have advantages over inorganic semiconductors and polymers that experience trouble from high cost and fabrication in a flexible substrate. In this direction, discotic liquid crystalline (DLC) materials are highly tempting as these are much easier to fabricate than single crystals and polymers and the molecular order is much higher than that of isotropic materials. Long range order in a material can be obtained relatively easily by using LCs and because they are liquid, it is easy to obtain highly ordered molecular structures over large domains as compared to other crystalline materials. Thus, design and synthesis of DLC materials with long range self-assembly make them promising in plastic electronic applications, such as OLEDs, organic photovoltaics devices and LC displays.

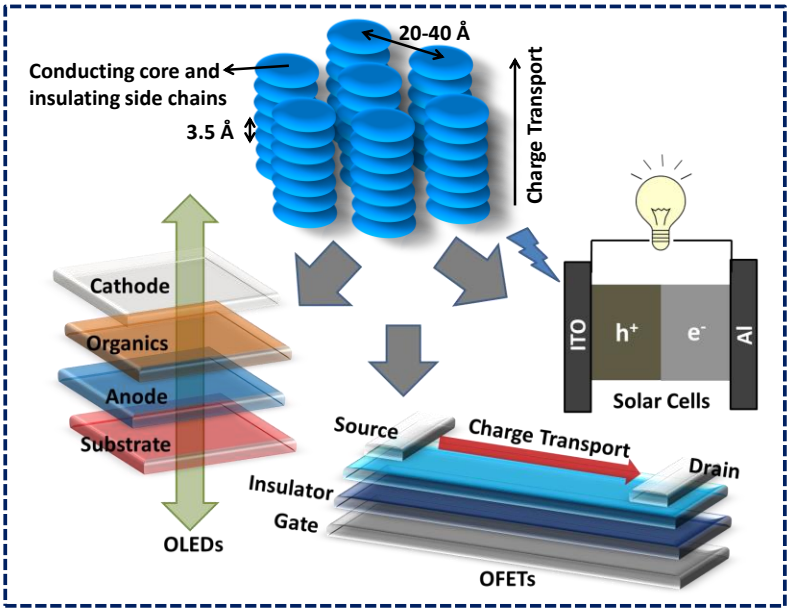

1.1 Overview

Over the last decade every aspect of our daily lives has become saturated with electronic devices such as notebook and tablet computers, smart phones, digital cameras, MP3 players, flat panel TVs as well as embedded systems in household appliances, automobiles and large industrial facilities etc. Much progress has been achieved up to now and extensive research efforts worldwide have been devoted to the development of novel materials for downsizing such electronic equipment in order to save cost, space, weight, energy and raw materials. In this regard, semiconducting organic materials are of utmost interest due to their easy fabrication, mechanical flexibility and low cost.[1,2] Many variations in chemical structures can be made which result in a wide range of properties. These materials find an extensive application in various fields for instance, organic photoconductors in copy machines and laser printers, organic field-effect transistors (OFETs), organic photovoltaics (OPVs) and organic light-emitting diodes (OLEDs) etc.[1,2]

Organic semiconductors are organic materials exhibiting semiconductor properties i.e., their properties lie in between those of conductors and insulators. Organic compounds generally act as insulators as the valence electrons are very tightly bound and fixed in place in covalent bonds. However, when a high degree of conjugation is present in the molecules and if the electrons exhibit a high degree of delocalization, then these organic compounds may act as semiconductors.[3]

In unsaturated organic compounds, the π_{pz} orbitals of the double bonds overlap to form a pair of π molecular orbitals. Out of these two orbitals, the one with lower energy level is known as the bonding molecular orbital and the higher energy orbital as the anti-bonding molecular orbital. In organic semiconductors, the bonding and anti-bonding orbitals are known as highest occupied molecular orbitals (HOMO) and lowest unoccupied molecular orbitals (LUMO), respectively. This can be regarded as equivalent to valence band and conduction band of semiconductors or conductors. Consequently, band gap is the energy difference between the HOMO and LUMO of an organic semiconductor.[4] For all the electronic devices, charges must travel over relatively large distances through the material and so good molecular order is necessary to obtain good charge transport. In this regard, the major

drawback of organic semiconductors compared to inorganic semiconductors is their low charge carrier mobility.[5-8] However, due of their low cost and flexibility, the use of organic semiconductors will be more profitable for many applications compared to inorganic semiconductors.[1,2]

Organic semiconductors can be single molecules, oligomers or polymers. In case of polymers, the processing cost is low. But, the molecular ordering in polymer systems is difficult to control as homogenous polymers are difficult to prepare. Therefore, to obtain highly ordered molecular organization small and low molecular weight semiconducting molecules are often required. In order to avoid packing defects which reduce charge transport, single crystals are needed. However, the fabrication of single crystals over large distances, as will be needed in future organic-based optoelectronic devices, is rather difficult. An intermediate solution would be to consider the use of organic liquid crystal (LC) materials. The fabrication of LCs is much easier than that of single crystals and the molecular order is much higher than that of isotropic materials. Long range order in a material can be obtained relatively easily by using LCs and because they can flow like a liquid, it is easy to obtain highly ordered molecular structures over large domains as compared to other crystalline materials.[9]

In this thesis, synthesis and evaluations of novel discotic liquid crystalline (DLC) materials for use in plastic electronic applications, such as OLED, OPV devices and LC display is presented. The aim of the thesis is to synthesize such discotic materials which are easier to process and exhibit mesomorphic behavior at or near to room temperature. It also focuses on the study of relationship between chemical structures and mesomorphic behavior, LC transition temperatures and energy levels of new compounds.

1.2 Liquid crystals

LCs are unique functional soft materials which combine both order and mobility on a molecular, supramolecular and macroscopic level. LCs are accepted as the fourth state of matter after solid, liquid and gas. LCs form a state of matter intermediate between solid and liquid state (Figure 1.1). For this reason, they are referred to as intermediate phases or

mesophases. This is a true thermodynamic stable state of matter. The constituents of the mesophase are called mesogens. While rigid core of the mesogen is responsible for structural order, alkyl chains provide necessary mobility within LC phase. Hierarchical self-assembly in LCs offers a powerful strategy for producing nanostructured mesophases.[10-18]

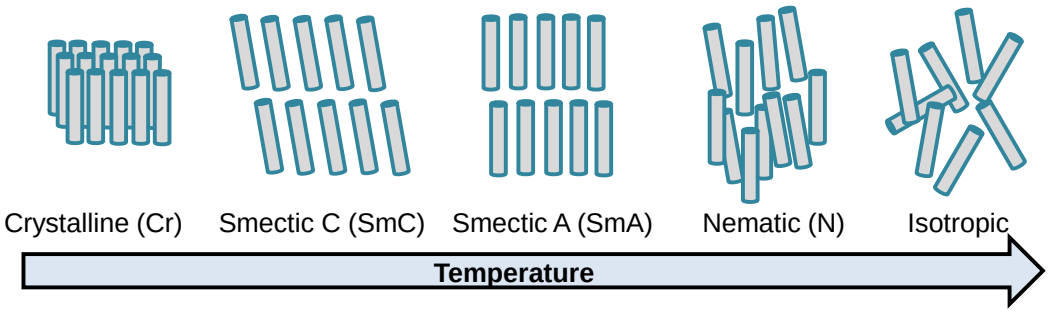

Figure 1.1 Schematic of arrangement of molecules in various phases.

The unique feature of LCs is that both order and high degree of mobility is retained in the mesophase. This combination leads to self-healing, adaptive and stimuli-responsive behavior of these supramolecular systems. Hence, such supramolecular systems are becoming the quintessential self-assembling molecular materials of the modern area.

LCs have made huge effects on the development of human societies today and in future. LCs are advanced technological materials found in low power consuming LC displays (LCDs) which are being used in the last decades for development of mobile data processing and communication tools. It is quite possible that LCDs might or might not be replaced by other technologies in the future but, the fundamental knowledge gained with LCs can be used for the self-assembly of a huge variety of other materials.[19-22]

1.3 Brief history of liquid crystals

In 1888 Friedrich Reinitzer,[23,24] Professor of botany and technical microscopy at the German Technical University in Prague was investigating cholesterol derivatives which he had extracted from carrots. While measuring the melting point of cholesteryl benzoate at 145.5 °C, he found a second melting point at 178.5 °C and in between these two transitions, there was a milky liquid phase and above 178.5 °C, the phase was clear. Under the polarizing

microscope, he observed distinct violet and blue color phenomena at both phase transitions. He also made similar observations with another derivative of cholesterol namely, cholesteryl acetate which has a monotropic cholesteric phase. He then contacted physicist Otto Lehmann,[25] an expert in the area of physical isomerism of crystals. He was having a polarizing microscope with a hot stage and was thus able to investigate more precisely than Reinitzer. Reinitzer, the biologist, therefore is seen as the discoverer of LCs and Lehmann, the physicist, is hailed as the founder of LC research.

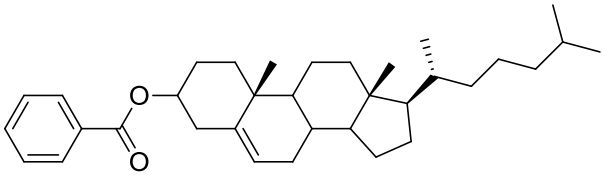

Cholesteryl Benzoate

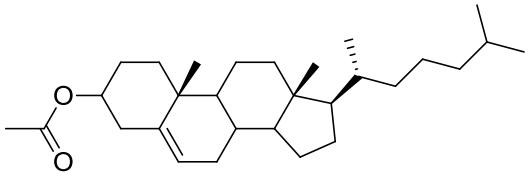

Cholesteryl Acetate

In 1890, Gatterman and Ritschke prepared the first totally synthetic LC *p*-azoxyanisole.[26] Then in 1922, a French chemist, Georges Freidel classified LCs into different mesophases.[27] This is one of the most important developments in the history of LCs. After this, Vörlander designed a programme to study the structure-LC properties of different molecules.[28] In his laboratory, about 1100 LCs were prepared and based on the synthesis, he suggested that compounds exhibiting mesophases must have elongated (rod-like) shape. These molecules nowadays are known as calamitic molecules. To date more than hundred thousand calamitic LC compounds are known in the literature.

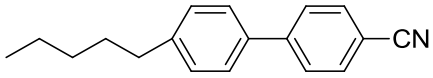

Cr 23 N 35 I

4'-Pentyl-4-cyanobiphenyl

Later in 1950s, Onsager and Flory[29,30] gave the theory to explain relationships between the molecular structure and formation of LC phases. These theories guided and promoted further research in the field of LCs. In 1973, Gray *et al.* made the most important discovery in the field of LCs by synthesizing a new class of thermotropic, calamitic LCs, known as the 4'-alkyl-4-cyanobiphenyls which exhibit either a smectic or nematic phase at or near to room

temperature.[31-33] These molecules have been found to be highly stable (chemically, photo-chemically, electrochemically and thermally) and are responsible for the development of early LCDs. For example, nematic mixture E7 containing some 4'-alkyl-4-cyanobiphenyls and the corresponding terphenyls was used for the early LCDs.[31-33]

In 1923, Vorländer suggested the possibility of formation of LC phases with a packing behavior similar to "Voltas columns" while studying flat molecules such as triphenylene and perylene.[34] Unfortunately, he was not able to observe any mesomorphism for these compounds which are now well known archetypal core units of many discotics. The experimental breakthrough came in September 1977, when Sivaramakrishna Chandrasekhar and his colleagues at the Raman Research Institute reported *"...what is probably the first observation of thermotropic mesomorphism in pure, single component systems of relatively simple plate like, or more appropriately disc-like molecules"*.[35] They prepared a number of benzene hexa-*n*-alkanoates and from thermodynamic, optical and X-ray studies, it was established that these materials form a new class of LCs in which molecules stacked one on the top of other in columns and the columns further constitute a hexagonal arrangement.[35] This is today considered as the birth of DLCs. Currently more than 3000 DLCs are known in the literature and are being explored for a variety of applications.[9,36-49]

The latest addition in the LC family is banana-shaped molecules which have been discovered very recently in 1996.[50-56] The molecular structure of these molecules can be regarded as being composed of three units; an angular central unit, two linear rigid cores and terminal chains. These molecules can display not only classical nematic or smectic phases but, also novel types of smectic-like phases called "B" phases. The discovery of ferroelectricity in non-chiral banana shaped molecules has led to a very intense research activity in this field. Not only this, various new applications of these materials include nonlinear optics, flexoelectricity, photoconductivity, molecular electronics and the design of biaxial nematic phase. Several hundred bent molecular shape compounds have been synthesized so far.

The work discussed in this thesis revolves around the development (synthesis and characterization) of new DLCs for optoelectronic and display applications.

1.4 Discotic liquid crystals: phase types and structure

An archetypal discogenic molecule has a rigid, planar core surrounded by flexible side chains. The cores are commonly composed of a single phenylene group, several phenylene groups or metal ion complexes. The flexible side chains are most necessary to form LC mesophases of these compounds. They are linked to the core directly or *via* an ether, thioether, ester, alkanoyloxy or amide groups.[9,36-49]

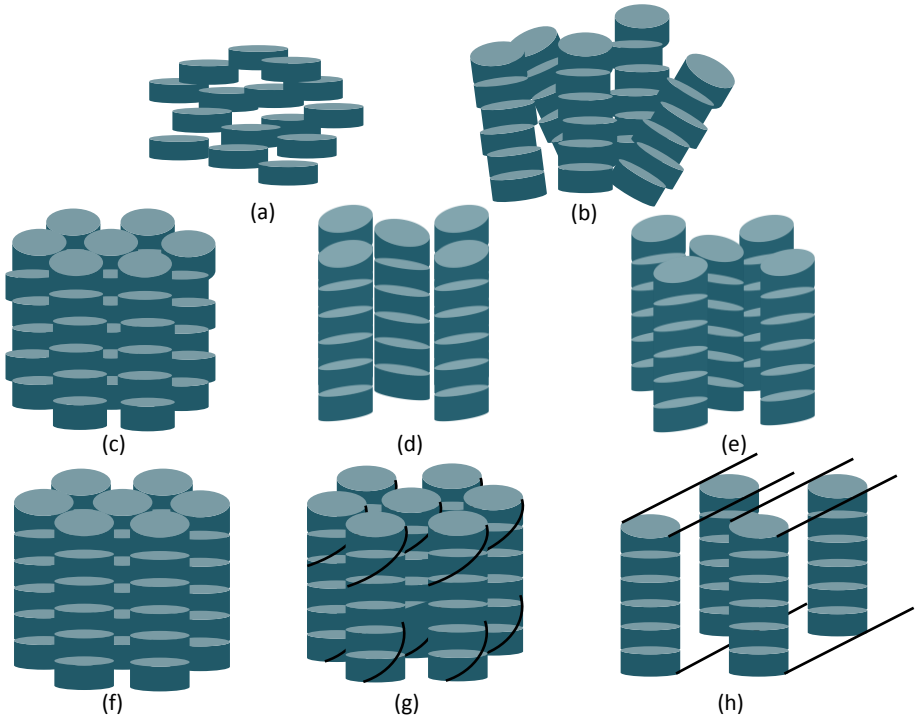

Figure 1.2 Schematic representation of mesophases formed by disc-like molecules: (a) discotic nematic, (b) columnar nematic (N_{col}), (c) hexagonal columnar (Col_h), (d) rectangular columnar (Col_r), (e) columnar oblique (Col_{ob}), (f) columnar plastic (Col_p), (g) columnar helical (H) and (h) columnar lamellar (Col_L) phase.

Achiral DLCs exhibit two different types of mesophases namely nematic (N) and columnar (Col) phases.[9,36-49] The nematic phase of discotics is similar to the nematic phase of rod-like molecules in possessing orientational order (Figure 1.2a). Another variant of nematic phase is columnar nematic phase (N_{col}), in which nematic structure is formed by columns (Figure 1.2b). The most common phase exhibited by disc-like molecules is the columnar phase, in

which discs self-assemble to give 1D columns which then self-organize into 2D mesophases (Figure 1.2c-h). Columnar LCs show a rich polymorphism and can be classified into six categories namely: (a) columnar hexagonal, (b) columnar rectangular, (c) columnar oblique, (d) columnar plastic, (e) columnar helical and (f) columnar lamellar. The stacking of discs within the columns can be ordered or disordered. In columnar hexagonal (Col_h) phase, the constituent molecules can have either an aperiodic arrangement (liquid-like) or long-range positional order within the column and columns are arranged in a hexagonal packing. Columnar rectangular (Col_r) and columnar oblique (Col_{ob}) phases are characterized by a liquid-like molecular order along the columns, in which the columns are arranged either in a rectangular or oblique packing, respectively. Columnar plastic (Col_p) phase is characterized by three-dimensional crystal-like order in a hexagonal lattice, while the discs within the columns are able to rotate about the column axis. In columnar helical phase (H), helical columns develop which interdigitate in groups of three columnar stacks. In the columnar lamellar phase (Col_L), discotic molecules stack to form columns and these columns are arranged in layers, where the columns in layers can slide. But, the columns in different layers do not possess any positional correlation. The discotic cores which have been explored to create novel LCs are triphenylene, phthalocyanines, anthraquinone, ethynyl benzene, hexa-*peri*-hexabenzocoronens, tricycloquinazolines, macrocycles with a large cavity at the centre, metallo-discogens containing copper, molybdenum, nickel and palladium etc.[36-49] By the introduction of chiral chains around the periphery of discotic cores, various chiral DLCs have also been prepared.

Interestingly, chiral discotics forming columnar mesophase have also been found to exhibit ferroelectric switching properties which appear to have some advantages over its tilted smectic counterpart in electro-optical displays. The discotic nematic mesophase is now considered as better medium for display applications especially with respect to viewing angle problems.[57] Added to this, the recent commercialization of discotic nematic in the production of optical compensation films by Fuji Film Company[58,59] has created an immense interest in this area. The potential use of discotic materials, especially those exhibiting columnar phases, as quasi-one dimensional conductors, photoconducting systems, ferroelectrics, light emitting diodes, photovoltaic solar cells, field effect transistors, gas sensors, optical storage devices,

hybrid computer chips for molecular electronics, xerographic processes etc. are attracting considerable attention.[10]

1.5 Characterization of mesophases

In our studies, a combination of different experimental techniques has been used to characterize the phase behavior of LC materials. They include direct space techniques such as polarized optical microscopy (POM) and wide- and small-angle X-ray scattering (WAXS and SAXS). Differential scanning calorimetry (DSC) was employed to study the thermal transitions occurring in LC systems during heating and cooling ramps. Importantly, none of the above mentioned techniques alone would suffice for a complete structural characterization of a LC system. For example, the temperatures and types of phase transitions can be conveniently studied by DSC. The type of mesophase can also be identified by POM, whereby defects of the structure give rise to the formation of characteristic textures well documented in literature. However, we observed that, in some instances, the transitions which are not detected by DSC, could still be observed in POM and vice versa. It is also clear that the phase characterization by means of POM alone is almost never unambiguous since different phases can display similar textures. Therefore, the use of X-ray scattering is necessary to identify different phases and obtain quantitative information on their structure.

1.5.1 Polarizing optical microscopy (POM)

POM is a routine technique used for the LC phase identification. If it is an isotropic liquid, the light is extinguished, so a black optical appearance is observed in the field of view. When LC samples are placed under microscope, the transmitted light is not completely extinguished and an optical texture appears because of the alternation of orientation of polarized light.[13] This is due to the birefringent nature of these compounds. LC compounds exhibit various characteristic textures under POM which yields important information about the structural arrangement of the LC phases. For example, for nematic phases typical schlieren texture is generally observed under microscope. For smectic phases, focal conic fan textures have been observed under POM. Focal conic, fan-shaped, mosaic and dendritic textures are characteristics of columnar phases observed under microscope.

1.5.2 Differential scanning calorimetry (DSC)

Generally, DSC measures the power released or absorbed by material during temperature treatments that can include dynamic (i.e., heating or cooling ramps) or isothermal segments. The measurement is performed by comparing the temperature of the sample and that of the reference material. The instantaneous heat flux is computed from this temperature difference using instrumental calibration constants. Standard sample like pure indium with known transition enthalpies and temperatures has been used for calibration of the instrument. In studies of LC systems, the measure of the enthalpy variation can allow to assign a given thermal event to a crystal-crystal or to a mesophase-mesophase transition. This is based on the fact that the enthalpy variation associated with crystal melting is very large than the one corresponding to the mesophase-mesophase or mesophase-isotropic phase transitions.

The main advantage of DSC is that it is a fast and convenient tool to measure the temperatures and transition enthalpies in order to determine the phase diagram of the system and to study the kinetics of transitions as a function of heating/cooling rates or as a function of time. DSC can also be used to identify the presence of glass transitions which is almost impossible to determine using POM and to determine the corresponding glass transition temperature.

1.5.3 Wide- and small- angle X-ray scattering (WAXS and SAXS)

The supramolecular organization and the corresponding packing parameters in each phase can be studied in detail by X-ray scattering This technique is generally considered as the proof for the existence of mesophase in compounds. The peaks in the small and wide angle region confirm existence of a particular mesophase. Based on the X-ray scattering pattern, different kinds of mesophases can be distinguished from each other. Different kinds of nematic mesophases for the discotic mesogens have also been distinguished from each other based on X-ray scattering. For example, for the discotic nematic mesophase, one peak comes in small angle region and one in wide angle region. The peak in the small angle region corresponds to the diameter of the discs and peak in the wide angle region is related to the lateral distance between the cores. An X-ray pattern of a columnar nematic phase shows

relatively sharp reflection in the wide-angle regime that corresponds to regular stacking of discotic molecules on top of each other. The reflections in small-angle regime are rather diffuse and broadly related to liquid-like arrangement of the columns. In N_L phase, relatively sharp reflections are found in both small-angle and wide-angle regions of the X-ray scattering pattern. Hence, X-ray scattering is a powerful technique to distinguish between these nematic phases.[37]

The DLCs investigated in this thesis work exhibited Col_h mesophase mostly and one DLC demonstrated Col_r mesophase. These different types of columnar phases have also been distinguished from each other by X-ray scattering.[37] For Col_h phase, the 2D X-ray scattering pattern and X-ray scattering profiles exhibited four diffraction rings in small-angle region, whose spacings are in ratio of $1:1/\sqrt{3}:1/\sqrt{4}:1/\sqrt{7}$ along with two broad peaks in the wide-angle region. Out of the two wide-angle reflections, one corresponds to the liquid-like packing of flexible alkyl chains and the other one which is relatively narrow, corresponds to intracolumnar stacking of discotic cores.

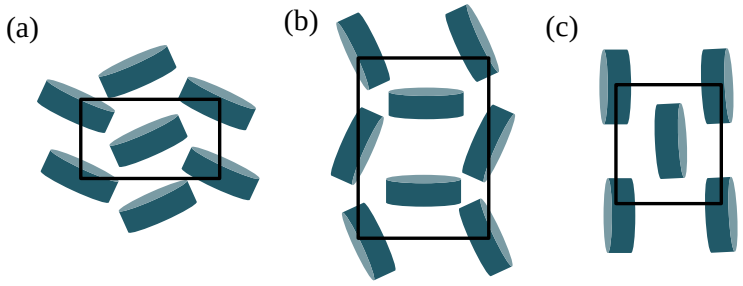

Figure 1.3 Schematic representation of three different types of symmetries; (a) $P2_1/a$, (b) P2/a and (c) C2/m.

Two strong reflections (results by splitting of (10) reflection of hexagonal lattice) in the small angle region of X-ray scattering pattern are characteristic of a rectangular columnar phase. X-ray scatterinhg has allowed to distinguish between different kinds of symmetries for this phase. Based on the X-ray scattering pattern, Col_r mesophase has been divided into three different types depending on the mutual orientation of the molecules and the number of columns per unit cell in the lattice. The symmetry of the 2D lattices are specified by three

different planar space group, that is, $P2_1/a$, P2/a and C2/m (Figure 1.3) which do not have any translational order in the direction of columns.

1.6 Discotic liquid crystalline packing and charge transport

1.6.1 Discotic liquid crystals (DLCs) as organic semiconductors

All the electronic devices, such as solar cells, light-emitting diodes and field-effect transistors rely on the transport of electrical charges between two electrodes. For these devices, inorganic semiconductors like crystalline Si are generally used due to their high charge carrier mobility. The dense packing of these materials in the crystalline state leads to significant orbital overlap of single atoms and hence broad energy bands are formed (several eV wide).[49] As a result of these broad bands, recombination of charge carriers is hindered and due to easy creation of free charge carriers, silicon fulfills the requirements for its application in microelectronic systems. The charge carrier mobility is one of the crucial parameters for the application of semiconductors in electronic devices because, fast switching times can only be achieved with high mobilities. Charge transport in inorganic semiconductors also depends on temperature. With increasing temperature, lattice vibrations increase that results in increase of scattering of charge carriers and thus decrease their mobility. The mobility also depends on the degree of crystallinity. In a single crystal of silicon, a very high electron mobility up to 1400 $cm^2\ V^{-1}\ s^{-1}$ at room temperature can be observed.[60] The processing of crystalline silicon is however expensive and it is difficult to prepare flexible electronic components from the hard material. In this direction, semi-conductive organic materials are attractive for the production of flexible and cheaper devices, as they are soluble in organic solvents and can easily be deposited on a substrate. For organic materials, the charge carrier mobility is not their intrinsic property. It is actually a material property and requires hopping of charges between the molecules.[5-8] For good charge carrier transport, strong π-π interaction between the neighboring molecules is the preliminary requirement. The typical intermolecular distances occur in the range of Angstroms, so, this intermolecular hopping process of charges occurs many times before reaching the opposite electrodes which have a distance of 100 nm (minimum) to several mm. In order to achieve high charge carrier mobilities, monodomain of a properly packed organic material is needed.

LC ordering offers the possibility to easily orient organic semiconducting molecules[9] and to prepare monodomain samples.[10,61] LC phases possess a higher degree of order than the isotropic melt (amorphous order) but, lesser than highly ordered crystals. Thus π-conjugated molecules with LC phases are attractive to improve the charge carrier mobility. In this context, DLCs have been investigated most thoroughly. Discotic mesogens of appropriate molecular shape can self-assemble to give columnar LC phases with intra-columnar stacking distance less than 3.5 Å. With an aromatic π-system in the center of the mesogens, an overlap between the π-orbitals (HOMOs or LUMOs) of adjacent molecules can be observed (Figure 1.4).

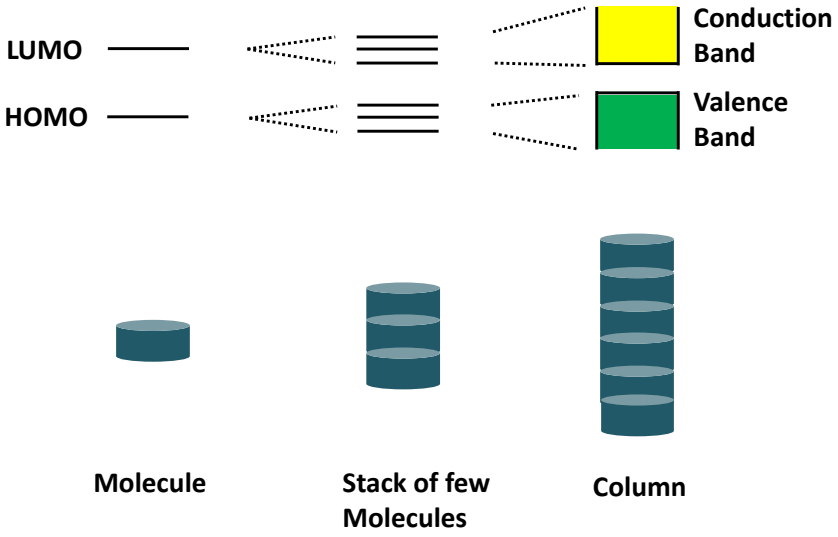

Figure 1.4 Cartoon illustrating the transition from individual energy levels to energy bands as the extension of π electron overlap grows along the columns of a columnar liquid crystal phase.

However, due to large HOMO-LUMO energy gap, no intrinsic charge carriers exist in the material. But, charge carriers can be generated in the columnar system by chemical doping (oxidation or reduction)[62] or can be transported through the material. In columnar LC phases, the transport of electrons and holes is only possible parallel to the columns along the stacked aromatic mesogen centers. The exchange of charge carriers between neighboring columns is strongly hindered due to the insulating alkyl chains (Figure 1.5). Columnar LCs are hence considered as quasi one dimensional semiconductors. While any defects or grain boundaries

inside a crystalline lattice lower the charge carrier mobility, these are less likely to appear in a LC semiconductor. Instead, the director can bend smoothly over the sample and local defects can be overcome by a self-healing procedure.[63-67] Thus, the pinning of charge carriers at grain boundaries is much less problematic in organic semiconducting materials with LC order than in polycrystalline samples.

Flexible aliphatic chains provide the mobility necessary for the discotic phase and act as insulating layer around stacked columns of aromatic cores. They also prevent any charge transport between molecules in neighboring columns.[68,69] The distance between neighboring columns ranges between 20-40 Å (Figure 1.5). The formation of columnar assembly can be seen as a nano-segregation between the conjugated cores and flexible insulating side chains.[63] As the charges has to move over macroscopic distances (>100 nm) which is well above the length of an individual undisturbed column, the side chains become important for macroscopic charge transport as determined by time of flight measurements.

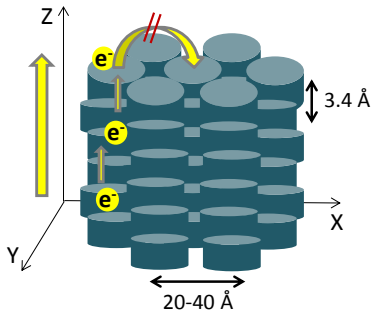

Figure 1.5 Schematic representation of the charge carrier transport along the columns. Transfer of charges between the columns is suppressed by insulating alkyl chains.

On increasing the length of side chains, both packing order and charge hopping between the columns gets reduced.[70-72] This readily illustrates the key problem of DLCs: any discontinuity in a column disrupts the charge motion. Therefore the choice of DLCs from a variety of discotics for use as semiconductors is highly important, as the combination of aromatic core, anchoring side chains and LC ordering determines the electronic properties of the discotics. Nowadays, there are many companies which focus on the fabrication of flexible

displays based on organic semiconducting materials.[73] Furthermore, organic light emitting diodes and organic photovoltaic cells are well-established in practice.[74]

1.6.2 Organic light emitting diodes (OLEDs)

Organic light emitting diode (OLED) is based on the principle of light generation by electrical excitation. Electrons are injected into the LUMO of the acceptor and holes into the HOMO of the donor and transported by an applied electric field. Electron and hole then combine to form an exciton which upon relaxation produces luminescence. In a multilayer device, electron and hole transporting layers are sandwiched between a metal cathode and a transparent indium tin oxide (ITO) anode (Figure 1.6). In between these layers, emitter material is kept whose energy levels are matched to trap electrons and holes. Between the two electrodes, discotics are kept in homeotropic alignment for best possible charge transport.

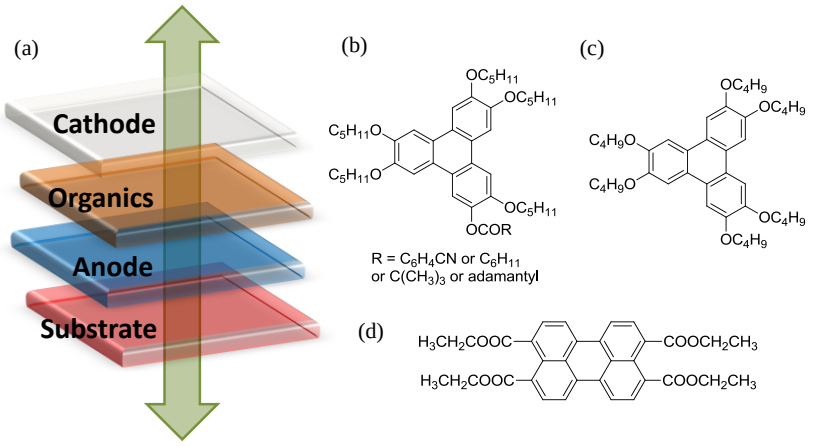

Figure 1.6 (a) Schematic of a simple OLED device, (b) Triphenylene monoester, (c) hole transporter triphenylene and (d) electron transporter perylene DLCs discussed in the text.

Till now, only a few DLCs have been explored for the preparation of OLEDs.[75-80] The very first OLED based on DLCs was single-layer with a very thin film of the LC sandwiched between hole-injecting ITO and electron injecting aluminum electrodes. Wendorff and co-workers[81,82] have shown that the monoesters of triphenylene (Figure 1.6b) in their Col_p phase and main chain polymers of triphenylene in the Col_h phase show electroluminescence. The

fields required are of the order of 105 V cm^{-1} and the lifetimes of the devices are probably not very long. The bilayer devices made by Bock and co-workers,[80,83] e.g., aluminum/ perylene (Figure 1.6d) (electron transporter)/ triphenylene (Figure 1.6c) (hole transporter)/ ITO was made from LC materials but, they were characterized at room temperature i.e., below the solid to LC transition temperature. These red-light emitters have a lifetime of 1 day under a dry nitrogen atmosphere.

1.6.3 Organic photovoltaics (OPVs)

OPV devices are the reverse of OLEDs, as in them dissociation of an exciton into electron and hole takes place after absorption of a photon and output is current (Figure 1.7). The high charge carrier mobility of inorganic crystalline semiconductors made this effect much more pronounced than in the organic materials. As in the latter materials, electron and hole are strongly bound to each other because of lower dielectric constant and lower charge carrier mobility of the material.[2] However, the processability of crystalline photovoltaic materials is rather difficult and expensive.

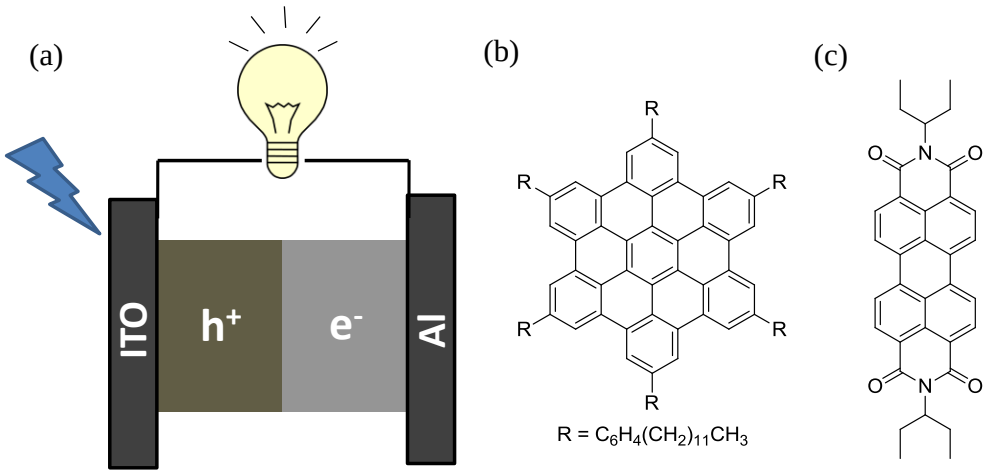

Figure 1.7 (a) Schematic representation of OPV device, (b) hole transporting hexa-*peri*-hexabenzocoronene DLC and (c) electron transporting perylene crystal discussed in the text.

Compared to them solution processable organic materials provide a means for the production of thin and flexible solar cells, often in a more cost-effective manner. There are many barriers that need to be overcome in order to produce a good OPV cell.[59] First, there needs to

be an efficient light absorption. Further, there should be a high probability of exciton diffusion to the interface between hole and electron transporting layers (where charge separation usually occurs), efficient charge separation at this interface, escape of the charges from the interface and efficient charge transport to the electrodes. Failure at any of these stages can result in overall failure of the device. Thus LC materials and especially discotics become interesting in this regard. The main advantage of DLCs is that these are free from grain boundaries which in crystalline molecular solids act as exciton traps. Another advantage of DLCs is that they possess large exciton diffusion lengths.[84,85] Many OPV devices have been reported in the literature containing triphenylene, phthalocyanine, porphyrin and hexa-*peri*-hexabenzocoronene (HBC) as the hole transporting layer and perylene as the electron transporting layer.[86-92] However, the best OPV devices consisted of HBC and perylene discogens.[90-92]

A solution of a mixture of HBC (Figure 1.7b) (a hole transporter which is LC at room temperature) and perylene (Figure 1.7c) (an electron transporter which is crystalline at room temperature) was spin-coated onto an ITO electrode. As the film dries, phase separation occurs and perylene crystallites got deposited on top of the HBC layer. An aluminum electrode is then evaporated on the top. Due to the space filling by the LC between the perylene molecules, there is a very large effective surface area between the hole and electron transporting units.[89] Annealing further improves the device performance which seems to increase interpenetration between two components of the films.[90] External quantum efficiencies up to 34 % at 490 nm are reported.[90] It has further been suggested that HBCs with shorter side chains gave better performance.[92]

1.6.4 Organic field effect transistors (OFETs)

An OFET device is made of a semiconductor and three terminals which are called source, gate and drain (Figure 1.8). Depending on the type of semiconductor, either electrons or holes are conducted between source and drain. The drain to source current flow is controlled by applied voltage between them. The applied gate voltage modulates channel conductivity by either increasing or decreasing the channel size. Columnar DLCs acting as anisotropic charge carriers can be used in these devices in the planar alignment. In an OFET, the ideal

columnar phase to use is that of a HBC, as these molecules prefer to lie in the planar alignment. However, to ensure the conduction pathway between source to drain, zone-casting[93] or a PTFE-rubbed substrate[94] are used. Unaligned films of HBCs gave OFET mobilities ~10^{-5} cm^2 V^{-1} s^{-1}, but when the hexadodecyl HBC (Figure 1.8b) is aligned by the zone-casting method, the mobility at room temperature rises to 5×10^{-3} cm^2 V^{-1} s^{-1}.[93] The high number of aromatic units allows the alignment of the HBC derivatives with a magnetic field. Such oriented films exhibit field-effect mobilities 10 times larger than FET devices from isotropically aligned films.[95]

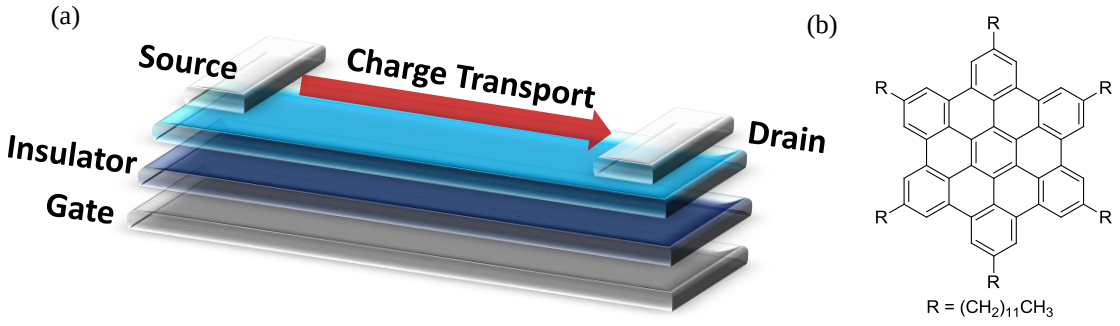

Figure 1.8 (a) Schematic representation of OFET device and (b) hexadodecyl-hexabenzocoronene DLC discussed in the text.

However, all the OFETs based on DLCs have been characterized below the Cr-Col transition temperature i.e., below the temperature at which the special properties and potential advantages of the LC phase are relevant. The most probable reason for this is that above the Cr-Col transition temperature, thin open to the air films of DLCs become unstable. Another reason is above the Cr-Col transition temperature, surface tension forces can come into play and films can move and dewet from the surface.[96]

Compared to well-established inorganic semiconductors, the charge carrier mobilities of DLCs are two orders of magnitude lower. In this regard, a better understanding of the structure-property relationship of the LCs can further improve their electronic properties. The ability to tailor components with specific properties and to easily process them in solution makes them a promising alternative to classic inorganic semiconductor materials.

1.7 Outline of thesis

The results described in this thesis were obtained on a variety of low molecular weight materials forming columnar and nematic mesophases. Good long-range order in organic semiconducting materials is necessary to obtain high charge transport mobilities. In this thesis, the synthesis of various novel series of LC semi-conducting materials is presented. In order to have a good understanding of the molecular order, the chemical structures of LCs are kept simple.

Chapter 2 describes the microwave (MW) assisted synthesis of new oligomeric DLCs based on rufigallol core. The synthesis of the target compounds was challenging since classical reactions failed to produce these hybrids. Specifically, we note that whereas, traditional form of heating failed to produce any desired product, MW dielectric heating resulted cleaner synthesis of these oligomers within minutes in good yield. We have demonstrated that the combination of rod and disc-like moieties in the rufigallol-cyanobiphenyl series has sufficiently perturbed the molecular shape to yield calamitic mesophases. Interestingly, the higher homologues of the series showed the SmA phase whereas, the lower one exhibited mixed N phases. We also reported a new series of rufigallol-based mesogens with branched alkyl chains at the peripheral positions. The introduction of various types of branched chains has sufficiently perturbed the system resulting into LC systems with mesophase stabilised up to room temperature. Such systems are good candidates for various mesophase device fabrications with high charge-carrier mobility.

Chapter 3 addresses non-conventional approach to the synthesis of DLC materials based on perylene core. The synthesis, optical properties and thermal behavior of non-conventional 3,4,9,10-tetrasubstituted perylene-based discotic oligomers are investigated consisting of a perylene core attached to which are four 4-cyanobiphenyl, triphenylene units *via* flexible alkyl spacers and branched alkyl chains. All the derivatives self-assemble into a mesophase and exhibit excellent fluorescence emission properties making them suitable for various optoelectronic applications. Whereas, the attachment of cyanobiphenyl units to the perylene core led to the formation of N phase, triphenylene and branched alkyl chains resulted a regular hexagonal mesophase. Comparison between the UV-vis and photo-luminescent

properties in the solution and solid state demonstrated large spectral shifts. The formation of thin films of these materials via Langmuir Blodgett technique has also been demonstrated. In the thin film state, these materials were found to exhibit charge transport properties. Such materials combine an exceptionally high degree of self-organization at the nanometer scale with the advantages that LCs provide.

Chapter 4 talks about the first discotic system based-on alkoxy (tri- & di-) substituted hexa-*peri*-hexabenzocoronene (HBC) that self-organizes into room temperature columnar structure. This system is a promising candidate as an active component of OLEDs, due to its facile processability, low band gap, luminescence and exceptionally higher ordered self-organization behavior in the mesophase derived from X-ray scattering studies. The role of alkoxy substituents in determining the geometrical preferences of the Scholl reaction for the formation of dodecylalkoxy substituted HBC core has also been reported in this chapter. Evidences from the ab-initio calculation of arenium cation reaction mechanism at a B3LYP/6-31G (d) level of theory gave an explanation for nature of products formed and reaction mechanism. We found that regioselectivity of Scholl reaction is highly dependent on the position of all the electron donating groups on the ring with respect to each other. Adjacent (i.e., ortho) alkoxy groups resulted in partially cyclized product and non-adjacent (i.e., meta) resulted in complete cyclodehydrogenation to form the fully cyclized product. These findings can also be applied for the synthesis of large polycyclic aromatic systems.

This thesis is concluded with **Chapter 5** which summarizes the results presented in all of the above chapters.

In addition to the above chapters, **Appendix** at the end of each chapter contains the structural analyses (^{1}H and ^{13}C NMR, IR, DSC) of representative products.

References

(1) O'Neill, M.; Kelly, S. M. *Adv. Mater.* **2003**, *15*, 1135-1146.

(2) Fleischmann, E.-K.; Zentel, R. *Angew. Chem. Int. Ed.* **2013**, *52*, 8810-8827.

(3) McGinness, J. E. *Science* **1972**, *177*, 896-897.

(4) Kaoand, K. C.; Hwang, W. in *Organic semiconductors* in Electrical Transport in Solids, Pergamon, Oxford, 1981.

(5) Bässler, H. *Phys. Status Solidi B* **1993**, *175*, 15-56.

(6) Boden, N.; Bushby, R.; Clements, J.; Movaghar, B.; Donovan, K.; Kreouzis, T. *Phys. Rev. B* **1995**, *52*, 13274-13280.

(7) Cordes, H.; Baranovskii, S.; Kohary, K.; Thomas, P.; Yamasaki, S.; Hensel, F.; Wendorff, J.-H. *Phys. Rev. B* **2001**, *63*, 094201.

(8) Kohary, K.; Cordes, H.; Baranovskii, S.; Thomas, P.; Yamasaki, S.; Hensel, F.; Wendorff, J.-H. *Phys. Rev. B* **2001**, *63*, 094202.

(9) Sergeyev, S.; Pisula, W.; Geerts, Y. H. *Chem. Soc. Rev.* **2007**, *36*, 1902-1929.

(10) Handbook of Liquid Crystals, Demus, D.; Goodby, J.; Gray, G. W.; Spiess, H. W.; Vill, V., Ed., Wiley-VCH, Weinheim, 1998, Vol 1-3.

(11) Liquid Crystals-Application and Uses, Bahadur, B., Ed., World Scientific, Singapore, 1990, Vol 1-3.

(12) Chandrasekhar, S. in Liquid Crystals, Cambridge University Press, Cambridge, 1992, Vol 2.

(13) Collings, P. J.; Hird, M. in Introduction to Liquid Crystals-Chemistry and Physics, Taylor & Francis Ltd., London, 1997.

(14) Collings, P. J.; Patel, S. J. in Handbook of Liquid Crystal Research, Oxford University Press, Oxford, 1997.

(15) Kelker, H.; Hatz, W. in Handbook of Liquid Crystals, VCH, Deerfield Beach, FL, 1980.

(16) Collings, P. J. in Liquid Crystals: Nature's delicate Phase of Matter, Princeton University Press, 1990.

(17) de Gennes, P. G.; Prost, J. in The Physics of Liquid Crystals, Oxford University Press, New York, 1993, Vol 2.

(18) Sluckin, T. J.; Dunmur, D. A.; Stegemeyer, H. in Crystals that flow, Classic papers from the history of liquid crystals, Taylor & Francis, London, 2004.

(19) Lagerwall, J. P. F.; Scalia, G. *Curr. Appl. Phys.* **2012**, *12*, 1387-1412.

(20) Hird, M. *Chem. Soc. Rev.* **2007**, *36*, 2070-2095.

(21) Kawamoto, H. *Proc. IEEE* **2002**, *90*, 460-500.

(22) Haas, W. E. *Mol. Cryst. Liq. Cryst.* **1983**, *94*, 1-31.

(23) Reinitzer, F. *Monatsh. Chem.* **1886**, *7*, 597-608.

(24) Reinitzer, F. *Monatsh. Chem.* **1888**, *9*, 421-441.

(25) Lehmann, O. *Z. Phys. Chem.* **1889**, *4*, 462-472.

(26) Gattermann, L.; Rischke, A. *Ber. Dtsch. Chem. Ges.* **1890**, *23*, 1738-1750.

(27) Friedel, G. *Ann. Phys.* **1922**, *18*, 273-474.

(28) Vörlander, D. in Chemische Kristallographie der Flüssigkeiten, Akadem, Verlagsanstalt, Leipzig, 1924.

(29) Onsager, L. *Ann. N. Y. Acad. Sci.* **1949**, *51*, 627-659.

(30) Flory, P. J. *Proc. Roy. Soc. Ser. A. London* **1956**, *234*, 73-89.

(31) Gray, G. W.; Harrison, K. J.; Nash, J. A. *J. Chem. Soc. Chem. Commun.* **1974**, 431-432.

(32) Gray, G. W.; Mosley, A. *J. Chem. Soc. Perkin Trans. 2* **1976**, *11*, 97-102.

(33) Bremer, M.; Kirsch, P.; Klasen-Memmer, M.; Tarumi, K. *Angew. Chem. Int. Ed.* **2013**, *52*, 8880-8896.

(34) Vorländer, D. *Z. Phys. Chem.* **1923**, *105*, 211-254.

(35) Chandrasekhar, S.; Sadashiva, B. K.; Suresh, K. A. *Pramana* **1977**, *9*, 471-480.

(36) Kumar, S. *Chem. Soc. Rev.* **2006**, *35*, 83-109.

(37) Kumar, S. in Chemistry Of Discotic Liquid Crystals: From Monomers to Polymers; Percec, V., Ed., CRS Press, Taylor & Francis Group: Boca Raton, FL, 2011.

(38) Kato, T.; Yasuda, T.; Kamikawa, Y.; Yoshio, M. *Chem. Commun.* **2009**, 729-739.

(39) Laschat, S.; Baro, A.; Steinke, N.; Giesselmann, F.; Hagele, C.; Scalia, G.; Judele, R.; Kapatsina, E.; Sauer, S.; Schreivogel, A.; Tosoni, M. *Angew. Chem. Int. Ed.* **2007**, *46*, 4832-4887.

(40) Wu, J.; Pisula, W.; Mullen, K. *Chem. Rev.* **2007**, *107*, 718-747.

(41) Boden, N.; Bushby, R. J.; Clements, J.; Movaghar, B. *J. Mater. Chem.* **1999**, *9*, 2081-2086.

(42) Bushby, R. J.; Lozman, O. R. *Curr. Opin. Solid State Mater. Sci.* **2002**, *6*, 569-578.

(43) Bushby, R. J.; Lozman, O. R. *Curr. Opin. Colloid Interface Sci.* **2002**, *7*, 343-354.

(44) Takezoe, H.; Kishikawa, K.; Gorecka, E. *J. Mater. Chem.* **2006**, *16*, 2412-2416.

(45) Ohta, K.; Hatsusaka, K.; Sugibayashi, M.; Ariyoshi, M.; Ban, K.; Maeda, F.; Naito, R.; Nishizawa, K.; van de Craats, A. M.; Warman, J. M. *Mol. Cryst. Liq. Cryst.* **2003**, *397*, 25-45.

(46) Kouwer, P. H. J.; Jager, W. F.; Misj W. J.; Picken, S. J. *Macromolecules* **2001**, *34*, 7582-7584.

(47) Chandrasekhar, S. *Liq. Cryst.* **1993**, *14*, 3-14.

(48) Chandrasekhar, S.; Ranganath, G. S. *Rep. Prog. Phys.* **1990**, *53*, 57-84.

(49) Wöhrle, T.; Wurzbach, I.; Kirres, J.; Kostidou, A.; Kapernaum, N.; Litterscheidt, J.; Haenle, J. C.; Staffeld, P.; Baro, A.; Giesselmann, F.; Laschat, S. *Chem. Rev.* **2016**, *116*, 1139-1241.

(50) Niori, T.; Sekine, T.; Watanabe, J.; Furukawa, T.; Takazoe, H. *J. Mater. Chem.* **1996**, *6*, 1231-1233.

(51) Pelzi, G.; Diele, S.; Weissflog, W. *Adv. Mater.* **1999**, *11*, 707-724.

(52) Tschierske, C.; Dantlgraber, G. *Pramana-J. Phys.* **2003**, *61*, 455-481.

(53) Ros, M. B.; Serrano, J. L.; De la Fuente, M. R.; Folcia, C. L. *J. Mater. Chem.* **2005**, *15*, 5093-5098.

(54) Reddy, R. A.; Tschierske, C. *J. Mater. Chem.* **2006**, *16*, 907-961.

(55) Takezoe, H.; Takanishi, Y. *Jpn. J. Appl. Phys.* **2006**, *45*, 597-625.

(56) Etxebarria, J.; Ros, M. B. *J. Mater. Chem.* **2008**, *18*, 2919-2926.

(57) Chandrasekhar, S.; Krishna Prasad, S.; Nair, G. G.; Rao, D. S. S.; Kumar, S.; Manickam, M. US Patent, 6, 558, 759, B2, 2003.

(58) Kawata, K. *Chem. Rec*. **2002**, *2*, 59-80.

(59) Bushby, R. J.; Kawata, K. *Liq. Cryst.* **2011**, *38*, 1415-1426.

(60) Costa, J.; Peczalski, A.; Shur, M. *J. Appl. Phys.* **1989**, *66*, 674-679.

(61) Topics in physical chemistry; Stegemeyer, H., Ed., Steinkopff, Darmstadt, 1994, Vol. 3.

(62) Boden, N.; Bushby, R. J.; Clements, J.; Movaghar, B.; Donovan, K. J.; Kreouzis, T. *Phys. Rev. B: Condens. Matter Mater. Phys.* **1995**, *52*, 13274-13280.

(63) Tschierske, C. *J. Mater. Chem.* **1998**, *8*, 1485-1508.

(64) Barber, J.; Rakitin, O. A.; Ros, M. B.; Torroba, T. *Angew. Chem. Int. Ed.* **1998**, *37*, 296-299.

(65) Bayer, A.; Zimmermann, S.; Wendorff, J. H. *Mol. Cryst. Liq. Cryst.* **2003**, *396*, 1-22.

(66) Kohary, K.; Cordes, H.; Baranovskii, S. D.; Thomas, P.; Wendorff, J.-H. *Phys. Status Solidi B* **2004**, *241*, 76-82.

(67) Brinker, C. J.; Lu, Y.; Sellinger, A.; Fan, H. *Adv. Mater.* **1999**, *11*, 579-585.

(68) Boden, N.; Bushby, R. J.; Cammidge, A. N.; Clements, J.; Luo, R.; Donovan, K. J. *Mol. Cryst. Liq. Cryst.* **1995**, *261*, 251-257.

(69) Balagurusamy, V. S. K.; Prasad, S. K., Chandrasekhar, S.; Kumar, S.; Manickam, M.; Yelamaggad, C. V. *Pramana J. Phys.* **1999**, *53*, 3-11.

(70) Morale, F.; Date, R. W.; Guillon, D.; Bruce, D. W.; Finn, R. L.; Wilson, C.; Blake, A. J.; Schrçder, M.; Donnio, B. *Chem. Eur. J.* **2003**, *9*, 2484-2501.

(71) Lai, C. K.; Tsai, C.-H.; Pang, Y.-S. *J. Mater. Chem.* **1998**, *8*, 1355-1360.

(72) Zheng, H.; Lai, C. K.; Swager, T. M. *Chem. Mater.* **1995**, *7*, 2067-2077.

(73) http://www.emd-Performance-Materials.com/en/index.html. 16.02.2015.

(74) http://www.heliatek.com/. 16.02.2015.

(75) Seguy, I.; Jolinat, P.; Destruel, P.; Farenc, J.; Mamy, R.; Bock, H.; Ip, J.; Nguyen, T. P. *J. Appl. Phys.* **2001**, *89*, 5442-5448.

(76) Hassheider, T.; Benning, S. A.; Kitzerow, H.-S.; Achard, M.-F.; Bock, H. *Angew. Chem. Int. Ed.* **2001**, *40*, 2060-2063.

(77) Schwab, M. G.; Qin, T.; Pisula, W.; Mavrinskiy, A.; Feng, X.; Baumgarten, M.; Kim, H.; Laquai, F.; Schuh, S.; Trattnig, R.; List, E. J. W.; Mullen, K. *Chem. Asian J.* **2011**, *6*, 3001-3010.

(78) Stapff, I. H.; Stumpflen, V.; Wendorff, J. H.; Spohn, D. B.; Mobius, D. *Liq. Cryst.* **1997**, *23*, 613-617.

(79) Lssem, G.; Wendorff, J. H. *Polym. Adv. Technol.* **1998**, *9*, 443-460.

(80) Seguy, I.; Destruel, P.; Bock, H. *Synth. Met.* **2000**, *111-112*, 15-18.

(81) Lussem, G.; Wendorff, J. H. *Polym. Adv. Technol.* **1998**, *9*, 443-460.

(82) Stapff, I. H.; Stumpflen, V.; Wendorff, J. H.; Spohn, D. B.; Mobius, D. *Liq. Cryst.* **1997**, *23*, 613-617.

(83) Seguy, I.; Jolinat, P.; Destruel, P.; Farenc, J.; Mamy, R.; Bock, H.; Ip, J.; Nguyen, T. P. *J. Appl. Phys.* **2001**, *89*, 5442-5448.

(84) Markovitsi, D.; Marguet, S.; Bondkowski, J.; Kumar, S. *J. Phys. Chem. B* **2001**, *105*, 1299-1306.

(85) Cisse, L.; Destruel, P.; Archambeau, S.; Seguy, I.; Jolinat, P.; Bock, H.; Grelet, E. *Chem. Phys. Lett.* **2009**, *476*, 89-91.

(86) Oukachmih, M.; Destruel, P.; Seguy, I.; Ablart, G.; Jolinat, P.; Archambeau, S.; Mabiala, M.; Fouet, S.; Bock, H. *Sol. Energy Mater. Sol. Cells* **2005**, *85*, 535-543.

(87) Petritsch, K.; Friend, R. H.; Lux, A.; Rozenberg, G.; Moratti S. C.; Holmes, A. B. *Synth. Met.* **1999**, *102*, 1776-1777.

(88) Li, L. F.; Kang, S. W.; Harden, J.; Sun, Q. J.; Zhou, X. L.; Dai, L. M.; Jakli, A.; Kumar S.; Li, Q. *Liq. Cryst.* **2008**, *35*, 233-239.

(89) Schmidt-Mende, L.; Fechtenkotter, A.; Mullen, K.; Moons, E.; Friend, R. H.; MacKenzie, J. D. *Science* **2001**, *293*, 1119-1122.

(90) Schmidt-Mende, L.; Fechtenkotter, A.; Mullen, K.; Moons, E.; Friend, R. H.; MacKenzie, J. D. *Physica E* **2002**, *14*, 263-267.

(91) Schmidtke, J. P.; Friend, R. H.; Kastler, M.; Mullen, K. *J. Chem. Phys.* **2006**, *124*, 174704/1-6.

(92) Hesse, H. C.; Weickert, J.; Al-Hussein, M.; Doessel, L.; Feng, X.; Mulen, K.; Schmidt-Mende, L. *Sol. Energy Mater. Sol. Cells* **2010**, *94*, 560-567.

(93) Pisula, W.; Menon, A.; Stepputat, M.; Lieberworth, I.; Kolb, U.; Tracz, A.; Sirringhaus, H.; Pakula T.; Mullen, K. *Adv. Mater.* **2005**, *17*, 684-689.

(94) Wittmann, J. C.; Smith, C. *Nature* **1991**, *352*, 414-417.

(95) Shklyarevskiy, I. O.; Jonkheijm, P.; Stutzmann, N.; Wasserberg, D.; Wondergem, H. J.; Christianen, P. C. M.; Schenning, A. P. H. J.; de Leeuw, D. M.; Tomovic, Z.; Wu, J.; Mullen, K.; Maan, J. C. *J. Am. Chem. Soc.* **2005**, *127*, 16233-16237.

(96) Bramble, J. P.; Tate, D. J.; Revill, D. J.; Sheikh, K. H.; Henderson, J. R.; Liu, F.; Zeng, X. B.; Ungar, G.; Bushby, R. J.; Evans, S. D. *Adv. Mater.* **2010**, *20*, 914-920.

Chapter 2

Anthraquinone based Discotic Liquid Crystals for Optoelectronic Applications

PART A

Microwave-assisted green syntheses of five new oligomeric liquid crystals have been reported consisting of rufigallol-based core attached to which 8-cyanobiphenyl units via flexible alkyl spacers. Classical reaction didn't result in formation of any product. The liquid crystalline behavior of the synthesized compounds was investigated by polarizing optical microscopy, differential scanning calorimetry and X-ray scattering.

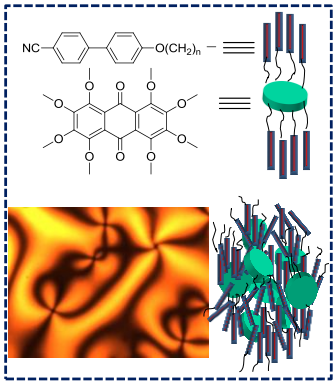

PART B

Microwave-assisted syntheses of five new series of rufigallol based mesogens have been reported with branched alkyl chains at the peripheral positions. The chemical structures of these newly synthesized compounds were determined by ^{1}H nuclear magnetic resonance (NMR), ^{13}C NMR, IR spectroscopy, UV-vis spectroscopy and elemental analysis. The thermotropic LC properties were investigated by polarizing optical microscopy, differential scanning calorimetry and X-ray scattering. Most of the derivatives were found to be liquid crystalline over a wide temperature range.

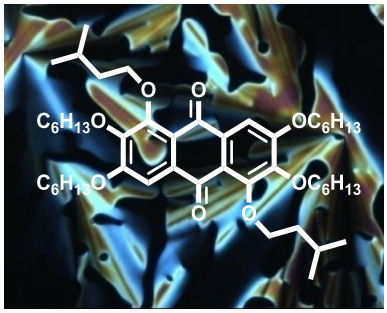

2.1 Part A: Microwave-assisted synthesis of novel oligomeric rod-disc hybrids

2.1.1 Introduction

Recently, there has been a considerable interest in the realization of elusive biaxial nematic (N_b) phase owing to produce interesting and possibly advantageous effects in liquid crystal (LC) devices such as optical compensation films. Freiser[1-5] first predicted the N_b phase in 1970 and since then there have been several attempts in the demonstration of this phase as a real entity.[1-6] Although some of these attempts bridge the gap between differently shaped LCs, the actual existence of the phase is still not clear. The most unambiguous example for the N_b phase is reported in a ternary lyotropic and most recently in thermotropic systems.[7-8]

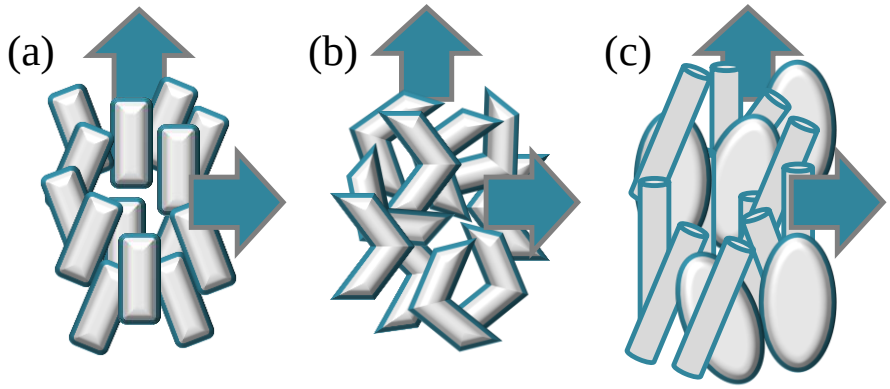

Figure 2.1 Schematic representation of three types of approaches for biaxial nematic phase; (a) board like molecules, (b) bent core molecules and (c) mixture of rod-like and disc-like molecules.

In considering the molecular design for this phase, mainly two options are apparent which includes either the molecular shape biaxiality or the supramolecular interactions leading to biaxiality. Based on the molecular shape biaxiality, the approaches can be divided into three major categories namely; (a) board like molecules, (b) bent core molecules and (c) mixture of rod-like and disc-like molecules[9] (Figure 2.1). In a mixture of rod-like and disc-like mesogens, rod-like molecules align with their long axis perpendicular to the short axis of the disc-like molecules. Theoretical studies and mean field calculations[10,11] have shown that the

N_b phase is obtained by changing shape biaxiality parameter (η) between a rod at one extreme (η = 0) and a disc (η =1) at the other. The N_b phase exists over ranges, such as $0.2 \leq \eta \leq 0.8$, and is most stable at η = 0.4. Such a structure is then properly intermediate between a rod and a disc and this led to proposals that the N_b phase might be realized in rod/disc mixtures.

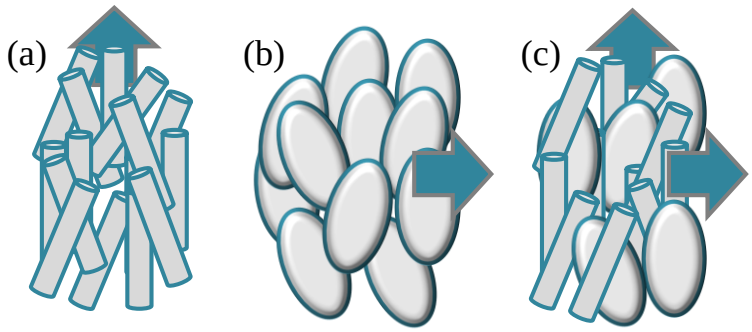

Figure 2.2 Schematic representation of packing arrangement and director configuration in; (a) rod like molecules, (b) disc like molecules and (c) mixture of rod like and disc like molecules.

In such a mixture, the optimum packing arrangement has the long axes of the rods arranged perpendicularly to the short axes of the discs and hence, the system has two directors (Figure 2.2).

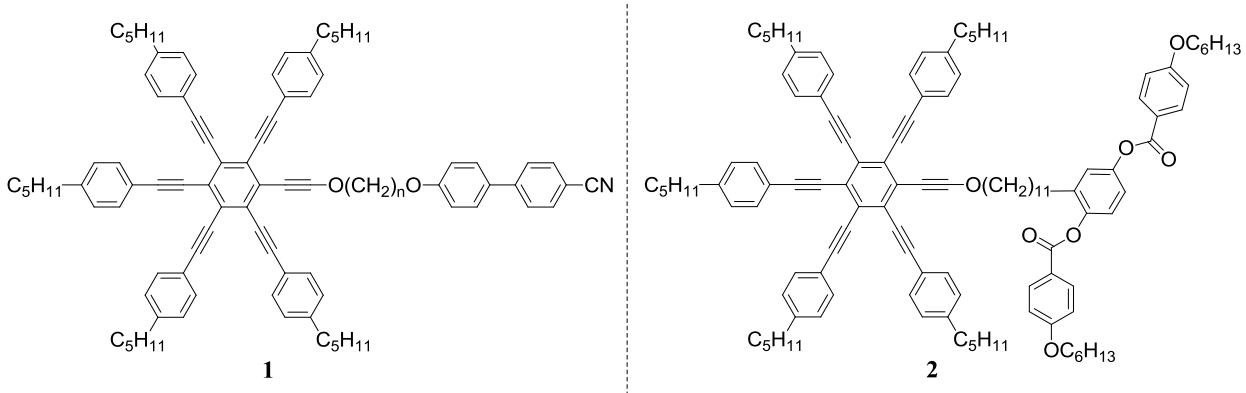

This idea was investigated in theoretical approaches to the N_b phase formed from binary mixtures of rod- and disc-like molecules.[12] But, in real systems physical mixtures of rod and

disc separate into two uniaxial nematic phase and thus biaxiality could not be experimentally verified.[13] To tackle this problem a number of molecular designs have been demonstrated where rod and disc-like mesogens are linked covalently *via* flexible alkyl spacers. Attachment of one disc and one rod like mesogen (so called rod-disc dimers) covalently leads to the formation of an amphiphile possessing features of a rod and features of a disc, so called a shape amphiphile. For example, Luckhurst *et al.*[14] synthesized the first rod-disc dimers (**1**) by joining together the disc-shaped [pentakis(4-pentylphenylethynyl)] benzene and the rod shaped 4-cyanobiphenyl moieties through an ether linkage. Bruce and co-workers[15,16] examined the molecular biaxiality by synthesizing compound **2** in which a pentyne disc was joined to the lateral rod-like molecules. Mehl and co-workers[17] confirmed complete miscibility in the nematic phase of molecule **3** which contain one rod and one disc with either rod or disc shaped molecules.

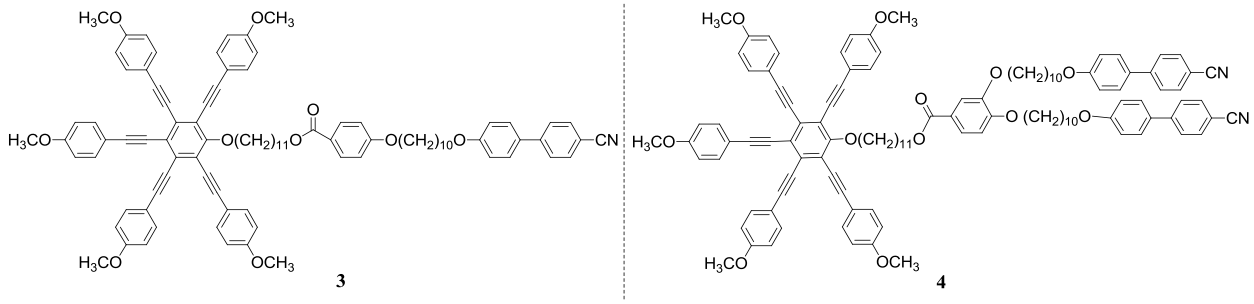

3 **4**

Whereas, incompatible combination (which does not induce nematic mesophase) of two or three rod-like mesogens with disc shaped mesogens in **4**, **5** and **6** induces the formation of a smectic phase with alternating layers of discs and rod-shaped mesogens, compatible combination (which induces nematic mesophase) of rod and disc mesogens resulted a nematic phase.[17-20]

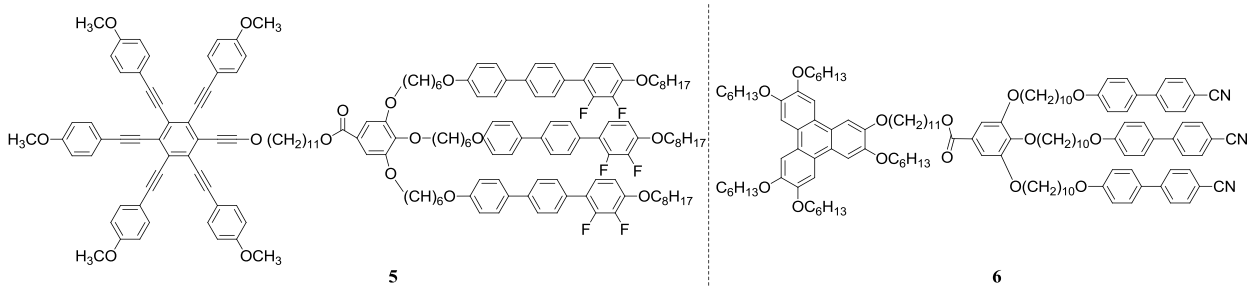

5 **6**

Subsequently, the approach of linking rod-disc moieties together has been extended where, six rods attached radially to a central discotic core that resulted several micro-segregated mesophase morphology due to change in the overall molecular shape. For example, linking six nitroazobenzene and cyanobiphenyl moieties with disc-shaped triphenylene (**7**, **8** and **9**) leads to a N phase in which the former promotes to form a calamitic N phase whereas the latter a discotic N phase indicating central units play an important role in controlling the average molecular shape.[21-24]

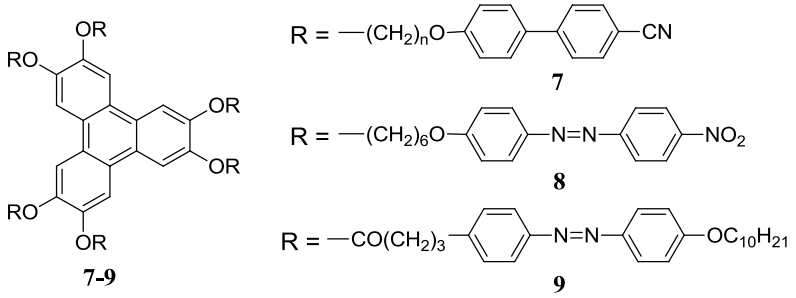

7-9

Not only molecular shape, various intra and intermolecular interactions play a significant role in determining the supramolecular organization in rod-disc hybrids as demonstrated recently with tricycloquinazoline discotic cores (**10**).[25]

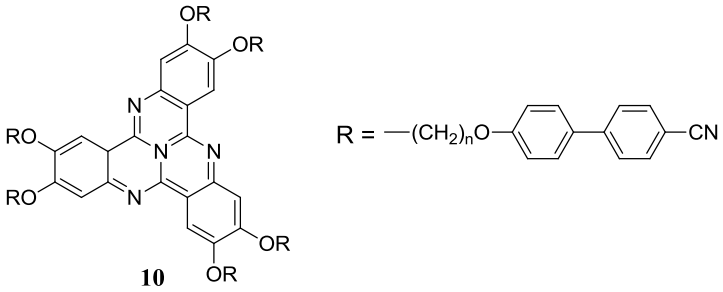

10

Though all these systems do not furnish a N_b phase but, veritably exploited to scaffold the gap between these differently shaped LC's (rod & disc) providing a greater insight into the structure-mesophase morphology.[26]

2.1.2 Objective

The past studies have used one, two, three and up to six rod like moieties with a single disc in the hunt of N_b phase. We have extended this approach and prepared a series of molecules **11**

in which eight rod-like 4-cyanobiphenyl (CB) moieties are connected to a central octahydroxyanthraquinone (OHA) core *via* flexible alkyl spacers. This study was motivated by two goals. First, by increasing number of rod-like mesogens around the central disc core (change in molecular shape), we sought to provide additional insight into the structure-mesophase morphology in the system. Second, we sought to determine the influence of spacer length in determining the supramolecular organization in disc-rod hybrid oligomers.

Anthraquinone (AQ) core was chosen because it is one of the earliest systems reported to exhibit columnar phases over a wide range of molecular framework and has a very versatile synthetic chemistry.[27] It has been found to be the critical component for the development of a variety of applications, such as the dye industry,[28] drug synthesis[29] and organic materials.[30,31] AQs are expected to be highly useful in devices as the redox reactions are generally reversible with stabilized radical anion intermediates leading to long-term stability in devices.[32]

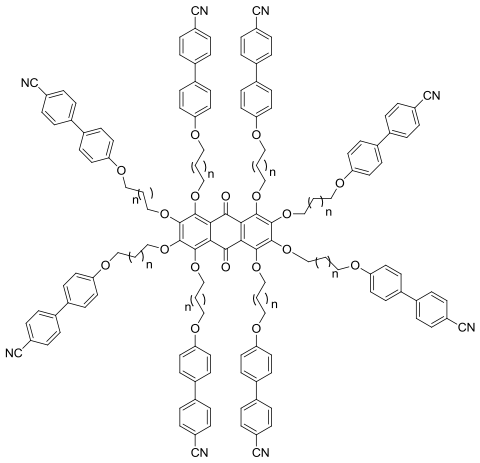

11

2.1.3 Results and Discussion

2.1.3.1 Synthesis and characterization

Compound **11** [OHA(nCB)$_8$] were synthesized by the route shown in Scheme 2.1. OHA **15** and ω-bromo substituted alkoxycyanobiphenyl were prepared following literature methods.[21,33] Acid-catalysed self-condensation of gallic acid **12** yielded crude rufigallol **13** which was purified through its hexa-acetate **14.** Pure rufigallol, obtained by the hydrolysis of

hexa-acetate was converted to octahydroxy anthraquinone **15** on reaction with mercuric oxide and boric acid which was further recrystallized with pyridine. The [OHA(*n*CB)$_8$] oligomers **11** were then prepared by reacting **15** with ω-bromo terminated alkoxycyanobiphenyl in the presence of cesium carbonate under microwave dielectric heating (MW) for 12 min.

The chemical structures of all these oligomers **11a-e** were confirmed through spectral and elemental analysis and details are given in the experimental section and representative spectra in Appendix I (Figures A1, A2 A9 and A14). It should be noted here that the etherification of hydroxyl groups of octahydroxyanthraquinone with ω-bromo substituted alkoxycyanobiphenyl failed to produce any desired product under classical reaction conditions. Only MW irradiation resulted in the formation of these oligomers. Failure of reaction under classical conditions could be due to steric hindrance resulted from simultaneously attaching eight cyanobiphenyl moieties. It is worth mentioning here that MW-assisted chemical synthesis of LC materials has attracted considerable attention recently.[34-36]

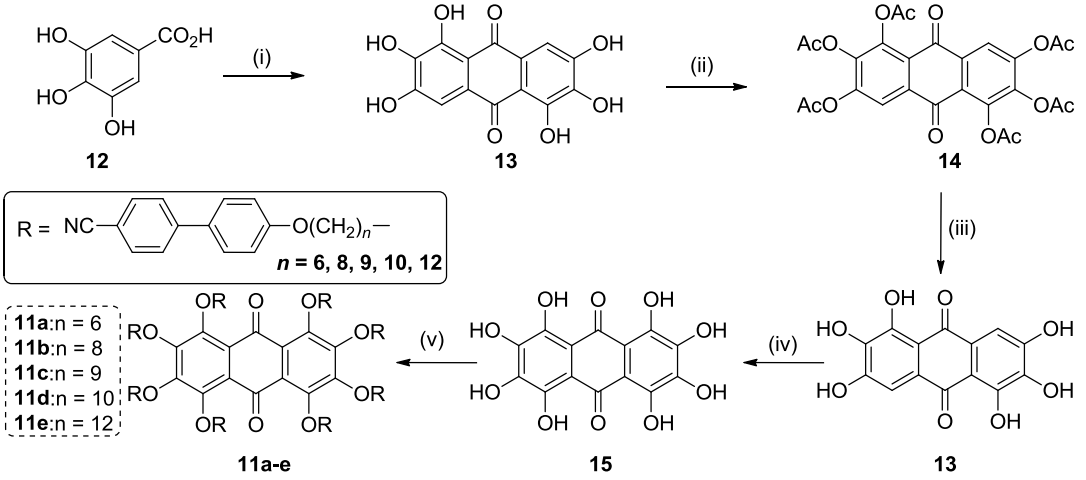

Scheme 2.1 Synthesis of the target compound **11**. *Reagents and conditions*: (i) H_2SO_4, MW, 90s, 90 %; (ii) Ac_2O, Pyridine, reflux, 12 h, 60 %; (iii) EtOH, 5% *aq*. NaOH, reflux, 2 h, 50 %; (iv) H_3BO_3, HgO, H_2SO_4, 45 %; (v) RBr, Cs_2CO_3, NMP, MW (800 W), 12 min, 45 %.

Nowadays, most of the organic reactions have been performed using the efficiency of MW

dielectric heating.[37-39] Also, whereas, classical form of heating is slow and inefficient method of transferring energy into a reaction mixture, the MW-irradiation produces efficient internal heating by directly coupling of microwave energy with the molecules that are present in the reaction mixture. Here, MW-assisted green chemistry endeavours resulted cleaner synthesis of these oligomers with easier work-up.

2.1.3.2 Thermal behavior

The thermal behavior (phase transition temperatures and associated enthalpy values) of all these materials (listed in Table 2.1) was investigated by polarizing optical microscopy (POM) and differential scanning calorimetry (DSC). Compound **11a** on heating melted at about 86 °C to a N phase and finally cleared (isotropic) at 169 °C. Before melting it displayed a crystal to crystal transition (partially crystallized states) at about 69 °C (ΔH = 0.3 kJ mol^{-1}) which could be due to some conformational reorganization of molecules by passing into different crystalline configurations.

Table 2.1 Phase behavior of mesogens**11a-e.**[a,b]

Mesogen	Heating run	Cooling run
11a	Cr_1 69 (0.3) Cr_2 86 (0.6) N 169 (2.6) I	I 168 (3.3) N
11b	SS 49 (15.7) SS 87 (1) N 161 (12) I	I 159.5 (12.6) N
11c	N 85 (0.5) I	I 84 (0.85) N
11d	SmA 138 (13) I	I 135 (13.6) SmA
11e	Cr_1 55 (57) Cr_2 71 (2.9) SmA 109 (12) I	I 104 (10) SmA

[a]Transition Temperatures in °C and latent heat values (in kJ mol^{-1} in brackets).

[b]Phase assignments: Cr = crystal; SS = semi solid; N = nematic phase; SmA = smectic A; I = isotropic.

These transitions in thermal analysis (DSC) arise from the different stability of two crystalline polymorphs; evidence accompanying by POM textures and powder X-ray scattering studies as observed by several researchers in past studies.[40-53] We also observed minor structural changes at Cr–Cr transition temperatures of the compounds reported here under POM and the samples remained solid even after these transitions. On cooling, the phase appeared at 168 °C which was stable down to room temperature. On second heating

and cooling, the peak re-appeared at 169 °C and 167 °C, respectively indicating the existence of phase which was further confirmed by POM as shown in Figure 2.3a.

Compound **11b** was semi-solid at room temperature and showed two endothermic transitions prior to isotropic transition at 161 °C (Figure A16). On cooling, the isotropic to mesophase transition peak appeared at 159.5 °C. However, no crystallization peak was observed up to room temperature. Under the microscope, a typical schlieren texture of the nematic phase is displayed, as shown in Figure 2.3b. Compound **11c** was nematic LC at room temperature and showed mesophase to isotropic transition temperature at 85 °C. On cooling, mesophase appeared at 84 °C which was characterized by typical schlieren texture as shown in Figure 2.3c. As expected, with the increasing length of the methylene spacer of the cyanobiphenyl units connecting to the anthraquinone discotic core, crystal to mesophase and mesophase to isotropic temperature decreases.

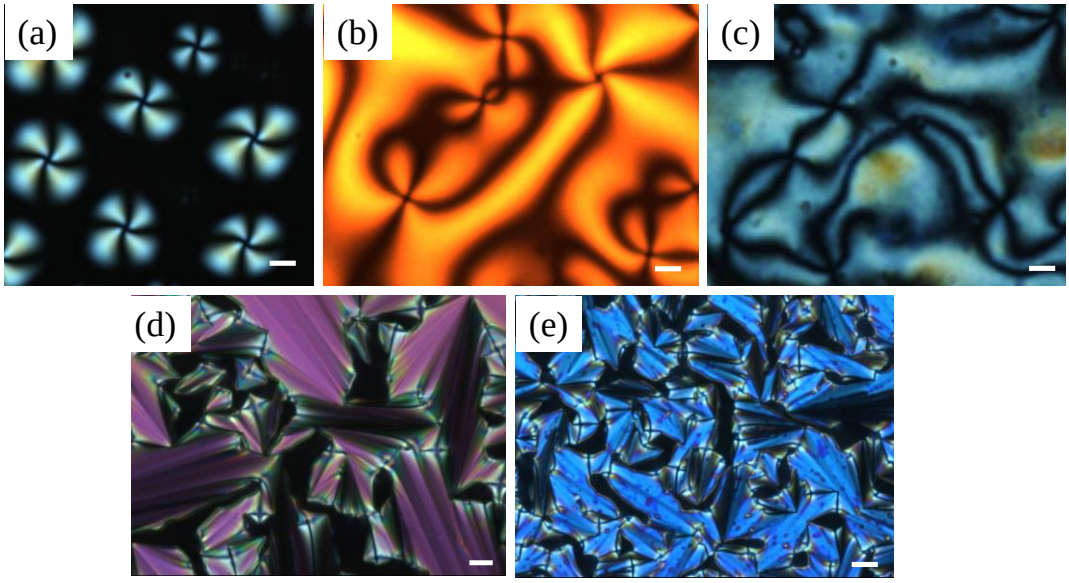

Figure 2.3 Optical photomicrograph of compounds (a) **11a,** (b) **11b,** (c) **11c,** (d) **11d** and (e) **11e** at 166.9 °C, 154.7 °C, 83.8 °C, 132 °C and 71.1 °C, respectively (on cooling, cross polars, scale bar 5 µm).

Two important trends were observed from the DSC plot regarding transition enthalpies of the compounds (**11a** to **11c**) associated with the mesophase (N) to isotropic phase transition: (i) the transition enthalpy for mesophase to isotropic transition for compound **11b** (ΔH = 12 kJ

mol^{-1}) is much higher than that of compound **11a** (ΔH = 2.6 kJ mol^{-1}). Such high difference in transition enthalpy suggests the role of flexible spacers in the efficient packing arrangement in the mesophase with increasing spacer length. (ii) With further increase in the number of methylene units in the alkoxy side chain (**11c**), the transition enthalpy decreases (ΔH = 0.5 kJ mol^{-1}). It has been proposed that even chain homologues (even number of methylene units in the side chain) showed higher enthalpies with respect to their highly packed solid structures compared to odd numbered ones. This sort of molecular organization (showing odd-even effect) has been studied in detail using a polarized light microscope, an electron microscope and wide angle X-ray scattering techniques.[54-57] Compound **11d** and **11e** were prepared to examine the effect of spacer length. Compound **11d** showed SmA phase at room temperature. On heating, SmA to isotropic transitions occurred at 138 °C, while on cooling the phase appeared at 135 °C (Figure 2.3d, focal conic fan texture). On the other hand, compound **11e** on heating showed a Cr-Cr transition before it went to SmA phase which finally cleared at 109 °C. On cooling, isotropic to SmA transition (Figure 2.3e) occurred at 104 °C which was stable down to room temperature. It is noticeable that the transition enthalpies associated with the mesophase to isotropic transitions of these compounds (**11d** and **11e**) are higher than the compounds showing the N phase in the order of ca. 14 kJ mol^{-1}. Such high transition enthalpies suggest a highly ordered organization (formation of a smectic phase) of the mesogens in the mesophase as observed in several past studies.[25] Interestingly, no crystallization peak up to room temperature was observed in any of these rod-disc oligomers. However, these materials were not deformed at room temperature probably because of vitrification and formation of a stable supercooled phase. Surprisingly, we did not observe any peak in DSC corresponding to glass transition while cooling from isotropic to room temperature. Noticeably, glass transitions are generally seen as a shift in the baseline and often may not be visible because they can be very weak. Under microscope, no difference in textural change was observed while cooling from the mesophase to room temperature. Such behavior has also been observed in other disc-like and disc-rod hybrid materials by several researchers in past studies.[25,45-47] However, these materials were not deformed at room temperature probably because of vitrification and formation of a stable super-cooled phase.

2.1.3.3 X-ray scattering studies

The supramolecular organization of these rod-disc oligomers in the mesophase was further investigated by X-ray scattering studies. In the N phase of compounds **11a**, **11b** and **11c**, two diffuse reflections were observed in the wide- and small-angle region (Figure 2.4a). These indicate the absence of any positional order in the mesophase and thereby exclude the existence of smectic and columnar phase structure of these hybrids, consistent with their microscopy textures.

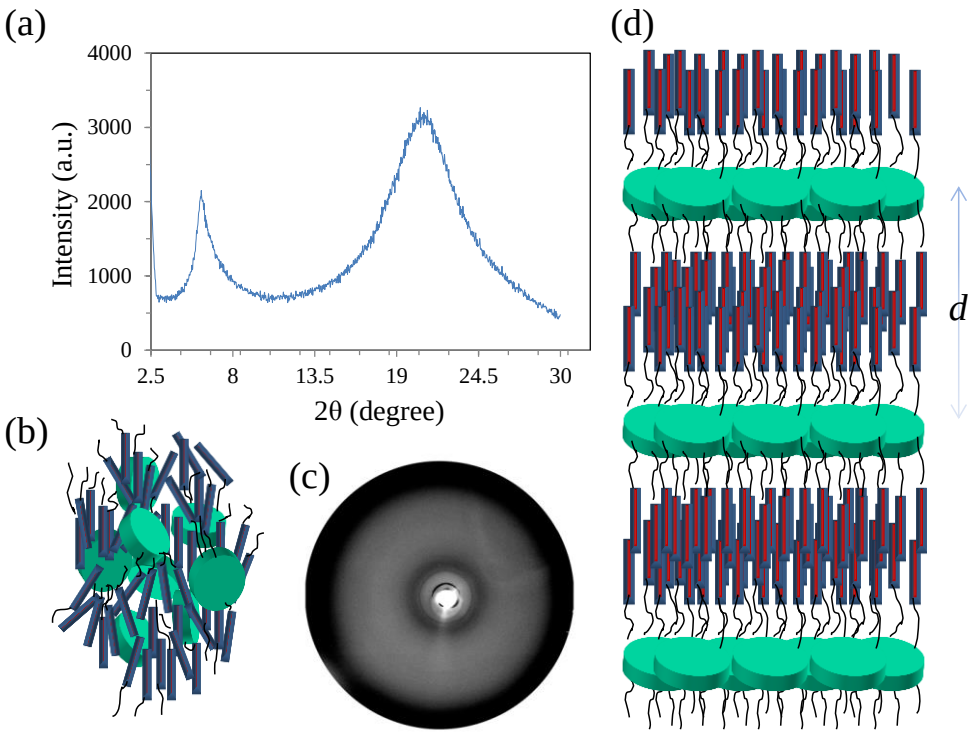

Figure 2.4 (a) An intensity *vs. 2θ* graph derived from the X-ray scattering pattern of compound **11b** in the mesophase. (b) Sketch of the order in the mixed nematic phase. (c) X-ray scattering pattern of compound **11e** in the mesophase. (d) Proposed model of the order of SmA phase of the oligomers of higher chain length.

The broad small angle reflection for **11a** showed a *d*-spacing of 13.28 Å in the mesophase (at 135 °C). This corresponds to the average length and diameter of the rod (~ 20 Å) and discs (~8 Å), respectively indicating a molecularly mixed N phase. Obviously, much smaller

reflection at small angle than that of the total length of the hybrid confirms the compatibility (homogeneously mixed) of both two components (disc and rod) in the mesophase and no nanophase segregation occurs between them. Similar scattering pattern was observed for certain mesogenic compounds having both rod- and disc-like moieties.[17] The small angle halos shifts to 14.77 Å at 140 °C in the N phase of **11b**, consistent with the increase in the length of the spacer. Based on the X-ray scattering studies and microscopy textures, we propose a sketch of the order of N phase (Figure 2.4b). Although biaxiality is likely to be seen at small length scales, as a result of large aspect ratios between two components, there is no direct evidence for the formation of biaxial N phase in our study. The *d*-spacings for all the compounds are gathered in Table 2.2. In all cases, we observed a very diffuse peak at around 4.5 Å and is attributed to the average lateral separation of the molecules in these fluid (N) phases. X-ray scattering pattern of higher chain length oligomers (**11d** and **11e**) show similar scattering pattern in the mesophase. In the small angle region two sharp peaks are observed, attributed to the layer formation (Figure 2.4c) which is consistent with their microscopic textures. The smectic periodicity *d*, for **11d** and **11e** is found to be 39.7 and 42.6 Å, respectively. The ratio of *d* with respect to full length (*l*) of each of these two molecules is close to 0.70 (*d*/*l*). This corresponds to the partial intercalation and orientational disorder of the rod-like moieties together with conformational flexibility in the spacers as observed by several researchers.[25,26]

Table 2.2 *d*-spacings of compounds **11a**, **11b**, **11d** and **11e** as found from the X-ray scattering data in the mesophase.

Compound	*d*-spacings (wide angle region)	*d*-spacings (small angle region)
11a	4.5 Å	13.28 Å
11b	4.5 Å	14.77 Å
11d	4.3 Å	14.7 Å, 39.7 Å
11e	4.3 Å	17.2 Å, 42.6 Å

Interestingly, in the SmA phase, a diffuse peak is observed in the small angle region at around 17.2 Å for **11e**. This spacing corresponds to the side-to-side distance between the discs and slightly decreases with decrease in spacer length (14.7 Å for **11d**) as expected. The diffuse peak in the wide-angle region at 4.3 Å confirms to the average separation of the rods and face-on spacing of the discs. Based on the X-ray microscopy data, we propose a sketch of the order of SmA phase (Figure 2.4d). Interestingly, we do not see any sharp reflections at 3.8 Å. This suggests that rufigallol discs are highly disordered similar to those reported earlier for other cores.[25] In fact, the discs behave like common rod-like mesogens in the layers, having only short range positional order associated with the organization of disc-like moieties.

2.1.4 Conclusions

In conclusion, a novel series of disc-rod oligomers have been synthesized using microwave-flash heating. Specifically, we note that whereas, traditional form of heating failed to produce any desired product, microwave dielectric heating resulted cleaner synthesis of these oligomers within minutes in good yield. We demonstrated that the combination of rod and disc-like moieties in the rufigallol-cyanobiphenyl series has sufficiently perturbed the molecular shape to yield calamitic mesophases. Interestingly, the higher homologues of the series showed SmA phase whereas, the lower one exhibited mixed N phases. Such hybrid materials combine an exceptionally high degree of organization at the nanometer scale with the advantages that LC's adduce.

2.2 Part B: Microwave assisted synthesis of novel mixed tail rufigallol derivatives

2.2.1 Introduction

In recent years, there has been a considerable attention in the development of molecular electronics. In this regard, discotic liquid crystals (DLCs) play an important role due to their unique optical[58] and non-linear properties.[59] DLCs exhibiting discotic nematic phase[21,60] are potential candidates to be used in optical compensation films to enhance the viewing angle capability.[61] Also, the hierarchical self-assembly of DLCs and their supramolecular columnar architecture are of fundamental importance not only as models for one-dimensional transportation of charge, ion and energy, but also as functional materials for the enhancement of properties through formation of self-organized monodomain on macroscopic scales.[62] For example, excellent charge transports through columns were achieved for π-conjugated DLCs.[62-71] In addition, due to their high charge carrier mobility,[63-71] self-healing of defects,[72,73] defect free long range order and tendency to form highly ordered films of various thickness,[74] these materials can be regarded as potential candidates for a number of molecular electronic devices. But, for all the device applications, columnar LCs with an appropriate chemical structure and morphology are required. The main prerequisite for an efficient engineering and processing of a columnar LCs by either thermal processing[75,76] or solution processing[77,78] in the form of devices is the presence of desired properties like appropriate thermal behavior and solubility.[75-78] Additionally, the operating temperature for all these devices is usually at room temperature. So, it is highly important to obtain materials with good intermolecular interactions and packing at ambient conditions.

In order to achieve this apposite isotropization as well as melting temperature various methods have been suggested in the literature which include heteroatom substitution,[79-81] branching,[82-94] unsaturation[83] etc. Assorted examples are there in the literature which has shown the effect of branching on melting and isotropic temperatures. Among them, use of branched alkyl chains to tune the mesophase behavior of various LC materials has been well documented in the literature. For example, effect of branched chains to modify the mesomorphism from lamellar to columnar mesophase has been reported by Ohta *et al.*[84]

Collard and Lillya[83] reported that introduction of branch points into the side chains of hexakis(*n*-alkanoyloxy)benzenes **16** and hexakis(*n*-alkanoyloxy)cyclohexanes **17** widens the temperature range of columnar mesophase without affecting the type of mesophase behavior.

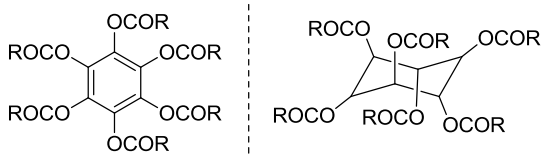

16 **17**

R = branched chain

Similarly, Schouten *et al.*[82,85] has shown the effect of branched chains on charge migration in phthalocyanine molecules. Liquid crystalline octaalkoxycarbonyl phthalocyanines with different branched chains **18** have been synthesized by Sergeyev *et al.*[86]

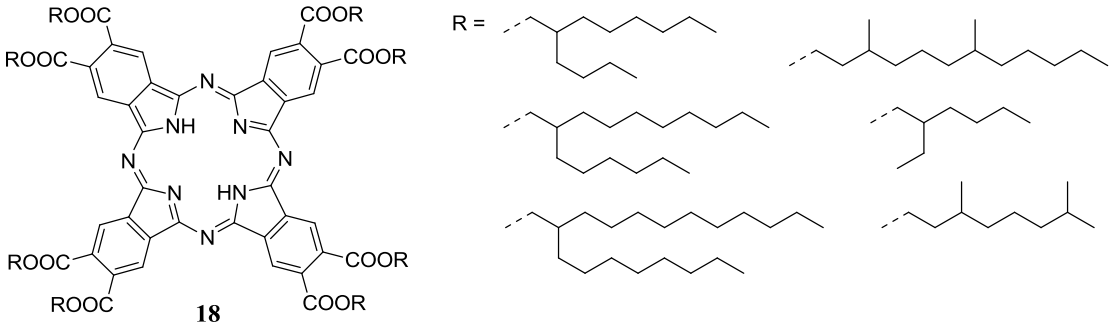

18

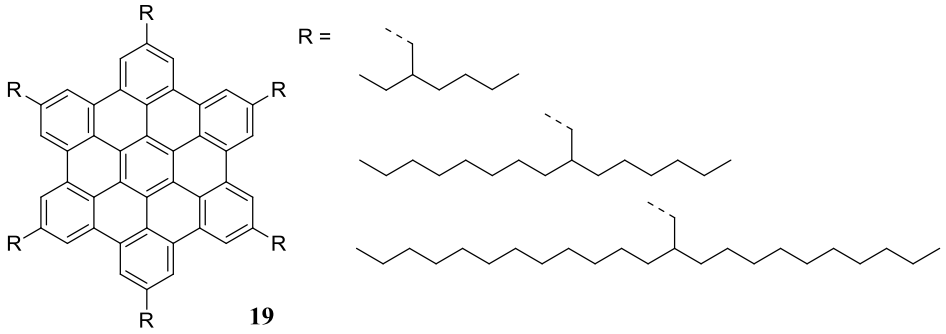

19

In case of hexabenzocoronenes **19**,[87] mesophase range was broadened by using branched peripheral chains but, type of mesophase was not affected. The same strategy has also been applied to tricycloquinazoline discotics **20** which were found to be mesogenic at room temperature, having a very broad mesophase range.[88]

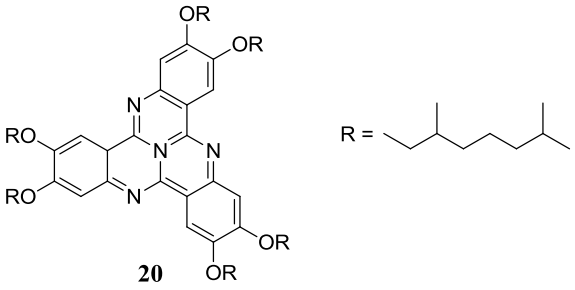

20

Bisoyi *et al.*[89] and Stackhouse *et al.*[90]reported a series of triphenylene-based DLCs **21** and **22,** respectively with peripheral branched chains. Branched chains in them significantly affected the intermolecular forces of attraction and packing in these molecules. This intern affected melting and isotropization temperatures of the LC materials.

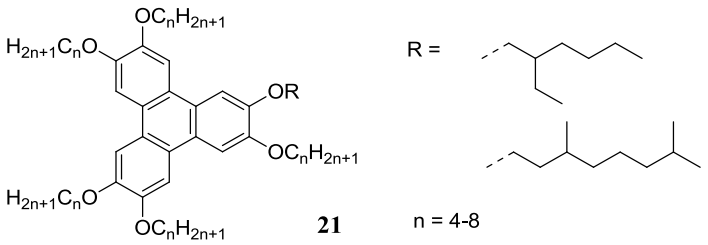

21

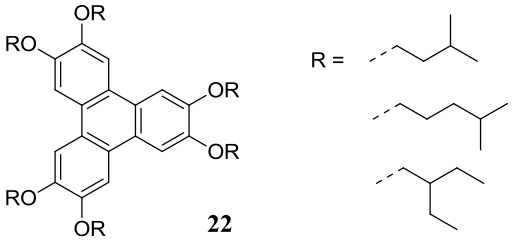

22

Very recently, Nakanishi *et al.* reported fullerene (C_{60}) derivatives **23** with branched aliphatic chains. The introduction of branched chains not only softens these C_{60} based materials, but also enables formation of thermotropic LCs and room temperature nonvolatile liquids.[91]

Kumar *et al.* synthesized several branched chain substituted benzene hexa- and pentaalkynes **24** which show very broad range of discotic nematic mesophase, stable well below and above the room temperature.[92,93] The decrease in transition temperatures could be due to the steric effect of branch (disorderness) and the reduction in symmetry associated with them.

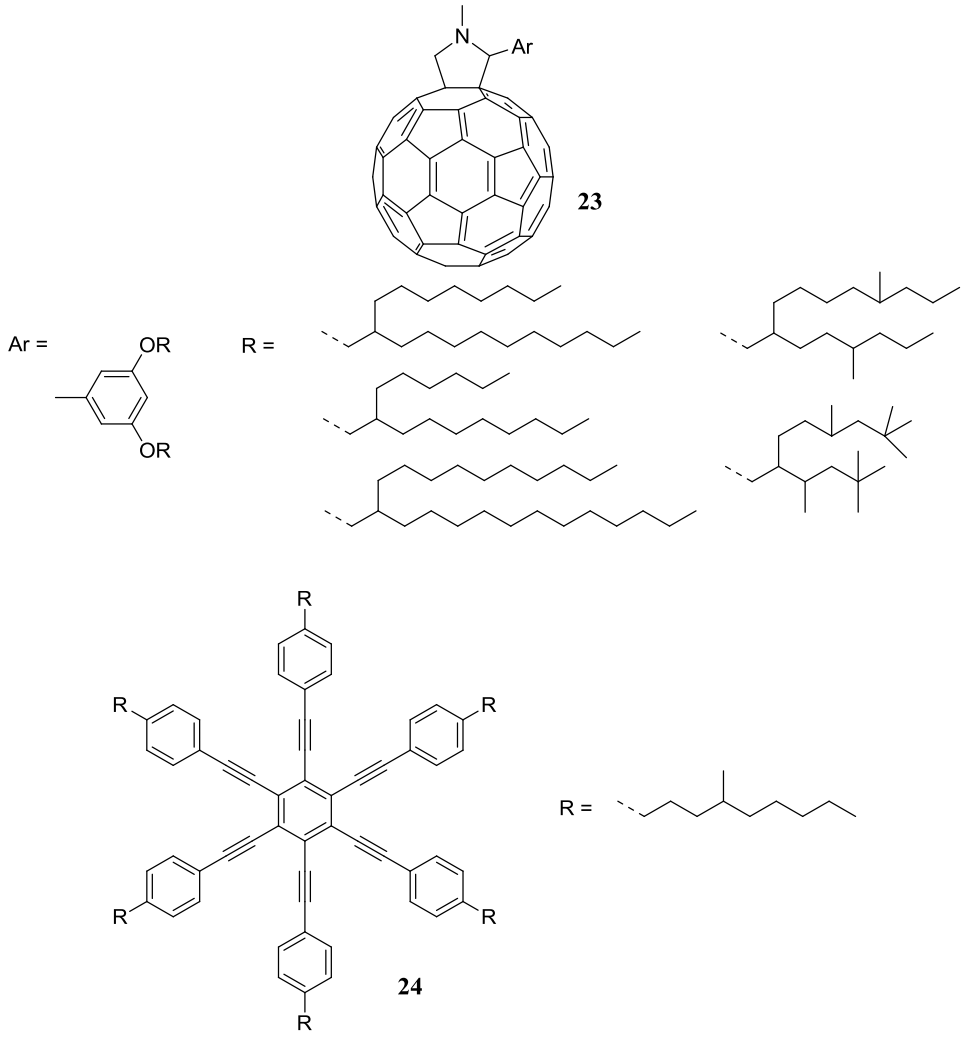

2.2.2 Objective

Not only lowering the transition temperatures, materials softness and crystallization tendency, introduction of branched aliphatic chains has a pronounced influence on the self-organization of molecules which can bring new functionalities such as enhanced charge carrier mobility in π-conjugated systems. With this idea keeping in mind, we have synthesized five series of mixed tail hexaethers of anthraquinone.

We chose to modify anthraquinone core because of the stable redox properties associated with the core which make it suitable for device fabrication. Recently, rufigallol based discotics with branched chains were reported by Bisoyi and Kumar.[94] But, they have shown the effect with only one branched chain. We have designed and synthesized a library of 20

molecules of five different series using microwave flash heating having branched alkyl substituted rufigallol core. The aim of the study was mainly two fold. First, we sought to determine the effect of different branched substituted chains on the mesomorphism in the rufigallol discotics. In particular, we wished to determine the effect of mesophase behavior with respect to the position of the side alkyl groups such as methyl, ethyl and so on. Secondly, we sought to provide additional insight into the mesophase stability by varying alkyl chains for a particular peripheral branched chain. Overall, the study represents a useful advance in the design of molecular systems enabling fresh insight into structure-mesophase morphology relationships.

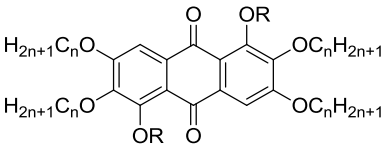

25-29

2.2.3 Results and Discussion

2.2.3.1 Synthesis and characterization

The synthesis of monomers **25-29** was achieved as shown in Scheme 2.2. Microwave assisted self-condensation of gallic acid in conc. H_2SO_4 yielded hexahydroxyanthraquinone **13**. The unequal reactivity of six phenolic groups of anthraquinone **13**, two of which are less reactive by virtue of being intra-molecularly H-bonded to the adjacent quinone carbonyls has been explored. Etherification of rufigallol was then performed using NaOH and appropriate alkyl bromide in DMSO which yielded various 1,5 dihydroxy tetraalkoxy anthraquinones **16**.[95] These tetraalkoxy derivatives were further alkylated with appropriate branched alkyl bromide with the help of microwave dielectric heating under mild basic conditions to produce compounds **25-29** within 20 min as shown in Scheme 2.2.

The chemical structures of all these oligomers **25-29** were confirmed through spectral and elemental analysis and details are given in the experimental section and representative spectra in Appendix I (Figures A3-8, A10-13, and A15).

2.2.3.2 Thermal behavior

The phase transition temperatures of all the new compounds together with transition enthalpy values determined by DSC are given in Table 2.3. The transition temperatures and associated enthalpy values were determined using a differential scanning calorimeter operated at a scanning rate of 5 °C min^{-1} both on heating and cooling. Textural observations of the mesophase were carried out using polarizing optical microscopy. As can be seen from Table 2.3, the first series of compounds (**25a-d)** with two branched 3-methylbutyl chains at the 1- and 5- positions and four *n*-alkyl chains (R = - C_6H_{13}, -C_8H_{17}, -$C_{10}H_{21}$, -$C_{12}H_{25}$) at 2-,3-,6-,7-positions were found to be LC over a wide temperature range except the one having longest *n*-alkyl spacer (**25d**, R = -$C_{12}H_{25}$).

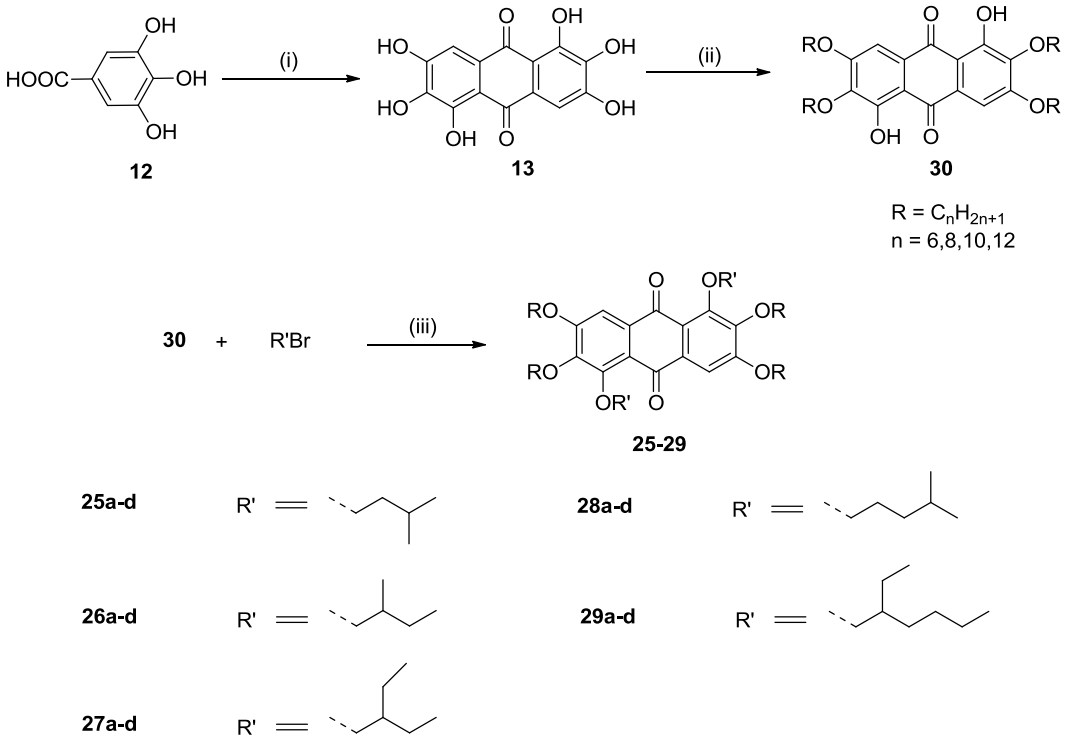

Scheme 2.2 Synthesis of compounds **25-29**. *Reagents and conditions:* (i) H_2SO_4, 90 s, MW, 90 %; (ii) NaOH, RBr, DMSO, reflux, 18 h, 55 %; (iii) Cs_2CO_3, NMP, 20 min, MW, 90 %.

Compound **25a** on heating melted at about 61.2 °C to the mesophase (ΔH = 13.2 kJ mol^{-1}) and finally cleared (isotropic) at 92 °C (ΔH = 8.4 kJ mol^{-1}). On cooling, it showed a transition in DSC centered at around 89.2 °C (ΔH = 8.2 kJ mol^{-1}) followed by crystallization at 44 °C

(ΔH = 12.7 kJ mol^{-1}). Under POM, it exhibited a well-defined texture of columnar mesophase (Figure 2.5a). Compound **25b** and **25c** were prepared to examine the effect of spacer length at the 2-, 3-, 6-, 7- positions without affecting the branched substitution at 1- and 5- positions. Compound **25b** having octyloxy chains exhibited crystal to mesophase transition at 66 °C and finally went to isotropic at around 70.7 °C. On cooling, the isotopic to mesophase transition peak appeared at 68.8 °C (ΔH = 17.4 kJ mol^{-1}).

Table 3. Phase behavior of mesogens[a,b,c].

Mesogen	Heating Run	Cooling Run
25a	Cr 61.24 (13.27) Col_h 92.03 (8.44) I	I 89.20 (8.24) Col_h 44.05 (12.75) Cr
25b	Cr 66.08 (18.83) Col_h 70.77 (14.73) I	I 68.89 (17.40) Col_h 48.42 (11.39) Cr
25c	Cr_1 37.37 (37.78) Cr_2 59.38 (64.58) I	I 58.70 (2.99) Col_h 53.00 (33.01) Cr
25d	Cr_1 40.30 (5.98) Cr_2 48.59 (16.98) I	-
26a	Cr_1 50.93 (1.04) Cr_2 58.07 (30.92) I	I 46.99 (9.84) Col_h 34.32 (17.57) Cr
26b	SS 54.89 (22.06) I	-
26c	Cr 50.35 (82.76) I	-
26d	Cr_1 41.09 (9.76) Cr_2 52.24 (199.67) I	-
27a	SS 54.23 (12.01) I	-
27c	Cr 46.16 (130.57) I	-
27d	Cr_1 40.02 (7.70) Cr_2 56.54 (185.68) I	I 29.47 (187.47) Cr
28a	Cr 64.14 (13.79) Col_h 99.87 (14.87) I	I 98.12 (14.69) Col_h
28b	Cr 41.15 (15.08) Col_h 73.12 (17.52) I	I 71.21 (17.33) Col_h
28c	Cr 41.15 (67.48) Col_h 52.89 (9.62) I	I 50.57 (9.04) Col_h
28d	Cr_1 40.46 (1.70) Cr_2 48.42 (121.50) I	-
29c	Cr_1 37.75 (7.42) Cr_2 52.31 (179.15) I	-
29d	Cr 49.68 (100.94) I	I 29.05 (102.21) Cr

[a]Phase assignment: Cr = crystal; SS = semisolid; Col_h = columnar hexagonal mesophase; I = isotropic.

[b]The phase transition temperatures in °C and enthalpy change values in kJmol^{-1} (in brackets).

[c]**27b**, **29a** and **29b** were isolated as isotropic liquids and for compounds **25d**, **26a**, **26c**, **26d**, **27a**, **27c**, **28d** and **29c** no peak was observed in the cooling scan.

While compound **25c** exhibited monotropic LC behavior showing isotropic to mesophase transition at 58.7 °C (ΔH = 3.0 kJ mol^{-1}), compound **25d** was found to be non-liquid

crystalline. The latter exhibited a crystal-crystal transition (at 40.3 °C, ΔH = 5.9 kJ mol^{-1}) which could be due to some conformational reorganization of molecules by passing into different crystalline configurations[51-53] before it went to isotropic at 48.6 °C and didn't return back to crystalline state on cooling to room temperature. It should be noted that with increasing peripheral chain length a significant change in isotropic temperature was observed. This could be due to the reduced π-π interactions among anthraquinone moieties with increasing spacer length.

In order to examine the effect of position of the methyl substituent on the mesomorphic behavior, a second series of even homologues (**26a-d**) were prepared by replacing 3-methyl butyl chains with 2-methyl one. It was observed that introduction of methyl group at 2-position resulted in destabilization of the mesophase as observed in some past studies.[83] In DSC, compounds **26b-d** exhibited only crystal to isotropic transition and didn't get crystallized down to room temperature. However, compound **26a** showed a monotropic phase transition (ΔH = 9.8 kJ mol^{-1}) while cooling from isotropic melt at 46.9 °C which crystallized at around 34.3 °C (ΔH = 17.6 kJ mol^{-1}).

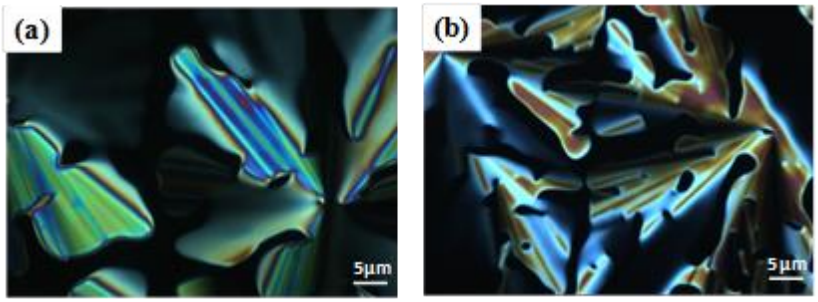

Figure 2.5. Orthoscopic images of rufigallol discotics under cross polars for (a) **25a** at 79.7 °C and (b) **28c** at 52.5 °C on cooling from isotropic liquid.

The 3rd series of compounds (**27a-d**) were prepared to explore the mesomorphic behavior of the anthraquinone derivatives (**26b-d**) by replacing methyl group to ethyl one in the peripheral branched chain at 2 position. Noticeably, the replacement leads to complete loss of mesomorphism. Compound **27a** was semisolid at room temperature. In DSC, **27a** and **27c** exhibited a crystal to isotropic transition at around 54.2 °C (ΔH = 12.0 kJ mol^{-1}) and 46.16 °C (ΔH = 130.5 kJ mol^{-1}), respectively and no peak corresponding to isotropic to crystalline

transition was observed in DSC. Compound **27d** melted at around 56.5 °C (ΔH = 185.7 kJ mol^{-1}) to the isotropic phase. Before melting, it displayed a low energy crystal to crystal transition at about 40 °C (ΔH = 7.7 kJ mol^{-1}). The non-mesomorphic nature of these compounds could be due to the steric nature of the ethyl substituent close to the aromatic core. The detrimental effect of this ethyl group is so high that compound **27b** was isolated as an isotropic liquid at room temperature.

The fourth set of compounds (**28a-d**) having 4-methyl pentyl group as the peripheral branched substituent at 1- and 5- positions were prepared to explore the mesomorphic behavior. Except compound **28d** with longer alkyl spacer (R = $-C_{12}H_{25}$), all compounds exhibited columnar hexagonal phase. In DSC, compound **28a** melted at around 64 °C (ΔH = 13.8 kJ mol^{-1}) to the Col_h mesophase which finally went to isotropic at around 99.8 °C (ΔH = 14.8 kJ mol^{-1}). On cooling, it showed isotropic to columnar mesophase peak centered at 98 °C (ΔH = 14.7 kJ mol^{-1}) and no other crystallization peak was observed up to room temperature (Figure A17). Similarly, compound **28b** and **28c** showed enantiotropic columnar mesophase exhibiting two transitions in DSC. In compound **28b**, the mesophase started at around 41 °C (ΔH = 15.0 kJ mol^{-1}) and completely changed to an isotropic phase at 73.1 °C (ΔH = 17.5 kJ mol^{-1}). On cooling mesophase appeared at 71.2 °C (ΔH = 17.3 kJ mol^{-1}) which remained stable down to room temperature. Compound **28c** exhibited a mesophase transition at a temperature (i.e., 41 °C) similar to **28b** but, the mesophase to isotropic transition drastically reduced to 52.8 °C (ΔH = 9.6 kJ mol^{-1}). On cooling, the mesophase appeared at 50.5 °C (ΔH = 9.0 kJ mol^{-1}) which was found to be stable down to room temperature. The classical columnar mesophase of **28c** was observed under POM as shown in Figure 2.5b. On the other hand, compound **28d** showed only one crystal to crystal transition before going to isotropic phase and didn't returned to crystalline state while cooling to room temperature and was found to be non-mesomorphic. Probably, the space filling effect of the branched chain is insufficient to cause the mesomorphic behavior with higher *n*-alkyl spacer (i.e., R= $-C_{12}H_{25}$).

The final series of compounds were prepared upon introduction of 2-ethyl hexyl branched chain. Interestingly, we did not observe any mesomorphic behavior upon addition of this branched chain. The two compounds **29a** and **29b** were found to be isotropic liquid at room temperature. Compound **29c** was solid at room temperature and went to isotropic at 52.3 °C

(ΔH = 179.1 kJ mol^{-1}). Before going to isotropic, it displayed a crystal to crystal transition at 37.8 °C (ΔH = 7.4 kJ mol^{-1}). However, while cooling to room temperature, no peak corresponding to any transition was observed for this compound. Compound **29d** showed crystal to isotropic transition at 49.68 °C (ΔH = 100.9 kJ mol^{-1}). The non-mesomorphic behavior could be due to the disorder caused by the ethyl branched chains and stereo-heterogeneity (racemic branched alkyl side chains can generate a mixture of different components in space which lead to disorder).

2.2.3.3 X-ray scattering studies

In order to reveal the mesophase structure and hence the supramolecular organization of these compounds, X-ray scattering experiments were carried out using unoriented samples. X-ray scattering patterns for two compounds **28a** and **28c** were recorded in the LC phase while cooling from the isotropic phase as shown in the Figure 2.6.

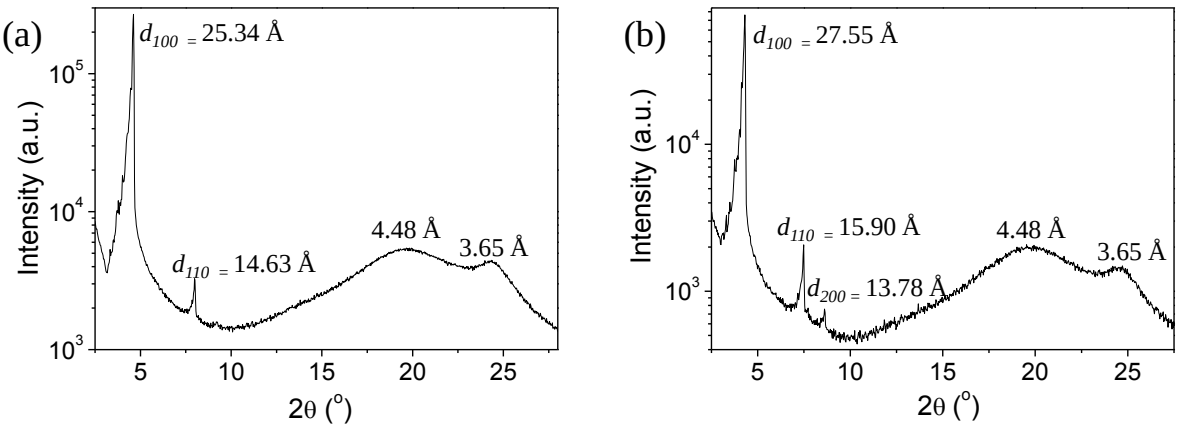

Figure 2.6 X-ray scattering profile of (a) **28a** at 55 °C and (b) **28c** at 45 °C on cooling from isotropic melt.

As can be seen from the Figure 2.6, in the small angle region, three sharp peaks, one very strong and two weak reflections are seen whose *d*-spacings are in the ratio of 1: 1/√3: 1/√4 that are indexed to the 10, 11 and 20 reflections, respectively consistent with a two-dimensional hexagonal lattice.[96] In the wide-angle region, a diffuse reflection appears at 4.48 Å. This corresponds to the liquid-like order of the aliphatic chains. A sharp reflection at 3.65

Å for these compounds indicates the core-core interaction in the columns. The intercolumnar distances, *a*, calculated by using the relation $a = d_{10}/(\cos 30°)$, where d_{10} is the spacing corresponding to the strongest peak in the small angle region, were found to be 21.95 and 23.86 Å, respectively for **28a** and **28c**. All the features fit into the well-known model for the Col_h phase in which the disc-like core of the molecules stack one on top of the other to form columns surrounded by alkyl chains and these columns in turn arrange themselves in a two-dimensional hexagonal lattice.

2.2.4 Conclusions

A library of 20 similar molecules based on rufigallol core showing the effect of various branched chains on the mesomorphic nature has been synthesized. In general, type, chain length, stereo-heterogeneity and substituent position have large effect on the mesomorphic behavior. The introduction of various types of branched chain has sufficiently perturbed the system to cause some room temperature LC systems with mesophase stabilized up to room temperature. The steric demand in close proximity to the aromatic core has some detrimental effects on the mesomorphic behavior. Such systems are good candidates for various mesophase device fabrications with high charge carrier mobility.

2.3 Experimental section

2.3.1 Measurements

Structural characterization of the compounds was carried out through a combination of infrared spectroscopy (Perkin Elmer Spectrum AX3), ^{1}H NMR and ^{13}C NMR (Bruker Biospin Switzerland Avance-iii 400 MHz and 100 MHz spectrometers, respectively), UV-vis-NIR spectrophotometers (Perkin Elmer Lambda 900) and Elemental analysis (carlo-Erba 1106 analyser). IR spectra were recorded in Nujol mull for intermediate compounds and KBr discs for target compounds. ^{1}H NMR spectra were recorded using deuterated chloroform ($CDCl_3$) as solvent and tetramethylsilane (TMS) as an internal standard. The transition temperatures and associated enthalpy values were determined using a differential scanning calorimeter (DSC, Perkin-Elmer, Model Pyris 1D) which was operated at a scanning rate 5 °C min^{-1} both on heating and cooling. The apparatus was calibrated using indium as a

standard. Textural observations of the mesophase were performed with Nikon Eclipse LV100POL polarizing microscope provided with a Linkam heating stage (LTS 420). All images were captured using a Q-imaging camera. X-ray scattering was carried out on powder samples using Cu-K_α (λ = 1.54 Å) radiation from DY 1042-Empyrean X-ray diffractometer with PCS and Pixel system (Diffractometer System-Empyrean, Measuring program-Focusing mirror, scans axis-gonioKAlpha-1.54060, Goniometer Radius-240mm, and Modification editor-Panalytical).

2.3.2 Synthesis of 1,2,3,5,6,7-hexahydroxyanthraquinone (13) Rufigallol was prepared following the reported procedure.[94] In a vial, gallic acid (2.0 g) and sulfuric acid (6.0 mL) were taken. The vial was then covered with a loose septum and was irradiated in microwave oven for 15 s. The vial was removed from the oven and left to stand for about 1 min and again irradiated for 15 s. This process was repeated 6 times and then the reaction mixture was poured into cold water. The resultant solid was filtered and washed with water and dried to give 1,2,3,5,6,7-hexahydroxyanthraquinone in 80 % yield (1.4 g). This compound was used as such without any further purification.

2.3.3 Synthesis of 1,2,3,4,5,6,7,8-octahydroxy-9,10-anthraquinone (15) Crude rufigallol **13** was purified by refluxing with acetic anhydride and pyridine for 12 h. Resulting hexaacetate **14** was then hydrolyzed to give pure rufigallol. Then, heating 1,2,3,5,6,7-hexahydroxyanthraquinone with boric acid and mercuric acid in concentrated sulfuric acid at 250 °C gave 1,2,3,4,5,6,7,8-octahydroxy-9,10-anthraquinone in 35 % yield. Elemental Analysis (calculated for $C_{14}H_8O_{10}$): C: calc. 50.01 %, found 49.54 %; H: calc. 2.38 %, found 2.59 %.

2.3.4 Synthesis of 4'-(*n*-bromoalkaneoxy)-4 cyano biphenyl A mixture of 4'-hydroxy-4-cyanobiphenyl (1 equiv.), K_2CO_3 (3 equiv.) and dibromoalkane (2.5 equiv.) in 2-butanone was heated to reflux under nitrogen atmosphere for 18 h. The reaction mixture was then filtered and washing were given with DCM. The mother liquor was then evaporated to dryness and the product was purified through column chromatography (silica gel, ethylacetate/hexane) to give white crystalline solid. ^{1}H NMR (400 MHz, $CDCl_3$): δ 7.64-7.57 (m, 4H), 7.48-7.46 (m, 2H), 6.94-6.92 (m, 2H), 3.95 (t, 2H), 3.35 (t, 2H), 1.81-1.73 (m, 4H),

1.41-1.26 (m, alkyl chain). ^{13}C NMR (100 MHz, $CDCl_3$): δ 159.80, 145.30, 132.59, 131.27, 128.34, 127.09, 119.15, 115.08, 110.04, 68.15, 34.087, 32.82, 29.44, 29.37, 29.33, 29.22, 28.75, 28.16.

2.3.5 Synthesis of Octa-cyanobiphenyl substituted rufigallols 11a A mixture of 1,2,3,4,5,6,7,8-octahydroxyanthraquinone **15** (60 mg, 0.18 mmol), 4'-(*6*-bromoalkaneoxy)-4 cyano biphenyl (0.527 g, 2.16 mmol) and cesium carbonate (1.17 g, 3.6 mmol) in N-methyl-2-pyrrolidone (NMP) was irradiated in microwave oven for 1 min. The vial was removed from the oven and left to stand for about 1 min and again irradiated for 1 min. This process was repeated 14 times until the reaction was complete (TLC monitoring). The product obtained was purified through column chromatography over silica gel (eluent: 20-90 % DCM in hexane and 1% methanol in DCM) to give pure product as orange reddish semisolid in 45% yield. ^{1}H NMR (400 MHz, $CDCl_3$): δ 7.69-7.65 (m, 16H, ArH), 7.62-7.52 (m, 16H, ArH), 7.49-7.45 (m, 16H, ArH), 7.02-6.92 (m, 16H, ArH), 4.20-3.96 (m, 32H, OCH_2), 1.67-1.50 (m, 64H, alkyl chain CH_2). ^{13}C NMR (100 MHz, $CDCl_3$): δ 159.65, 145.04, 132.58, 131.38, 128.32, 127.03, 119.07, 115.03, 110.12, 68.06, 30.34, 29.27, 26.02. IR (KBr): ν_{max}/cm^{-1} 3041, 2938, 2223 (CN), 1667, 1602, 1574, 1518, 1494, 1467, 1393, 1310, 1289, 1249, 1178, 1115, 1084, 1030, 994, 850, 730, 709. UV-vis (MeOH): λ_{max}/nm 208, 294. Elemental Analysis (calculated for $C_{166}H_{160}N_8O_{18}$): C: calc. 78.06 %, found 78.41 %; H: calc. 6.27 %, found 5.89 %; N: calc. 4.39 %, found 4.32 %.

2.3.6 Synthesis of 11b Compound was synthesized according to a similar procedure to **11a.** ^{1}H NMR (400 MHz, $CDCl_3$): δ 7.69-7.65 (m, 16H, ArH), 7.63-7.58 (m, 16H, ArH), 7.52-7.47 (m, 16H, ArH), 7.01-6.94 (m, 16H, ArH), 4.18-3.95 (m, 32H, OCH_2), 1.59-1.42 (m, 96H, alkyl chain CH_2). ^{13}C NMR (100 MHz, $CDCl_3$): δ 159.73, 145.12, 132.57, 131.30, 128.32, 127.02, 119.09, 115.02, 110.12, 68.07, 30.32, 29.45, 26.02. IR (KBr): ν_{max}/cm^{-1} 3037, 2932, 2224 (CN), 1664, 1603, 1577, 1520, 1494, 1471, 1393, 1320, 1289, 1250, 1179, 1122, 1089, 1030, 995, 850, 726, 709. UV-vis (MeOH): λ_{max}/nm 208, 294. Elemental Analysis (calculated for $C_{182}H_{192}N_8O_{18}$): C: calc. 78.67 %, found 78.44 %; H: calc. 6.92 %, found 6.92 %; N: calc. 4.03 %, found 3.71 %.

2.3.7 Synthesis of 11c Compound was synthesized according to a similar procedure to **11a.** ^{1}H NMR (400 MHz, $CDCl_3$): δ 7.69-7.65 (m, 16H, ArH), 7.63-7.60 (m, 16H, ArH), 7.54-7.49 (m, 16H, ArH), 7.00-6.95 (m, 16H, ArH), 4.17-3.98 (m, 32H, OCH_2), 1.65-1.38 (m, 112H, alkyl chain CH_2). ^{13}C NMR (100 MHz, $CDCl_3$): δ 159.72, 145.18, 132.54, 131.23, 128.28, 127.01, 119.05, 115.01, 110.03, 68.08, 30.30, 29.47, 26.02. IR (KBr): ν_{max}/cm^{-1} 2924, 2852, 2227 (CN), 1667, 1603, 1573, 1517, 1494, 1469, 1390, 1310, 1289, 1250, 1179, 1115, 1091, 1030, 995, 850, 730, 709. UV-vis (MeOH): λ_{max}/nm 200, 286. Elemental Analysis (calculated for $C_{190}H_{208}N_8O_{18}$): C: calc. 78.95 %, found 78.59 %; H: calc. 7.20 %, found 7.07 %; N: calc. 3.88 %, found 3.23 %.

2.3.8 Synthesis of 11d Compound was synthesized according to a similar procedure to **11a.** ^{1}H NMR (400 MHz, $CDCl_3$): δ 7.68-7.66 (m, 16H, ArH), 7.64-7.60 (m, 16H, ArH), 7.53-7.49 (m, 16H, ArH), 7.01-6.95 (m, 16H, ArH), 4.17-3.96 (m, 32H, OCH_2), 1.64-1.35 (m, 128H, alkyl chain CH_2). ^{13}C NMR (100 MHz, $CDCl_3$): δ 159.72, 145.13, 132.53, 131.22, 128.28, 126.99, 119.04, 115.00, 110.05, 68.09, 30.38, 29.49, 26.07. IR (KBr): ν_{max}/cm^{-1} 3041, 2923, 2224 (CN), 1693, 1603, 1520, 1494, 1472, 1393, 1271, 1250, 1164, 1134, 1093, 1032, 994, 846, 746, 720. UV-vis (MeOH): λ_{max}/nm 206, 292. Elemental Analysis (calculated for $C_{198}H_{224}N_8O_{18}$): C: calc. 79.2 %, found 79.55 %; H: calc. 7.47 %, found 6.97 %; N: calc. 3.73 %, found 3.21 %.

2.3.9 Synthesis of 11e Compound was synthesized according to a similar procedure to **11a.** ^{1}H NMR (400 MHz, $CDCl_3$): δ 7.70-7.66 (m, 16H, ArH), 7.65-7.61 (m, 16H, ArH), 7.53-7.50 (m, 16H, ArH), 7.00-6.96 (m, 16H, ArH), 4.06-3.97 (m, 32H, OCH_2), 1.59-1.30 (m, 160H, alkyl chain CH_2). ^{13}C NMR (100 MHz, $CDCl_3$): δ 159.72, 145.19, 132.51, 131.18, 128.25, 127.02, 119.05, 115.00, 109.95, 68.10, 30.63, 29.38, 25.97. IR (KBr): ν_{max}/cm^{-1} 3032, 2919, 2224 (CN), 1665, 1603, 1574, 1519, 1495, 1472, 1315, 1290, 1260, 1179, 1113, 1091, 1030, 994, 850, 716. UV-vis (MeOH): λ_{max}/nm 219, 294. Elemental Analysis (calculated for $C_{214}H_{248}N_8O_{18}$): C: calc. 79.6 %, found 79.55 %; H: calc. 7.69 %, found 7.27 %; N: calc. 3.47%, found 3.97 %.

2.3.10 Synthesis of 1,5-Dihydroxy-2,3,6,7-tetraalkoxy-9,10-anthraquinone (30) All the tetraethers were prepared following the reported procedure.[36] To a stirred solution of NaOH

(4 equiv.) in dry DMSO (50 mL) added crude rufigallol **13** (1 equiv.) and 1-bromoalkane (4.4 equiv.) and the mixture was heated to 70 °C and held at the same temperature under N_2 for 18 h. The reaction mixture was cooled, diluted with aq. HCl and extracted with chloroform (80 mL × 5). The combined chloroform extracts were washed with water and dried over anhydrous Na_2SO_4. Product was crystallized from EtOH : $CHCl_3$ (4:6) in 45 % yield (yellow solid). All the compounds gave similar spectra differing in only the number of alkyl chain CH_2 protons. ^{1}H NMR (400 MHz, $CDCl_3$): δ 12.77 (s, 2H), 7.39 (s, 2H), 4.21-4.15 (m, 8H), 1.9-1.3 (m, alkyl chain CH_2), 1.0 (t, 12H).). ^{13}C NMR (100 MHz, $CDCl_3$): 186.37, 158.03, 157.19, 141.09, 128.81, 111.75, 104.69, 73.74, 69.37, 31.68, 31.50, 30.30, 30.23, 29.05, 25.66, 25.58, 22.65, 22.61, 14.09, 14.03.

2.3.11 Synthesis of Hexaalkoxy anthraquinone discotics (25a) A mixture of 1,5-dihydroxy-2,3,6,7-tetrahexyloxy anthraquinone **30** (150 mg, 0.23 mmol), 3-methylbutylbromide (138.92 mg, 0.92 mmol, 0.13 mL) and cesium carbonate (304.9 mg, 0.94 mmol) in N-methyl-2-pyrrolidone (NMP) was irradiated in microwave oven for 1 min. The vial was removed from the oven and left to stand for about 1 min and again irradiated for 1 min. This process was repeated 20 times until the reaction was complete (TLC monitoring). The product obtained was purified through column chromatography over silica gel to give pure product in 45 % yield. ^{1}H NMR (400 MHz, $CDCl_3$): δ 7.57 (s, 2H, ArH), 4.13 (t, 4H, J = 7.9 Hz, OCH_2), 4.08-4.02 (m, 8H, OCH_2), 1.87-1.73 (m, 12H, $OCH_2C\underline{H}_2$), 1.56-1.29 (m, 26H, aliphatic CH_2), 0.97 (d, 6H, J = 4.6 Hz, CH_3), 0.91-0.87 (m, 18H, CH_3). ^{13}C NMR (100 MHz, $CDCl_3$): δ 181.27, 157.48, 153.93, 146.93, 132.68, 120.37, 107.00, 74.16, 73.28, 69.15, 39.07, 31.71, 31.52, 30.27, 29.04, 25.72, 25.03, 22.77, 22.67, 22.61, 14.10, 14.05. IR (Diamond ATR): ν_{max} /cm^{-1} 2954.37, 2928.20, 2865.38, 1663.50, 1571.94, 1466.33, 1425.90, 1378.03, 1317.04, 1267.85, 1125.65, 1093.99, 1043.66, 993.67, 915.86, 870.10, 788.54, 731.93, 711.59, 631.71. UV-Vis (DCM): λ_{max} /nm 369, 321, 287. Elemental Analysis (calculated for $C_{48}H_{76}O_8$): C: calc. 73.81 %, found 73.50 %; H: calc. 9.81 %, found 9.92 %. All the other three compounds of the series **25b, 25c** and **25d** display similar data differing only in the number of alkyl chain H atoms in ^{1}H NMR.

2.3.12 Synthesis of 26b Compound was synthesized according to a similar procedure to **25a.** ^{1}H NMR (400 MHz, $CDCl_3$): δ 7.61 (s, 2H, ArH), 4.18 (t, 4H, OCH_2, J = 6.4 Hz), 4.07 (t,

4H, OCH_2, *J* = 8.0 Hz), 3.86 (d, 2H, *J* = 8.0 Hz), 3.83 (d, 2H, *J* = 8.0 Hz), 2.10-1.87 (m, 2H), 1.82-1.68 (m, 10H, $OCH_2C\underline{H}_2$), 1.54-1.47 (m, 8H, aliphatic CH_2), 1.33-1.27 (m, 34H, aliphatic CH_2), 1.11 (d, 6H, *J* = 4.6 Hz, CH_3), 1.01 (d, 6H, *J* = 4.6 Hz, CH_3),.0.91 (t, 6H, *J* = 4.6 Hz, CH_3) ^{13}C NMR (100 MHz, $CDCl_3$): δ 181.19, 157.51, 154.21, 146.72, 132.76, 120.31, 106.91, 79.72, 74.23, 69.14, 35.68, 31.88, 31.83, 30.27, 29.50, 29.33, 29.27, 29.11, 26.11, 26.06, 22.70, 16.40, 14.12, 11.37. IR (Diamond ATR): ν_{max} /cm^{-1} 2953.80, 2924.28, 2855.51, 1663.67, 1572.44, 1466.19, 1426.08, 1377.93, 1318.58, 1266.83, 1126.39, 1094.09, 1024.45, 953.82, 870.71, 819.63, 789.85, 732.86, 713.82, 632.13. UV-vis (DCM): λ_{max} /nm 369, 320, 287. Elemental Analysis (calculated for $C_{56}H_{92}O_8$): C: calc. 75.61%, found 75.67 %; H: calc. 10.50 %, found 10.82 %. All the other three compounds of the series **26a, 26c** and **26d** display similar data differing only in the number of alkyl chain H atoms in ^{1}H NMR.

2.3.13 Synthesis of 27c Compound was synthesized according to a similar procedure to **25a.** ^{1}H NMR (400 MHz, $CDCl_3$): δ 7.56 (s, 2H, ArH), 4.18 (t, 4H, OCH_2, *J* = 8.0 Hz), 4.07 (t, 4H, OCH_2), 3.96 (d, 4H, OCH_2), 1.92-1.88 (m, 4H, $OCH_2C\underline{H}_2$), 1.82-1.78 (m, 4H, $OCH_2C\underline{H}_2$), 1.65-1.63 (m, 2H, $OCH_2C\underline{H}_2$), 1.60-1.25 (m, 64H, aliphatic CH_2), 0.94 (t, 12H, *J* = 8.1 Hz, CH_3), 0.88-0.84 (m, 12H, CH_3). ^{13}C NMR (100 MHz, $CDCl_3$): δ 181.15, 157.47, 154.29, 146.69, 132.80, 120.34, 106.88, 74.24, 69.13, 41.76, 31.93, 30.26, 29.68, 29.64, 29.60, 29.57, 29.39, 29.37, 29.12, 26.07, 22.86, 22.86, 22.71, 14.14, 11.07. IR (Diamond ATR): ν_{max} /cm^{-1} 2956.51, 2918.60, 2851.00, 1686.26, 1568.54, 1463.72, 1423.99, 1375.41, 1316.03, 1264.95, 1128.03, 1091.31, 1063.80, 1023.50, 987.78, 873.16, 800.19, 744.28, 720.64, 631.53. UV-vis (DCM): λ_{max} /nm 369, 320, 288. Elemental Analysis (calculated for $C_{66}H_{112}O_8$): C: calc. 76.69 %, found 76.66 %; H: calc. 10.92 %, found 11.06 %. All the other three compounds of the series **27a, 27b** and **27d** display similar data differing only in the number of alkyl chain H atoms in ^{1}H NMR.

2.3.14 Synthesis of 28a Compound was synthesized according to a similar procedure to **25a.** ^{1}H NMR (400 MHz, $CDCl_3$): δ 7.57 (s, 2H, ArH), 4.13 (t, 4H, OCH_2, *J* = 8.0 Hz), 4.06-4.00 (m, 8H, OCH_2), 1.93-1.74 (m, 12H, $OCH_2C\underline{H}_2$), 1.65-1.29 (m, 30H, aliphatic CH_2), 0.92-0.90 (m, 24H, CH_3). ^{13}C NMR (100 MHz, $CDCl_3$): δ 181.29, 157.48, 153.91, 146.94, 132.64, 126.39, 107.01, 74.97, 74.16, 69.13, 35.02, 31.72, 31.52, 30.30, 29.04, 28.25, 28.01, 25.72, 25.70, 22.67, 22.65, 22.61, 14.09, 14.04. IR (Diamond ATR): ν_{max} /cm^{-1} 2953.68, 2929.63,

2867.81, 1663.33, 1571.98, 1466.59, 1426.17, 1377.60, 1317.91, 1264.39, 1125.49, 1093.99, 1041.16, 994.79, 917.41, 869.90, 787.53, 732.21, 711.63, 631.67. UV-vis (DCM): λ_{max} /nm 369, 320, 288. Elemental Analysis (calculated for $C_{50}H_{80}O_8$): C: calc. 74.22 %, found 73.99 %; H: calc. 9.97 %, found 10.09 %. All the other three compounds of the series **28b, 28c** and **28d** display similar data differing only in the number of alkyl chain H atoms in ^{1}H NMR.

2.3.15 Synthesis of 29c Compound was synthesized according to a similar procedure to **25a.** ^{1}H NMR (400 MHz, $CDCl_3$): δ 7.57 (s, 2H, ArH), 4.18 (t, 4H, OCH_2, J = 7.9 Hz), 4.06 (t, 4H, OCH_2, J = 7.9 Hz), 3.95 (d, 4H, OCH_2, J = 6.4 Hz), 1.95-1.78 (m, 10H, $OCH_2C\underline{H}_2$), 1.6 -1.29 (m, 72H, aliphatic CH_2), 1.01-0.88 (m, 24H, CH_3). ^{13}C NMR (100 MHz, $CDCl_3$): δ 181.05, 157.35, 154.15, 146.58, 132.79, 120.35, 106.84, 74.20, 69.11, 40.35, 31.88, 31.83, 29.53, 29.34, 29.28, 29.08, 26.06, 23.24, 22.70, 14.21, 14.07. IR (Diamond ATR): ν_{max} /cm^{-1} 2988.91, 2958.17, 2926.10, 2855.25, 1663.66, 1571.69, 1466.31, 1384.04, 1319.33, 1275.40, 1123.06, 1094.74, 1023.50, 983.75, 897.07, 873.58, 764.19, 749.79. UV-vis (DCM): λ_{max} /nm 369, 320, 288. Elemental Analysis (calculated for $C_{70}H_{120}O_8$): C: calc. 77.15 %, found 77.22 %; H: calc. 11.10 %, found 11.60 %. All the other three compounds of the series **29a, 29b** and **29d** display similar data differing only in the number of alkyl chain H atoms in ^{1}H NMR.

References

(1) Luckhurst, G. R. *Nature* **2004**, *430*, 413-414.

(2) Kato, T.; Mizoshita, N.; Kishimoto, K. *Angew. Chem. Int. Ed.* **2005**, *45*, 38-68.

(3) Kato, T.; Hirai, Y.; Nakaso, S.; Moriyama, M. *Chem. Soc. Rev*. **2007**, *36*, 1857-1867.

(4) Bruce, D. W. *Chem. Rec*. **2004**, *4*, 10-12.

(5) Tschierske, C.; Photinos, D. J. *J. Mater. Chem*. **2010**, *20*, 4263-4294.

(6) Frieser, M. J. *Phys. Rev. Lett.* **1970**, *24*, 1041-1043.

(7) Yu, L. J.; Saupe, A. *Phys. Rev. Lett.* **1980**, *45*, 1000-1003.

(8) Madsen, L. A.; Dingemans, T. J.; Nakata, M.; Samulski, E. T. *Phys. Rev. Lett*. **2004**, *92*, 145505-1/4.

(9) Tschierske, C.; Photinos, D. J. *J. Mater. Chem.* **2010**, *20*, 4263-4294.

(10) Straley, J. P. *Phys. Rev. A* **1974**, *10*, 1881-1887.

(11) Boccara, N.; Mejdani, R.; De Seze, L. *J. Phys*. **1977**, *38*, 149-151.

(12) Alben, R. *J. Chem. Phys*. **1973**, *59*, 4299-4304.

(13) Hashim, R.; Luckhurst, G. R.; Prata, F.; Romano, S. *Liq. Cryst.* **1993**, *15*, 283-309.

(14) Fletcher, I. D.; Luckhurst G. R. *Liq. Cryst*. **1995**, *18*, 175-183.

(15) Date, R. W.; Bruce, D. W. *J. Am. Chem. Soc.* **2003**, *125*, 9012-9013.

(16) Hunt, J. J.; Date, R. W.; Timimi, B. A.; Luckhurst, G. R.; Bruce, D. W. *J. Am. Chem. Soc*. **2001**, *123*, 10115-10116.

(17) Apreutesei, D., Mehl, G. *Mol. Cryst. Liq. Cryst.* **2006**, *449*, 107-115.

(18) Kouwer, P. H. J.; Mehl, G. H. *J. Am. Chem. Soc.* **2003**, *125*, 11172-11173.

(19) Kouwer, P. H. J.; Mehl, G. H. *Angew. Chem. Int. Ed.* **2003**, *42*, 6015-6018.

(20) Kouwer, P. H. J.; Pourzand, J.; Mehl, G. H. *Chem. Commun.* **2004**, 66-67.

(21) Imrie, C. T.; Lu, Z.; Picken, S. J.; Yildirim, Z. *Chem. Commun.* **2007**, 1245-1247.

(22) Leong, K. U.; Jing, A. J.; Monsdorf, B.; Graham, M. J.; Harris, F. W.; Cheng, S. Z. D. *J. Phys. Chem. B* **2007**, *111*, 767-777.

(23) Rahman, M. L.; Tschierske, C.; Yusoff, M.; Silong, S. *Tetrahedron Lett.* **2005**, *46*, 2303-2306.

(24) Shimizu, Y.; Kurobe, A.; Monobe, H.; Terasawa, N.; Klyohar, K.; Uchida, K. *Chem. Commun.* **2003**, 1676-1677.

(25) Bisoyi, H. K.; Raghunathan, V. A.; Kumar, S. *Chem. Commun.* **2009**, 7003-7005.

(26) Kouwer, P. H. J.; Mehl, G. H. *J. Mater. Chem.* **2009**, *19*, 1564-1575.

(27) Kumar, S. *Phase Transitions* **2008**, *81*, 113-128.

(28) Ferreira, E. S. B.; Hulme, A. N.; McNab, H.; Quye, A. *Chem. Soc. Rev.* **2004**, *33*, 329-336.

(29) Maier, M. E.; Bosse, F.; Niestroj, A. J. *Eur. J. Org. Chem.* **1999**, *1999*, 1-13.

(30) Catellani, M.; Luzzati, S.; Lupsac, N.-O.; Mendichi, R.; Consonni, R.; Famulari, A.; Meille, S. V.; Giacalone, F.; Segura, J. L.; Martin, N. *J. Mater. Chem.* **2004**, *14*, 67-74.

(31) Mamada, M.; Nishida, J.-i.; Tokito, S.; Yamashita, Y. *Chem. Commun.* **2009**, 2177-2179.

(32) Murschell, A. E.; Sutherland, T. C. *Langmuir* **2010**, *26*, 12859-12866.

(33) Billard, J.; Luz, Z.; Poupko, R.; Zimmermann, H. *Liq. Cryst.* **1994**, *16*, 333-337.

(34) Kumar, S.; Bisoyi, H. S.; Pal, S. K. *Mol. Cryst. Liq. Cryst.* **2008**, *480*, 287-294.

(35) Bisoyi, H. S.; Kumar, S. *Phase Transitions* **2006**, *79*, 285-292.

(36) Gupta, S. K.; Raghunathan, V.; Kumar, S. *New J. Chem.* **2009**, *33*, 112-118.

(37) Herrero, M. A.; Kremsner, J. M.; Kappe, C. O. *J. Org. Chem.* **2008**, *73*, 36-47.

(38) Hoz, A.; Diaz-Orti, A.; Moreno, A. *Chem. Soc. Rev.* **2005**, *34*, 164-178.

(39) Nuchter, M.; Ondruchka, B.; Bonrath, W.; Gum, A. *Green Chem.* **2004**, *6*, 128-141.

(40) Johnson, L.; Ringstrand, B.; Kaszynski, P. *Liq. Cryst.* **2009**, *36*, 179-185.

(41) Wang, G.-T.; Zhao, X.; Li, Zhan-Ting *Tetrahedron* **2011**, *67*, 48-57.

(42) Zhao, K. Q.; Guo, J. Z.; Yu, W. H.; Wang, L.; Hu, P.; Wang, B. Q.; Monobe, H.; Shimizu, Y. *Mol. Cryst. Liq. Cryst.* **2011**, *542*, 559-569.

(43) Majumdara, K. C.; Ghosh, T.; Chakravortya, S.; Pala, N.; Raob, D. S. S.; Prasad, S. K. *Liq. Cryst.* **2010**, *37*, 1539-1547.

(44) Goossens, K.; Lava, K.; Nockemann, P.; Hecke, K. V.; Meervelt, L. V.; Pattison, P.; Binnemans, K.; Cardinaels, T. *Langmuir* **2009**, *25*, 5881-5897.

(45) Majumdar, K. C.; Chakravorty, S.; Pal, N.; Sinha, R. K. *Tetrahedron* **2009**, *65*, 7998-8006.

(46) Wu, C. C. *Liq. Cryst.* **2007**, *34*, 283-288.

(47) Kumar, S.; Pal, S. K. *Tetrahedron Lett.* **2005**, *46*, 4127-4130.

(48) Pal, S. K.; Raghunathan, V. A.; Kumar, S. *Liq. Cryst.* **2007**, *34*, 135-141.

(49) Kaszynski, P.; Pakhomov, S.; Tesh, K. F.; Young, V. G., Jr. *Inorg. Chem.* **2001**, *40*, 6622-6631.

(50) Miura, H.; Ushio, T.; Nagai, K.; Fujimoto, D.; Lepp, Z.; Takahashi, H.; Tamura, R. *Cryst. Growth Des.* **2003**, *3*, 959-965.

(51) Choudhury, A. R.; Nagarajan, K.; Guru Row, T. N. *Cryst. Eng. Comm.* **2006**, *8*, 482-488.

(52) Fujimoto, D.; Tamura, R.; Lepp, Z.; Takahashi, H.; Ushio, T. *Cryst. Growth Des.* **2003**, *3*, 973-979.

(53) Gonnade, R. G.; Bhadbhade, M. M.; Shashidhar, M. S. *Cryst. Eng. Comm.* **2010**, *12*, 478-484.

(54) Goel, M.; Jayakannan, M. *J. Phys. Chem. B* **2010**, *114*, 12508-12519.

(55) Ungar, G.; Feijoo, J. L.; Keller, A.; Yourd, R.; Percec, V. *Macromolecules* **1990**, *23*, 3411-3416.

(56) Duer, M. J.; Roper, C. *Phys. Chem. Chem. Phys.* **2003**, *5*, 3034-3041.

(57) Taylor, R. A.; Ellis, H. A. Mol. Cryst. *Liq. Cryst.* **2011**, *548*, 37-54.

(58) Khoo, C.; Wu, S. T. in Optics and Nonlinear Optics of Liquid Crystals. World Scientific: Singapore, 1993.

(59) Simoni, F. in Nonlinear Optical Properties of Liquid Crystals and Polymer Dispersed Liquid Crystals. World Scientific: Singapore, 1997.

(60) Pal, S. K.; Kumar, S. *Liq. Cryst.* **2013**, *40*, 281-292.

(61) Bushby, R. J.; Kawata, K. *Liq. Cryst.* **2011**, *38*, 1415-1426.

(62) Kumar, S. *Chem. Soc. Rev.* **2006**, *35*, 83-109.

(63) Ohta, K.; Hatsusaka, K.; Sugibayashi, M.; Ariyoshi, M.; Ban, K.; Maeda, F.; Naito, R.; Nishizawa, K.; Van de Craats, A. M.; Warman, J. M. *Mol. Cryst. Liq. Cryst.* **2003**, *397*, 25-45.

(64) Boden, N.; Bushby, R. J.; Clements, J.; Movaghar, B. *Phys. Rev. B* **1995**, *52*, 13274-13280.

(65) Kumar, S. *Liq. Cryst.* **2005**, *32*, 1089-1113.

(66) Kumar, S. *Liq. Cryst.* **2004**, *31*, 1037-1059.

(67) An, Z.; Yu, J.; Jones, S. C.; Barlow, S.; Yoo, S.; Domercq, B.; Prins, P.; Siebbeles, L. D. A.; Kippelen, B.; Marder, S. R. *Adv. Mater.* **2005**, *17*, 2580-2583.

(69) An, Z.; Yu, J.; Domercq, B.; Jones, S. C.; Barlow, S.; Kippelen, B.; Marder, S. R. *J. Mater. Chem.* **2009**, *19*, 6688-6698.

(70) Zhao, K.-Q.; Chen, C.; Monobe, H.; Hu, R.; Wang, B.-Q.; Shimizu, Y. *Chem. Commun*. **2011**, *47*, 6290-6292.

(71) Feng, X.; Marcon, V.; Pisula, W.; Hansen, M. R.; Kirkpatrick, J. Grozema, F. Andrienko, D. Kremer, K.; Mullen, K. *Nature Mater*. **2009**, *8*, 422-426.

(72) Kaafarani, B. R. *Chem*. *Mater*. **2011**, *23*, 378-396.

(73) Simpson, C. D.; Wu, J.; Watson, M. D.; Mullen, K. *J. Mater. Chem.* **2004**, *14*, 494-504.

(74) Sergeyev, S.; Pisula, W.; Geerts, Y. H. *Chem. Soc. Rev.* **2007**, *36*, 1902-1929.

(75) Wang, L.; Park, S.-Y.; Kim, S.-M.; Yoon, S.; Lee, S.-H.; Lee, E.; Jeong, K.-U.; Lee, M.-H. *Liq. Cryst.* **2012**, *39*, 795-801.

(76) Charlet, E.; Grelet, E. *Phys. Rev. E: Stat. Nonlin. Soft Matter. Phys.* **2008**, *78*, 041707/1-041707/8.

(77) Tracz, A.; Jeszka, J. K.; Watson, M. D.; Pisula, W.; Mullen, K.; Pakula, T. *J. Am. Chem. Soc.* **2003**, *125*, 1682-1683.

(78) Zimmermann, S.; Wendorff, J. H.; Weder, C. *Chem. Mater.* **2002**, *14*, 2218-2223.

(79) Lillya, C. P.; Collard, D. M. *Mol. Cryst. Liq. Cryst.* **1990**, *182B*, 201-207.

(80) Collard, D. M.; Lillya, C. P. *J. Org. Chem.* **1991**, *56*, 6064-6066.

(81) Tabushi, I.; Yammamura, K.; Okada, Y. *J. Org. Chem.* **1987**, *52*, 2502-2505.

(82) Schouten, P. G.; van der Pol, J. F.; Zwikker, J. W.; Drenth, W.; Picken, S. J. *Mol. Cryst. Liq. Cryst.* **1991**, *195*, 291-305.

(83) Collard, D. M.; Lillya, C. P. *J. Am. Chem. Soc.* **1991**, *113*, 8577-8583.

(84) Ohta, K.; Morizumi, Y.; Ema, H.; Fujimoto, T.; Yamamoto, I. *Mol. Cryst. Liq. Cryst.* **1991**, *208*, 55-63.

(85) Schouten, P. G.; Warman, J. M.; de Haas, M. P.; van Nostrum, C. F.; Gelinck, G. H.; Nolte, R. J. M.; Copyn, M. J.; Zwikker, J. W.; Engel, M. K.; Hanack, M.; Chang, Y. H.; Ford, W. T. *J. Am. Chem. Soc.* **1994**, *116*, 6880-6894.

(86) Sergeyev, S.; Pouzet, E.; Debever, O.; Levin, J.; Gierschner, J.; Cornil, J.; Aspe, R. G.; Geerts, Y. H. *J. Mater. Chem.* **2007**, *17*, 1777-1784.

(87) Pisula, W.; Kastler, M.; Wasserfallen, D.; Mondeshki, M.; Piris, J.; Schnell, I.; Mullen, K. *Chem. Mater.* **2006**, *18*, 3634-3640.

(88) Kumar, S.; Rao, D. S. S.; Prasad, S. K. *J. Mater. Chem.* **1999**, *9*, 2751-2754.

(89) Bisoyi, H. K.; Kumar, S. *J. Phys. Org. Chem.* **2008**, *21*, 47-52.

(90) Stackhouse, P. J.; Hird, M. *Liq. Cryst.* **2008**, *35*, 597-607.

(91) Li, H.; Babu, S. S.; Turner, S. T.; Neher, D.; Hollamby, M. J.; Seki, T.; Yagai, S.; Deguchi, Y.; Mohwald, H.; Nakanishi, T. *J. Mater. Chem. C* **2013**, *1*, 1943-1951.

(92) Kumar, S.; Varshney, S. K. *Angew. Chem. Int. Ed.* **2000**, *17*, 3140-3142.

(93) Kumar, S.; Varshney, S. K.; Chauhan, D. *Mol. Cryst. Liq. Cryst.* **2003**, *396*, 241-250.

(94) Bisoyi, H. K.; Kumar, S. *Tetrahedron Lett.* **2007**, *48*, 4399-4402.

(95) Kumar, S.; Naidu, J.; Varshney, S. K. *Mol. Cryst. Liq. Cryst.* **2004**, *411*, 355-362.

(96) Carfagna, C.; Iannelli, P.; Roviello, A.; Sirigu, A. *Liq. Cryst.* **1987**, *2*, 611-616.

Appendix I

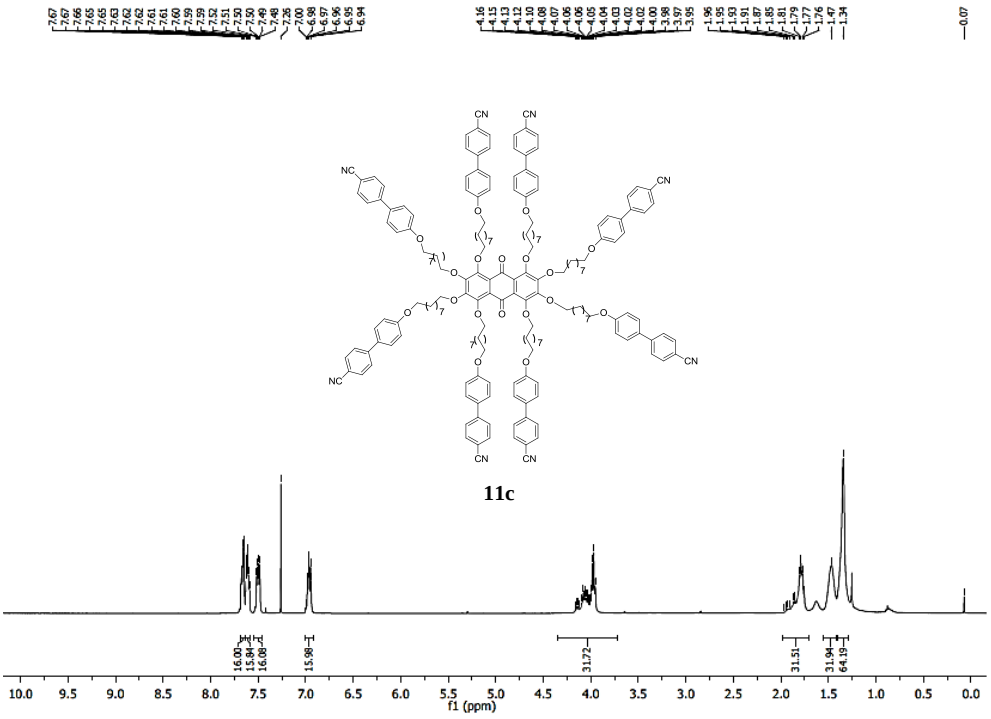

Figure A1 ^{1}H NMR spectrum of compound **11c**.

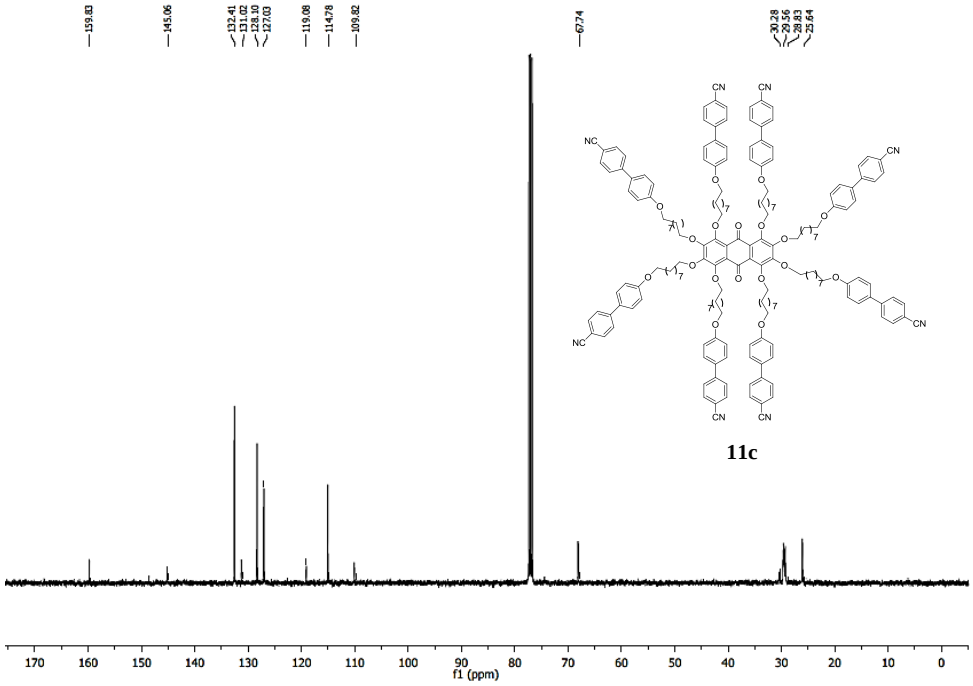

Figure A2 ^{13}C NMR spectrum of compound **11c**.

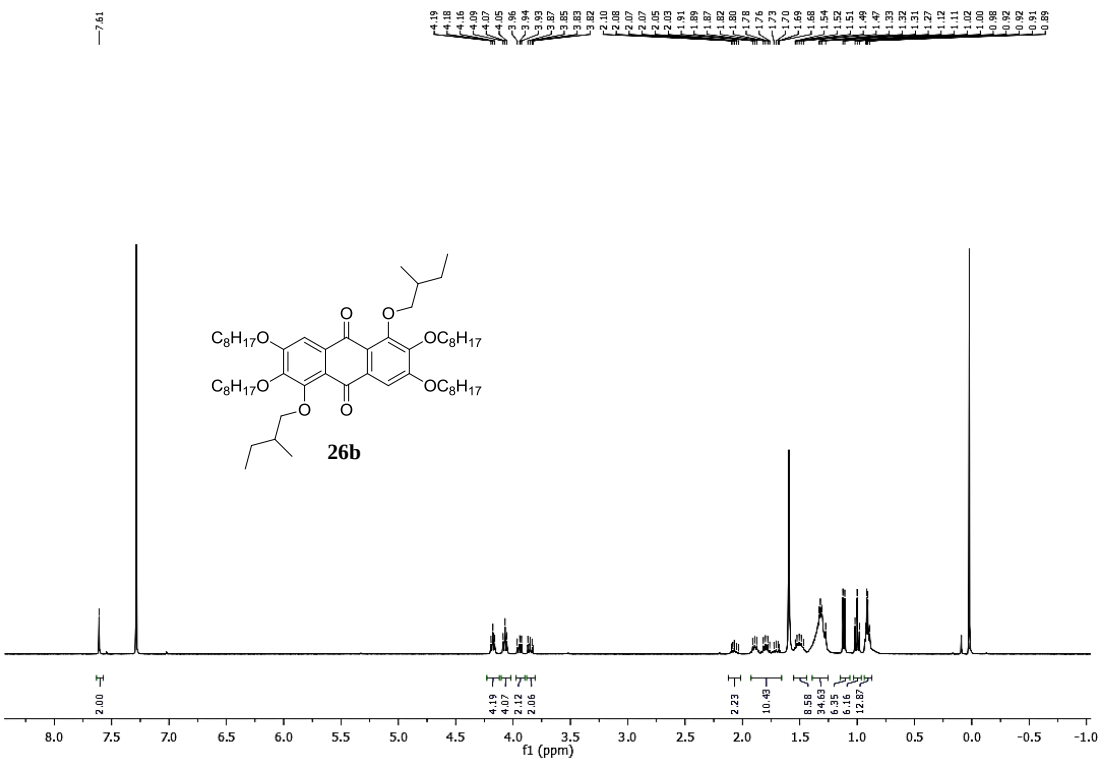

Figure A3 ^{1}H NMR spectrum of compound **26b.**

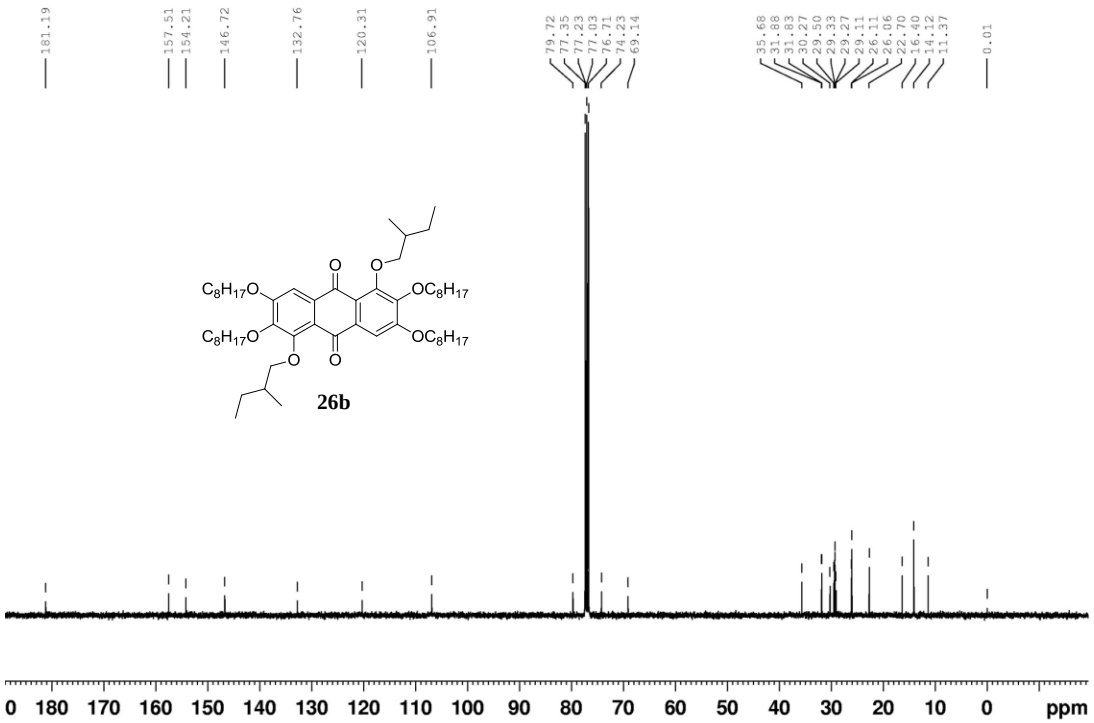

Figure A4 ^{13}C NMR spectrum of compound **26b.**

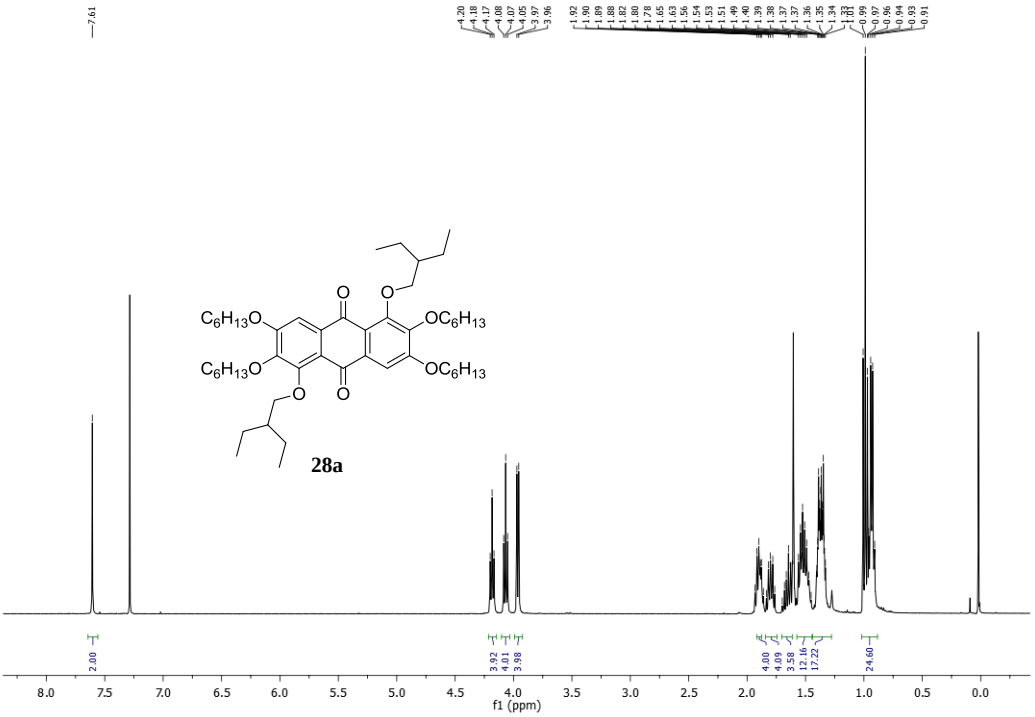

Figure A5 ^{1}H NMR spectrum of compound **28a.**

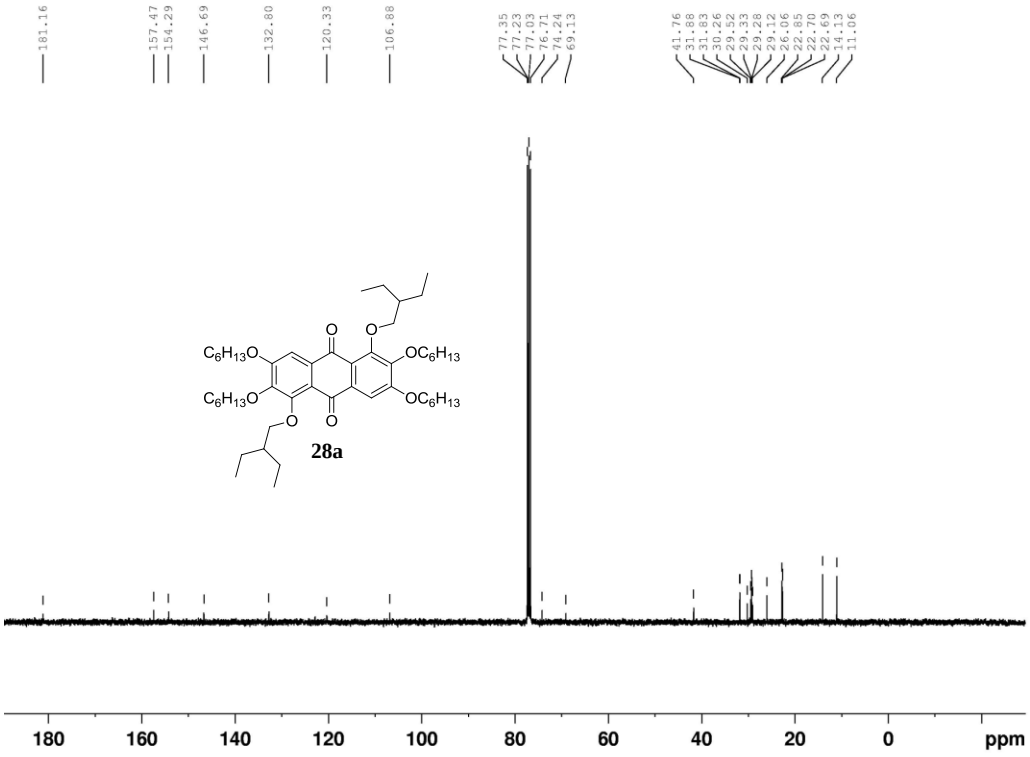

Figure A6 ^{13}C NMR spectrum of compound **28a.**

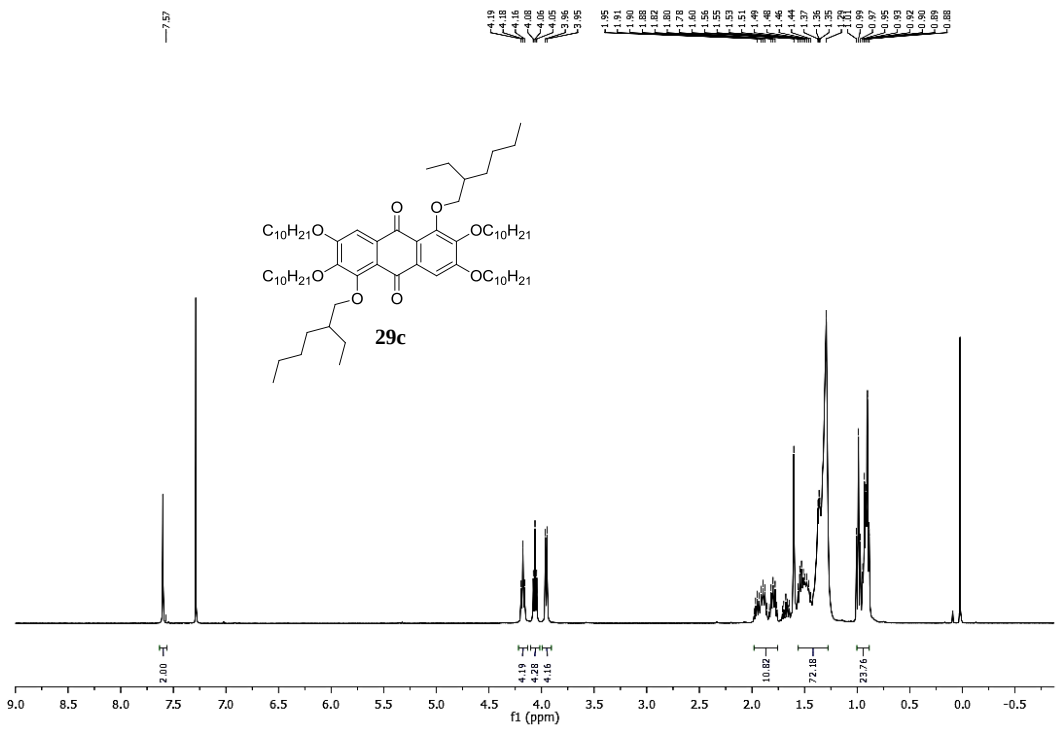

Figure A7 ^{1}H NMR spectrum of compound **29c.**

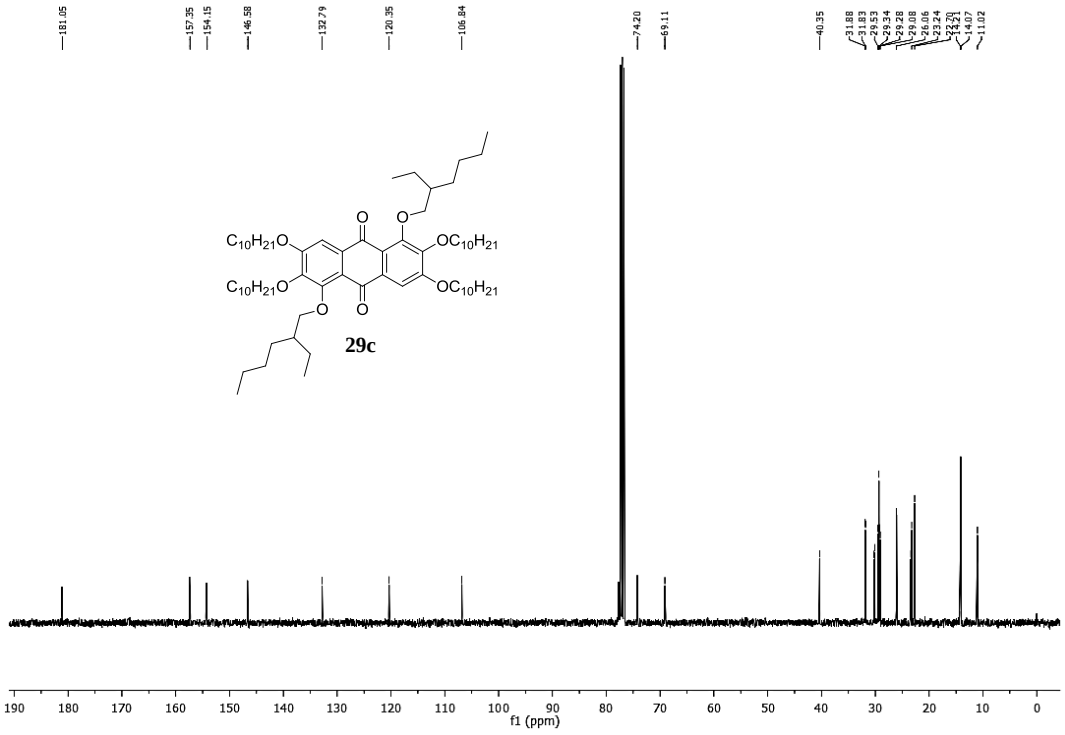

Figure A8 ^{13}C NMR spectrum of compound **29c.**

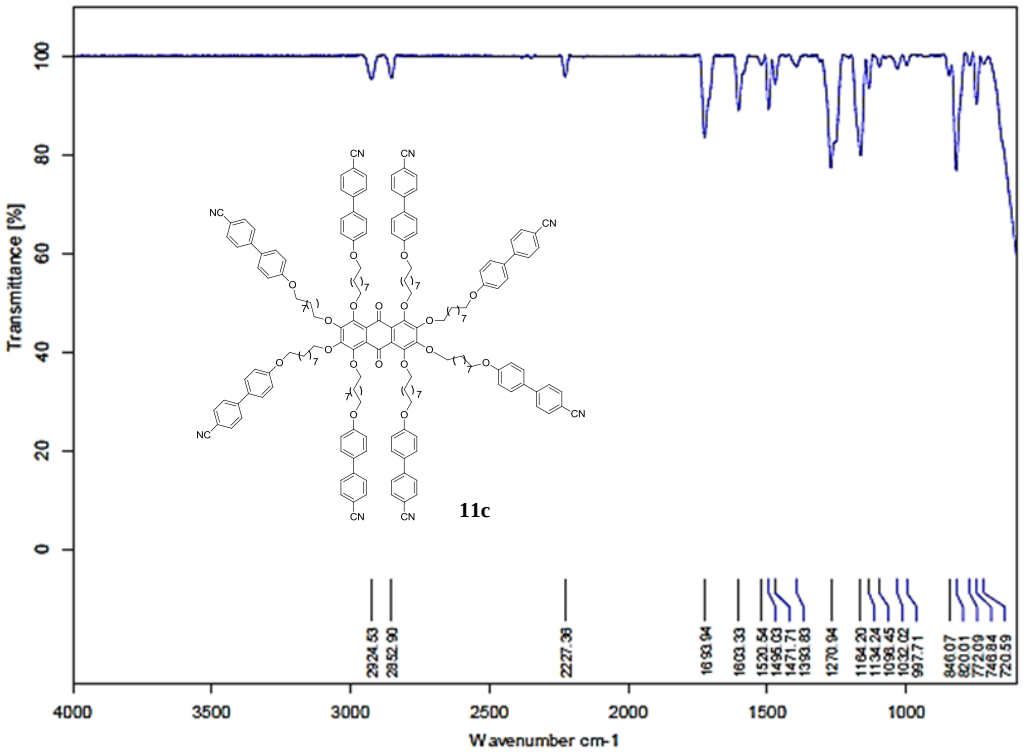

Figure A9 IR spectrum of compound **11c.**

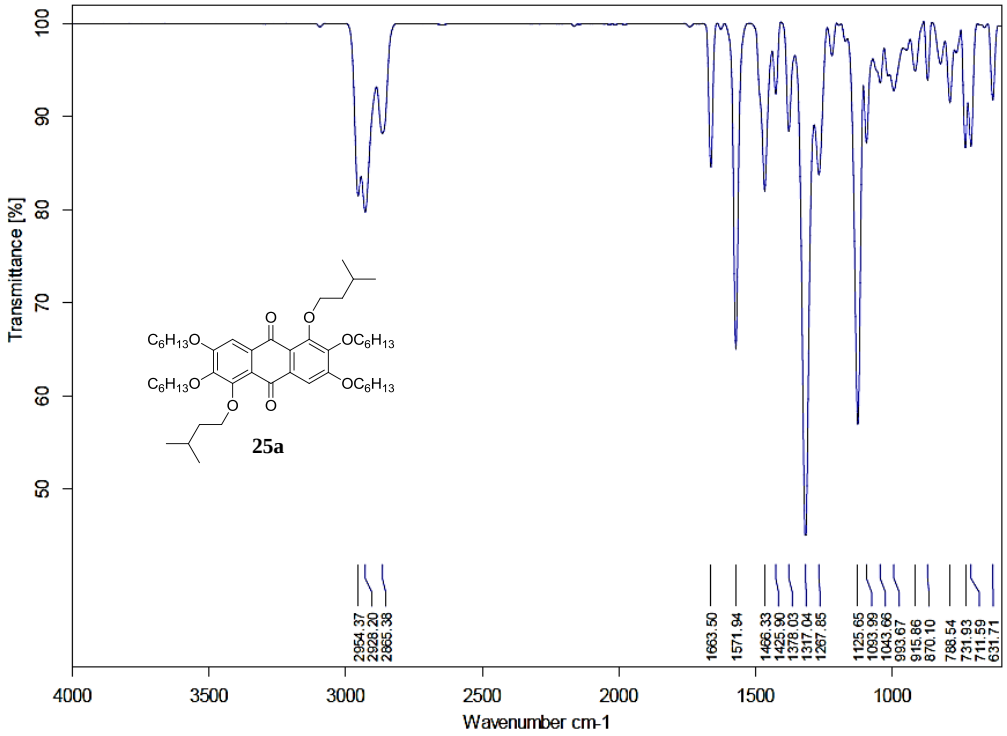

Figure A10 IR spectrum of compound **25a.**

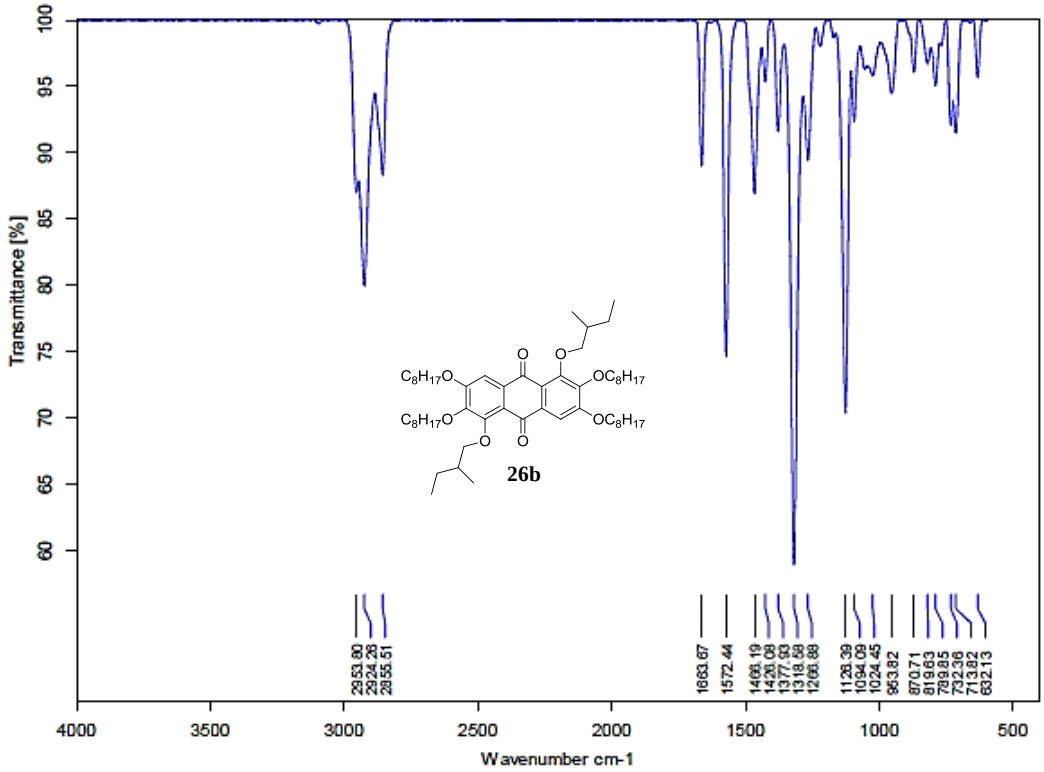

Figure A11 IR spectrum of compound **26b.**

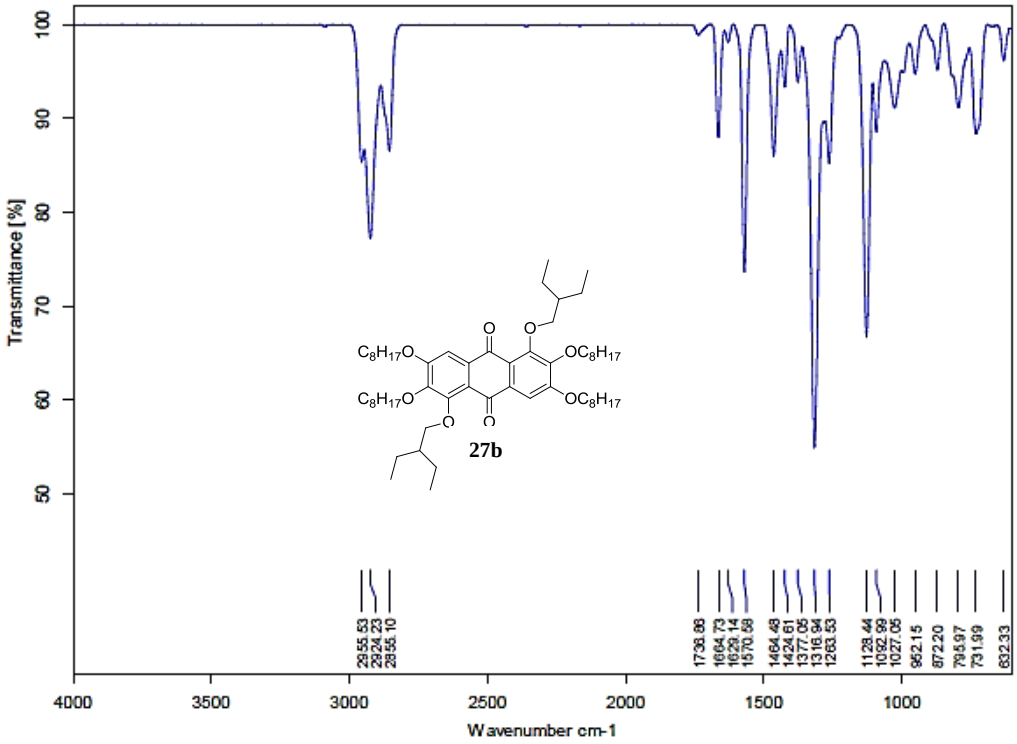

Figure A12 IR spectrum of compound **27b.**

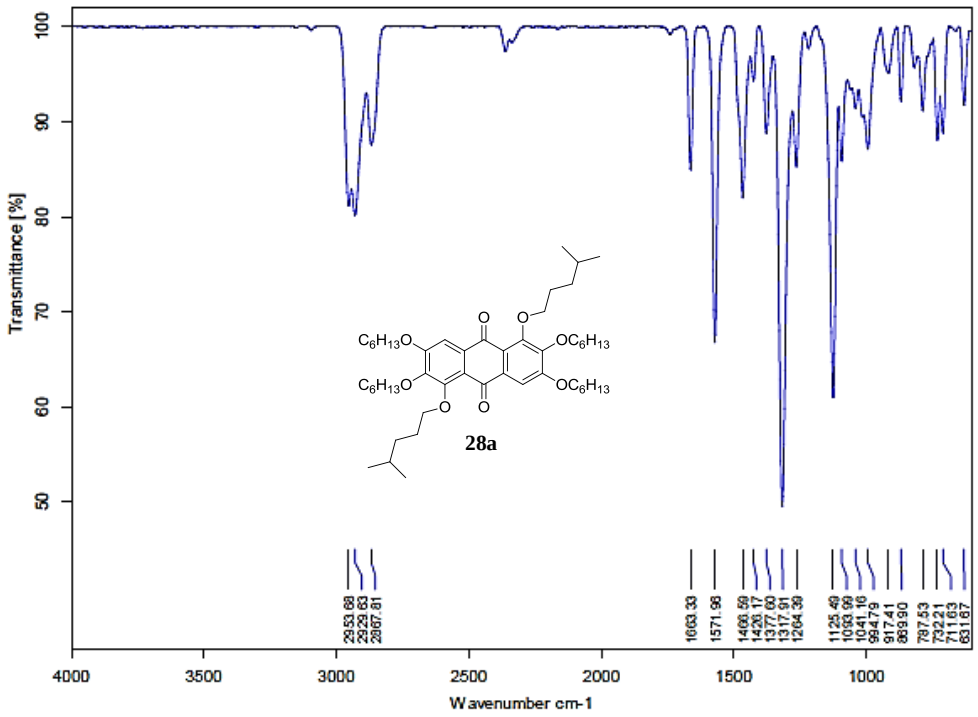

Figure A13 IR spectrum of compound **28a.**

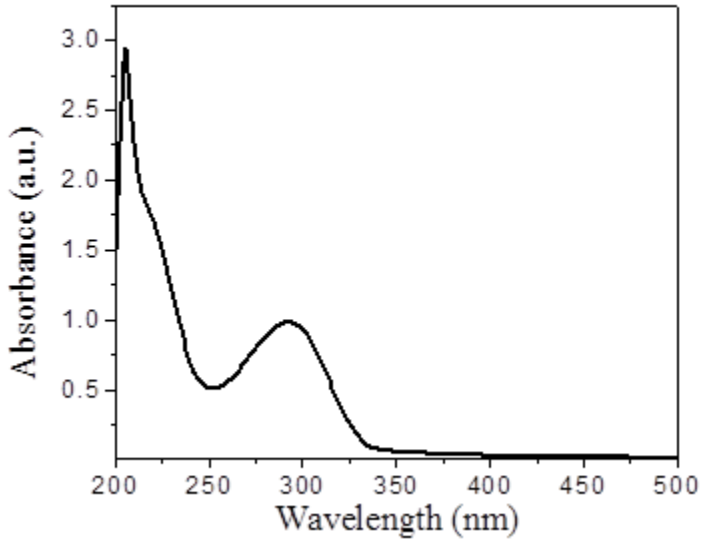

Figure A14 UV-vis spectrum of compound **11c.**

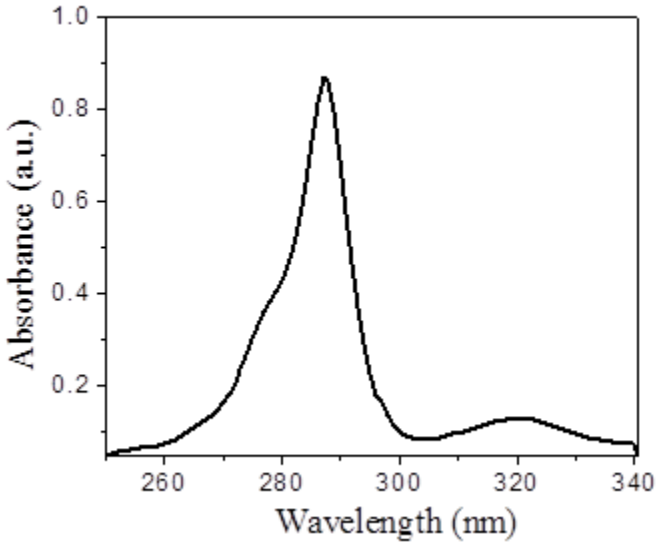

Figure A15 UV-vis spectrum of compound **25a.**

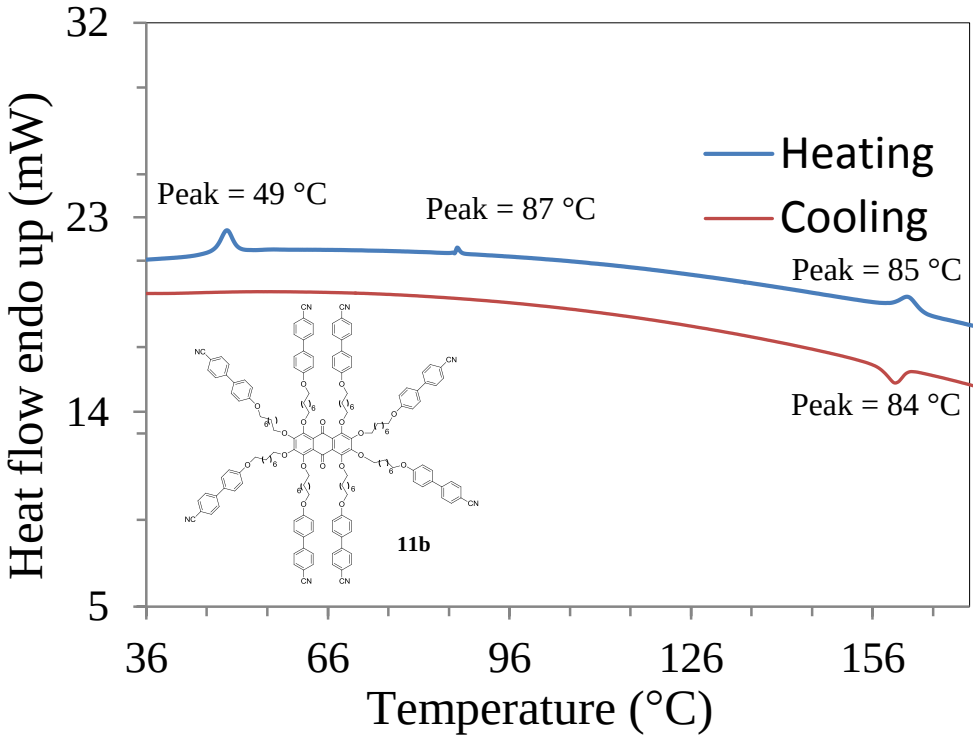

Figure A16 DSC thermogram of compound **11b**.

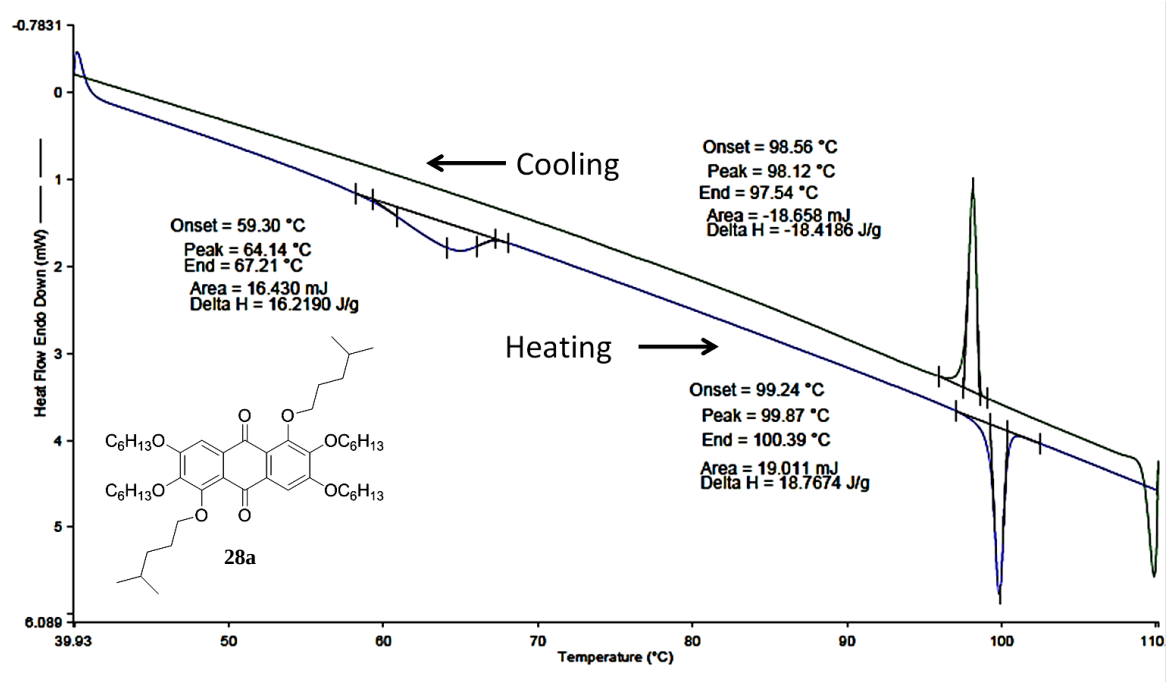

Figure A17 DSC thermogram of compound **28a**.

Chapter 3

Synthesis, Characterization and Physical Properties of Mesogenic Perylene Tetraesters

A series of perylene tetraesters based liquid crystals bearing four triphenylene, cyanobiphenyl linked *via* flexible chains and branched chain substituents have been synthesized and their thermotropic properties have been studied by a combination of thermogravimetric analysis, differential scanning calorimetry, polarizing optical microscopy and X-ray scattering. All the compounds with triphenylene and branched chains units were found to stabilize columnar hexagonal mesophase over a broad range of temperature, while with cyanobiphenyl exhibited nematic mesophases. Six compounds showed columnar mesophase at room temperature. From investigations of the spectroscopic properties and aggregation behavior of two compounds in solvents and solid states by absorption and fluorescence optical spectroscopy, it was revealed that they form H-type aggregates. All these compounds showed yellow-green fluorescence even under day-light conditions. The high stability and bright fluorescence of several of the compounds make them promising for applications as components in optoelectronic devices.

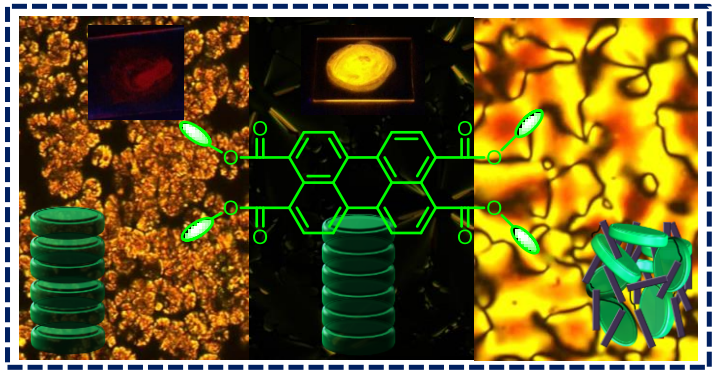

3.1 Introduction

Organic chromophores, such as perylene and its derivatives have remained the subject of much current research due to their unique features such as facile structural functionalization, outstanding light-harvesting in the visible region, high thermal, chemical, photo & environmental stability, near-unity fluorescence quantum yields in the molecular state, light fastness and *n*-type semiconductor properties.[1] Due to these properties, perylene has been recognized as an ideal candidate for fabricating organic optoelectronic materials and devices, such as organic photovoltaics (OPVs), organic field effect transistors (OFETs), dye lasers, fluorescent sensors, organic light-emitting diodes (OLEDs), xerographic photoreceptors etc.[1-10] The optical and electronic properties of these derivatives are caused by the local π-π stacking interactions of perylene skeleton leading to molecular aggregation.[11-14] This aggregation further enables the efficient conduction of electrons within the aggregates.[15,16] The π interactions between the perylene molecules can be modulated by the introduction of peripheral groups. Two or more radiating side groups can lead to the formation of discotic liquid crystals (DLCs) which can self-assemble into 2D columnar superstructures.[17-23] In this regard, proper management of the molecular structure is highly important as it can preserve the LC behavior up to room temperature for long term sustainability and can also lead to spontaneous self-alignment in the mesophase. Compounds with LC behavior at room temperature, low clearing temperature, mesophase stability over a wide range of temperatures and single mesophase structure are anticipated for all the potential device applications.[24,25] All these factors critically depend on the side chains attached to the perylene core, as these side chains play a crucial role in molecular self-assembly. Therefore, properly substituted LC perylene derivatives with good self-assembly properties are obligatory for the envisioned applications.

The molecular self-assembly also gets affected by the addition of solvents. In general, a good solvent leads to solvation of the π-system and no aggregation or molecular self-assembly can take place at low concentration. However, a poor solvent tends to facilitate the molecular self-assembly as it cannot dissolve the π-aggregates.[26,27] Furthermore, perylenes could be of potential interest in showing biaxial nematic (N_b) phases. Molecular shape biaxiality can lead to the formation of biaxial nematic thermotropic LC materials. Conceptually mixing board-

like molecules i.e., perylenes with different size or aspect ratios could reduce the formation of positionally ordered phases and might lead to the N_b phase.[28-33]

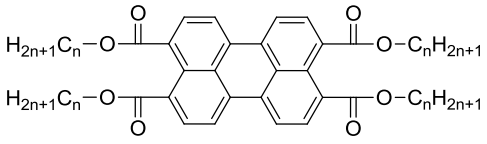

1

So far, only a few LC perylene tetraester derivatives have been synthesized.[34-38] For example, Wang and co-workers[34,35] have synthesized a series of perylene tetraesters with normal alkyl chains, out of which derivatives with n = 4, 6, 8, 10 were found to possess columnar hexagonal mesophases. Bock and co-workers[36] have prepared different LCs based on cores like triphenylene, coronene, perylene, pyrene etc. by attaching 2-ethylhexyl chains at the periphery. All these derivatives were found to stabilize columnar hexagonal mesophase. But, the clearing temperatures of all these derivatives varied, perylene being an exception having highest clearing temperature among all of them. 3,4,9,10-tetra-(2,2,3,3,4,4,5,5,5-tetrafluoro-pentenyl)-perylene was synthesized[37,38] and studied for its properties in nematic LCs and LB films.

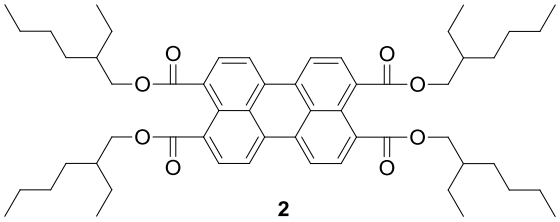

2

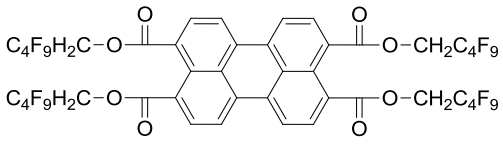

3

3.2 Objective

With the aim of studying the influence of substituents on the perylene core, we have synthesized three series of perylene tetraesters. Our molecular design is such that it contains

discotic perylene moiety at the center and perylene has been connected from four sides to four discotic triphenylene core (**5.1**-**5.5**), calamitic 4-cyanobiphenyl moieties (**6.1**-**6.8**) *via* flexible methylene spacers and different branched alkyl chains (**7.1**-**7.7**) in three different molecules (Scheme 3.1). This study represents a simple but useful advance in the design of a molecular system that enables fundamental insights into unconventional structure-mesophase morphology relationship. This investigation was motivated by two goals. First, by changing the connection of structurally different units i.e., cyanobiphenyl (*CB*) around periphery of perylene core (*PE*), we sought to provide insight into structure-mesophase behavior in the system.

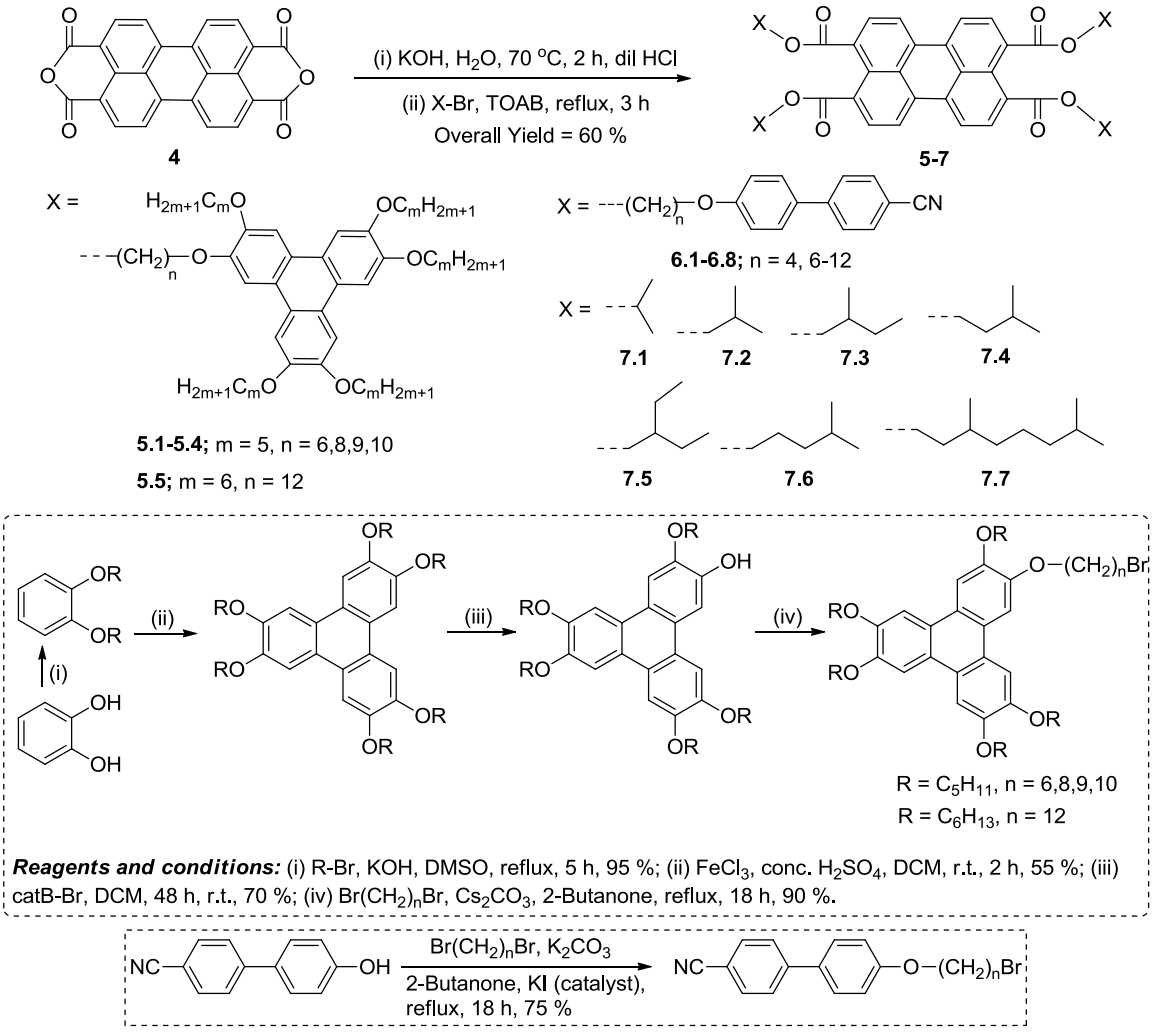

Scheme 3.1 Synthesis of perylene tetraesters **5-7** prepared in this study.

Additionally, we sought to explore the possibility of hole and electron transport properties by attaching electron rich *TP* and electron deficient *PE* moieties. These molecular double-cables, owing to their incommensurate core sizes, may stack one on top of the other in the columns to give columnar versions of double cable polymers, which could ultimately provide side-by-side percolation pathways for electrons and holes in solar cells. Additionally, since perylene is associated with very high clearing temperatures, various branched chains have been selected to facilitate self-assembly at or near to room temperature. The thermotropic behavior in the pristine state was investigated by polarizing optical microscopy (POM), differential scanning calorimetry (DSC), thermogravimetric analysis (TGA) and X-ray scattering (WAXS and SAXS). We also report the extensive and comprehensive investigation of the spectroscopic properties and aggregation behavior in solvents for compounds with triphenylene and branched moieties for their application in optoelectronics. We have discovered that without additional non-covalent interactions like hydrogen bonding, metal ion, van der Waals interactions, dipole etc. five out of these compounds formed hexagonal columnar mesophases at room temperature with low clearing transition. The very first step for the successful fabrication of any organic electronics involves the creation of thin films of the organic molecules. In these thin films, interfacial molecular orientation plays an important role. For the creation of the thin films, Langmuir-Blodgett technique offers a unique method in which molecular organization and interfacial interactions can be determined very easily. We have used this technique to prepare thin films of these compounds. For applications in organic electronics, charge transport in the thin film state is also a prerequisite. So, we have measured the charge transport in these films. Additionally, low band gap values, good fluorescence quantum yields, high purity and green luminescence under day-light conditions make these derivatives promising for the fabrication of various electronics.

3.3 Results and Discussion

3.3.1 Synthesis and characterization

The synthetic protocol for the preparation of all the perylene derivatives is outlined in Scheme 3.1. All the final molecules **5-7** were prepared by applying a method already

described in literature with some modification in the synthetic method.[34,35] Tetraesters of perylene has been synthesized by various other methods also.[39-42] These methods involve (a) treatment of perylene-3,4,9,10-tetracarboxylic dianhydride with a mixture of alkyl halide/alkyl tosylate and alkyl alcohol by refluxing in presence of potassium carbonate for 2-7 days;[39,40] (b) refluxing a mixture of perylene-3,4,9,10-tetracarboxylic dianhydride, alcohol, alkyl halide and 1,8-diazabicyclo[5.4.0]undec-7-ene (DBU) in acetonitrile for overnight;[41] (c) transesterification of tetramethyl ester of perylene-3,4,9,10-tetracarboxylic acid with suitable alcohol by boiling in presence of sodium alcoholate for 80 h[38] and (d) another track goes *via* hydrolysis of perylene-3,4,9,10-tetracarboxylic acid dianhydride by refluxing it in aqueous potassium hydroxide followed by acidification to pH 8–9 with aqueous dilute H_2SO_4 or HCl to provide perylene-3,4,9,10-tetracarboxylic acid.[34,35] This was followed by addition of the corresponding alkyl bromide and tetraoctylammonium bromide (TOAB) as phase transfer catalyst and refluxing the mixture vigorously for 1-2 h. After this, the reaction mixture was cooled down to room temperature and extracted with chloroform. Chloroform was then evaporated to give the crude product which was further purified by column chromatography. We have used this method for the synthesis of our materials. Details of the synthesis are provided in the experimental section. The chemical structures of these compounds were determined using spectroscopic techniques (^{1}H NMR, ^{13}C NMR, FTIR and MALDI-MS) as detailed in the experimental section and representative spectra are given in appendix II (Figures A1-A12).

3.3.2 Thermal behavior

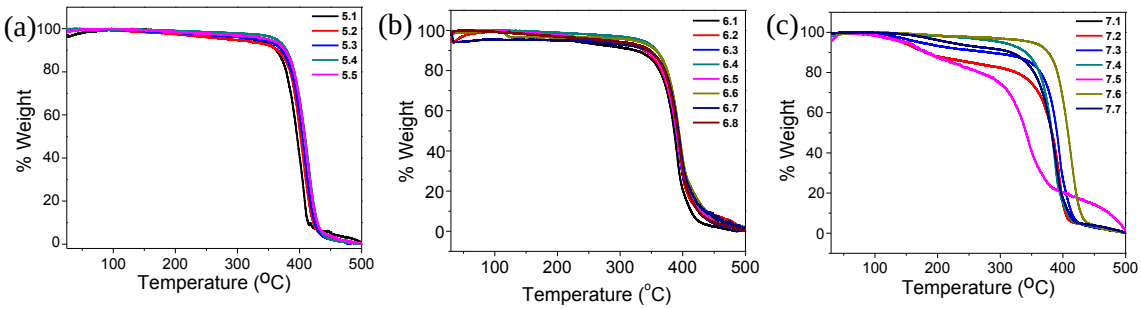

Figure 3.1 TGA curves of compounds (a) **5**, (b) **6** and (c) **7**. All the measurements were performed under a nitrogen atmosphere, with heating and cooling rates of 10 °C/min.

Table 3.1 Phase behavior of mesogens **5.1**-**7.7**.[a,b]

Mesogen	Heating Cycle	Cooling Cycle
5.1	Col_h 111.20 (8.37) I	I 98.59 (11.09) Col_h
5.2	Col_h 107.85 (21.29) I	I 96.16 (19.19) Col_h
5.3	Col_h 125.69 (10.25) I	I 113.42 (10.34) Col_h
5.4	Col_h 124.74 (11.08) I	I 112.99 (14.61) Col_h
5.5	Col_h 103.9 (78.83) I	[c]I 101 Col_h
6.1	Cr 224.44 (89.45) I	-
6.2	Cr 222.90 (114.56) I	I 95.62 (4.02) N
6.3	Cr_1 69.20 (13.72) Cr_2 225.37 (92.84) I	I 180.29 (83.05) Cr_2 42.66 (12.34) Cr_1
6.4	N 105.3 (5.54) I	I 89.6 (2.87) N
6.5	Cr_1 163.35 (88.18) Cr_2 172.68 (10.31) I	I 140.82 (3.66) N 122.25 (52.61) Cr
6.6	Cr 123.74 (75.21) I	I 113.16 (3.09) N
6.7	Cr_1 116.72 (15.14) Cr_2 153.45 (101.67) I	I 125.21 (12.11) N 100.67 (71.06) Cr
6.8	Cr 125.39 (110.46) I	I 110.71 (3.52) N 46.61 (28.25) Cr
7.1	Cr_1 162.28 (11.32) Cr_2 > 286.37 Dec[d]	-
7.2	Cr_1 179.60 (28.70) Cr_2 > 303.02 Dec[d]	-
7.3	Cr 124.50 (30.90) Col_h > 321.81 Dec[d]	-
7.4	Cr_1 42.13 (0.82) Cr_2 86.93 (36.29) Col_h > 306.53 Dec[d]	-
7.5	Cr_1 100.78 (32.42) Cr_2 > 318.52 Dec[d]	-
7.6	Cr 100.28 (25.45) Col_h 227.30 (2.04) I	I 186.56 (0.83) Col_h 42.52 (29.24) Cr
7.7	Col_h 150.2 (6.23) I	I 147 (0.40) Col_h

[a]Transition temperatures in °C and latent heat values (in kJ mol^{-1} in brackets).
[b]Phase assignments: Cr = crystalline; Col_h = columnar hexagonal; N = nematic; I = isotropic; Dec = decompose.
[c]From POM.
[d]Decomposition temperatures from TGA.

The thermal behavior of all the compounds was monitored by a combination of thermo gravimetric analysis (TGA), differential scanning calorimetry (DSC) and polarizing optical microscopy (POM) and small- and wide angle X-ray scattering (SAXS and WAXS). TGA measurements revealed that compounds **5.1**-**5.5** and **6.1**-**6.8** were thermally stable with 5% weight loss up to ~ 300 °C under nitrogen atmosphere and complete decomposition occurred at 500 °C (Figure 3.1). However, for compounds **7.1**-**7.7** stability varied depending on the

branched alkyl bromide used. All the compounds were then subjected to DSC to study their thermal transition behavior. The transition temperature and associated enthalpy data obtained from the heating and cooling cycles of DSC or POM are collected in Table 3.1. The peak temperatures are given in degree Celsius and the numbers in parentheses indicate the transition enthalpy (ΔH) in kJ mol^{-1}. Compounds **5.1**-**5.5** showed enantiotropic mesomorphic behavior and were found to be LC glassy materials in their neat form at room temperature. Compound **5.1** with hexyl spacer between perylene and triphenylene exhibited single transition in the heating cycle corresponding to mesophase to isotropic phase at 111.20 °C with an enthalpy change of 8.37 kJ mol^{-1}. On cooling from isotropic liquid, mesophase started appearing at 98.6 °C and was stable down to room temperature (Table 3.1). However, on further cooling up to -100 °C, no signature of crystallization appeared. LC morphology of all the compounds was checked under POM with a hot stage (Figure A17 in appendix II). Fresh samples were kept between a glass slide and cover slip. The images were captured under cross polars on cooling from the isotropic phase in the LC window using a high resolution camera. Under POM, on cooling from the isotropic phase typical flower shaped texture characteristic for the formation of columnar phase was displayed.

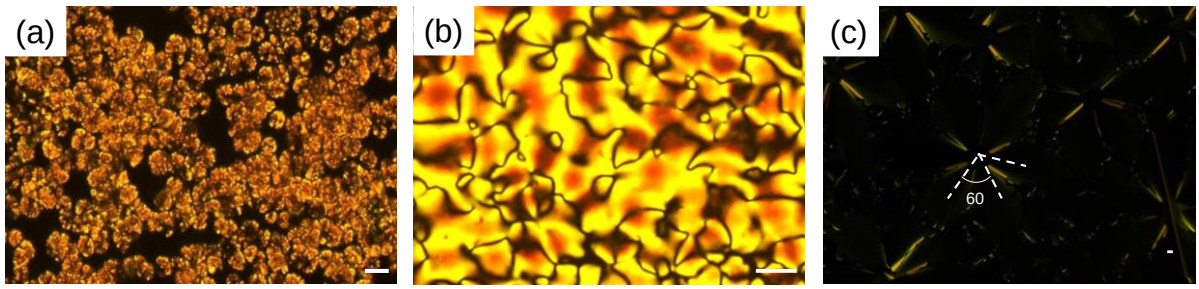

Figure 3.2 Polarizing optical microscope images of compounds (a) **5.3**, (b) **6.6** and (c) **7.6** at 112.3 °C, 105.1 °C and 182.5 °C, respectively (on cooling, crossed polars, scale bar = 10 μm). The broken lines in (c) indicates the growth directions of the dendritic texture.

Compounds **5.2**-**5.4** were prepared to see the effect of spacer length on the mesophase behavior. Compound **5.2** with octyl spacer also exhibited enantiotropic mesophase formation at room temperature. It showed mesophase to isotropic transition at 107.9 °C. In cooling scan, it displayed only one transition corresponding to mesophase formation at 96.2 °C with no signature of crystallization up to -100 °C. Under POM, it also exhibited flower shaped

texture formation. Similar to **5.1** and **5.2**, compounds **5.3** and **5.4** with nonyl and decyl spacers, respectively also showed only a single transition in DSC. **5.3** became isotropic at 125.7 °C and **5.4** became isotropic at 124.7 °C. Under POM also, both the compounds exhibited flower shaped texture (Figure 3.2a). Compound **5.5** (Figure A13) was prepared to investigate the effect of spacer length as well as the length of alkoxy chains attached to triphenylene. This compound underwent mesophase to isotropic transition at 103.9 °C. In the cooling scan, no peak corresponding to any transition has been observed. However, under POM, this compound exhibited textures typical of Col_h phase in the cooling run. It can be seen that the effect of spacer length is not much on the clearing transition, only increase of the alkoxy chain length led to a decrease in the clearing temperature. Interestingly, the clearing temperatures of all these compounds were ~120 °C which was very less compared to the previous reports.[42] Hence, these compounds can be very easily processed for their use in various optoelectronics. It is noteworthy that mesophase range of perylene - triphenylene oligomers is much higher as compared to that for hexaalkoxytriphenylene reported earlier.[43]

Compound **6.1** with butyl spacer was found to be non-mesomorphic and exhibited crystal to isotropic transition at 224.5 °C and no peak corresponding to isotropic to crystal transition was observed in DSC. Compound **6.2** with hexyl spacer was found to exhibit monotropic mesophase on cooling. On first heating in DSC, it showed a melting transition at 222.2 °C and on cooling mesophase appeared at 95.6 °C which was stable down to room temperature. Under POM, this displayed schlieren texture typical of nematic mesophase formation. Compound **6.3** with heptyl spacer demonstrated crystal to crystal transition at 69.2 °C and finally cleared at 225.4 °C. These transitions in thermal analysis (DSC) arise from the different stability of two crystalline polymorphs; evidence accompanying by POM textures and powder X-ray scattering studies as observed in past reports.[44,45] Compound **6.4** (Figure A14) with octyl chain exhibited enantiotropic mesomorphism and isolated as the room temperature nematic compound. In DSC, it showed nematic to isotropic transition at 105.3 °C in the heating cycle. In the cooling run, it exhibited isotropic to nematic transition at 89.6 °C. Under POM, this also displayed schlieren texture typical of nematic mesophase. Compounds **6.5** and **6.7** with nonyl and undecyl spacers (odd spacers) demonstrated crystal to crystal transition at 163.4 and 116.7 °C, respectively and cleared on heating at 172.7 and

153.5 °C, respectively. In the cooling scan, mesophase started appearing at 140.8 and 125.2 °C, respectively for compounds **6.5** and **6.7**, consistent with the observation of schlieren texture under POM. On further cooling, mesophase to crystalline transition occurred at 122.3 and 100.7 °C, respectively in DSC for compounds **6.5** and **6.7**. Under microscope, we have observed appearance of spherulitic growth which slowly covered the whole sample area consistent with the formation of crystalline state. In DSC, compounds **6.6** and **6.8** with decyl and dodecyl spacer unveiled only a single transition corresponding to crystal to isotropic phase at 123.7 and 125.4 °C, respectively. In the cooling scan, for compound **6.6** only a single transition (isotropic to mesophase) was observed. However, for compound **6.8**, DSC thermogram displayed two transitions (isotropic to nematic and nematic to crystal). Figure 3.2b represents the schlieren texture of the nematic phase for compound **6.6** as a representative case. The compounds of this series displayed odd-even effect in their melting and clearing temperatures. Odd spacer compounds (n = 7, 9, 11) have higher clearing temperatures than the even analogues (n = 6, 8, 10, 12). Noticeably, compounds with odd spacers also exhibit polymorphism in the crystalline state which was not observed in the even analogues.

Compound **7.1** was prepared to see the effect of 2-propyl chain (branching position directly attached to core) in inducing the mesophase. During the heating cycle in DSC, only a single transition was observed at 162 °C. Based on the POM analysis, this transition was assigned to the crystal to crystal transition. No peak corresponding to melting or clearing temperature was observed. Probably, this compound directly decomposed during the heating scan before going to isotropic state. Under POM also, we didn't observe any transition corresponding to the isotropic state. The decomposition temperature was then assigned based on the TGA analysis. In compound **7.2** (2-methylpropyl), branching position was close to the core but, not directly attached as in case of compound **7.1**. This compound was found to be non-mesomorphic and exhibited only a single transition in DSC in the heating run at 179.60 °C (ΔH = 28.70 kJ/mol) corresponding to crystal to crystal mesomorphism. Compound **7.3** with 2-methyl butyl chains in the periphery when observed under microscope, exhibited an undefined mobile texture during heating with an increase of birefringence. In DSC, this compound displayed one transition corresponding to crystal to mesophase. Similar to

previous compounds, this also decomposed during heating. Compound **7.5** was prepared by substituting the methyl branch in **7.3** with ethyl group. Interestingly, this replacement leads to a complete loss of mesomorphism as observed by both POM and DSC studies. Compound **7.4** with 3-methylbutyl peripheral chains was found to stabilize columnar mesophase. Under POM, this compound exhibited dendritic texture with homeotropic appearance in some region. Compound **7.6** was prepared by the introduction of 4-methyl pentyl chains at the periphery. On heating, this compound showed a crystal to mesophase transition at 100.3 °C as evidenced by DSC with an enthalpy change of about 25.45 kJ mol^{-1}. On further heating, mesophase transformed into isotropic liquid at 227.3 °C. On cooling this isotropic liquid at a rate of 5 °C min^{-1}, a dark field of view with only a little birefringence was observed as shown in Figure 3.2c. It has been reported in the literature that the homeotropically aligned columnar mesophases results in loss of birefringence.[46-52] It can be seen that this is a dendritic texture and the branching of this dendritic started at 60° to the main center.[50,51] This feature is characteristic of a highly ordered hexagonal columnar phase. Organic photovoltaics and OLEDs require homeotropic alignment of the columnar phase, in which all the molecules arrange in face-on alignment on the substrate.[48,52] Compound **7.7** (Figure A15) with 3,7-dimethyloctyl chain was isolated in the columnar mesophase at room temperature and showed the mesophase to isotropic transition at 150.2 °C. For this compound, mesophase range was broadened and the clearing temperature was also very low compared to the previous derivatives. This derivative also showed homeotropic alignment of the columnar mesophase as observed for compound **7.6**.

3.3.3 X-ray scattering studies

In order to reveal the mesophase structure and hence the supramolecular organization of these compounds, X-ray scattering experiments were carried out using unoriented samples filled in a glass capillary. The SAXS and WAXS patterns were recorded for compounds **5.1**-**5.5** in the LC phase on cooling from the isotropic phase. Table 3.2 summarizes results of observed and calculated *d*-spacings, indexing and lattice parameters of compounds **5.1**-**5.5** and **7.1**-**7.7**. The X-ray scattering profile for compound **5.1** showed seven reflections in the small and wide angle region. These reflections can be assigned to a two-dimensional rectangular lattice in which molecules stack one on top of another and the columns generated

adopt a rectangular packing with rectangular lattice constants: a =43.78 and b =20.01 Å. The symmetry of the phase was assigned as *p2gg* symmetry owing to the presence of 21 reflection. The sublattice compression ratio, q_{hex} which expresses the distortion of Col_r lattice relative to hexagonal lattice, equals 1.3 corresponding to a compression of the lattice along b direction and the tilt angle q ($q=\cos^{-1}(b/a)$, where a and b are the lattice constants) along this direction takes value of 60°.

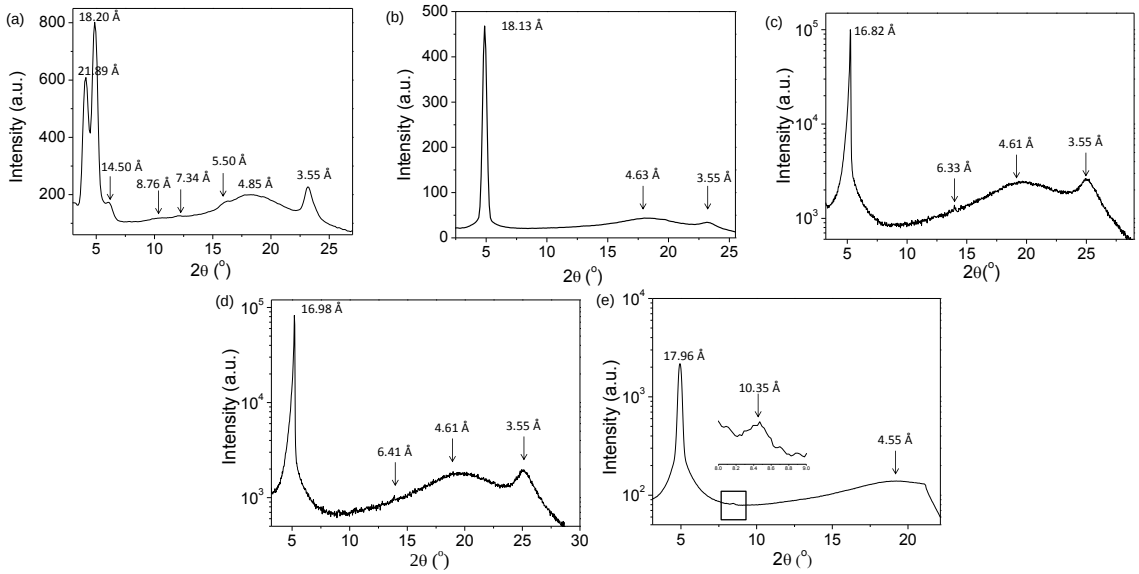

Figure 3.3 X-ray scattering patterns of compounds (a) **5.1** at 70 °C, (b) **5.2** at 70 °C, (c) **5.3** at 90 °C, (d) **5.4** at 90 °C and (e) **5.5** at 90 °C after cooling from isotropic phase.

For compound **5.2**, the reflection in the small angle region was indexed as 100. There were two diffused peaks in the wide-angle region at 4.61 and 3.55 Å. The first of these peaks corresponds to the packing of alkyl chains and the second corresponds to core–core stacking. The intercolumnar distances, a, calculated by using the relation, $a = d_{100}*2/\sqrt{3}$, where d_{100} is the spacing corresponding to the strong peak in the small angle region was found to be 20.94 Å. This is approximately 5 % less than the diameter obtained from the molecular model in its full trans conformation. This can be ascribed to the folding of the flexible chains or the possible interdigitation of flexible chains in the neighboring columns. This value is lower as compared to the scattering data reported in case of hexahexyloxytriphenylene (H6TP) and 3,4,9,10-tetra-(*n*-decyloxy-carbonyl)-perylene reported earlier.[34,35] It can be assumed that

columns are dominated by triphenylene disks rather than perylene disks and these columns are arranged in hexagonal pattern to construct the mesophase. This shrinkage of the intercolumnar distance in the pentamer is expected upon covalent linking the two molecules.

Table 3.2 Experimental data of X-ray scattering of compounds **5.1**-**5.5** and **7.3**-**7.7**.

Compound	d_{obs} (Å)[a]	d_{calc} (Å)[a]	*hkl*[b]	Lattice constants (Å)[c]	Lattice parameters[d]
5.1	21.89	21.89	200	a = 43.78	T = 70 °C; Col_r, *P2gg*;
	18.20	18.20	110	b = 20.01	q_{hex} = 1.3;
	14.54	14.76	210	c = 3.55	S = 876.03 Å^2
	8.76	8.25	320		S_{col} = 438.02 Å^2
	7.34	7.30	600		V_m = 5912.36 Å^3 (d = 1 gcm^{-3});
	5.50	5.69	430		Z = 0.5; h_m = 3.55 Å
	4.65(br)				
	3.55				
5.2	18.13	18.13	100	a = 20.94	T = 70 °C; Col_{ho}, *P6mm*;
	4.63			c = 3.55	S = 379.73 Å^2
	3.55				S_{col} = 189.86 Å^2
					V_m = 6108.76 Å^3 (d = 1 g cm^{-3});
					Z = 0.2; h_m = 3.55 Å
5.3	16.82	16.82	100	a = 19.33	T = 90 °C; Col_{ho}, *P6mm*;
	6.33	6.35	210	c = 3.55	S = 323.58 Å^2
	4.61				S_{col} = 161.79 Å^2
	3.55				V_m = 6330.77 Å^3 (d = 1 g cm^{-3});
					Z = 0.2; h_m = 3.55 Å
5.4	16.98	16.98	100	a = 19.52	T = 90 °C; Col_{ho}, *P6mm*;
	6.41	6.43	210	c = 3.55	S = 329.97 Å^2
	4.65	17.87			S_{col} = 164.99 Å^2
	3.55	10.32			V_m = 6428.75 Å^3 (d = 1 g cm^{-3});
					Z = 0.2; h_m = 3.55 Å
5.5	17.87	17.87	100	a = 20.54	T = 90 °C; Col_{hd}, *P6mm*;
	10.35	10.32	110		S = 365.36 Å^2
	4.60				S_{col} = 182.68 Å^2
					V_m = 7114.61 Å^3 (d = 1 g cm^{-3});
					Z = 0.2; h_m > 3.55 Å

7.3	16.73	16.73	100	a = 19.23	T = 135 °C; Col_{ho}, *P6mm*;
	6.33	6.31	210	c = 3.50	S = 320.24 Å^2
	5.30				S_{col} = 160.12 Å^2
	3.50				V_m = 1278.37 Å^3 (d = 1 g cm^{-3});
					Z = 0.9; h_m = 3.50 Å
7.4	16.82	16.82	100	a = 19.31	T = 200 °C; Col_h, *P6mm*;
	6.40	6.35	210	c = 3.51	S = 322.91 Å^2
	5.32				S_{col} = 161.46 Å^2
	3.51				V_m = 1330.43 Å^3 (d = 1 g cm^{-3});
					Z = 0.9; h_m = 3.51 Å
7.6	17.70	17.70	100	a = 20.44	T = 120 °C; Col_h, *P6mm*;
	6.65	6.68	210	c = 3.48	S = 361.81 Å^2
	5.35				S_{col} = 180.91 Å^2
	3.48				V_m = 1364.71 Å^3 (d = 1 g cm^{-3});
					Z = 0.92; h_m = 3.48 Å
7.7	20.56	20.56	100	a = 23.75	T = 140 °C; Col_h, *P6mm*;
	11.99	11.87	110	c = 4.20	S = 488.48 Å^2
	10.37	10.28	200		S_{col} = 244.24 Å^2
	7.86	7.76	210		V_m = 1784.24 Å^3 (d = 1 g cm^{-3});
	5.36				Z = 1.1; h_m = 4.20 Å
	4.20				

[a]d_{obs} and d_{cal} are the measured and theoretical scattering spacings; d_{cal} is calculated from the following mathematical expression for the hexagonal phase: $1/d_{hk} = \sqrt{(1/ d_{100})}(h^2 + k^2 + hk)$ and for the columnar rectangular phase; $1/d_{hk} = \sqrt{ h^2/a^2 + k^2/b^2}$ where hk are the indices of the reflections corresponding to the hexagonal and rectangular symmetry, and a and b are the lattice parameters. [b]Proposed indexing. [c]For Col_h phase; $a = d_{100}*2/\sqrt{3}$; [d]S is the lattice area, for the Col_h, $S = a^2*\sqrt{3}/2$ and for Col_r, $S = a*b$. S_{col} is the columnar cross-section, $S_{col} = S/2$. V_m is Molecular volume, $V_m = M/\lambda d N_A$, where M is the molecular weight of the compound, N_A is the Avogadro number, d is the volume mass density (1 g cm^{-3} for organic compounds), and $\lambda(T)$ is the temperature correction coefficient at the temperature of the experiment (T), $\lambda = V_{CH2}(T_0)/V_{CH2}(T)$, where T_0 = 25 °C, $V_{CH2}(T) = 26.5616 + 0.02023T$. Z is the number of molecules per columnar slice of thickness h_m: $h_m S = ZV_m$.

The diffractogram of compound **5.3** at 90 °C (Figure 3.3c) showed one sharp reflection in the small angle region at a *d* spacing of 16.82 Å and one reflection at *d* spacings of 6.33 Å in the middle-angle region. These reflections can be indexed to a lattice of hexagonal Col phase with Miller indices of 100, 210 in the ratio 1:1/√7. Two diffused peaks are observed in the wide angle region at *d* spacings of 4.61 and 3.55 Å, corresponding to packing of flexible tails and stacking of discs within the column. The lattice constant *a* was found to be 19.33 Å (19.5 % lesser than the optimized molecule geometry) indicating interdigitation of alkoxy chains in

the columnar phase. The X-ray pattern of **5.4** consisted of two diffuse scattering halo in the wide-angle region, centered around 4.65 and 3.55 Å, corresponding to the liquid-like order of the molten aliphatic chains and core-core separation. In the small-angle region, two reflections were detected with the reciprocal spacings in the ratios of 1: $1/\sqrt{7}$. These were indexed as 100, 210, respectively. The lattice constant *a* was found to be 19.52 Å (24.5 % lesser than the fully stretched molecule).

For compound **5.5**, the X-ray scattering profile showed only one peak in the wide angle region at *d* = 4.60 Å corresponding to the liquid like order of the alkyl chains. The small angle region consisted of two peaks in the ratio of 1: $1/\sqrt{3}$. For this compound an interdigitation of about 35 % has been observed. Compounds **5.1**-**5.4** with pentyloxy chains in the triphenylene moieties exhibited peaks corresponding to the π-π stacking of the aromatic cores. But, this peak was missing in compound **5.5**. This suggested that probably an increase of the alkoxy chain length lead to the disordering of mesophase similar to those observed by previous studies[53] and the alkyl spacer length has not much effect on the mesophase. So the columnar phase in compound **5.1** and **5.2**-**5.4** can be assigned as columnar rectangular ordered (Col_{ro}) and columnar hexagonal ordered (Col_{ho}) and for compound **5.5** as columnar hexagonal disordered (Col_{hd}). The columnar slice thickness h_m is given by the core-core stacking distance which is 3.55 Å for compounds **5.1**-**5.4**. This is also known as the lattice constant *c*. The number of molecules per columnar slice of thickness h_m is designated as Z. This is calculated using the relation; $h_mS = ZV_m$, where V_m is Molecular volume, $V_m = M/\lambda dN_A$, where M is the molecular weight of the compound, N_A is the Avogadro number, d is the volume mass density (1 g cm^{-3} for organic compounds) and λ(T) is the temperature correction coefficient at the temperature of the experiment (T), $\lambda = V_{CH2}(T_0)/V_{CH2}(T)$, where T_0 = 25 °C, $V_{CH2}(T) = 26.5616 + 0.02023T$. Substituting these values, for compounds **5.2**-**5.5**, Z was found to be 0.2. Since in these compounds, all the five discs are joined together, so, value of Z suggested that each of the columnar slice is made of only one disc. The lattice area S is calculated by the relation, $S = a^2*\sqrt{3}/2$ for compounds **5.2**-**5.5**. As the size of the molecules is increasing from **5.2**-**5.5**, lattice area is also increasing. The columnar cross-section designated as S_{col}, calculated by the relation $S_{col} = S/2$. The value of this parameter also increased with increase in the molecular size. For compound **5.1**, Z was found to be 0.5.

The lattice area S calculated by the relation, S = $a \times b$ for compounds **5.1** was found to be 876.03 Å^2.

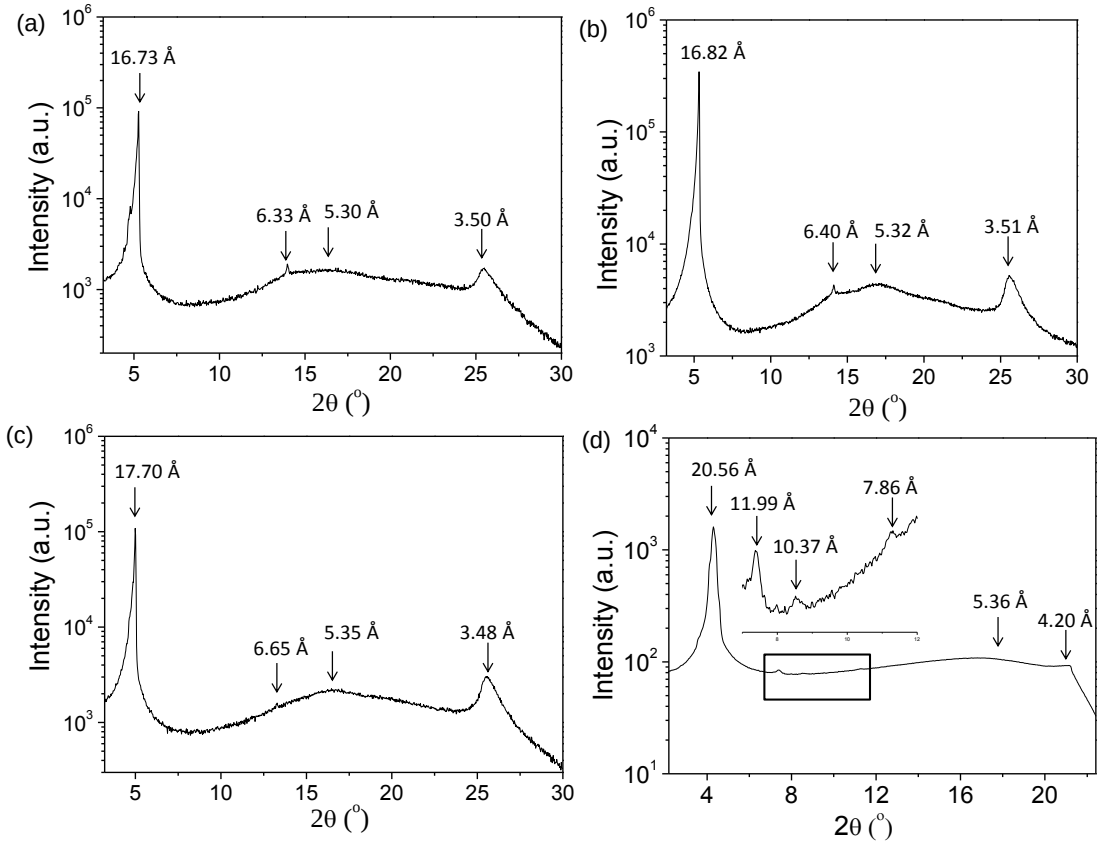

Figure 3.4 X-ray scattering patterns of compounds (a) **7.3** at 135 °C; (b) **7.4** at 200 °C on heating, (c) **7.6** at 120 °C and (d) **7.7** at 140 °C after cooling from isotropic phase.

X-ray scattering pattern of compounds **7.1**, **7.2** and **7.5** consisted of many peaks both in the small and wide angle region, indicating their crystalline nature. One-dimensional intensity *vs.* two theta (2θ) graph derived from the X-ray scattering pattern of compound **7.3** is shown in Figure 3.4a. As can be seen from the Figure, in the small angle region, two reflections, one very strong and one weak are present whose *d*-spacings are in the ratio of 1:1/√7, consistent with a two-dimensional hexagonal lattice. In the wide-angle region, a diffuse reflection appears at 5.30 Å. This corresponds to the liquid-like order of the aliphatic chains. The second peak at *d* = 3.50 Å can be attributed to the core-core separation. The intercolumnar distance, *a*, corresponding to the strongest peak in the small angle region was found to be

19.23 Å. This is 7 % lesser than the fully extended molecule indicating interdigitation of the alkyl chains. All the features fit into the well-known model for the Col_h phase in which the disc-like core of the molecules stack one on top of the other to form columns surrounded by alkyl chains and these columns in turn arrange themselves in a two-dimensional hexagonal lattice. In the X-ray diffractogram of compound **7.4**, the ratio between the scattering spacings of the 100 and 210 reflections of 1 : $1/\sqrt{7}$, typical for a hexagonal phase, is clearly visible (Figure 3.4b, Table 3.2). The reflection at d = 3.51 Å is assigned to be the inter disk distance and indicates that the phase is ordered. The intercolumnar distance, a, was found to be 19.31 Å which is slightly more than compound **7.3** owing to almost similar size of branched chain. A similarly ordered columnar hexagonal phase (Col_{ho}) was assigned to compound **7.6** based on the scattering pattern shown in Figure 3.4c.

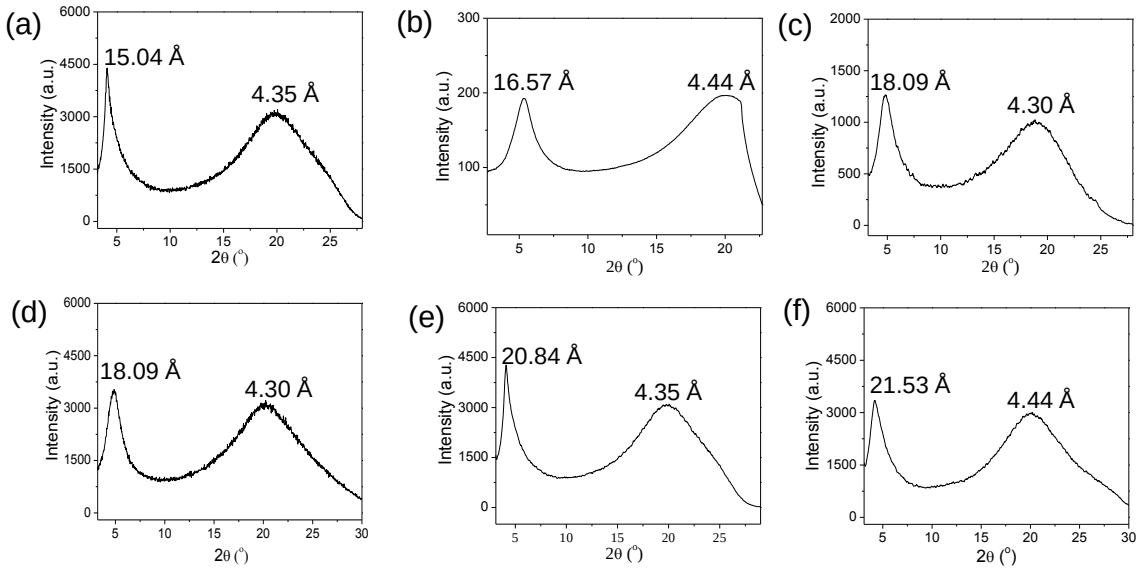

Figure 3.5 X-ray scattering patterns of compounds (a) **6.2** at 90 °C, (b) **6.4** at 80 °C, (c) **6.5** at 138 °C, (d) **6.6** at 105 °C, (e) **6.7** at 125 °C and (f) **6.8** at 100 °C after cooling from isotropic phase.

The X-ray scattering pattern of the compound **7.7** is different from those of the other compounds and consisted of many peaks. Figure 3.4d shows the scattering pattern for compound **7.7** at 140 °C as obtained upon cooling from the isotropic phase. The four Bragg reflections observed in the small angle region can be indexed as 100, 110, 200 and 210 being

in the ratio of 1: 1/√3: 1/√4: 1/√7 according to a two dimensional columnar hexagonal lattice. Surprisingly, for this molecule, the core-core separation was found to be 4.20 Å. This suggested that more number of branching points in the alkyl chains also affect the packing of discs in the mesophase.

The columnar slice thickness h_m or lattice constant *c* is ~3.50 Å for compounds **7.3**, **7.4**, **7.6** and 4.20 Å for **7.7**. The number of molecules per columnar slice of thickness h_m designated as Z was found to be ~ 1. The value of Z suggested that each of the columnar slice is made of single disc only. As the size of the molecules is increasing from **7.3** to **7.7**; lattice area S and columnar cross-section S_{col} is also increasing.

The broad small angle reflection for **6.2** showed a *d*-spacing of 15.04 Å in the mesophase (at 90 °C, Figure 3.6a). This corresponds to the average length and diameter of the rod (~24.4 Å) and discs (~7.6 Å), respectively indicating a molecularly mixed N phase. Obviously, much smaller reflection at small angle than that of the total length of the hybrid confirms the compatibility (homogeneously mixed) of both components (disc and rod) in the mesophase and no nanophase segregation occurs between them. The peak in the wide angle region at *d* = 4.35 Å corresponds to the lateral separation between the rod and disc moieties. Similar type of scattering pattern has been observed for all other compounds of this series, with increasing *d* values corresponding to the peak in the small angle region. The sketch of the molecularly mixed nematic phase in these compounds is shown in Figure 3.6. Although biaxiality is likely to be seen at small length scales, as a result of large aspect ratios between two components, there is no direct evidence for the formation of biaxial N phase in our study.

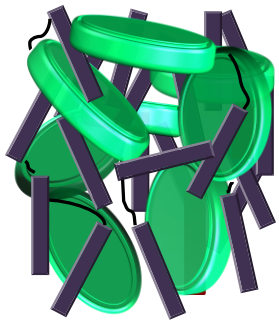

Figure 3.6 Sketch of the molecularly mixed nematic phase in compounds **6.2**, **6.4**-**6.8**.

3.3.4 Photophysical properties in $CHCl_3$

The optical properties of **5-7** were investigated by UV-vis and fluorescence spectroscopy. All the compounds exhibited yellowish-green fluorescence even under daylight conditions (Figure 3.7). All these compounds exhibited good solubility in solvents such as CH_2Cl_2, $CHCl_3$, acetone, ethylacetate, THF except for compound **6.3**. These derivatives were found to be insoluble in solvents such as methanol, ethanol, acetonitrile, hexane and water. The absorption spectra of mesogens **5.4**, **6.6** and **7.6** (as a representative case) in $CHCl_3$ at a concentration of 15×10^{-6} M is depicted in Figure 3.7 and optical data of all the compounds is summarized in Table 3.3. The absorption spectra of all the compounds exhibited the well-resolved vibronic structure of three bands at 416, 442 and 472 nm with increasing intensity representing the 2-0, 1-0 and 0-0 transitions, (designation of the transitions was carried out according to Spano and co-workers[54]) respectively. The S_0-S_1 band of the perylene chromophore polarized along the long molecular axis was observed with bands at 260, 269 and 278 nm for triphenylene moieties in **5.4** and at 296 nm for biphenyls in **6.6**.

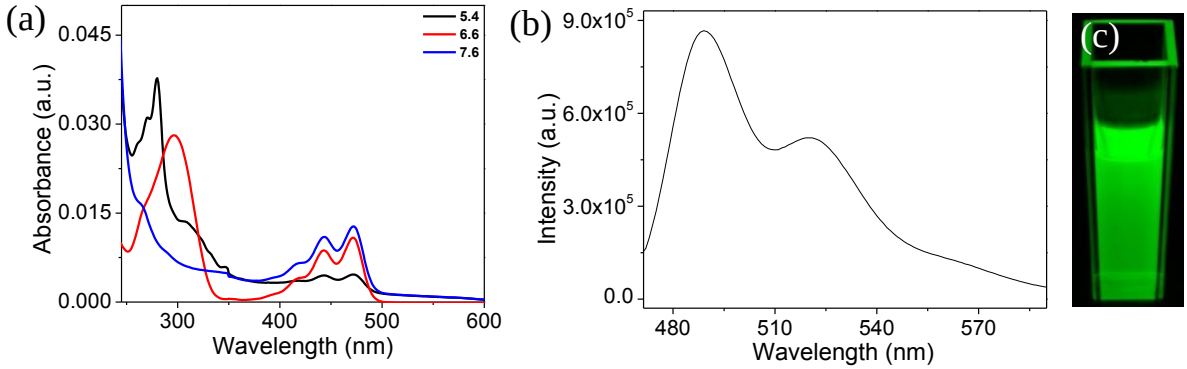

Figure 3.7 (a) UV−vis absorption spectra of **5.4** (black line), **6.6** (red line), **7.6** (blue line) and (b) representative emission spectra of **5.4** in 15 µM $CHCl_3$ solution. (c) Picture of µM solution of compound **5.6** in $CHCl_3$ under day-light conditions.

The fluorescence spectrum depicts the same peak structure in a mirror image of the absorption and displays two bands at ~ 490 and 519 nm with a stock shift between 15-20 nm for all the compounds. The overall shape of both UV-vis and fluorescence spectra, with the

0-0 transition being the strongest, suggested that in dilute solutions perylene molecules exist in non-aggregated state.[55-57]

Table 3.3 Summary of photo-physical properties of compounds **5.1**-**5.5**, **6.2**, **6.4**-**6.8** and **7.3**-**7.7**.

Mesogen	Absorption[a] (nm)	Emission[a,b] (nm)	Stokes shift (nm)	r_{av}[c] (ns)	Anisotropy	Band gap[d,e] (eV)
5.1	473, 444, 421, 346, 307, 280, 271, 260	487, 519	14	0.91	0.215	2.45
5.2	472, 443, 416, 346, 308, 280, 271, 261	490, 519	18	1.37	0.174	2.44
5.3	472, 443, 415, 346, 308, 280, 271, 261	491, 519	19	1.46	0.167	2.45
5.4	471, 443, 416, 346, 309, 280, 271, 261	489, 518	18	1.61	0.161	2.47
5.5	472, 442, 416, 346, 308, 280, 271, 261	489, 521	17	2.17	0.149	2.45
6.2	472, 443, 417, 296	490, 521	18	4.33	0.045	-
6.4	472, 443, 415, 296	488, 519	16	4.33	0.042	-
6.5	472, 443, 414, 296	488, 520	16	4.11	0.049	-
6.6	472, 443, 414, 297	488, 520	16	4.14	0.046	-
6.7	472, 443, 416, 296	489, 519	15	4.15	0.048	-
6.8	472, 443, 417, 296	488, 520	16	4.09	0.049	-
7.3	471, 443, 415	491, 519	20	4.11	0.015	2.45
7.4	471, 442, 415	491, 519	20	4.36	0.014	2.47
7.6	471, 443, 413	489, 519	18	4.12	0.018	2.46
7.7	472, 443, 415	489, 519	17	4.04	0.018	2.45

[a]Measured in $CHCl_3$ solution of at concentrations of approximately 15×10^{-6} M. [b]Excitation wanvelength is ~ 470 nm for all compounds. [c]Average Fluorescence life time. [d]Optical energy gap from the onset of absorption in solution from UV-vis data. [e]Not calculated for compounds **6.2**, **6.4**-**6.8**.

Evidence for the self-association behavior of **5.4** in $CHCl_3$ solution was provided by ^1H NMR spectrum at different concentrations (Figure 3.8). It has been well established that an upfield shift of aromatic proton signals is a signature of intermolecular association involving π-stacking interaction. Upon increasing the concentration from 0.81 to 13.61 mM at r.t., the

resonance of protons in **5.4** is upfield shifted by 0.02 ppm (from 8.26 to 8.24 ppm). However, for compound **7.6**, an upfield shift of 0.13 ppm (from 8.40 to 8.27 ppm) is recorded upon increasing concentration from 1.09 to 13.51 mM (Figure 3.8b). The upfield shifts of the aromatic proton resonances in concentrated solutions reflect a typical co-facial molecular stacking of aromatic cores. This co-facial stacking of perylene core in the concentrated solution was found to be more for **7.6** than for **5.4**, probably because of the triphenylene discs, perylene moieties are not in the same plane, leading to lesser interactions. Ghosh *et al.*[58] found that for perylene bisimides, no aggregation occurred in chloroform and this was attributed to the solvation of the π-cloud. In our case, we have observed that no aggregation occurred in chloroform in dilute conditions. However, significant changes in the chemical shifts have been observed when the concentration was increased.

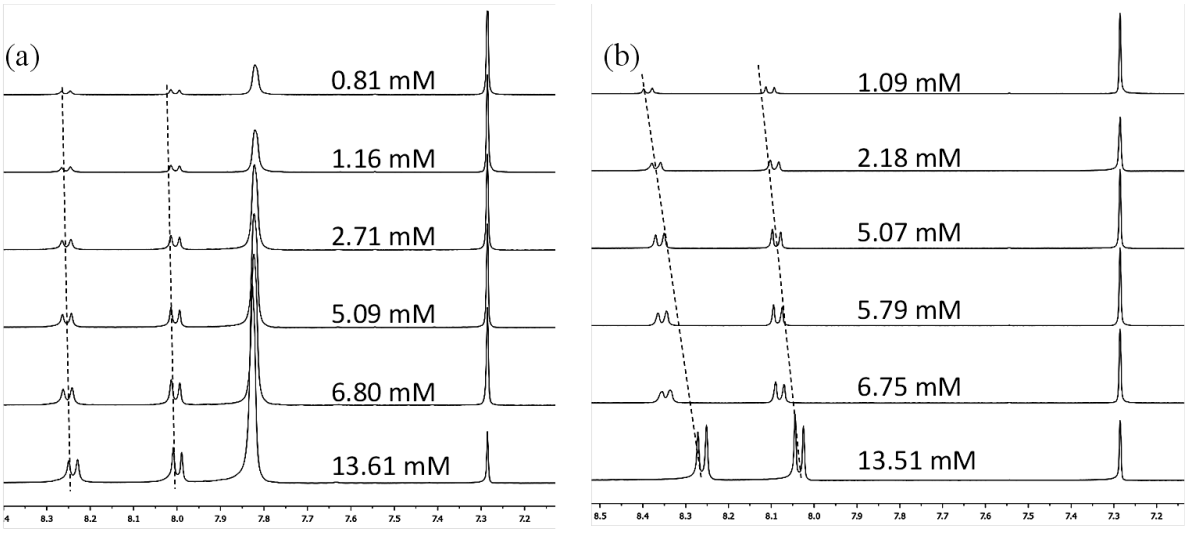

Figure 3.8 Aromatic region of ^{1}H NMR spectra of (a) **5.4** and (b) **7.6** recorded at various concentrations in $CDCl_3$ solution at r.t., 400 MHz.

The fluorescence quantum yields[59] of **5.4** and **7.6** were calculated in $CHCl_3$ solvent using quinine sulphate as the standard ($\Phi_r = 0.52$ in 0.1 N H_2SO_4) and the following equation:

$$\Phi_s = \Phi_r [F_s A_r / F_r A_s] (n_s/n_r)^2$$

Where Φ denotes the quantum yield, F is the integrated area under the fluorescence spectrum, n is the refractive index of solvent and A is the absorbance at the excitation wavelength. The

subscript r and s denote the reference and the sample. The quantum yields are given in Table 3.4. It is seen that quantum yield depends on the concentration of the sample and decreases with an increase in concentration in both cases. This can plausibly be due to the quenching of the excitation energy with increasing concentration.[60] Due to the high quantum yields in the diluted solutions, they could be used as standards for quantum yield measurements because of their high solubility in organic solvents (at 471-473 nm).

Table 3.4 Quantum yield of **5.4** and **7.6** in $CHCl_3$ at different concentrations.

Concentration	Quantum Yield
5.4	
7.64×10^{-7} M	1.01
2.29×10^{-6} M	0.53
3.01×10^{-6} M	0.49
7.6	
2.98×10^{-6} M	0.91
5.96×10^{-6} M	0.45
8.94×10^{-6} M	0.31

The optical energy gap was calculated from the onset of absorption in $CHCl_3$ and was found between 2.45-2.47 eV for compounds **5** and **7** which is comparable to the literature known perylene derivatives.[61]

In order to understand the changes in the nano-environment of the perylene-based hybrid fluorophores and their ordered molecular system, fluorescence lifetime (r_{av}) and steady state anisotropy measurements were performed in dilute solution (Table 3.3, 15 μM in $CHCl_3$). Interestingly, except for **5.1**-**5.5**, the measured life time in all other hybrids is close to 4 ns whereas, measured life time value reported for perylene is 5.2 ns in ethanol solution.[62] The observed decrease in the fluorescence life time could be due to higher non-radiative rate involved in the processes due to a change of size and shape of the hybrid molecules and thus molecular interactions. Surprisingly, among all the synthesized perylene hybrids, we noted a

high value of fluorescence anisotropy and shortest fluorescence lifetime in case of compounds **5.1**-**5.5**. We hypothesized that bulky triphenylene units attached to perylene core resulted in restricted molecular motion of the hybrid and thus increased fluorescence anisotropy. The lower anisotropy observed for compounds with branched chains could be due to higher rotational diffusion (because of less rigid molecular environment) that may occur during the lifetime of the excited state and displaces the emission dipole of the fluorophore. Further, we have observed that with increasing size of the molecule from **5.1** to **5.5**, the fluorescence lifetime was increasing. But, the anisotropy values are decreasing. However, in compounds with cyanobiphenyl moieties **6.1**-**6.8**, r_{av} decreases with increasing spacer length but, the values remain close to 4 ns (decrease is not significant as in case of triphenylene series) and the anisotropy values remain almost same.

3.3.5 Aggregation behavior in binary THF/water mixtures

The polarity of the solvent is gradually changed by the addition of water to the stock of 10 μM THF. We have investigated the influence of solvent polarity on the aggregation behavior of **5.4** using different concentrations of THF with water and compared with the aggregation behavior of compound **7.6**. Herein, we have made use of dilution method, in which specific amount of water was added to pure THF stock solution. All the samples were kept properly sealed to avoid unwanted evaporation of THF during the observation period.

Although aggregation of **5.4** and **7.6** does not occur in the non-aqueous solvents at very low concentrations, addition of water promoted the self-assembly in these two cases. Figure 3.9a,b shows that by adding increasing amount of water to the stock THF solution, the absorption spectra considerably changed. It is seen that on increasing water concentration, the intensities of the peaks gradually decreased and the spectral response becomes broader (starting from 7×10^{-6} M).[59,63] Also, with increasing water content, the intensities of 0-0 and 0-1 peaks became equal (at 4×10^{-6} M) and then intensity of 0-1 started increasing (at 3×10^{-6} M). The blue shift in the absorption maxima from 471 nm to 420 nm confirms the mode of aggregation being H-type.[64] However, the emission spectra in the binary solvent displayed complete quenching of the fluorescence intensity in 1:1 mixture of THF and water may be due to π-π electronic coupling.[26] Figure 3.9c,d indicates that dilution of the stock solution

with THF didn't lead to broadening of the spectral response which indicated that stacking occurs with the addition of a non-solvent that can-not dissolve the π-aggregates.

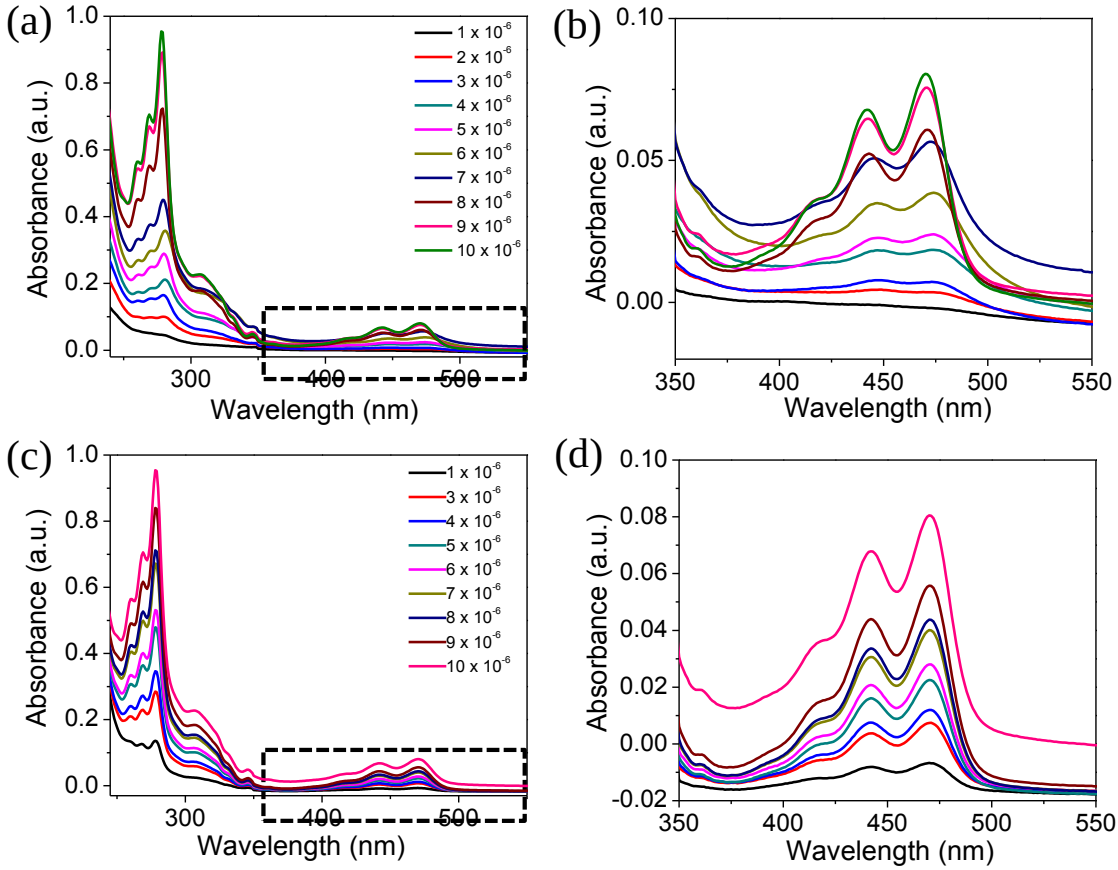

Figure 3.9 UV-vis spectra of titration of a 10 μM stock solution of **5.4** in THF (a) with water; (b) the corresponding enlarged portion between 350-550 nm; (c) with THF and (d) the corresponding enlarged portion between 350-550 nm (different concentrations were prepared by dilution of stock solution with water/THF).

The same trend has also been observed for compound **7.6** (Figure 3.10). Here also, with increasing water content, the intensities of 0-0 and 0-1 peaks became equal (at 4×10^{-6} M) and then intensity of 0-1 started increasing (at 3×10^{-6} M). The blue shift in the absorption spectra indicated the formation of H-type aggregates.[65-67] A comparison of similar dilution with THF indicated that spectral broadening occurred in case of water only.

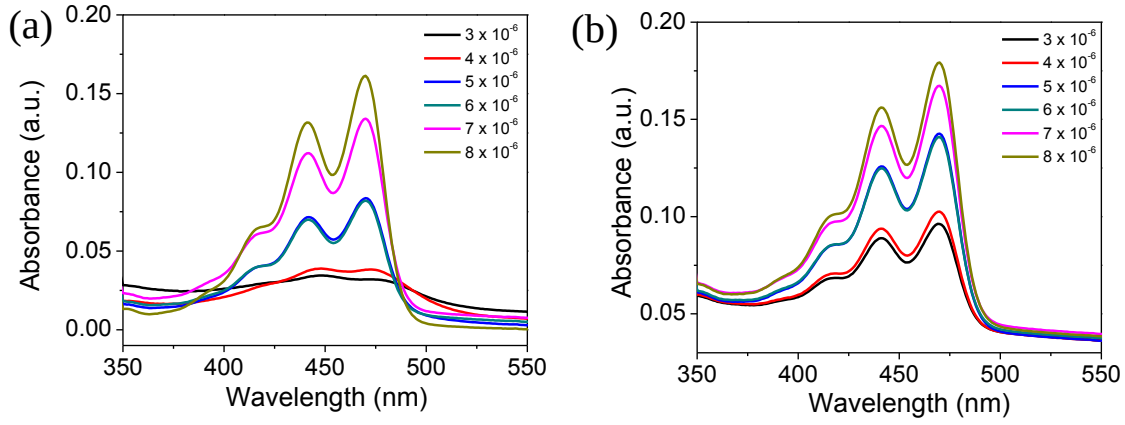

Figure 3.10 UV-vis spectra of titration of a 10 μM stock solution of **7.6** in THF (a) with water and (b) with THF (different concentrations were prepared by dilution of stock solution with water/THF).

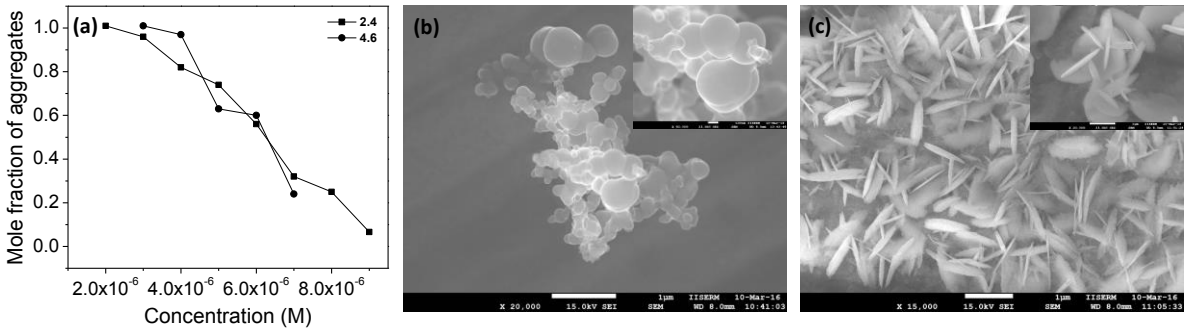

Figure 3.11 (a) Mole fraction of aggregates (α_{agg}) as a function of THF/water composition for compounds **5.4** and **7.6**. SEM images of the morphologies of the microstructures formed by slowly evaporating water/THF (90% addition of water to 10 μM THF stock) mixture of compound (b) **5.4** and (c) **7.6**.

The mole-fraction of aggregates[58,59] was estimated for both the compounds in THF-water mixtures by using the following relation:

$$\alpha_{agg} \approx (A_{mix}(T) - A_{nonagg}) / (A_{agg} - A_{nonagg})$$

Where, α_{agg} is the mole fraction of the aggregates at temperature T;

A_{mix} (T) is the absorbance at λ_{max} of the monomer at a given mixture of solvent;

A_{nonagg} and A_{agg} are the absorbances of the non-aggregated state and of the maximum aggregated states, respectively.

It can be seen from Figure 3.11 that for **5.4**, α_{agg} increases almost linearly with increasing water content and for **7.6**, this increase is abrupt. SEM images of the morphologies of the microstructures formed by slowly evaporating water/THF (90% addition of water to 10 µM THF stock) mixture of compound **5.4** and **7.6** indicates the presence of globular aggregates and needle shaped crystals as shown in Figure 3.11.

3.3.6 Characterizing molecular packing in the solid state

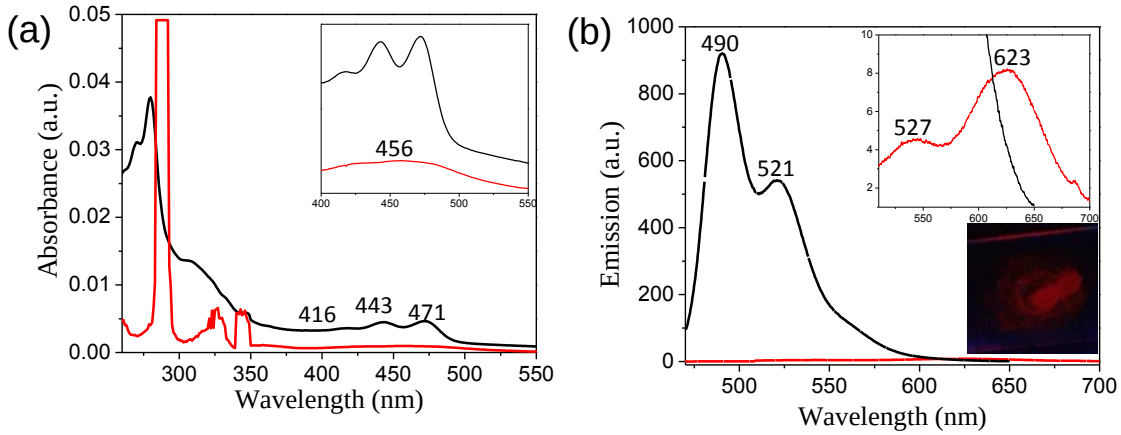

Figure 3.12 (a) Absorption and (b) emission spectra obtained for compound **5.4** in micromolar $CHCl_3$ solution (black trace) and in thin film (red trace) prepared from millimolar $CHCl_3$ solution. The inset in (b) corresponds to the pictures of same thin film of compound **5.4** as seen with the illumination of 365 nm UV light.

Figure 3.12 shows the absorption and emission spectra of a thin film of **5.4** prepared by drop-casting millimolar solution of compound in chloroform and its comparison with the solution state. Compared to the solution state, only a single band has been observed in the solid state at 456 nm in the absorption spectrum. This band is blue shifted compared to the maxima of the solution state (~ 15 nm). Even more interesting than the changes to the UV-vis absorption

spectra in the solid state are those of the emission spectra. Depending on the ratio of aggregated *vs.* total dye molecules, i.e., mole fraction of aggregation, α_{agg}, the color of the emitted light changes from green (α_{agg}, 0.3) to yellow ($\alpha_{agg} \approx 0.7$), orange ($\alpha_{agg} \approx 0.8$) and red ($\alpha_{agg} > 0.9$).[68]

As can be seen in Figure 3.12b, appearance of a new band at 623 nm and red shift of the monomer band at 521 to 527 nm can be attributed to the aggregate emission and the red color suggested that here $\alpha_{agg} > 0.9$. Moreover, the absorbance intensity is lesser compared to the solution state. The thin film showed very weak luminescence under UV light of 365 nm wavelength indicating that aggregation leads to quenching of fluorescence. Both spectral features are indicative of a close face-to-face stacking of the chromophores i.e., the formation of H-shaped aggregates.

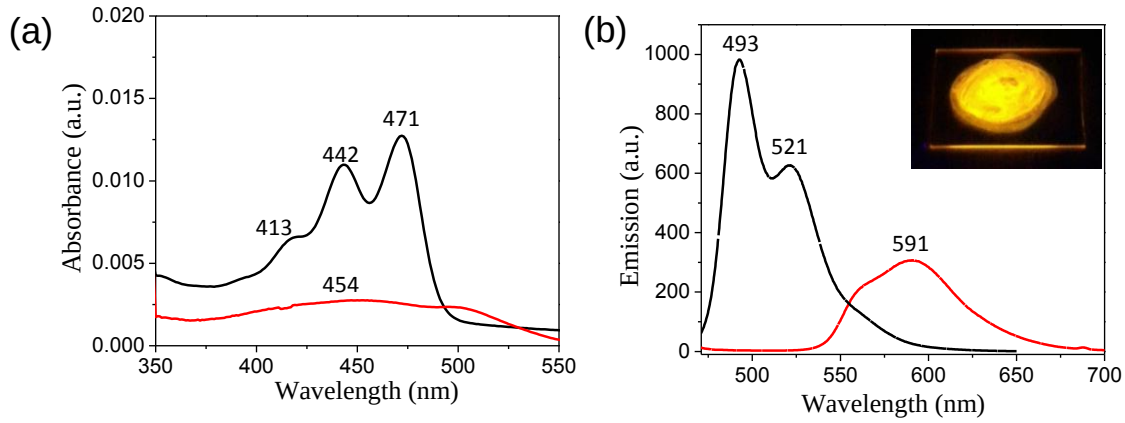

Figure 3.13 (a) Absorption and (b) emission spectra obtained for compound **7.6** in micromolar $CHCl_3$ solution (black trace) and in thin film (red trace) prepared from millimolar $CHCl_3$ solution. The inset in (b) corresponds to the pictures of same thin film of compound **7.6** as seen with the illumination of 365 nm UV light.

In case of compound **7.6**, the absorption spectra showed a similar blue shift of the maxima to 454 nm (~ 13 nm shift) in the solid state (Figure 3.13). The emission spectra revealed the presence of a broad band at 591 nm and yellow emission of the thin film in the 365 nm UV light suggested that here degree of aggregation is lesser as compared to **5.4**. These spectral

features suggested the presence of H-type aggregates in this molecule. AFM imaging of the thin film of these compounds also revealed the presence of aggregates (Figure 3.14).

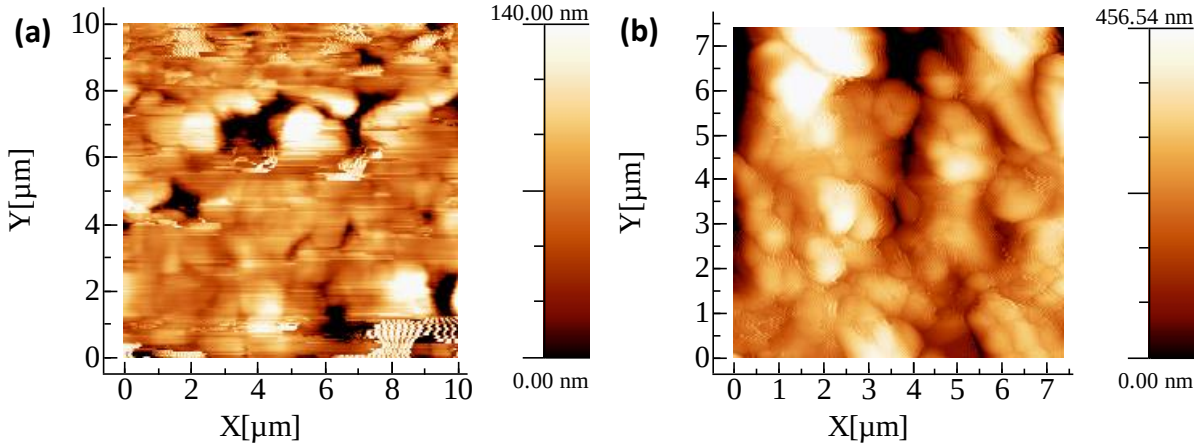

Figure 3.14 AFM topography image of the drop casted film of compound (a) **5.4** and (b) **7.6**.

3.3.7 Electrochemical properties

The electrochemical behavior of the perylene-triphenylene hybrid **5.4** and branched chain substituted derivative **7.6** was studied by cyclic voltammetry in 0.1 M tetrabutylammonium perchlorate (TBAP) as a supporting electrolyte in dry DCM, as shown in Figure 3.15. A single compartment cell equipped with $Ag/AgNO_3$ (0.1 M) reference electrode, platinum rod counter electrode and glassy carbon working electrode was used for the experiments. The reference electrode was calibrated with the ferrocene/ferrocenium (Fc/Fc^+) redox couple (absolute energy level of -4.80 eV to vacuum). The cyclic voltammograms were recorded with a scanning rate of 0.1 Vs^{-1}. According to the cyclic voltammogram, anodic and cathodic peak potential responses are observed corresponding to electrochemical oxidation and reduction processes. Both the compounds showed one oxidation potential and one reduction potential. The LUMO energy levels were calculated using the formula E_{LUMO} = -(4.8 - $E_{1/2,Fc,Fc}^{+}$ + $E_{red,onset}$) eV, whereas the HOMO energy levels were measured using the formula E_{HOMO} = -(4.8 - $E_{1/2,Fc,Fc}^{+}$ + $E_{oxd,onset}$) eV.[69-72] The HOMO and LUMO levels for compound **5.4** were found to be around −5.94 and −3.67 eV and the HOMO-LUMO gap was found to be 2.27 eV. For compound **7.6**, the HOMO and LUMO levels were found to be around – 6.14 and – 3.71 eV and the HOMO-LUMO gap was found to be 2.43 eV. A comparison of band

gaps *via* UV-vis and CV indicated that calculated absolute values of band gaps by CV are lesser as compared with UV-vis.

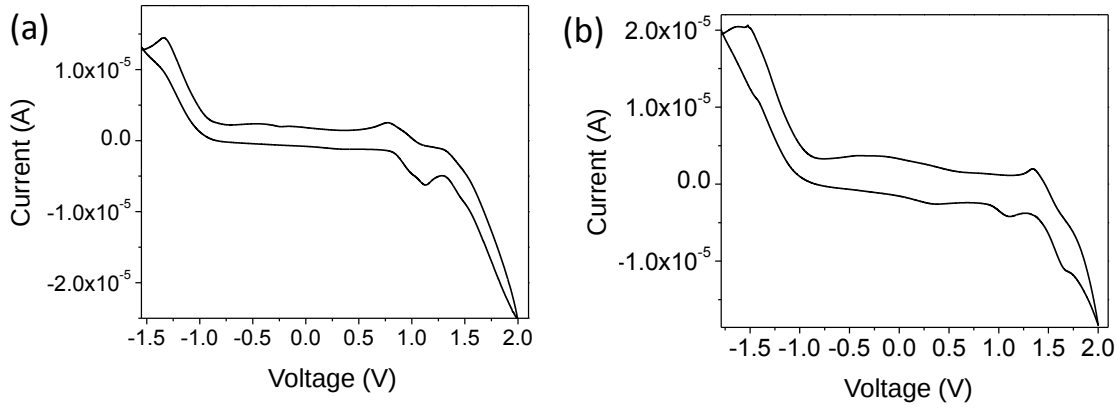

Figure 3.15 Cyclic Voltammogram of compound (a) **5.4** and (b) **7.6** in HPLC DCM solution of TBAP (0.1 M) at a scanning rate 0.1 V/s.

3.3.8 Surface manometry and Brewster angle microscopy

The surface pressure (π) - area per molecule isotherms recorded for compounds **5.3**, **5.5**, **6.2**, **6.4**, **6.5** and **6.8** at air-water interface at room temperature with a compression speed of 10 mm min^{-1} are presented in Figure 3.16. For perylene-triphenylene hybrids **5.3** and **5.5**, isotherm indicated that collapse pressure is lower compared to perylene-cyanobiphenyl derivatives **6.2**, **6.4**, **6.5** and **6.8.** For compound **5.3** and **5.5**, the isotherm showed a gradual rise up to 5 mN/m and 8 mN/m, respectively followed by a sharp rise. For compound **5.3**, isotherm exhibited a collapse pressure of about 19 mN/m. The area per molecule[73] calculated by extrapolating the corresponding region of the isotherm to the zero surface pressure spans a value of 2.52 nm^2. This value gives an estimate of the average area occupied by the individual molecules in the monolayer. Taking the measured limiting area of a "face on" orientation of this molecule to be 15 nm^2, albeit somewhat imperfectly, one can exclude the possibility of arrangement of these molecules to be "face on" on water subphase. From this, we infer that probably the molecules are arranging themselves in an edge on arrangement as shown in Figure 3.17. Similarly, for molecule **5.5**, the isotherm showed a collapse around 27

mN/m. The limiting area of 4.1 nm^2/molecule was found to be in agreement with the edge-on arrangement of the triphenylene moieties.

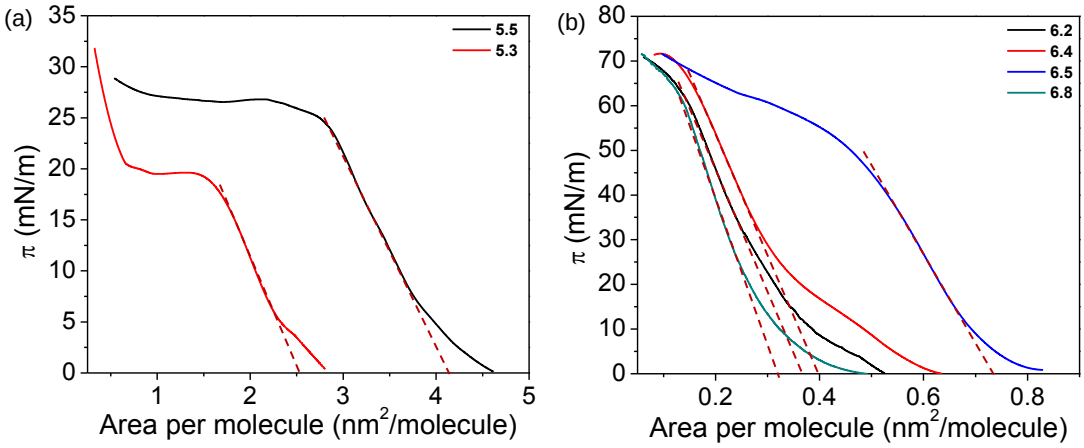

Figure 3.16 The surface pressure (π)- area per molecule isotherms obtained for compounds **5.3**, **5.5**, **6.2**, **6.4**, **6.5** and **6.8** at air-water interface at room temperature.

Compounds **6.2**, **6.4**, **6.5** and **6.8** with cyanobiphenyl moieties attached to perylene, exhibited collapse at a pressure of 71 mN/m. The high collapse pressure compared to the perylene-triphenylene hybrids can be due to the presence of highly polar cyano groups and strong inter-chain interactions between the cyanobiphenyl moieties.[73] Compound **6.4** with octyl spacer indicated a first change in the slope at a pressure of 20 mN/m. The surface pressure then rises rapidly till the monolayer collapses at around 71 mN/m. The extrapolation to the zero surface pressure of the rapidly increasing surface pressure region of the isotherm yields an area per molecule of around 0.40 nm^2. For a face-on conformation of the perylene-cyanobiphenyl molecule **6.4** on the water surface, the average molecular area should be around 6 nm^2. However, the area per molecule found is much lesser than the face on conformation. This can be accounted for by the edge on conformation of the molecules on the water surface, similar to the perylene-triphenylene hybrids.

Compound **6.2** with hexyl spacer exhibited a first change in the slope at 15 mN/m and then monolayer rose rapidly. For this compound, the area per molecule was found to be 0.39 nm^2. Hence, this molecule also existed in the edge on conformation similar to compound **6.4**. Compound **6.8** with dodecyl spacer showed a first slope change at 20 mN/m. The area per

molecule of 0.36 nm^2 confirmed an edge on conformation. We hypothesized that owing to the long spacers, this compound arranges itself in an ordered monolayer and hence, the area per molecule is lesser compared to oligomer **6.4**.

Compound **6.5** with nonyl spacer (odd) showed first slope change at 15 mN/m and then an abrupt rise in surface pressure similar to other compounds of this series. Surprisingly, the area per molecule for this compound was found to be 0.76 nm^2, which is almost double than that observed for the other three compounds. This diverse behavior can be correlated to the presence of odd spacer in this molecule which disrupts the packing. Hence, the inefficient packing of this molecule led to increase of the area per molecule as compared to others.

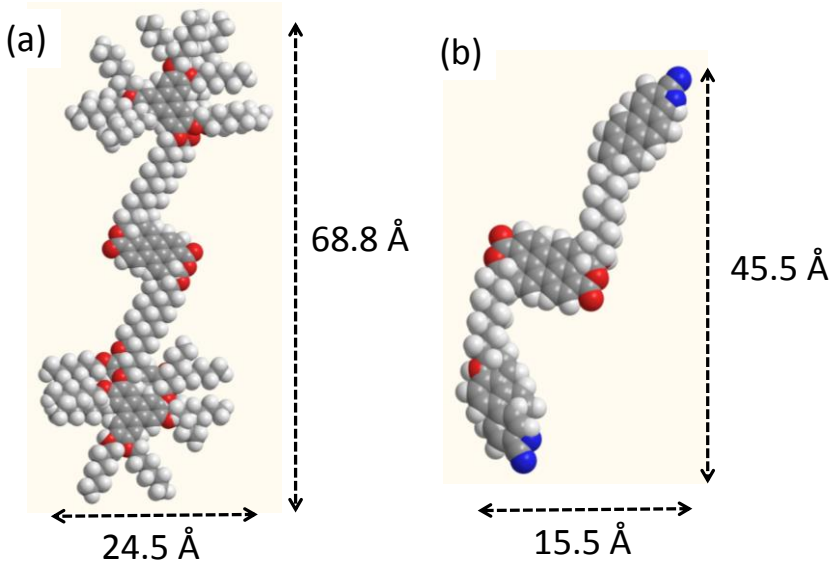

Figure 3.17 Approximate molecular dimensions of compounds (a) **5.5** and (b) **6.4** calculated using chem draw software.

The observations under Brewster angle microscopy (BAM) for compound **5.5** as a representative case indicated that for area per molecule greater than 4.5 nm^2, partially dark and grey regions existed indicating a two phase region. With compression, BAM images showed that the two phase region transformed to uniform grey region (Figure 3.18b). On further compression, BAM images showed bright regions indicating the collapse of the monolayer (Figure 3.18c). For compound **6.4**, at area per molecule of 0.61 nm^2, BAM images

showed the coexistence of partially dark and grey regions similar to compound **5.5**. At area per molecule of 0.35 nm^2, a very uniform grey colored region was observed corresponding to monolayer state. On further compression, the brightness increases gradually. The completely bright regions as shown in Figure 3.19c correspond to the collapse state.

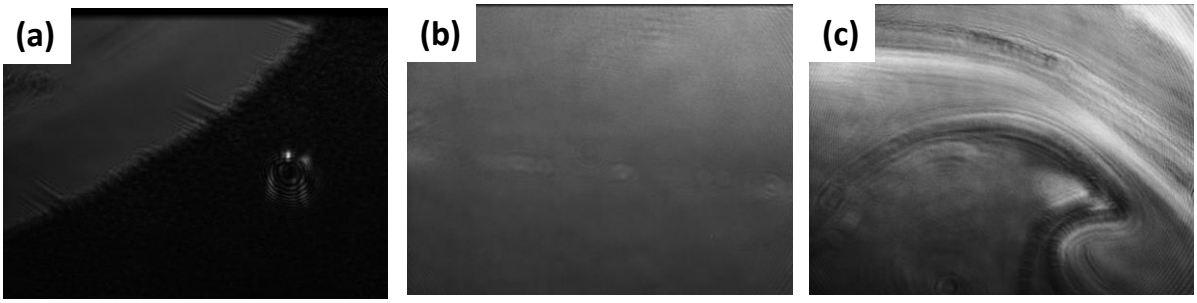

Figure 3.18 BAM images of the perylene-triphenylene oligomer **5.5** at air-water interface. (a) two phase region at area per molecule of 4.3 nm^2, (b) uniform grey region at an area per molecule of 3.5 nm^2 and (c) collapsed film at 27 nm^2. Here all images are of dimension 1010 × 900 µm.

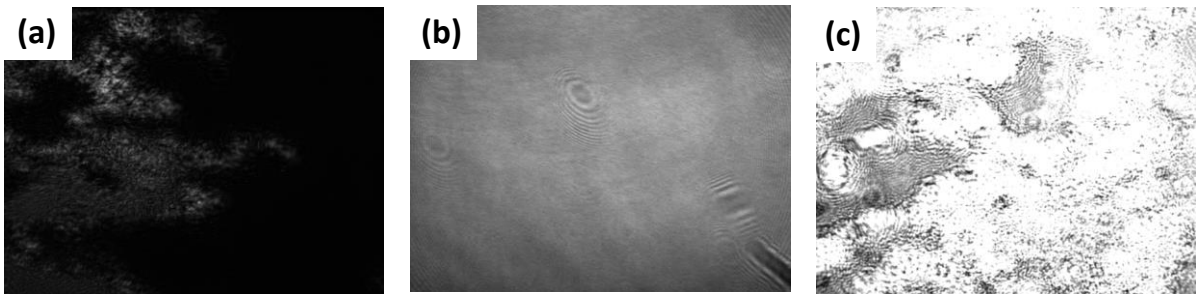

Figure 3.19 BAM images of the perylene-cyanobiphenyl oligomer **6.4** at air-water interface. (a) two phase region at area per molecule of 0.61 nm^2, (b) uniform grey region at an area per molecule of 0.35 nm^2 and (c) collapsed film at 0.15 nm^2. Here all images are of dimension 1010 × 900 µm.

3.3.9 Atomic Force Microscopy (AFM)

In order to obtain the morphology and film structure at air-solid interface, AFM studies of the LB monolayer of compounds **5.5** and **6.4** transferred onto a ITO coated hydrophilic glass

substrate at a target pressure of 20 and 40 mN/m, respectively were carried out. The deposition of a single layer of LB films was done by a single upstroke of the dipper in a vertical direction. We have employed non-contact mode of AFM to obtain the topography image of the film at air-solid interface. Figure 3.20 shows the stability measurement of the films of both the compounds at the air-water interface.

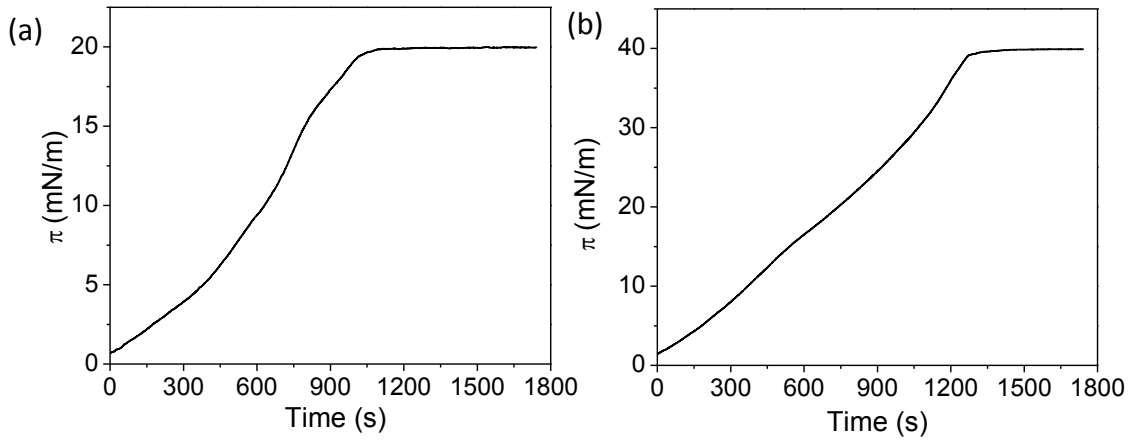

Figure 3.20 Stability measurement of the film of compound (a) **5.5** and (b) **6.4** at air-water interface at a control pressure of 20 and 40 mN/m, respectively.

The AFM topography image of compound **5.5** (Figure 3.21a) shows bright domains grown over a less bright background. The average height of such bright domains is 6.5±0.3 nm. With the alkyl chains fully stretched and in all-trans conformation, the value turns out to be ~ 6.8 nm to a vertical orientation of this molecule. The average height of the less bright region is around 4.0±0.5 nm. This can be accounted for by a tilt of the molecules.[74] The bright domains do not show any preferential growth direction and are found to be grown randomly. This feature has been observed earlier for tricycloquinazoline-cyanobiphenyl hybrids.[74]

The AFM topography image of compound **6.4** (Figure 3.21b) shows the height of the film to be about 5.0 ±0.3 nm. For comparison, we estimated the height of a single molecule using ChemDraw software (Figure 3.17). With the alkyl chains fully stretched and in all-trans conformation, the value turns out to be ~ 4.7 nm to a vertical orientation of this molecule. So,

in this case, all the molecules were found to be in the same orientation as compared to compound **5.5**.

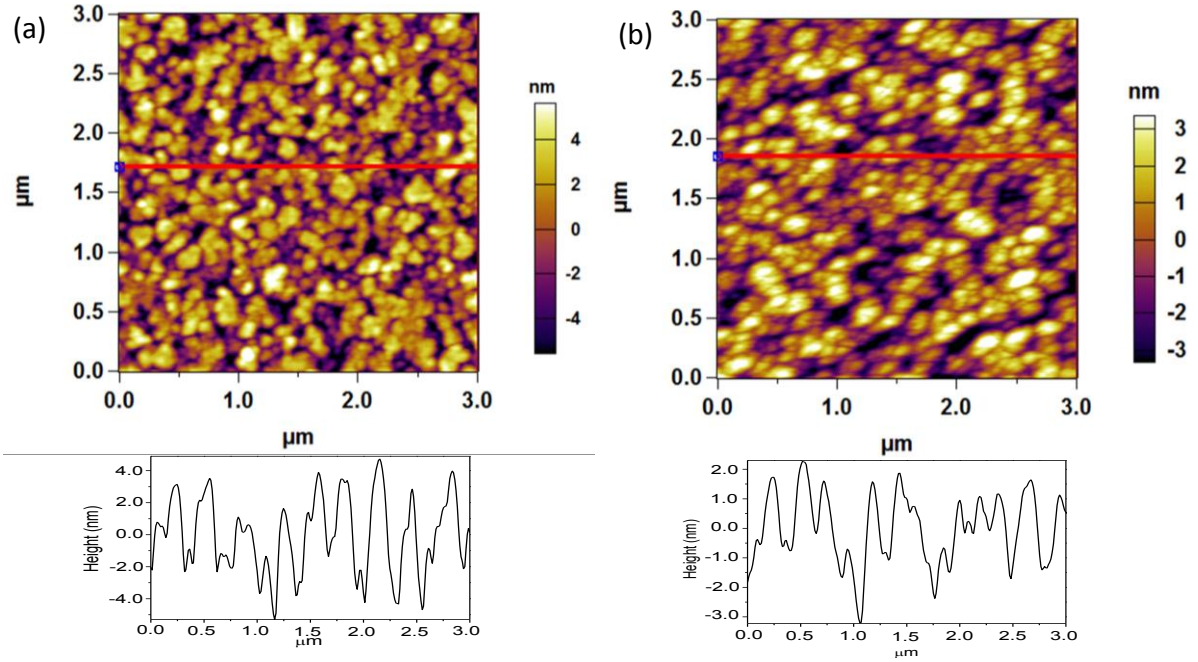

Figure 3.21 Non-contact mode AFM mode topography image of monolayer of compound (a) **5.5** and (b) **6.4** on ITO-coated glass substrate transferred at a surface pressure of 20 and 40 mN/m, respectively.

3.3.10 Current sensing atomic force microscopy (CS-AFM)

For the measurement of nanoscale electrical conductivity across the thin films, we have carried out the CS-AFM studies in contact mode for samples **5.5** and **6.4** being room temperature LC. We have studied the electrical conductivity across LB monolayer films deposited on ITO coated glass substrates. The conducting tip-LB monolayer-conducting substrate forms a system of M-I-M junction. Voltage bias was applied to the substrate and current was measured at the tip. The tip was placed at different places on the sample surface to carry out the I-V measurements. A voltage ramp of -2.0 to + 2.0 V was applied with a scan rate of 1 Hz and current was measured at the tip. Figure 3.22 reveals the non-linear I-V characteristics of the M-I-M junction formed by the monolayer between conducting substrate (**5.5**) and conducting tip. Electrical conductivity between two electrodes separated by an

insulating film can be either due to Schottky emission or electron tunneling. The shape of the I-V curves suggests a tunneling barrier to electron transport exists at the interface of monolayer and the metal electrodes as reported earlier for ferritin-gold[75] as well as triphenylene polymer-gold[76] systems. Thus the electrical conductivity through the metal-monolayer-metal junction herein is dominated by tunneling process rather than the thermionic emission.[75] The tunneling process can be either injection tunneling or direct tunneling. So, in order to find the possible charge transport mechanism, we have plotted variation of $\ln(I/V^2)$ against 1/V as shown in Figure 3.22b. The logarithimic variation of $\ln(I/V^2)$ against 1/V suggest direct tunneling to be the best possible mechanism.[77]

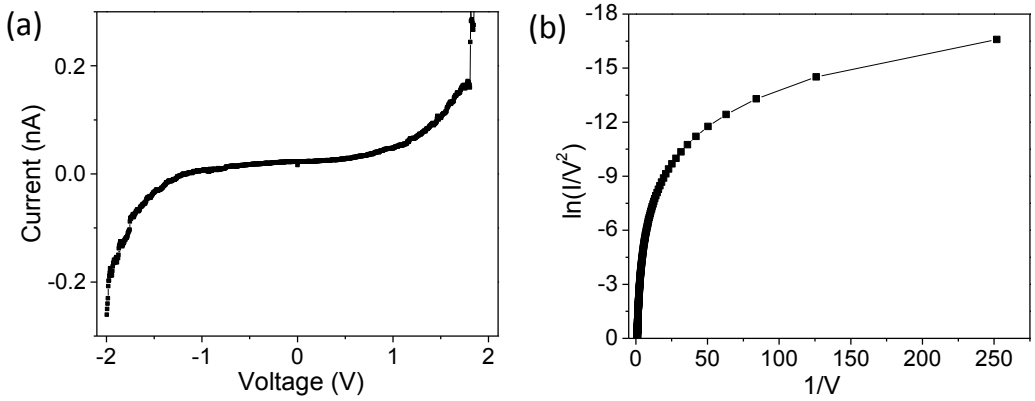

Figure 3.22 (a) The AFM I-V measurements of monolayer of compound **5.5** deposited on ITO coated glass slide. (b) Variation of $\ln(I/V^2)$ as a function of 1/V.

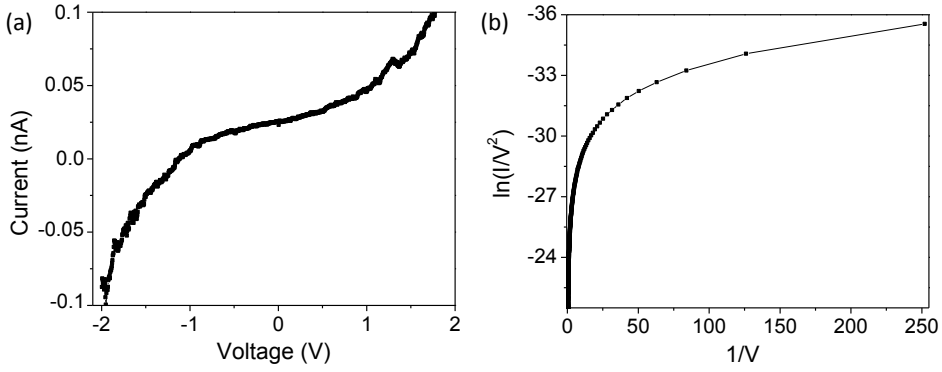

Figure 3.23 (a) The AFM I-V measurements of monolayer of compound **6.4** deposited on ITO coated glass slide. (b) Variation of $\ln(I/V^2)$ as a function of 1/V.

The I-V characteristics of the M-I-M junction formed by the monolayer between compound **6.4** and conducting tip are shown in Figure 3.23. The non-linear shape of the I-V curves suggests a tunneling barrier to electron transport similar to compound **5.5**. However, the current values measured for this compound **6.4** (~ 0.1 nA) were found to lesser than compound **5.5** (0.2 nA). Figure 3.22 shows the variation of $\ln(I/V^2)$ against 1/V which suggest direct tunneling to be the best possible mechanism for the charge transport for this molecule also.[77]

3.3.11 Characterizing perylene-cyanobiphenyl doped 5CB LC films for LC displays

As already mentioned above that compound **6.4** i.e., perylene-cyanobiphenyl oligomer shows nematic mesophase at room temperature and also shows green fluorescence. We hypothesized that if this LC can be used in the LC mixture of the LC display, then it might serve as a source of green light in the display, as **6.4** exist in the room temperature nematic phase which is required for the LC display. It is well known that the LCs used in the LC display does not produce light by itself. Each pixel of the colored LC display contains red, blue and green sub-pixels which together create full picture. For this, we have doped 4'-pentyl-4-cyanobiphenyl (5CB, one of the component of the LC mixture of LC display) with 1 wt% of compound **6.4**.

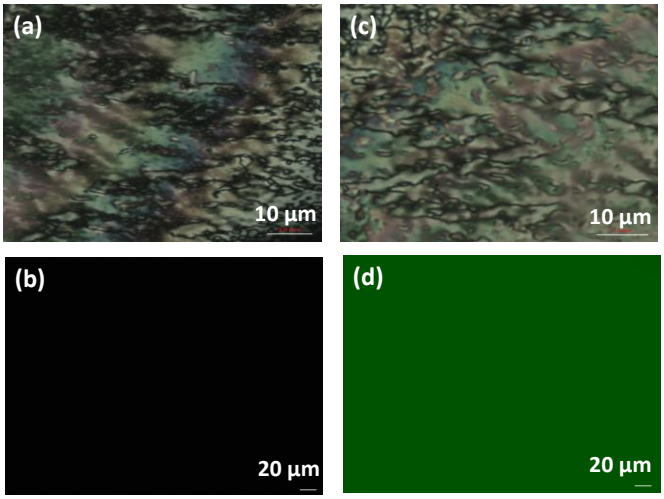

Figure 3.24 Polarizing optical and epi-fluorescence micrographs (below) of (a), (b) 5CB and (c), (d) 1 wt % PE8CB doped 5CB.

In order to see whether LC properties of 5CB are still retained, we have observed both doped and undoped 5CB LC under POM. Figure 3.24 indicated that the textures of 5CB and 1 wt % doped 5CB are similar at room temperature.

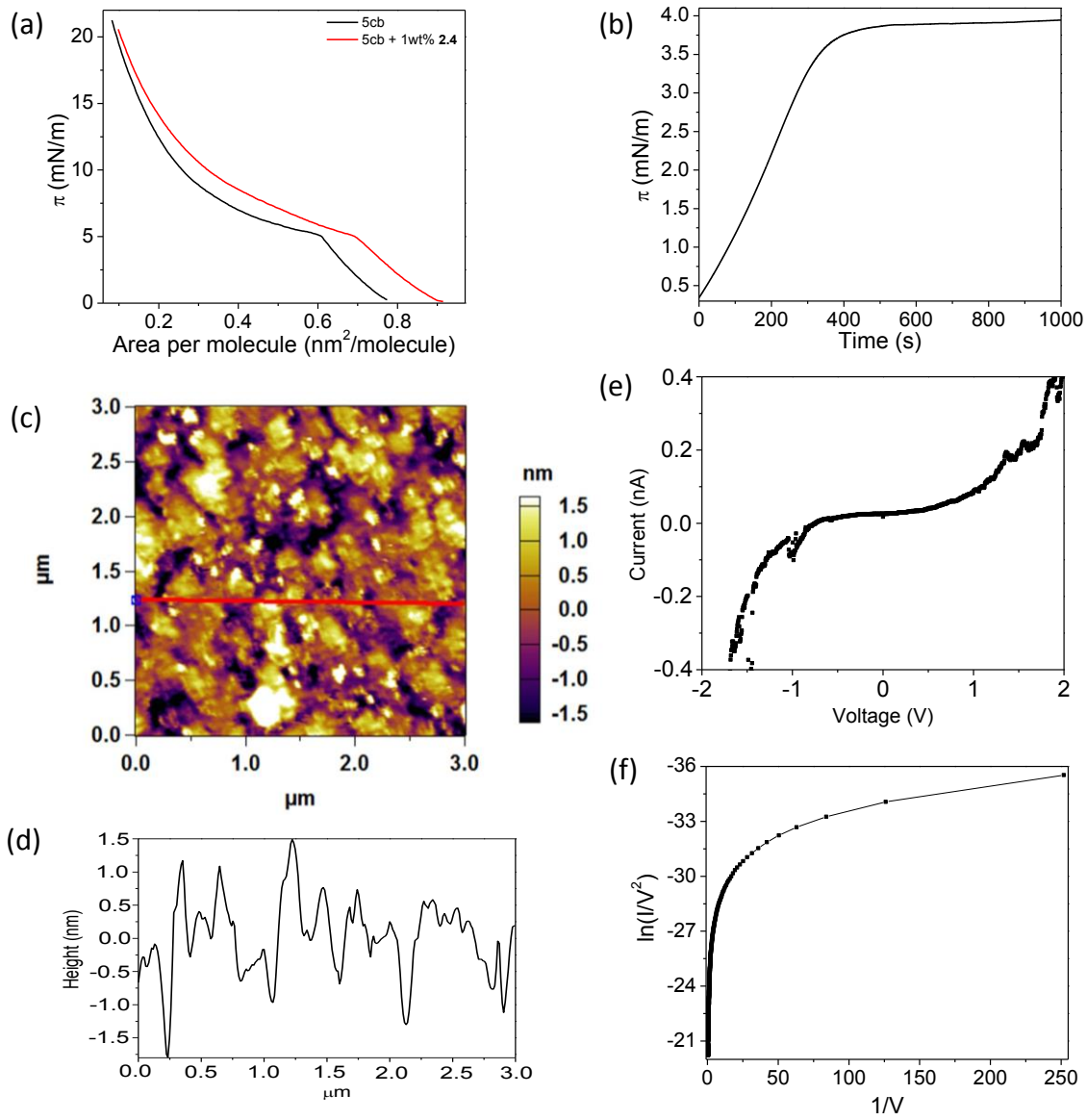

Figure 3.25 (a) The surface pressure (π)- area per molecule isotherms obtained for 5CB and 1 wt % doped 5CB at air-water interface at room temperature. (b) Stability measurement of the film of 1 wt % doped 5CB at 4 mN/m surface pressure. (c) Non-contact mode AFM mode topography image of monolayer of 1 wt % doped 5CB and the corresponding height profile

in (d). (e) The AFM I-V measurements of monolayer of 1 wt % doped 5CB deposited on ITO coated glass slide. (f) Variation of $\ln(I/V^2)$ as a function of 1/V.

To see whether doping has provided sufficient fluorescence to non-fluorescent 5CB, we have compared the epi- fluorescence micrographs of both LCs. Figure 3.24 shows that with 1 wt % doping, 5CB LC shows bright green fluorescence, even visible by naked eye.

For LC display applications, LCs must be deposited on ITO coated glass slides. In order to see, whether doping has any effect on the thin film formation and charge transport of 5CB LC, we have done surface manometry experiments and deposited the thin film of doped LC on ITO coated glass slides. The surface pressure (π) - area per molecule isotherms recorded for 5CB and 1 wt% doped 5CB at air-water interface at room temperature with a compression speed of 5 mm min^{-1} are shown in Figure 3.25. Both the compounds exhibited similar isotherms. For both the compounds, isotherm exhibited a collapse pressure of about 5 mN/m. The area per molecule spans a value of 0.78 nm^2 for 5CB and 0.84 nm^2 for 1 wt% doped 5CB which indicated only a small change in the area per molecule on doping.

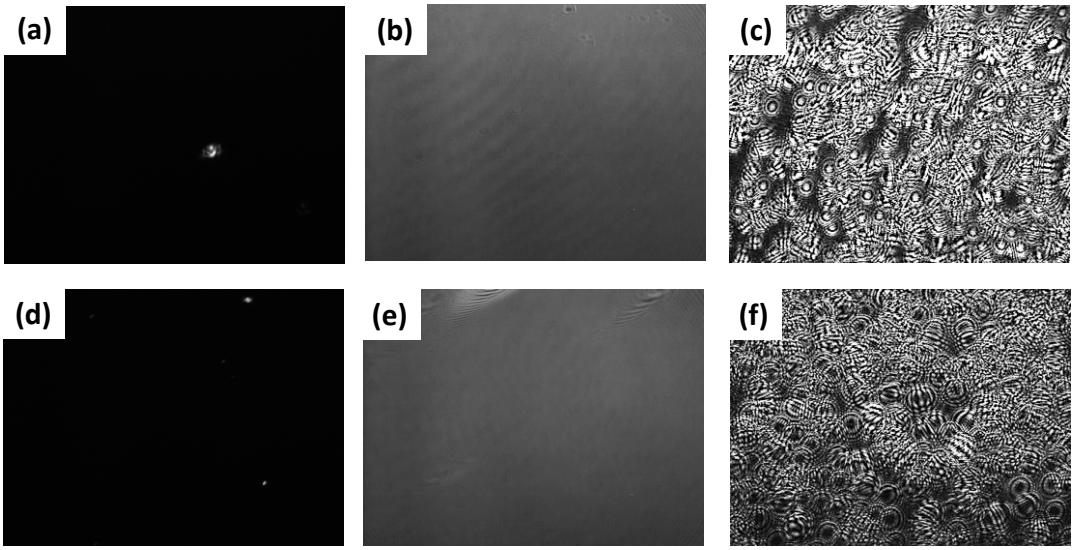

Figure 3.26 BAM images at air-water interface (a-c) for 5CB (a) at area per molecule of 0.80 nm^2, (b) at area per molecule of 0.70 nm^2, (c) collapsed film at 0.2 nm^2 and (d-f) for 1 wt % **2.4** doped 5CB (d) at area per molecule of 0.92 nm^2, (e) at area per molecule of 0.83 nm^2, (f) collapsed film at 0.3 nm^2 Here all images are of dimension 1010 × 900 μm.

For 5CB, at area per molecule of 0.8 nm^2, BAM images showed completely dark regions similar to compound **5.5**. At area per molecule of 0.65 nm^2, a very uniform grey colored region was observed corresponding to monolayer state. On further compression, the brightness increases gradually. The completely bright regions as shown in Figure 3.26c correspond to the collapse state. Similar observations have been made on doped 5CB suggesting that doping has not much effect on the thin film formation (Figure 3.26).

The AFM topography image of thin film of doped 5CB (Figure 3.25d) formed on ITO coated glass substrate shows bright domains grown over a less bright background. The average height of such bright domains is 2.8±0.3 nm and that of less bright region is around 1.5 nm. The bright domains do not show any preferential growth direction, and are found to be grown randomly. This observation suggested that LC monolayer on an air-water interface underwent a first-order transition to a stable phase that is composed of a monolayer plus an interdigitated bilayer (3-layer film). Formation of this stable 3-layer film can likely be due to a delicate balance between molecular interactions in the system as reported earlier for the 8CB systems.[77]

We have further determined the I-V characteristics of the M-I-M junction formed by the monolayer of doped 5CB and conducting tip as shown in Figure 3.25. This suggested that after doping also, charge transport can take place through this monolayer as observed for 9CB and 10CB molecules. Thus, compound **6.4** might serve as a fluorescent green light emitter for LC displays.

3.4 Conclusions

In conclusion, we have synthesized new DLCs based on perylene tetraesters in which perylene was peripherally attached to four triphenylenes, cyanobiphenyls *via* flexible alkyl spacers and branched chain moieties. Whereas, attachment of cyanobiphenyl units to the perylene core leads to the formation of nematic phase, triphenylene and branched alkyl chain resulted a regular hexagonal mesophase. We have demonstrated that the combination of rod and disc-like moieties has sufficiently perturbed the molecular shape to yield calamitic mesophases. Although biaxiality is likely to be seen at small length scales, as a result of large

aspect ratios between two components, there is no direct evidence for the formation of biaxial N phase in our study. We have shown that all the hybrid materials exhibit excellent fluorescence emission properties and nice quantum yields making them suitable for various optoelectronic applications. Further, the length of the alkyl chain has no effect on the photo-physical properties. The perylene-triphenylene and perylene-branched chain hybrids were found to form aggregates in THF/water mixtures. CV studies have shown that perylene-triphenylene and perylene-branched chain hybrids have lowered the gap between the HOMO and LUMO levels. Perylene-triphenylene and perylene-cyanobiphenyl oligomers were found to form stable monolayers at air-water interface. The monolayers were then transferred onto ITO coated glass substrates. The height profile for both the molecules indicated the existence of both tilted as well as non-tilted molecules. The substrate-LC molecules-Pt coated tip form M-I-M junction. The electrical conductivity through the junction was due to direct tunneling. 1 wt% perylene-cyanobiphenyl oligomer doped 5CB LCs have been found to exhibit greenish fluorescence for their use in LC displays as green light emitters. It has been shown that with doping also, 5CB was able to form stable monolayers keeping the topography and charge transporting similar to undoped 5CB. Thus, this series of compounds are highly promising in terms of LC behavior, fluorescent properties and charge transport. So these studies can further pave the way for the application of perylenes as fluorescent dyes in LCDs and as emitter materials in OLEDs. Such materials combine an exceptionally high degree of self-organization at the nanometer scale with the advantages that LCs provide.

3.5 Experimental Section

3.5.1 Measurements

Chemicals and solvents (AR quality) were used as received without any further purification. Column chromatographic separations were performed on silica gel (100–200 & 230-400 mesh). Thin layer chromatography (TLC) was performed on aluminum sheets pre-coated with silica gel (Merck, Kieselgel 60, F254). Structural characterization of the compounds was carried out through a combination of infrared spectroscopy (Bruker, Tensor Series), ^{1}H NMR and ^{13}C NMR (Bruker Biospin Switzerland Avance-iii 400 MHz and 100 MHz spectrometers, respectively), UV-vis-NIR spectrophotometers (Agilent Technologies, Cary

Series), Mass spectrometry (Water Synapt G-2-s QTOF with MALDI ion source and α-cyano-4-hydroxy-cinnamic acid). IR spectra were recorded in neat form for target compounds on Diamond ATR. ^{1}H NMR spectra were recorded using deuterated chloroform ($CDCl_3$) as solvent and tetramethylsilane (TMS) as an internal standard. Fluorescence spectra and Steady State anisotropy experiments were performed on Horiba Scientific Fluoromax Spectrofluorometer 4. Time resolved lifetime measurements were done on Time Correlated Single Photon Counter from Horiba Jobin Yvon. For Steady-state experiments excitation wavelength was 443 nm and emission wavelength was 488 nm. For Time resolved experiments, excitation was done by 440 nm Laser Diode, emission wavelength was 490 nm and emission slit was 1 nm. Thin film fluorescence studies were performed on Shimadzu spectrofluorophotometer –RF-5301PC. Raman spectra of the samples were recorded on an inVia Raman microscope with 180° scattering geometry (Renishaw, UK). Approximately 350 mW of 785 nm from an NIR laser was used as excitation source and focused on to the sample spot by 20X objective lens. The transition temperatures and associated enthalpy values were determined using a differential scanning calorimeter (Mettler Toledo Model DSC 821^{e} or Perkin Elmer DSC 8000 coupled to a controlled liquid nitrogen accessory (CLN 2)) which was operated at a scanning rate 5 °C min^{-1} both on heating and cooling. Textural observations of the mesophase were performed with Nikon Eclipse LV100POL polarizing microscope provided with a Linkam heating stage (LTS 420). All images were captured using a Q-imaging camera. Thermogravimetric analysis (TGA) was carried out from 25 to 500 °C (at a heating rate of 10 °C min^{-1}) under nitrogen atmosphere on a Shimadzu DTG-60 instrument. X-ray scattering was carried out on powder samples filled in glass capillaries using Cu-K_α (λ = 1.54 Å) radiation from DY 1042-Empyrean X-ray diffractometer with PCS and Pixel system (diffractometer system-empyrean, Measuring program-Focusing mirror, scans axis-gonioKAlpha-1.54060, Goniometer Radius-240 mm, and Modification editor-Panalytical) or Xeuss (Model C HP100 fm) X-ray diffractometer from Xenocs equipped with GeniX3D source operating at 50 kV and 0.6 mA in conjunction with a multilayer mirror and Pilatus 200 hybrid pixel detector from Dectris. The scanning electron microscopy images were captured with Jeol JSM-7600F Field emission Scanning Electron Microscope. The AFM images for aggregation were collected by Bruker Atomic Force Microscope in AC mode. Cyclic voltammetry experiments were performed on CH Instruments, electrochemical

workstation. The surface manometry experiments were carried out using an APEX LB-2007 and a NIMA 611M trough. The subphase used was the ultrapure deionised water obtained from a Millipore Milli-Q system. The stock solutions were prepared using chloroform (HPLC grade, Merck). After spreading it on the air–water interface, the film was left for 20 min, allowing the solvent to evaporate. The π-Am isotherm was obtained by the symmetric compression of barriers with a constant barrier speed of 10 mm/min. The surface pressure (π) was measured using the standard Wilhelmy plate technique. Brewster angle microscopy images were taken by Accurion imaging Ellipsometer EP4 by keeping angle of incidence 53.15°, polariser, compensator and analyser at 0°. Film deposition was done by transferring single layer of films using LB technique onto hydrophilic substrates at different surface pressure (πt) with a dipping speed of 1 mm min^{-1} on ITO coated glass substrates. AFM studies on these LB films were performed using Asylum Research MFP 3D. Pt/Ir-coated tip of length 240 ± 10 µm, width 35 ± 5 µm, height 15-20 µm with a force constant of 0.7-9.0 Nm^{-1} and a resonance frequency of 50-130 kHz was used. Non-contact mode was used to obtain the topography of the film. AFM was carried out at room temperature (25 °C). To obtain the I-V characteristics of the film, the conducting tip was kept at ground and a voltage ramp (-2V to +2V) was applied to the ITO substrate. The I-V measurements were performed by placing the tip at the desired position on the film. The current values in the range of 1 pA to 20 nA can be measured. The epi-fluorescence micrographs were obtained with Zeiss, Axio Scope A1, Germany fluorescence microscope equipped with a 100 W mercury lamp and Axio cam camera. The samples were viewed using a fluorescent filter cube with a 460 nm excitation filter and a 534 nm emission filter.

3.5.2 Synthesis of 2-(*n*-bromoalkaneoxy)-3,6,7,10,11-pentakis(alkoxy)triphenylene A mixture of catechol (1 equiv.), n-bromoalkane (2.5 equiv.) and crushed KOH (3 equiv.) in DMSO were heated with stirring at 70 °C for 4 h. The reaction mixture was then cooled to room temperature and poured into water and extracted with hexane. Hexane was then evaporated to give brown colored liquid which was used for the next step without any further purification. In the next step, the dialkoxybenzene (1 equiv.) obtained was dissolved in DCM and then 1-2 drops of conc. H_2SO_4 was added. After stirring for about 5 min, $FeCl_3$ (3 equiv.) was added and the mixture was stirred for 45min-1h and then poured over ice cold methanol.

The solid formed was filtered off and subjected to column chromatography (silica gel, ethylacetate/hexane) to give pale yellow solid i.e, triphenylene. Triphenylene (1 equiv.) was dissolved in DCM in a RBF and Cat B-Br (3.6 equiv.) was added. The RBF was then stoppered and stirred at room temperature for 48 h. After this, the reaction mixture was poured into water and extracted with DCM. DCM layer was evaporated and resulting solid was purified through column chromatography to give monohydroxytriphenylene. Monohydroxytriphenylene (1 equiv.), dibromoalkane (7 equiv.), K_2CO_3 (4 equiv.) were mixed in 2-butanone and refluxed for 18 h under nitrogen atmosphere. 2-butanone was then evaporated and the crude product was purified by column chromatography. ^{1}H NMR (400 MHz, $CDCl_3$): δ 7.86 (s, 6H), 4.26 (t, 12H, J = 6.8 Hz), 3.43 (t, 2H, J = 6.8 Hz), 2.01-1.84 (m, alkyl chain), 1.62-1.36 (m, alkyl chain), 1.02-0.98 (m, 15H). ^{13}C NMR (100 MHz, $CDCl_3$): δ 146.18, 145.80, 126.13, 123.11, 119.21, 106.31, 73.13, 72.89, 33.41, 33.13, 29.54, 29.33, 28.61, 28.53, 25.49, 22.71, 14.11.

3.5.3 Synthesis of 4'-(*n*-bromoalkaneoxy)-4 cyano biphenyl A mixture of 4'-hydroxy-4-cyanobiphenyl (1 equiv.), K_2CO_3 (3 equiv.) and dibromoalkane (2.5 equiv.) in 2-butanone was heated to reflux under nitrogen atmosphere for 18 h. The reaction mixture was then filtered and washing were given DCM. The mother liquor was then evaporated to dryness and the product was purified through column choromatography (silica gel, ethylacetate/hexane) to give white crystalline solid. ^{1}H NMR (400 MHz, $CDCl_3$): δ 7.64-7.57 (m, 4H), 7.48-7.46 (m, 2H), 6.94-6.92 (m, 2H), 3.95 (t, 2H), 3.35 (t, 2H), 1.81-1.73 (m, 4H), 1.41-1.26 (m, alkyl chain). ^{13}C NMR (100 MHz, $CDCl_3$): δ 159.80, 145.30, 132.59, 131.27, 128.34, 127.09, 119.15, 115.08, 110.04, 68.15, 34.087, 32.82, 29.44, 29.37, 29.33, 29.22, 28.75, 28.16.

3.5.4 Synthesis of 5.1 18.8 mg of perylene-3,4,9,10-tetracarboxylic dianhydride was heated at 70 °C in a solution of 0.1M potassium hydroxide solution (15 mL) for about 2 h. The reaction mixture was transformed in to a clear solution having green fluorescence of tetra-potassium salt of perylene tetracarboxylic acid. The solution was allowed to cool down to room temperature, filtered and acidified with dilute hydrochloric acid to get a solution with pH value of 8-9. To this solution, was then added 320.3 mg of the corresponding triphenylene bromide and 10.5 mg of tetraoctyl ammonium bromide (TOAB). The reaction

mixture was refluxed under vigorous stirring for 2-3 h. The solution became almost colourless and red or brown coloured insoluble oily or glassy material was floating on the top of solution. The reaction mixture was cooled to room temperature and extracted with chloroform. The organic layer was separated and washed with aqueous sodium chloride solution and then distilled water. The chloroform was removed by rotary evaporation and the resulting residue was first purified by repeated (minimum three times) column chromatography over silica gel (silica: 230-400 mesh, eluent: 5% ethyl acetate in chloroform). The residue was then dissolved in dichloromethane and then cold methanol to afford **5.1** (Yield = 65.4 %). ^{1}H NMR (400 MHz, $CDCl_3$): δ 7.98 (d, 4H, J = 8.2 Hz), 7.88 (d, 4H, J = 8.0 Hz), 7.82-7.77 (m, 24H), 4.38 (t, 8H, J = 6.4 Hz), 4.26-4.21 (m, 48H), 1.95-1.90 (m, 48H), 1.88-1.76 (m, 8H), 1.56-1.23 (m, 96H), 0.97-0.87 (m, 60H). ^{13}C NMR (100 MHz, $CDCl_3$): δ 168.55 (C=O), 148.88, 148.84, 132.95, 130.29, 127.03, 121.26, 107.14, 69.56, 65.38, 29.14, 28.38, 25.91, 22.61, 14.16. IR (Diamond ATR): ν_{max}/cm^{-1} 2953.11, 2929.68, 2858.20, 1714.73 (COO), 1615.75, 1590.40, 1508.59, 1467.31, 1432.42, 1387.47, 1258.45, 1161.23, 1098.45, 1074.27, 1035.66, 893.26, 869.51, 833.06, 747.84, 729.84, 658.15, 598.49. Raman: ν_{max}/cm^{-1} 1708, 1621, 1578, 1462, 1406, 1358, 1320, 1281, 1077, 797, 759. MALDI-MS: m/z cald. for $C_{220}H_{300}O_{32}^{+}$: 3454.1848; found: 3454.1622.

3.5.5 Synthesis of 5.2 Compound was synthesized according to a similar procedure to **5.1** (Yield: 69.3 %). ^{1}H NMR (400 MHz, $CDCl_3$): δ 8.16 (d, 4H, J = 8.0 Hz), 7.93 (d, 4H, J = 8.0 Hz), 7.78 (s, 24H), 4.29 (t, 8H, J = 6.4 Hz), 4.20-4.15 (m, 48H), 1.95-1.90 (m, 48H), 1.88-1.76 (m, 8H), 1.56-1.23 (m, 112H), 0.97-0.87 (m, 60H). ^{13}C NMR (100 MHz, $CDCl_3$): δ 168.52 (C=O), 148.90, 148.87, 133.07, 130.37, 123.55, 121.34, 107.15, 69.60, 65.58, 29.72, 29.45, 29.36, 29.30, 29.13, 28.58, 28.37, 26.11, 25.97, 22.59, 22.73, 14.16, 14.14. IR (Diamond ATR): ν_{max}/cm^{-1} 2952.48, 2927.26, 2856.22, 1711.86 (COO), 1615.74, 1596.30, 1508.74, 1466.87, 1432.53, 1387.62, 1258.55, 1160.65, 1099.37, 1035.83, 893.27, 869.37, 831.01, 771.19, 747.89, 729.15, 623.82. Raman: ν_{max}/cm^{-1} 1707, 1619, 1576, 1438, 1394, 1358, 1319, 1280, 1076, 699. MALDI-MS: m/z cald. for $C_{228}H_{316}O_{32}^{+}$: 3568.9294; found: 3568.9387.

3.5.6 Synthesis of 5.3 Compound was synthesized according to a similar procedure to **5.1** (Yield: 60.2 %). ^{1}H NMR (400 MHz, $CDCl_3$): δ 8.21 (d, 4H, J = 8.0 Hz), 7.96 (d, 4H, J = 8.0

Hz), 7.77 (s, 24H), 4.29 (t, 8H, *J* = 6.8 Hz), 4.20-4.15 (m, 48H), 1.95-1.87 (m, 48H), 1.78-1.76 (m, 8H), 1.56-1.38 (m, 120H), 0.97-0.91 (m, 60H). ^{13}C NMR (100 MHz, $CDCl_3$): δ 168.53 (C=O), 148.90, 133.09, 130.40, 128.99, 123.54, 121.36, 107.25, 107.16, 69.61, 69.58, 65.59, 29.72, 29.54, 29.50, 29.45, 29.31, 29.14, 28.61, 28.37, 26.18, 26.01, 22.59, 14.14. IR (Diamond ATR): ν_{max}/cm^{-1} 2956.76, 2927.59, 2856.20, 1711.54 (COO), 1615.91, 1590.64, 1509.25, 1467.02, 1433.13, 1388.03, 1259.33, 1162.17, 1099.93, 1036.52, 893.86, 869.27, 831.66, 772.12, 747.91, 729.58, 656.94. Raman: ν_{max}/cm^{-1} 1705, 1623, 1576, 1461, 1405, 1358, 1319, 1280, 1074, 796, 751. MALDI-MS: m/z cald. for $C_{232}H_{324}O_{32}^{+}$: 3624.3793; found: 3624.3091

3.5.7 Synthesis of 5.4 Compound was synthesized according to a similar procedure to **5.1** (Yield: 70.1 %). ^{1}H NMR (400 MHz, $CDCl_3$): δ 8.26 (d, 4H, *J* = 8.0 Hz), 7.98 (d, 4H, *J* = 8.0 Hz), 7.79 (s, 24H), 4.27 (t, 8H, *J* = 6.8 Hz), 4.20-4.17 (m, 48H), 1.95-1.88 (m, 48H), 1.78-1.75 (m, 8H), 1.55-1.34 (m, 128H), 0.97-0.94 (m, 60H). ^{13}C NMR (100 MHz, $CDCl_3$): δ 168.50 (C=O), 148.91, 148.90, 133.15, 130.47, 130.41, 123.56, 121.43, 107.18, 69.63, 65.64, 29.73, 29.63, 29.54, 29.52, 29.45, 29.39, 29.14, 28.61, 28.38, 28.30, 26.23, 26.03, 22.60, 22.73, 14.16. IR (Diamond ATR): ν_{max}/cm^{-1} 2952.73, 2926.70, 2855.85, 1712.08 (COO), 1615.94, 1590.57, 1508.93, 1467.04, 1432.96, 1387.87, 1259.06, 1162.32, 1100.20, 1036.51, 893.57, 869.43, 832.33, 771.59, 747.88, 729.75, 656.72. Raman: ν_{max}/cm^{-1} 1709, 1621, 1576, 1461, 1406, 1357, 1318, 1280, 1076, 797, 756. MALDI-MS: m/z cald. for $C_{236}H_{332}O_{32}^{+}$: 3680.4419; found: 3680.4604.

3.5.8 Synthesis of 5.5 Compound was synthesized according to a similar procedure to **5.1** (Yield: 68.3 %). ^{1}H NMR (400 MHz, $CDCl_3$): δ 8.12 (d, 4H, *J* = 8.2 Hz), 7.94 (d, 4H, *J* = 8.1 Hz), 7.83 (s, 24H), 4.35 (t, 8H, *J* = 6.48 Hz, 4 Hz), 4.124 (t, 48H, *J* = 6.48 Hz), 2.00-1.93(m, 48H), 1.85-1.80 (m, 8H), 1.63-1.256 (m, 56H), 1.43-1.37 (m, 128H), 0.98-0.95 (m, 60H). ^{13}C NMR (100 MHz, $CDCl_3$): δ 168.55 (C=O), 148.93, 132.90, 130.32, 128.88, 128.67, 123.59, 121.30, 107.22, 69.65, 65.63, 31.93, 31.76, 31.58, 29.76, 29.73, 29.64, 29.57, 29.48, 28.68, 26.29, 26.09, 25.92, 25.73, 23.13, 22.89, 22.73, 22.55, 14.12. IR (Diamond ATR): ν_{max}/cm^{-1} 2925.17, 2855.09, 1713.00 (COO), 1616.42, 1590.89, 1513.47, 1467.56, 1433.99, 1389.32, 1259.77, 1164.16, 1100.14, 1039.48, 925.97, 865.34, 835.49, 803.65, 748.61, 726.34, 657.45.

Raman: ν_{max}/cm^{-1} 1707, 1620, 1576, 1461, 1405, 1358, 1319, 1280, 1076, 799, 756. MALDI-MS: m/z cald. for $C_{264}H_{388}O_{32}^{+}$: 4072.8801; found: 4072.8663.

3.5.9 Synthesis of 6.1 Compound was synthesized according to a similar procedure to **5.1** (Yield: 37.1 %). ^{1}H NMR (400 MHz, $CDCl_3$): δ 8.21 (d, 4H, J = 8.0 Hz), 7.98 (d, 4H, J= 8.0 Hz), 7.64-7.62 (m, 8H), 7.54-7.50 (m, 8H), 7.44-7.42 (m, 8H), 6.90-6.87 (m, 8H), 4.42 (t, 8H, J = 5.8 Hz), 4.04 (t, 8H, J = 5.8 Hz), 2.00-1.97 (m, 16H). ^{13}C NMR (100 MHz, $CDCl_3$): δ 168.39 (C=O), 159.52, 145.02, 133.10, 132.60, 131.31, 130.50, 130.41, 128.27, 126.95, 121.48, 115.02, 110.08, 67.41, 65.31, 26.09, 25.29. IR (Diamond ATR): ν_{max}/cm^{-1} 2986.52, 2858.03, 2223.90 (CN), 1710.26 (COO), 1600.91, 1519.26, 1493.16, 1470.45, 1391.57, 1269.43, 1248.13, 1203.60, 1162.72, 1134.32, 1098.66, 1068.27, 1033.91, 995.13, 956.13, 850.86, 819.58, 772.43, 748.10, 713.41, 658.82. Raman: ν_{max}/cm^{-1} 2229, 1716, 1605, 1575, 1524, 1459, 1357, 1319, 1287, 1260, 1182, 1072, 816, 520. MALDI-MS: m/z cald. for $C_{92}H_{72}N_4O_{12}^{+}$: 1424.5147; found: 1424.5126.

3.5.10 Synthesis of 6.2 Compound was synthesized according to a similar procedure to **5.1** (Yield: 42.5 %). ^{1}H NMR (400 MHz, $CDCl_3$): δ 8.22 (d, 4H, J = 8.0 Hz), 7.98 (d, 4H, J= 8.0 Hz), 7.65-7.63 (m, 8H), 7.57-7.55 (m, 8H), 7.46-7.44 (m, 8H), 6.93-6.91 (m, 8H), 4.34 (t, 8H, J = 6.4 Hz), 3.96 (t, 8H, J = 6.4 Hz), 1.84-1.81 (m, 16H), 1.23-1.20 (m, 16H). ^{13}C NMR (100 MHz, $CDCl_3$): δ 168.46 (C=O), 159.70, 145.11, 133.11, 132.58, 131.25, 130.51, 130.43, 128.28, 127.00, 121.44, 115.04, 110.06, 67.89, 65.52, 29.72, 29.00, 28.45, 25.76. IR (Diamond ATR): ν_{max}/cm^{-1} 2975.01, 2945.89, 2915.72, 2222.13 (CN), 1709.95 (COO), 1601.48, 1517.96, 1493.65, 1470.60, 1393.49, 1269.05, 1246.56, 1201.98, 1166.61, 1099.64, 1063.32, 1031.94, 1004.55, 854.29, 818.87. Raman: ν_{max}/cm^{-1} 2228, 1719, 1606, 1576, 1461, 1359, 1319, 1289, 1262, 1183, 1107, 1070, 952, 823, 560. MALDI-MS: m/z cald. for $C_{100}H_{88}N_4O_{12}^{+}$: 1536.6399; found: 1536.6361

3.5.11 Synthesis of 6.3 Compound was synthesized according to a similar procedure to **5.1** (Yield: 39.3 %). ^{1}H NMR (400 MHz, $CDCl_3$): δ 8.28 (d, 4H, J = 8.0 Hz), 8.03 (d, 4H, J= 8.0 Hz), 7.65-7.63 (m, 8H), 7.58-7.56 (m, 8H), 7.47-7.45 (m, 8H), 6.94-6.92 (m, 8H), 4.32 (t, 8H, J = 6.4 Hz), 3.96 (t, 8H, J = 6.4 Hz), 1.81-1.77 (m, 16H), 1.51-1.45 (m, 16H). IR (Diamond ATR): ν_{max}/cm^{-1} 2938.39, 2852.87, 2224.62 (CN), 1711.20 (COO), 1698.91,

1599.20, 1513.96, 1494.51, 1477.94, 1464.93, 1392.21, 1277.83, 1248.30, 1200.69, 1184.64, 1167.91, 1137.46, 1116.47, 1100.14, 1054.33, 1023.78, 995.37, 955.20, 903.39, 851.51, 819.76. Raman: ν_{max}/cm^{-1} 2231, 1716, 1603, 1573, 1459, 1357, 1313, 1285, 1265, 1186, 1113, 1069, 962, 798, 633, 564, 504. MALDI-MS: m/z cald. for $C_{104}H_{96}N_4O_{12}^+$: 1593.7058; found: 1593.7197.

3.5.12 Synthesis of 6.4 Compound was synthesized according to a similar procedure to **5.1** (Yield: 33.8 %). ^{1}H NMR (400 MHz, $CDCl_3$): δ 8.31 (d, 4H, J = 8.1 Hz), 8.06 (d, 4H, J= 7.9 Hz), 7.69-7.67 (m, 8H), 7.63-7.60 (m, 8H), 7.53-7.49 (m, 8H), 6.97-6.94 (m, 8H), 4.33 (t, 8H, J = 6.7 Hz), 3.98 (t, 8H, J = 6.5 Hz), 1.83-1.77 (m, 16H), 1.24-0.86 (m, 32H). ^{13}C NMR (100 MHz, $CDCl_3$): δ 168.50, 159.73, 145.17, 132.57, 131.24, 130.51, 130.43, 128.30, 127.03, 121.41, 119.14, 115.02, 110.02, 68.08, 65.62, 29.18, 28.55, 25.14. IR (Diamond ATR): ν_{max}/cm^{-1} 3041.55, 2926.53, 2853.72, 2223.91 (CN), 1710.46 (COO), 1602.02, 1516.31, 1493.80, 1470.17, 1392.18, 1269.74, 1251.01, 1200.02, 1177.62, 1161.92, 1137.24, 1100.37, 1068.97, 1030.09, 1013.31, 999.15, 849.07, 820.56, 806.80, 773.62, 748.99, 724.19, 660.04, 633.53. Raman: ν_{max}/cm^{-1} 2232, 1728, 1604, 1575, 1461, 1356, 1318, 1285, 1257, 1184, 1071, 955, 751, 633, 559, 501. MALDI-MS: m/z cald. for $C_{108}H_{104}N_4O_{12}^+$: 1649.7684; found:1649.7655.

3.5.13 Synthesis of 6.5 Compound was synthesized according to a similar procedure to **5.1** (Yield: 49.6 %). ^{1}H NMR (400 MHz, $CDCl_3$): δ 8.29 (d, 4H, J = 8.0 Hz), 8.03 (d, 4H, J= 8.0 Hz), 7.65-7.63 (m, 8H), 7.60-7.57 (m, 8H), 7.49-7.45 (m, 8H), 6.95-6.92 (m, 8H), 4.30 (t, 8H, J = 6.7 Hz), 3.95 (t, 8H, J = 6.4 Hz), 1.80-1.73 (m, 16H), 1.44-1.39 (m, 40H). ^{13}C NMR (100 MHz, $CDCl_3$): δ 168.50, 159.74, 145.20, 132.56, 131.24, 130.54, 130.44, 129.07, 128.30, 127.03, 121.42, 119.12, 115.04, 110.93, 68.11, 65.63, 29.39, 29.26, 29.20, 28.56, 25.99, 25.97. IR (Diamond ATR): ν_{max}/cm^{-1} 2924.72, 2852.92, 2225.11 (CN), 1715.01 (COO), 1601.71, 1518.13, 1494.07, 1470.73, 1394.51, 1271.71, 1164.35, 1099.46, 1029.04, 850.51, 820.14, 748.26, 721.72, 660.70. Raman: ν_{max}/cm^{-1} 2232, 1716, 1606, 1574, 1459, 1356, 1319, 1284, 1184, 1068, 950, 850, 619, 558. MALDI-MS: m/z cald. for $C_{112}H_{112}N_4O_{12}^+$: 1704.8277; found: 1704.8364.

3.5.14 Synthesis of 6.6 Compound was synthesized according to a similar procedure to **5.1** (Yield: 52.7 %). ^{1}H NMR (400 MHz, $CDCl_3$): δ 8.31 (d, 4H, J = 8.0 Hz), 8.03 (d, 4H, J= 8.0 Hz), 7.66-7.64 (m, 8H), 7.60-7.58 (m, 8H), 7.50-7.46 (m, 8H), 6.98-6.92 (m, 8H), 4.29 (t, 8H, J = 6.7 Hz), 3.96 (t, 8H, J = 6.4 Hz), 1.86-1.72 (m, 16H), 1.44-1.31 (m, 48H). ^{13}C NMR (100 MHz, $CDCl_3$): δ 168.50, 159.76, 145.23, 133.14, 132.56, 131.25, 130.55, 130.45, 128.31, 127.05, 121.43, 119.12, 115.05, 110.03, 68.14, 65.66, 29.46, 29.43, 29.34, 29.27, 29.21, 28.57, 26.04, 25.99. IR (Diamond ATR): ν_{max}/cm^{-1} 2924.53, 2852.90, 2227.36 (CN), 1725.20 (COO), 1603.33, 1520.54, 1495.03, 1471.71, 1393.83, 1270.94, 1164.20, 1134.24, 1096.45, 1032.02, 997.71, 846.07, 820.01, 772.09, 746.84, 720.59. Raman: ν_{max}/cm^{-1} 2234, 1731, 1607, 1573, 1529, 1461, 1356, 1317, 1260, 1185, 1120, 1069, 956, 840, 566, 503. MALDI-MS: m/z cald. for $C_{116}H_{120}N_4O_{12}^{+}$: 1760.8903; found: 1760.8785

3.5.15 Synthesis of 6.7 Compound was synthesized according to a similar procedure to **5.1** (Yield: 71.9 %). ^{1}H NMR (400 MHz, $CDCl_3$): δ 8.29 (d, 4H, J = 8.0 Hz), 8.01 (d, 4H, J= 8.0 Hz), 7.66-7.64 (m, 8H), 7.60-7.58 (m, 8H), 7.50-7.47 (m, 8H), 6.96-6.92 (m, 8H), 4.30 (t, 8H, J = 6.7 Hz), 3.96 (t, 8H, J = 6.4 Hz), 1.80-1.75 (m, 16H), 1.44-1.29 (m, 56H). ^{13}C NMR (100 MHz, $CDCl_3$): δ 168.51, 159.77, 145.23, 133.14, 132.56, 131.23, 130.55, 130.46, 128.31, 127.04, 121.43, 119.13, 115.05, 110.02, 68.14, 65.67, 29.53, 29.49, 29.38, 29.31, 29.22, 28.58, 26.03, 26.00. IR (Diamond ATR): ν_{max}/cm^{-1} 2923.11, 2851.74, 2227.82 (CN), 1723.73 (COO), 1602.46, 1520.41, 1494.43, 1470.62, 1394.92, 1270.06, 1164.12, 1098.73, 1035.84, 997.55, 933.78, 845.40, 819.69, 746.96, 719.79, 660.38. Raman: ν_{max}/cm^{-1} 2234, 1730, 1607, 1574, 1531, 1478, 1356, 1318, 1284, 1185, 1073, 958, 855, 633, 556, 505. MALDI-MS: m/z cald. for $C_{120}H_{128}N_4O_{12}^{+}$: 1816.9529; found: 1816.9451.

3.5.16 Synthesis of 6.8 Compound was synthesized according to a similar procedure to **5.1** (Yield: 68.5 %). ^{1}H NMR (400 MHz, $CDCl_3$): δ 8.32 (d, 4H, J = 8.0 Hz), 8.04 (d, 4H, J= 8.0 Hz), 7.67-7.64 (m, 8H), 7.61-7.59 (m, 8H), 7.50-7.47 (m, 8H), 6.96-6.94 (m, 8H), 4.29 (t, 8H, J = 6.7 Hz), 3.96 (t, 8H, J = 6.4 Hz), 1.79-1.74 (m, 16H), 1.43-1.20 (m, 40H). ^{13}C NMR (100 MHz, $CDCl_3$): δ 168.52, 159.77, 145.24, 133.31, 132.57, 131.23, 130.52, 130.45, 128.31, 127.05, 121.42, 119.14, 115.05, 110.01, 68.15, 65.59, 29.57, 29.53, 29.40, 29.34, 29.22, 28.59, 26.05, 26.01. IR (Diamond ATR): ν_{max}/cm^{-1} 2920.02, 2851.00, 2228.48 (CN), 1728.93 (COO), 1707.36, 1602.67, 1494.92, 1472.59, 1391.35, 1267.95, 1215.84, 1181.36,

1161.21, 1133.42, 1095.43, 1030.37, 998.62, 844.42, 818.94, 771.13, 745.76, 723.00, 660.82, 634.37. Raman: ν_{max}/cm^{-1} 2236, 1735, 1607, 1447, 1356, 1317, 1300, 1285, 1185, 1122, 1069, 959, 841, 634, 567. MALDI-MS: m/z cald. for $C_{124}H_{136}N_4O_{12}^+$: 1873.0155; found: 1873.1156

3.5.17 Synthesis of 7.1 Compound was synthesized according to a similar procedure to **5.1** (Yield: 49.6 %). ^{1}H NMR (400 MHz, $CDCl_3$): δ 8.22 (d, 4H, J = 8.0 Hz), 7.98 (d, 4H, J= 8.0 Hz), 5.22 (m, 4H), 1.44-1.42 (m, 24H). ^{13}C NMR (100 MHz, $CDCl_3$): δ 167.95, 132.98, 130.76, 130.25, 128.93, 121.29, 68.99, 29.71, 21.97. IR (Diamond ATR): ν_{max}/cm^{-1} 2978.56, 2920.96, 2849.86, 1703.14 (COO), 1589.65, 1513.73, 1455.65, 1407.58, 1383.56, 1372.55, 1346.99, 1308.58, 1259.01, 1199.83, 1177.74, 1159.53, 1133.49, 1092.02, 1026.40, 978.79, 938.37, 906.71, 828.02, 801.27, 771.42, 747.98, 636.99. Raman: ν_{max}/cm^{-1} 1707, 1699, 1607, 1578, 1460, 1360, 1318, 1282, 1190, 1076, 868, 756, 510. MALDI-MS: m/z cald. for $C_{36}H_{36}O_8^+$: 596.2410; found: 596.2421.

3.5.18 Synthesis of 7.2 Compound was synthesized according to a similar procedure to **5.1** (Yield: 61.5 %). ^{1}H NMR (400 MHz, $CDCl_3$): δ 8.31 (d, 4H, J = 8.0 Hz), 8.05 (d, 4H, J= 8.0 Hz), 4.09 (d, 8H, J= 6.4 Hz), 2.09-2.07 (m, 4H), 1.02-1.00 (m, 24H). ^{13}C NMR (100 MHz, $CDCl_3$): δ 168.47, 133.17, 130.58, 130.43, 121.44, 71.49, 30.97, 29.72, 27.81, 19.31. IR (Diamond ATR): ν_{max}/cm^{-1} 2959.03, 2917.15, 2874.02, 1720.94 (COO), 1703.18, 1587.34, 1513.53, 1474.73, 1410.31, 1383.59, 1368.44, 1342.76, 1328.41, 1307.55, 1297.97, 1270.11, 1204.53, 1185.34, 1167.51, 1136.36, 1097.41, 1005.09, 981.99, 940.24, 900.20, 842.76, 803.66, 791.62, 762.93, 747.37, 667.59, 639.60. Raman: ν_{max}/cm^{-1} 1709, 1608, 1574, 1462, 1355, 1316, 1276, 1199, 1073, 969, 869, 562, 513. MALDI-MS: m/z cald. for $C_{40}H_{44}O_8^+$: 652.3036; found: 652.3028.

3.5.19 Synthesis of 7.3 Compound was synthesized according to a similar procedure to **5.1** (Yield: 52.3 %). ^{1}H NMR (400 MHz, $CDCl_3$): δ 8.33 (d, 4H, J = 8.0 Hz), 8.07 (d, 4H, J= 8.0 Hz), 4.28-4.25 (m, 4H), 4.17-4.13 (m, 4H), 1.95-1.90 (m, 4H), 1.34-1.28 (m, 8H), 1.05 (d, 12H, J = 6.4 Hz), 1.00-0.98 (m, 12H). ^{13}C NMR (100 MHz, $CDCl_3$): δ 168.56, 132.93, 130.43, 130.26, 128.96, 128.78, 121.35, 70.08, 34.22, 29.72, 26.21, 22.72, 22.59, 16.57. IR (Diamond ATR): ν_{max}/cm^{-1} 2955.28, 2919.31, 2856.40, 1715.14 (COO), 1699.66, 1588.51,

1513.52, 1461.33, 1394.17, 1282.18, 1260.16, 1202.66, 1170.99, 1100.97, 1004.81, 974.73, 923.55, 849.37, 807.15, 777.12, 748.12, 678.02. Raman: ν_{max}/cm^{-1} 1708, 1697, 1609, 1576, 1459, 1360, 1322, 1285, 1260, 1189, 1070, 873, 798, 560. MALDI-MS: m/z cald. for $C_{44}H_{52}O_8^+$: 708.3662; found: 708.3679.

3.5.20 Synthesis of 7.4 Compound was synthesized according to a similar procedure to **5.1** (Yield: 49.6 %). ^{1}H NMR (400 MHz, $CDCl_3$): δ 8.18 (d, 4H, J = 8.0 Hz), 7.96 (d, 4H, J= 8.0 Hz), 4.35 (t, 8H, J = 6.4 Hz), 1.82-1.76 (m, 4H), 1.71-1.58 (m, 12H), 0.98-0.97 (m, 24H). ^{13}C NMR (100 MHz, $CDCl_3$): δ 168.57, 132.99, 130.37, 128.94, 121.38, 64.20, 37.27, 25.23, 22.58. IR (Diamond ATR): ν_{max}/cm^{-1} 2958.50, 2922.59, 2871.21, 1721.20 (COO), 1704.02, 1586.25, 1512.68, 1468.06, 1390.28, 1367.94, 1266.38, 1160.95, 1133.67, 1099.37, 1055.01, 981.99, 948.66, 924.37, 849.75, 828.53, 804.64, 774.80, 747.00. Raman: ν_{max}/cm^{-1} 1707, 1694, 1610, 1575, 1461, 1358, 1321, 1280, 1256, 1184, 1076, 1057, 863, 799, 756, 559, 510. MALDI-MS: m/z cald. for $C_{44}H_{52}O_8^+$: 708.3662; found: 708.3666.

3.5.21 Synthesis of 7.5 Compound was synthesized according to a similar procedure to **5.1** (Yield: 71.5 %). ^{1}H NMR (400 MHz, $CDCl_3$): δ 8.26 (d, 4H, J = 8.0 Hz), 8.00 (d, 4H, J= 8.0 Hz), 4.25 (t, 8H, J = 6.4 Hz), 1.72-1.67 (m, 4H), 1.56-1.42 (m, 16H), 0.97-0.93 (m, 24H). ^{13}C NMR (100 MHz, $CDCl_3$): δ 168.62, 132.99, 130.54, 130.20, 121.37, 67.52, 40.31, 23.35. IR (Diamond ATR): ν_{max}/cm^{-1} 2963.80, 2873.20, 1716.22 (COO), 1697.95, 1586.75, 1512.96, 1461.42, 1391.61, 1313.44, 1272.74, 1168.62, 1099.08, 1047.84, 1007.00, 953.77, 929.23, 895.12, 850.21, 801.80, 774.85, 747.87. Raman: ν_{max}/cm^{-1} 1702, 1698, 1607, 1575, 1462, 1360, 1322, 1260, 1184, 1107, 1067, 952, 851, 751, 657, 616, 561. MALDI-MS: m/z cald. for $C_{48}H_{60}O_8^+$: 764.4288; found: 764.4293.

3.5.22 Synthesis of 7.6 Compound was synthesized according to a similar procedure to **5.1** (Yield: 72.3 %). ^{1}H NMR (400 MHz, $CDCl_3$): δ 8.36 (d, 4H, J = 8.0 Hz), 8.09 (d, 4H, J= 8.0 Hz), 4.33 (t, 8H, J = 6.4 Hz), 1.83-1.79 (m, 8H), 1.66-1.58 (m, 4H), 1.37-1.31 (m, 8H), 0.95 (s, 12H), 0.94 (s, 12H). ^{13}C NMR (100 MHz, $CDCl_3$): δ 168.54, 133.15, 130.49, 130.47, 129.07, 128.89, 121.45, 65.92, 35.04, 29.72, 27.83, 26.51, 22.55. IR (Diamond ATR): ν_{max}/cm^{-1} 2951.66, 2925.86, 2867.43, 1717.92 (COO), 1702.72, 1588.05, 1512.49, 1462.20, 1445.62, 1310.13, 1264.38, 1226.36, 1200.84, 1184.60, 1157.93, 1096.37, 1051.35, 998.96,

975.81, 940.02, 893.66, 848.22, 805.05, 793.49, 775.19, 748.65, 673.31, 643.30. Raman: ν_{max}/cm^{-1} 1709, 1696, 1607, 1574, 1464, 1358, 1316, 1263, 1186, 1077, 1055, 867, 791, 751, 564, 510. MALDI-MS: m/z cald. for $C_{48}H_{60}O_8^+$: 764.4288; found: 764.4286.

3.5.23 Synthesis of 7.7 Compound was synthesized according to a similar procedure to **5.1** (Yield: 46.3 %). ^{1}H NMR (400 MHz, $CDCl_3$): δ 8.31 (d, 4H, *J* = 7.7 Hz), 7.91 (d, 4H, *J* = 7.8Hz), 4.34-4.38 (m, 8H), 1.88-1.85 (m, 4H), 1.66-1.50 (m, 12H), 1.40-1.14 (m, 28H), 1.00 (d, 12H, *J* = 6.3 Hz), 0.87 (d, 24H, *J* = 6.6 Hz). ^{13}C NMR (100 MHz, $CDCl_3$): δ 168.58, 132.76, 130.29, 128.79, 128.60, 121.27, 64.16, 39.42, 39.25, 39.07, 37.27, 35.53, 31.65, 30.24, 30.08, 29.72, 29.13, 29.04, 28.14, 27.97, 27.79, 24.69, 22.73, 22.63, 19.66. IR (Diamond ATR): ν_{max}/cm^{-1} 2953.68, 2925.50, 2868.66, 1718.05 (COO), 1590.13, 1514.27, 1461.19, 1408.65, 1383.46, 1365.73, 1308.09, 1267.13, 1197.94, 1156.62, 1129.44, 1098.04, 1071.75, 1040.03, 989.18, 840.58, 803.05, 769.78, 747.14. Raman: ν_{max}/cm^{-1} 1702, 1610, 1575, 1461, 1357, 1321, 1258, 1184, 1071, 800, 758, 639, 558, 508. MALDI-MS: m/z cald. for $C_{64}H_{92}O_8^+$: 988.6792; found: 988.6801.

References

(1) Chen, S.; Slattum, P.; Wang, C.; Zang, L. *Chem. Rev.* **2015**, *115*, 11967-11998.

(2) Balakrishnan, K.; Datar, A.; Oitker, R.; Chen, H.; Zuo, J. M.; Zang, L. *J. Am. Chem. Soc.* **2005**, *127*, 10496-10497.

(3) Li, C.; Wonneberger, H. *Adv. Mater.* **2012**, *24*, 613-636.

(4) Zhan, X. W.; Facchetti, A.; Barlow, S.; Marks, T. J.; Ratner, M. A.; Wasielewski, M. R.; Marder, S. R. *Adv. Mater.* **2011**, *23*, 268-284.

(5) Law, K.-Y. *Chem. Rev.* **1993**, *93*, 449-486.

(6) Dimitrakopoulos, C. D.; Malenfant, P. R. L. *Adv. Mater.* **2002**, *14*, 99-117.

(7) Jones, B. A.; Ahrens, M. J.; Yoon, M.-H. Facchetti, A.; Marks, T. J.; Wasielewski, M. R. *Angew. Chem. Int. Ed.* **2004**, *43*, 6363-6366.

(8) Tang, C. W. *Appl. Phys. Lett.* **1986**, *48*, 183-185.

(9) Schmidt-Mende, L.; Fechtenkötter, A.; Müllen, K.; Moons, E.; Friend, R. H.; MacKenzie, J. D. *Science* **2001**, *293*, 1119-1122.

(10) Breeze, A. J.; Salomon, A.; Ginley, D. S.; Gregg, B. A.; Tillmann, H.; Hörhold, H.-H. *Appl. Phys. Lett.* **2002**, *81*, 3085-3087.

(11) Würthner, F. *Chem. Commun.* **2004**, 1564-1579.

(12) Görl, D.; Zhang, X.; Würthner, F. *Angew. Chem. Int. Ed.* **2012**, *51*, 6328-6348.

(13) Ma, Y.-S.; Wang, C.-H.; Zhao, Y.-J.; Yu, Y.; Han, C.-X.; Qiu, X.-J.; Shi, Z. *Liq. Cryst.* **2007**, *19*, 141-149.

(14) Zhao, Q.; Zhang, S.; Liu, Y.; Mei, J.; Chen, S.; Lu, P.; Qin, A.; Ma, Y.; Sun, J. Z.; Tang, B. Z. *J. Mater. Chem.* **2012**, *22*, 7387-7394.

(15) Gregg, B. A. *J. Phys. Chem.* **1996**, *100*, 852-859.

(16) Marciniak, H.; Li, X.-Q.; Würthner, F.; Lochbrunner, S. *J. Phys. Chem. A* **2011**, *115*, 648-654.

(17) Kumar, S. *Chem. Soc. Rev.* **2006**, *35*, 83-109.

(18) Laschat, S.; Baro, A.; Steinke, N.; Giesselmann, F.; Hagele, C.; Scalia, G.; Judele, R.; Kapatsina, E.; Sauer, S.; Schreivogel, A.; Tosoni, M. *Angew. Chem. Int. Ed.* **2007**, *46*, 4832-4887.

(19) Wu, J.; Pisula, W.; Mullen, K. *Chem. Rev.* **2007**, *107*, 718-747.

(20) Boden, N.; Bushby, R. J.; Clements, J.; Movaghar, B. *J. Mater. Chem.* **1999**, *9*, 2081-2086.

(21) Bushby, R. J.; Lozman, O. R. *Curr. Opin. Solid State Mater. Sci.* **2002**, *6*, 569-578.

(22) Bushby, R. J.; Lozman, O. R. *Curr. Opin. Colloid Interface Sci.* **2002**, *7*, 343-354.

(23) Wöhrle, T.; Wurzbach, I.; Kirres, J.; Kostidou, A.; Kapernaum, N.; Litterscheidt, J.; Haenle, J. C.; Staffeld, P.; Baro, A.; Giesselmann, F.; Laschat, S. *Chem. Rev.* **2016**, *116*, 1139-1241.

(24) Gao, B.; Xia, D.; Zhang, L.; Bai, Q.; Bai, L.; Yang, T.; Ba, X. *J. Mater. Chem.* **2011**, *21*, 15975-15980.

(25) Bhavsar, G. A.; Asha, S. K. *Chem. Eur. J.* **2011**, *17*, 12646-12658.

(26) Balakrishnan, K.; Datar, A.; Naddo, T.; Huang, J.; Oitker, R.; Yen, M.; Zhao, J.; Zang, L. *J. Am. Chem. Soc.* **2006**, *128*, 7390-7398.

(27) Balakrishnan, K.; Datar, A.; Oitker, R.; Chen, H.; Zuo, J.; Zang, L. *J. Am. Chem. Soc.* **2005**, *127*, 10496-10497.

(28) Alben, R. *Phys. Rev. Lett.* **1973**, *30*, 778-781.

(29) Alben, R. *J. Chem. Phys.* **1973**, *59*, 4299-4304.

(30) Straley, J. P. *Phys. Rev. A* **1974**, *10*, 1881-1887.

(31) Vanakaras, A. G.; Bates, M. A. Photinos, D. J. *Phys. Chem. Chem. Phys.* **2003**, *5*, 3700-3706.

(32) Raton, Y. M.; Varga, S.; Velasco, E. *Phys. Rev. E: Stat. Nonlin. Soft Matter Phys.* **2008**, *78*, 031705-1/12.

(33) Tschierske, C.; Photinos, D. J. *J. Mater. Chem.* **2010**, *20*, 4263-4294.

(34) Mo, X.; Chen, H.-Z.; Shi, M.-M.; Wang, M. *Chem. Phys. Lett.* **2006**, *417*, 457-460.

(35) Mo, X.; Shi, M.-M.; Huang, J.-C.; Wang, M.; Chen, H.-Z. *Dyes Pigments* **2008**, *76*, 236-242.

(36) Saidi-Besbes, S.; Grelet, E.; Bock, H. *Angew. Chem. Int. Ed.* **2006**, *45*, 1783-1786.

(37) Wolarz, E.; Mykowska, E.; Martyński, T.; Stolarski, R. *J. Mol. Struct.* **2009**, *929*, 79-84.

(38) Stolarski, R.; Fiksiński, K. *Dyes Pigments* **1994**, *24*, 295-303.

(39) Benning, S.; Kitzerow, H.-S.; Bock, H.; Achard, M.-F. *Liq. Cryst.* **2000**, *27*, 901-906.

(40) Hassheider, T.; Benning, S. A.; Kitzerow, H.-S.; Achard, M.-F.; Bock, H. *Angew. Chem. Int. Ed.* **2001**, *40*, 2060-2063.

(41) Alibert-Fouet, S.; Seguy, I.; Bobo, J.-F.; Destruel, P.; Bock, H. *Chem. Eur. J.* **2007**, *13*, 1746-1753.

(42) Kumar, S. in Chemistry Of Discotic Liquid Crystals: From Monomers to Polymers; Percec, V., Ed., CRS Press, Taylor & Francis Group: Boca Raton, FL, 2011.

(43) Kumar, S. *Liq. Cryst.* **2004**, *31*, 1037-1059.

(44) Johnson, L.; Ringstrand, B.; Kaszynski, P. *Liq. Cryst.* **2009**, *36*, 179-185.

(45) Choudhury, A. R.; Nagarajan, K.; Guru Row, T. N. *Cryst. Eng. Commun.* **2006**, *8*, 482-488.

(46) Segeyev, S.; Pisula, W.; Geerts, Y. H. *Chem. Soc. Rev.* **2007**, *36*, 1902-1929.

(47) Eccher, J.; Faria, G. C.; Bock, H.; von Seggern, H.; Bechtold, I. H. *ACS Appl. Mater. Interfaces* **2013**, *5*, 11935-11943.

(48) Simpson, C.; Wu, J.; Watson, M.; Müllen, K. *J. Mater. Chem.* **2004**, *14*, 494-504.

(49) Hatsusaka, K.; Ohta, K.; Yamamoto, I.; Shirai, H. *J. Mater. Chem.* **2001**, *11*, 423-433.

(50) Pisula, W.; Tomovic, Z.; El Hamaoui, B.; Watson, M. D.; Pakula, T.; Müllen, K. *Adv. Funct. Mater.* **2005**, *15*, 893-904.

(51) Yang, T.; Pu, J.; Zhang, J.; Wang, W. *J. Org. Chem.* **2013**, *78*, 4857-4866.

(52) Bushby, R. J.; Kawata, K. *Liq. Cryst.* **2011**, *38*, 1415-1426.

(53) Lai, C. K.; Tsai, C.-H.; Pang, Y.-S. *J. Mater. Chem.* **1998**, *8*, 1355-1360.

(54) Kistler, K. A.; Pochas, C. M.; Yamagata, H.; Matsika, S.; Spano, F. C. *J. Phys. Chem. B* **2012**, *116*, 77-86.

(55) Hippius, C.; van Stokkum, I. H. M.; Zangrado, E.; Williams, R. M.; Wuerthner, F. *J. Phys. Chem. C* **2007**, *111*, 13988-13996.

(56) Chen, Z.; Fimmel, B.; Wurthner, F. *Org. Biomol. Chem.* **2012**, *10*, 5845-5855.

(57) Rodler, F.; Schade, B.; Jäger, C. M.; Backes, S.; Hampel, F.; Böttcher, C.; Clark, T.; Hirsch, A. *J. Am. Chem. Soc.* **2015**, *137*, 3308-3317.

(58) Ghosh, S.; Li, X.-Q.; Stepanenko, V.; Wurthner, F. *Chem. Eur. J.* **2008**, *14*, 11343-11357.

(59) Islam, M. R.; Dahan, E.; Saimani, S.; Sundararajan, P. R. *Eur. Polym. J.* **2012**, *48*, 1538-1554.

(60) Würthner, F.; Thalacker, C.; Diele, S.; Tschierske, C. *Chem. Eur. J.* **2001**, *7*, 2245-2253.

(61) Gupta, R. K.; Pathak, S. K.; Pradhan, B.; Rao, D. S. S.; Prasad, S. K.; Achalkumar, A. S. *Soft Matter* **2015**, *11*, 3629-3636.

(62) Bijak, K.; Janeczek, H.; Grucela-Zajac, M.; Schab-Balcerzak, E. *Opt. Mater.* **2013**, *35*, 1042-1050.

(63) Johansson, L. B.-Å.; Langhals, H. *Spectrochim. Acta* **1991**, *47A*, 857-861.

(64) Dulmage, W. J.; Light, W. A.; Marino, S. J.; Salzberg, C. D.; Smith, D. L.; Staudenmayer, W. J. *J. Appl. Phys.* **1978**, *49*, 5543-5554.

(65) Kasha, M.; Rawls, H. R.; El-Bayoumi, M. A. *Pure Appl. Chem.* **1965**, *11*, 371-392.

(66) Prabhu, D. D.; Sivadas, A. P.; Das, S. *J. Mater. Chem. C* **2014**, *2*, 7039-7046.

(67) Spano, F. C. *Acc. Chem. Res.* **2010**, *43*, 429-439.

(68) Würthner, F.; Chen, Z.; Dehm, V.; Stepanenko, V. *Chem. Commun.* **2006**, 1188-1190.

(69) Aotake, T.; Suzuki, M.; Aratani, N.; Yuasa, J.; Kuzuhara, D.; Hayashi, H.; Nakano, H.; Kawai, T.; Wu, J.; Yamada, H. *Chem. Commun.* **2015**, *51*, 6734-6737.

(70) Pankhurst, J. R.; Cadenbach, T.; Betz, D.; Finn, C.; Love, J. B. *Dalton Trans.* **2015**, *44*, 2066-2070.

(71) Zhang, Y.; Bao, X.; Xiao, M.; Tan, H.; Tao, Q.; Wang, Y.; Liu, Y.; Yang R.; Zhu, W. *J. Mater. Chem. A* **2015**, *3*, 886-893.

(72) Areephong, J.; Hendsbee, A. D.; Welch, G. C. *New J. Chem.* **2015**, *39*, 6714-6717.

(73) Bala, I.; Pal, S. K. *Liq. Cryst.* **2016**, DOI:10.1080/02678292.2016.1153733

(74) Gupta, R. K.; Manjuladevi, V.; Karthik, C.; Kumar, S. *J. Phys.: Conf. Ser.* **2013**, *417*, 012068/1-6.

(75) Xu, D.; Watt, G. D.; Harb, J. N.; Davis, R. C. *Nano Lett.* **2005**, *5*, 571-577.

(76) Gayathri, H. N.; Kumar. B.; Suresh, K. A.; Bisoyi, H. K.; Kumar, S. *Phys. Chem. Chem. Phys.* **2016**, *18*, 12101-12107.

(77) Xue, J.; Jung, C. S.; Kim, M. W. *Phys. Rev. Lett.* **1992**, *69*, 474-477.

Appendix II

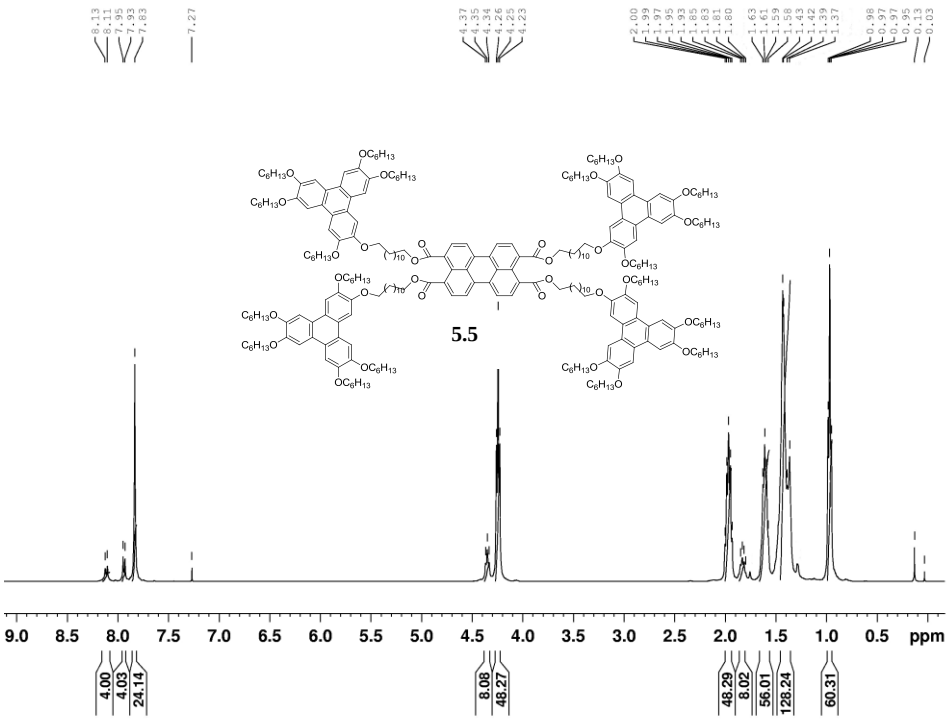

Figure A1 ^{1}H NMR spectrum of compound **5.5**.

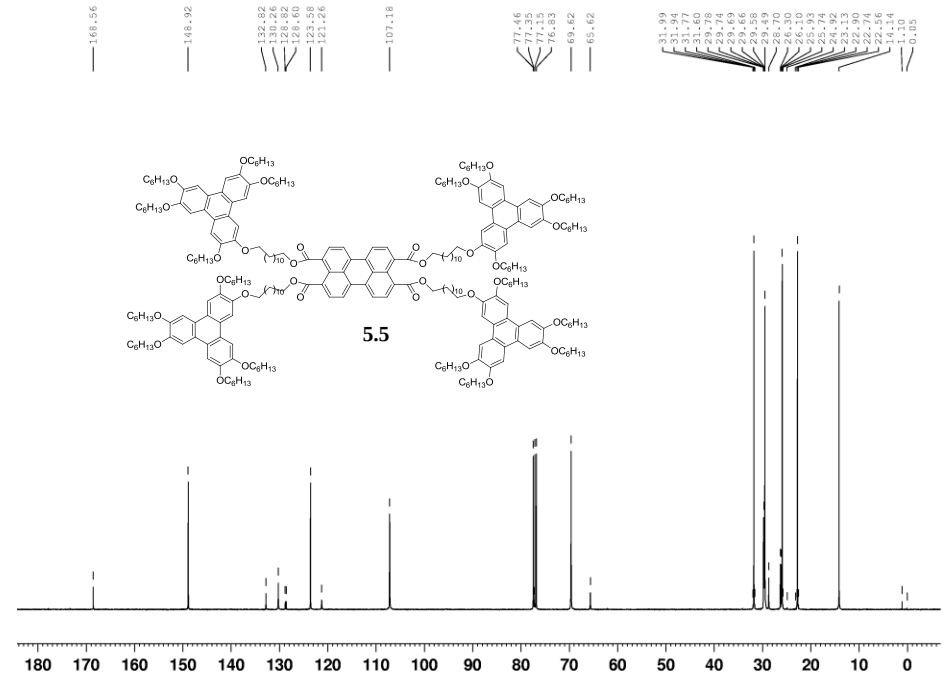

Figure A2 ^{13}C NMR spectrum of compound **5.5**.

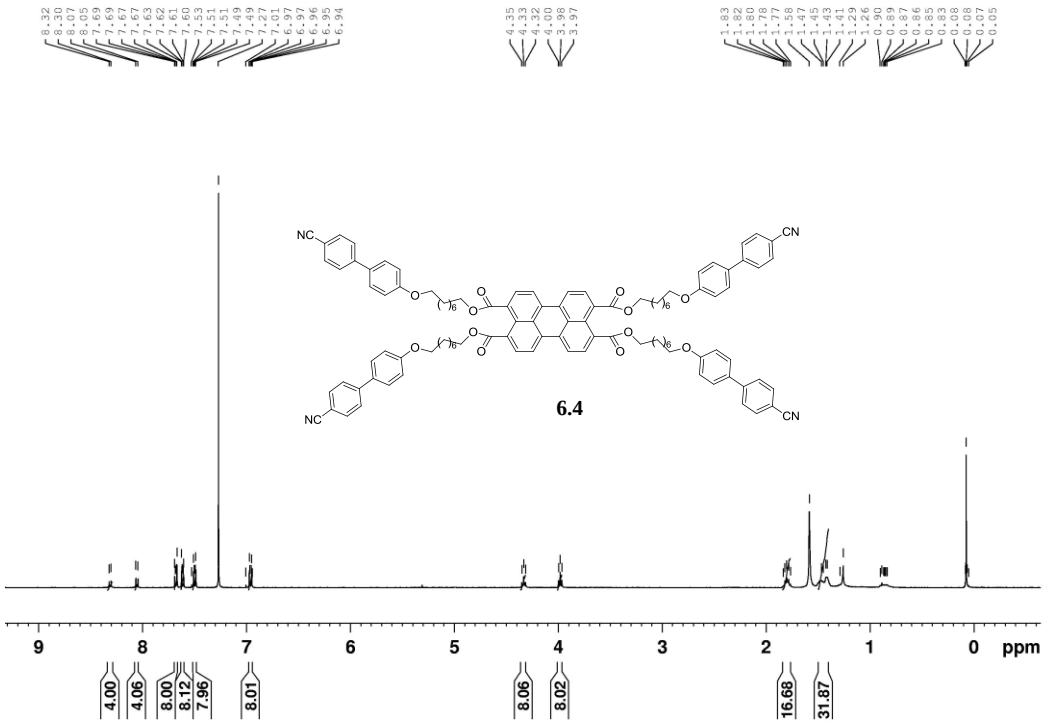

Figure A3 ^{1}H NMR spectrum of compound **6.4**.

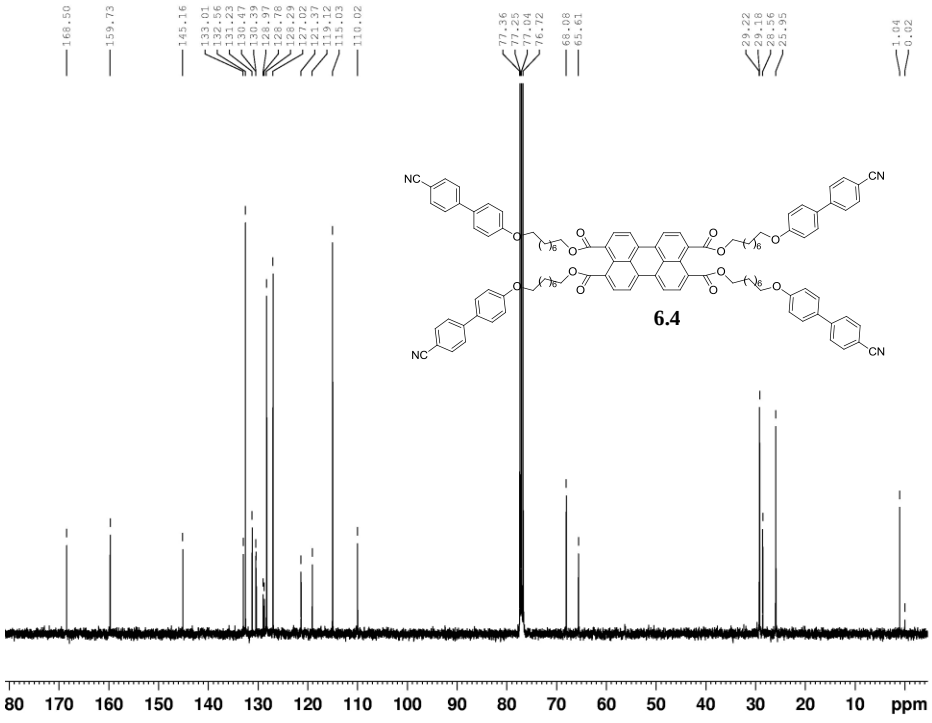

Figure A4 ^{13}C NMR spectrum of compound **6.4.**

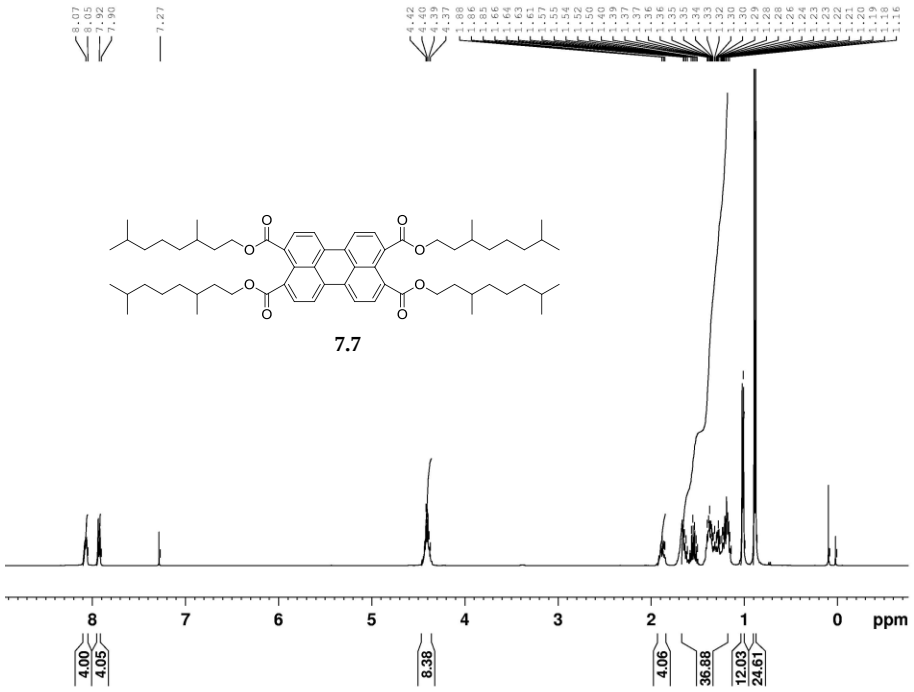

Figure A5 ^{1}H NMR spectrum of compound **7.7.**

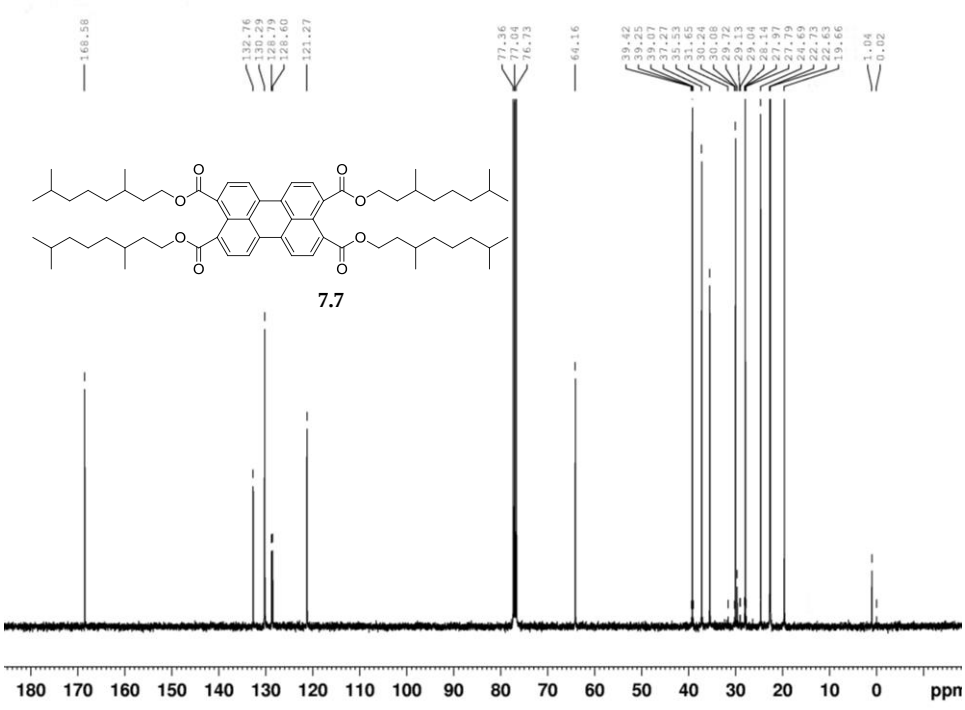

Figure A6 ^{13}C NMR spectrum of compound **7.7**.

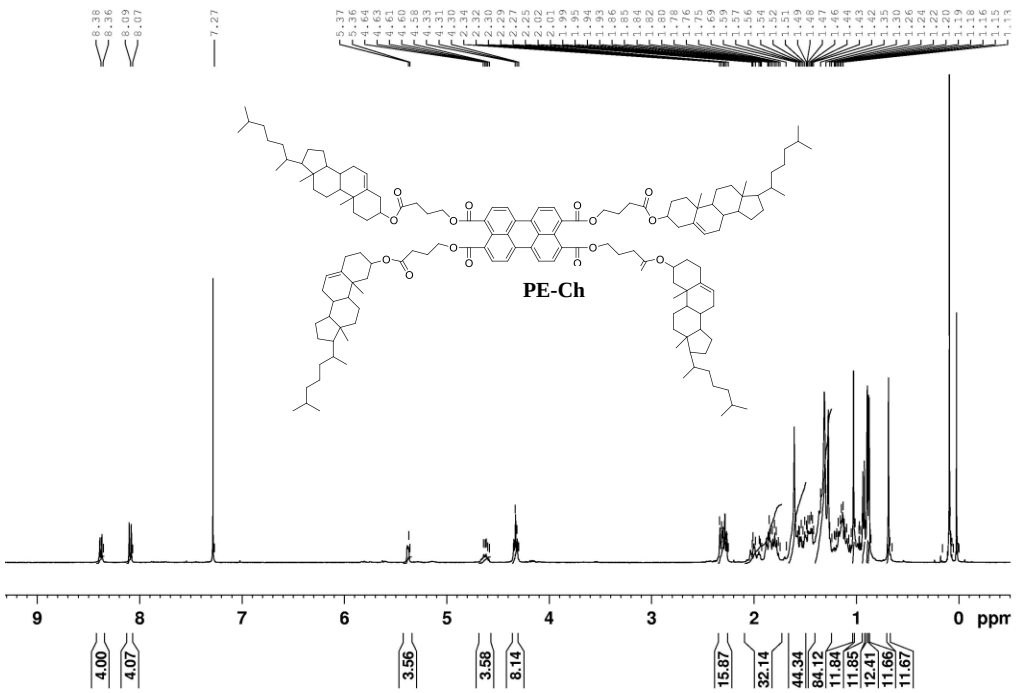

Figure A7 ^{1}H NMR spectrum of compound **PE-Ch.**

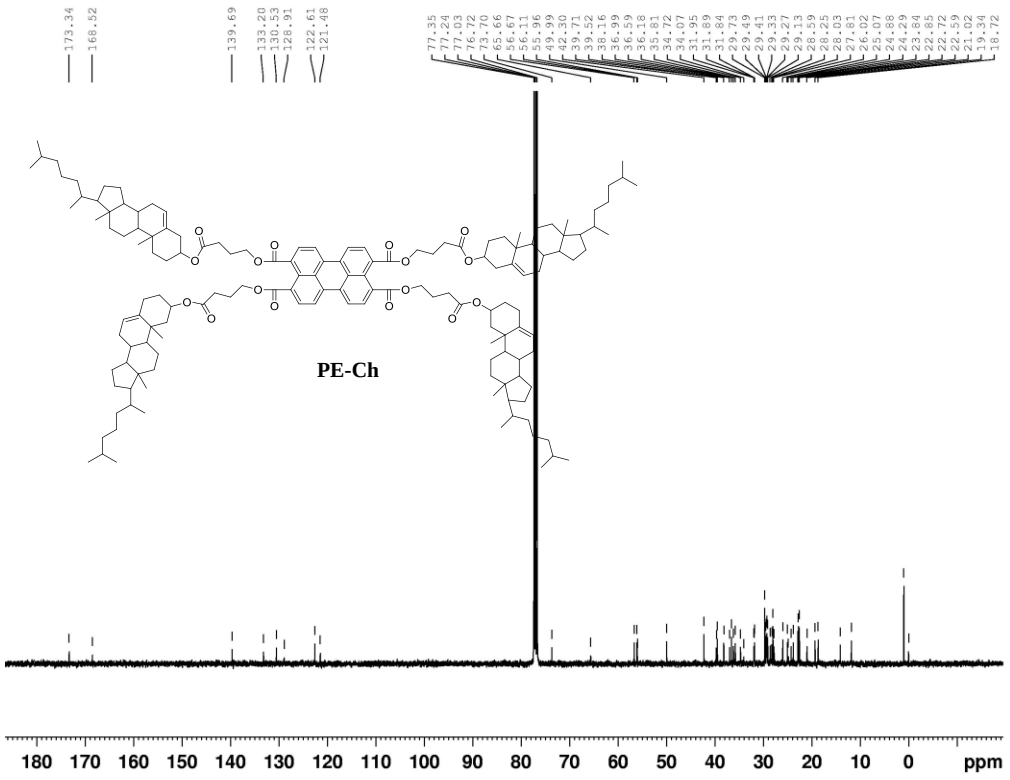

Figure A28 ^{13}C NMR spectrum of compound **PE-Ch.**

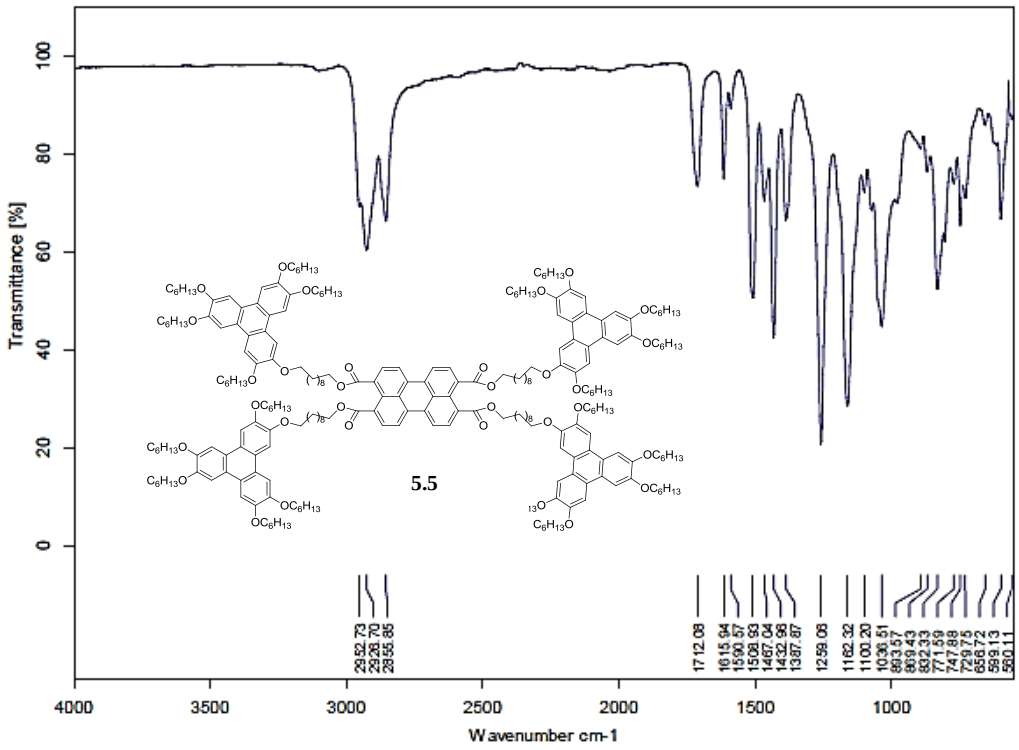

Figure A9 IR spectrum of compound **5.5.**

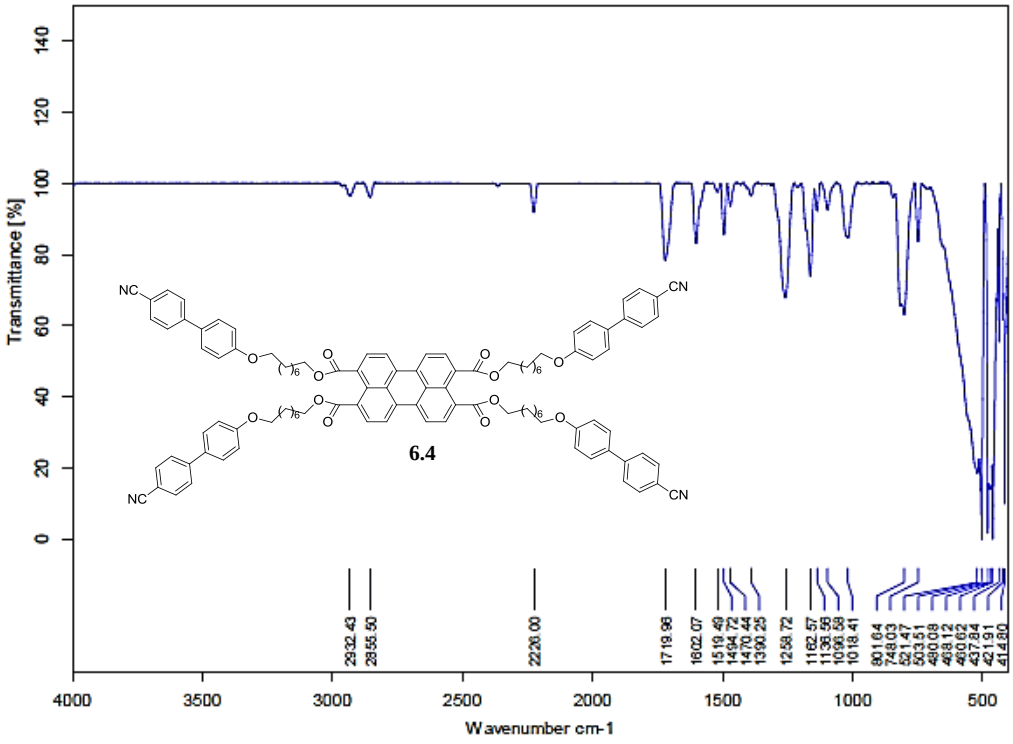

Figure A10 IR spectrum of compound **6.4.**

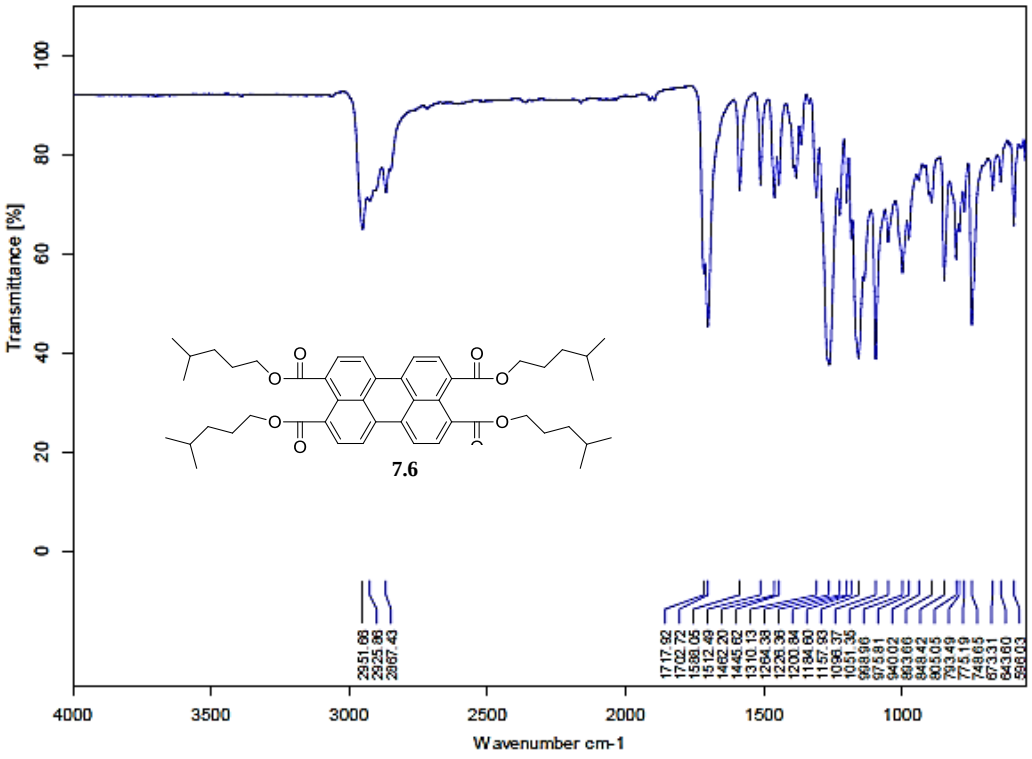

Figure A11 IR spectrum of compound **7.6.**

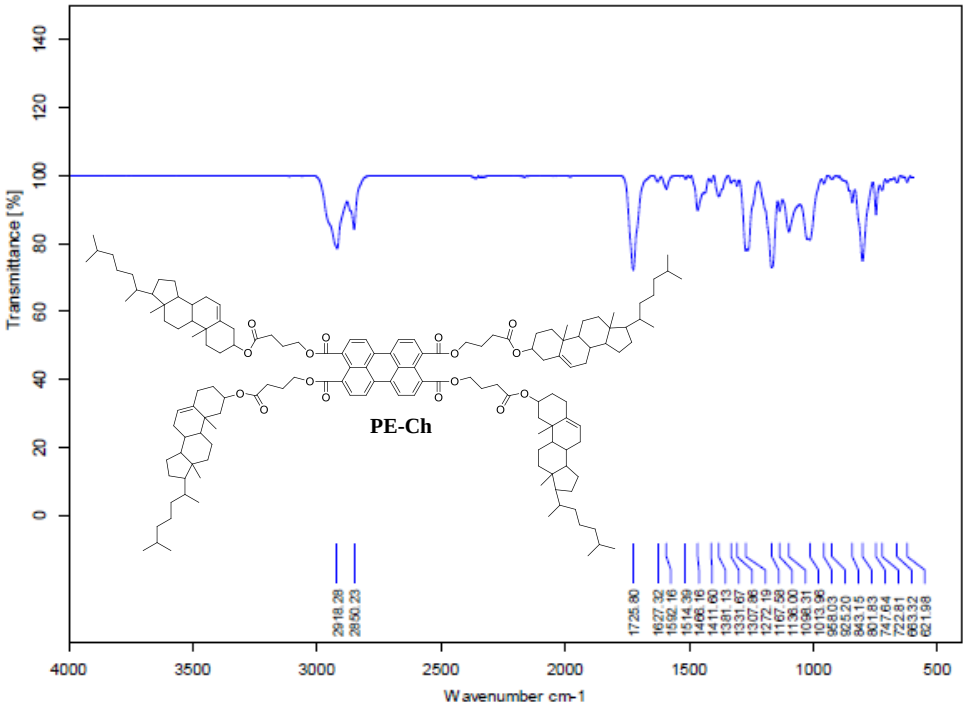

Figure A12 IR spectrum of compound **PE-Ch.**

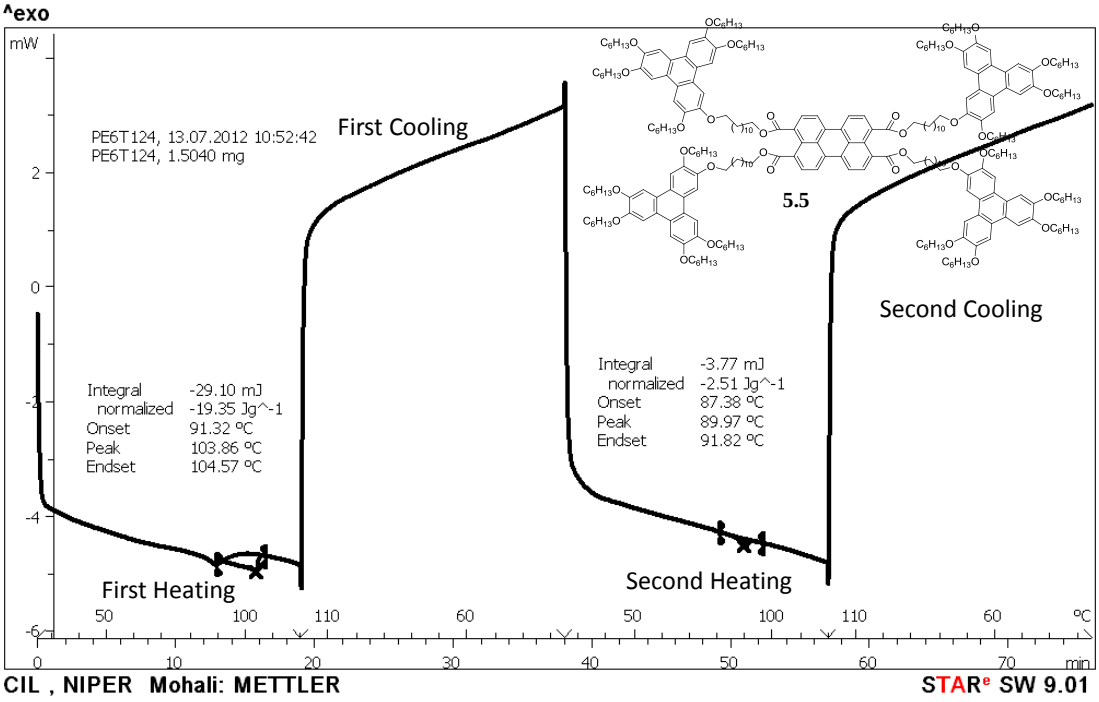

Figure A13 DSC thermogram of compound **5.5.**

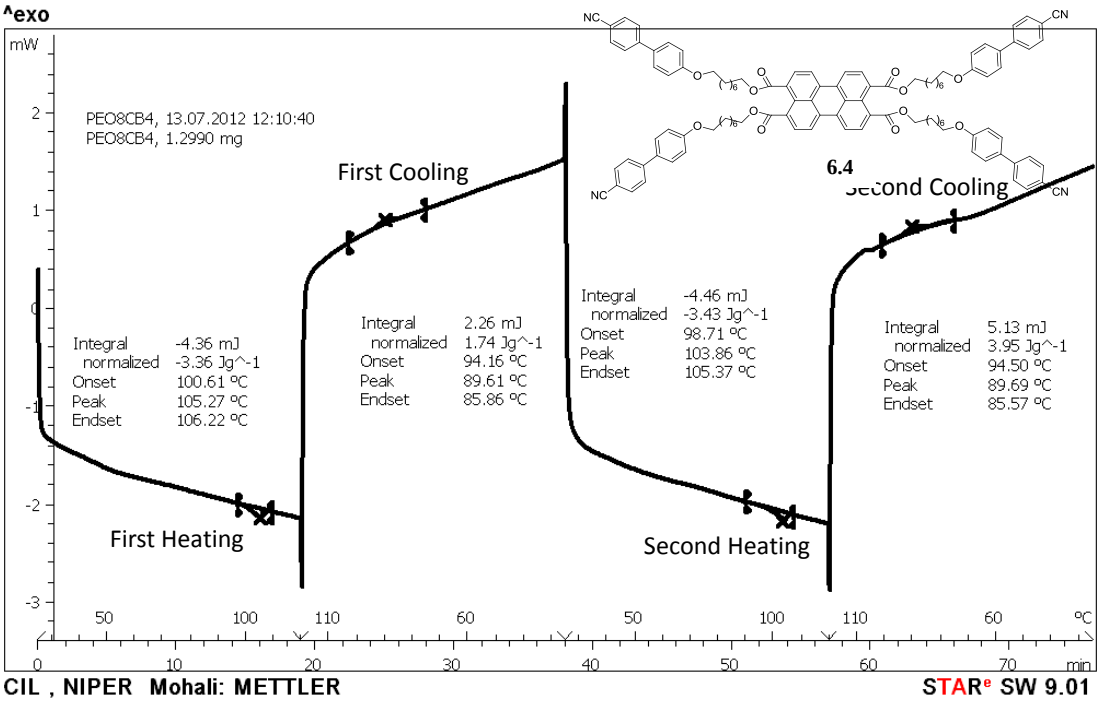

Figure A14 DSC thermogram of compound **6.4.**

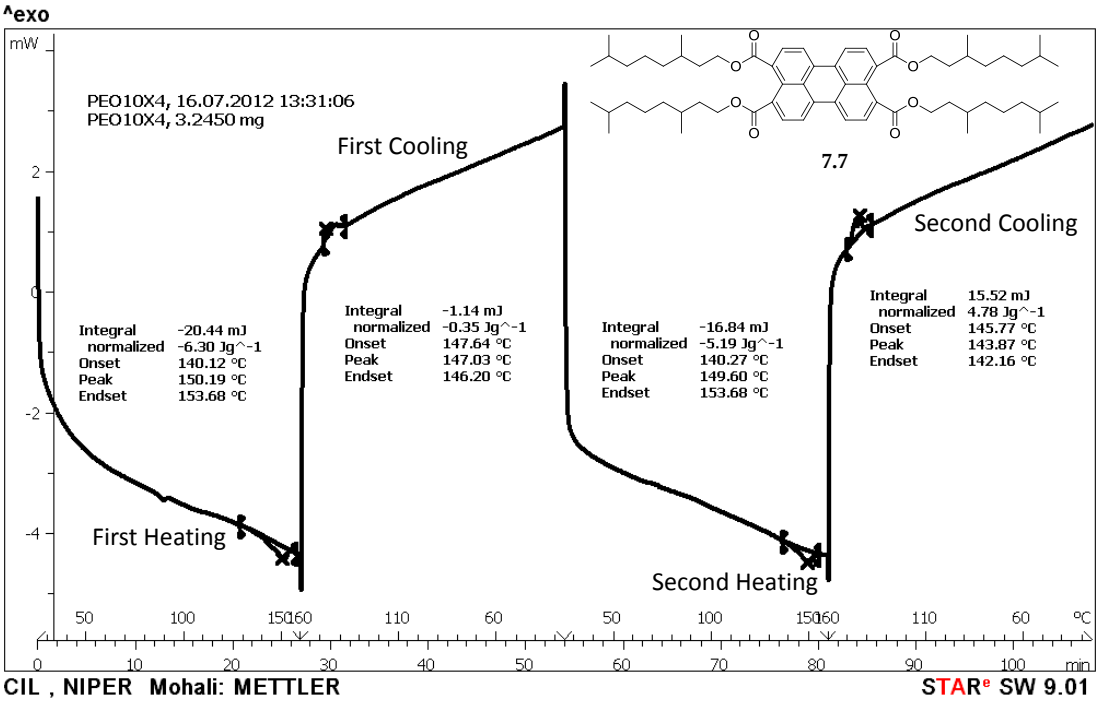

Figure A15 DSC thermogram of compound **7.7.**

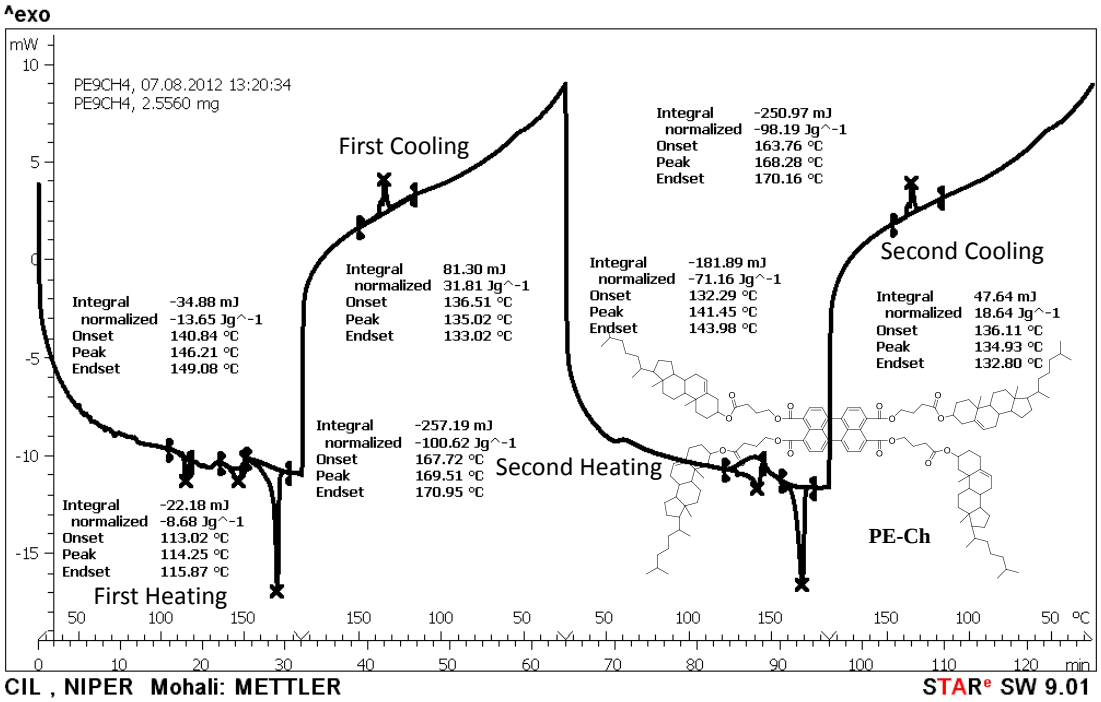

Figure A16 DSC thermogram of compound **PE-Ch.**

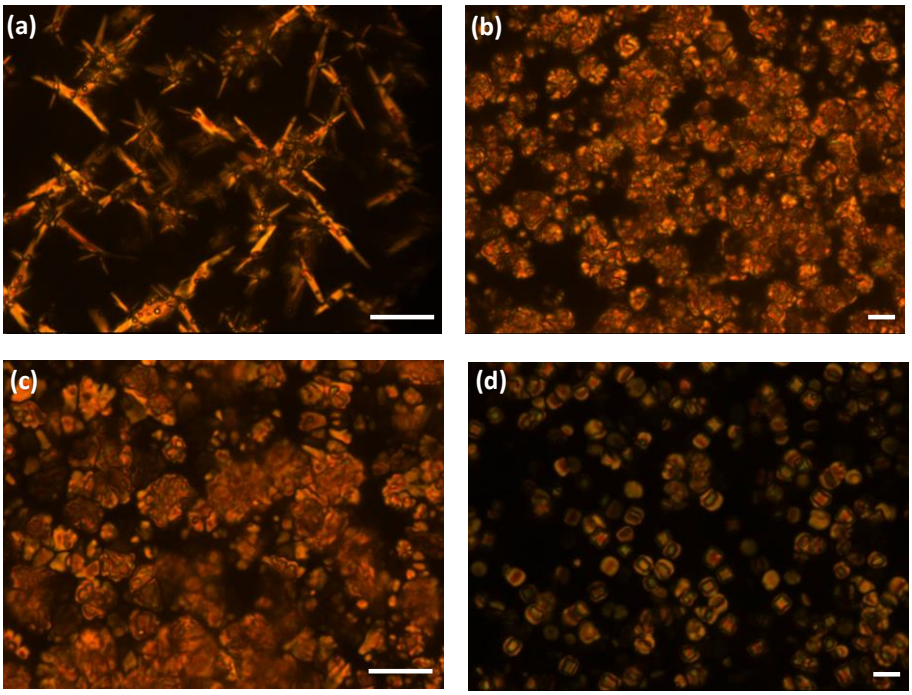

Figure A17 Polarizing optical micrographs of compounds (a) **5.1** at 88.4 °C, (b) **5.2** at 100.9 °C, (c) **5.3** at 123.4 °C and (d) **5.5** at 124.6 °C on cooling from the isotropic phase (scale bar = 10 μm).

In addition to the perylene tetraesters mentioned in chapter 3, we have also synthesized another mesogen based on cholesterol moiety according to the same procedure as already mentioned in that chapter (Figure A18). This cholesterol derivative was found to be non-liquid crystalline at room temperature. However, it exhibited a monotropic nematic (N*) phase on cooling. On first heating in DSC it showed a melting temperature at around 169.5 °C. Before melting it displayed two low energy crystal-to-crystal transitions at about 114.3 °C and 146.2 °C which could be due to some conformational reorganization of molecules by passing into different crystalline configurations. We also observed minor structural changes at Cr–Cr transition temperatures of the compounds reported here under POM and the samples remained solid even after these transitions. On cooling, it showed a transition in DSC centered at 135 °C, which was stable down to room temperature. The chiral nematic phase was assigned on the basis of the observation of fan texture when viewed through a polarized light microscope: representative texture is shown as Figure A17b. The fan texture gave the characteristic Grandjean texture upon shearing. The broad small angle reflection showed a *d*-

spacing of 18.35 Å (2θ = 4.82) at 150 °C (Figure A32c) in the N* phase (on cooling) which corresponds to the average length of the cholesterol moiety (~29.72 Å) and the discs (~7.6 Å) as expected. A very diffuse peak at around 5.60 (2θ = 15.75) Å indicates liquid like order.

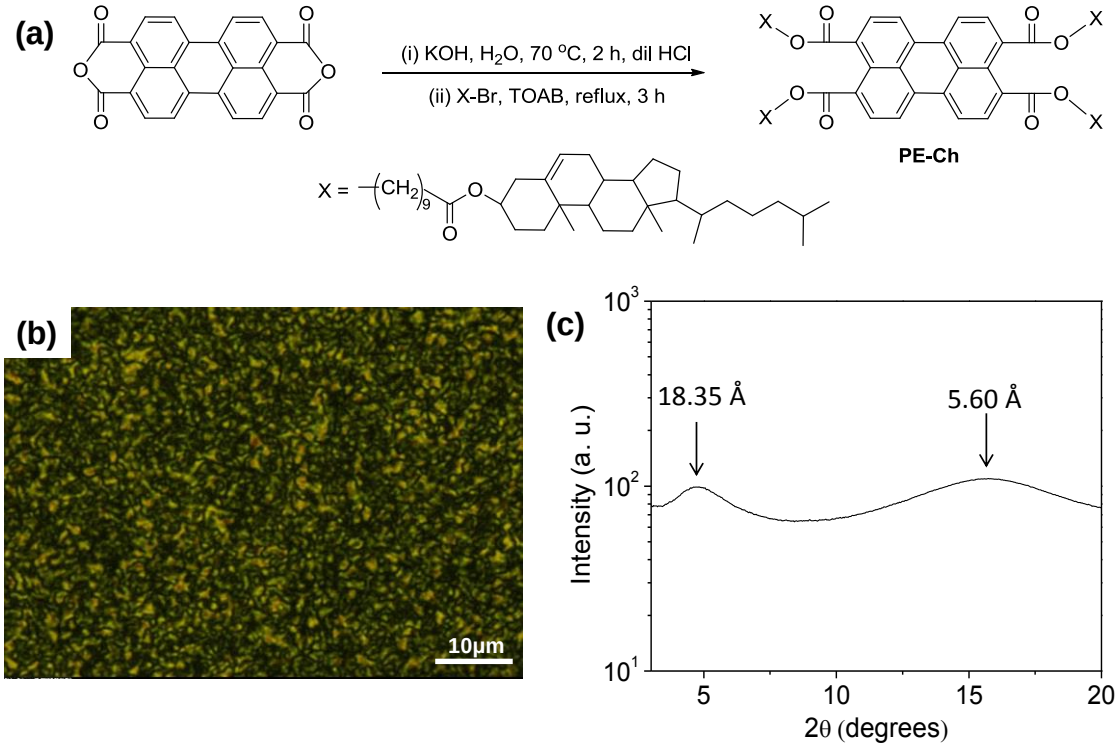

Figure A18 (a) Synthesis scheme of perylene tetraester based on cholesterol, (b) its polarizing optical micrograph in the mesophase and (c) an intensity vs. 2θ profile of the same compound as obtained after cooling from the isotropic phase.

Chapter 4

Development of Alkoxy Substituted Hexa-*peri*-hexabenzocoronene Discotics with Higher Order Mesophases at Room Temperature

PART A

In this work, the role of alkoxy substituents in determining the geometrical preferences of the Scholl reaction for the formation of dodecylalkoxy substituted hexa-*peri*-hexabenzocoronene core has been investigated experimentally and computationally. Experimentally, it has been found that when the alkoxy substituents are ortho to each other, the Scholl reaction resulted in partially cyclized products and when the alkoxy groups are meta to each other, completely fused product formed. The reaction path analysis suggested that high barrier is preventing further bond formation. The regioselectivity of Scholl reaction is highly dependent on the position of electron donating groups on the ring.

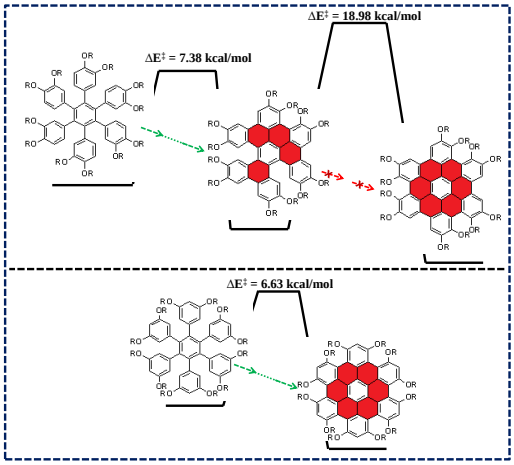

PART B

The first discotic systems based on alkoxy (tri- & di-) substituted hexa-*peri*-hexabenzocoronene that self-organizes into room temperature columnar structure has been prepared. Tri- and di- substituted HBC derivatives showed reddish and yellowish green fluorescence under long wavelength (365 nm) UV light illumination in solution as well as in thin films in the liquid crystalline (LC) state at room temperature, respectively. Tri-alkoxy derivative was found to self-organize into a highly ordered columnar rectangular mesophase, while the other (di-) possessed a columnar hexagonal mesophase.

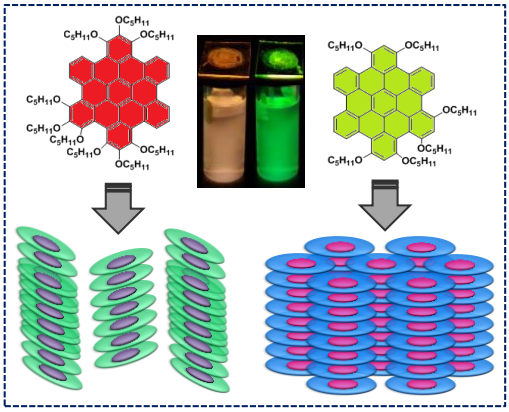

4.1 Part A: An expedient access towards alkoxy substituted hexa-*peri*-hexabenzocoronene core *via* regioselective Scholl reaction: Experimental and computational insights

4.1.1 Introduction

The backbone of all organic compounds is composed of C-C bonds and building a C-C linkage directly from two simple C-H bonds has emerged as an attractive and challenging task in the field of organic synthesis. The tandem oxidation of C-H bonds takes place in the presence of some reagents and these oxidations often reduce the number of steps required to achieve the target molecule.[1,2] In this regard, direct coupling reactions of arenes i.e., Scholl oxidations are highly attractive, since neither the aryl halide nor the organometallic reagents are required in these reactions.

The Scholl reaction has been effectively employed for the oxidative condensation of *o*-terphenyls (**1**) and hexaarylbenzenes (**3**) to produce the corresponding triphenylenes (**2**) and hexa-*peri*-hexabenzocoronenes (**4**) (HBC).[3-9]

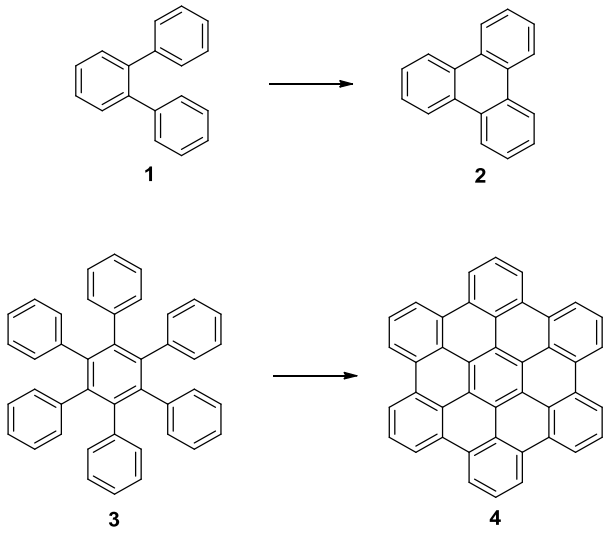

Among them HBCs, the smallest prototype of polycyclic aromatic hydrocarbons (PAH) are particularly interesting as they often exhibit strong π-π interactions in solution as well as in films.[10-14] Hence, HBCs are able to form highly ordered columnar structures that produce

high charge carrier mobilities of the order of 5 $cm^2 V^{-1} s^{-1}$.[15] Furthermore, with the alignment of HBC molecules organic field-effect transistors (OFET) mobility of 5×10^{-3} $cm^2 V^{-1} s^{-1}$ has been achieved in the columnar phase.[16] Due to the high charge-carrier mobility, self-healing of defects, defect free long-range order and tendency to form highly ordered films of various thicknesses, HBCs can be very promising as active semiconductors in OFETs and photovoltaic devices.[17-29] However, the introduction of various functional groups at the peripheral positions of the HBC core has been limited due to the poor solubility of this core[30] and the undesired reactions. In particular, the synthesis of alkoxy substituted HBC directly from a hexaphenyl benzene precursor is difficult due to severe side reactions such as cleavage of ether chains.[31,32]

Feng *et al.* reported that the topology and substituents influence the cyclisation of HBC precursors.[33] Bock and co-workers also pointed out that the outcome of the Scholl reaction remains only partially predictable.[34,35] In this context, it has been hypothesized that reactions of reasonably electron rich arenes with oxidants can lead to formation of C-C bonds.

4.1.2 Objective

Intrigued by this, we initiated an investigation of the effect of steric hindrance and electron donating groups (particularly alkoxy substituents) on the regioselectivity of Scholl reaction in case of HBCs. Particularly, two key questions have been analyzed here: how does the oxidative cross-coupling of aromatic compounds depend on the electron density and steric hindrance of the oligophenylenes and how cyclodehydrogenation reaction of oligophenylenes can be affected by the electronic effects.

Till now, only a few theoretical studies have been carried out to investigate the reaction pathway for the Scholl oxidation of hexaphenylbenzene to HBC. Some reports followed the radical cation pathway[36] and some advocated the existence of arenium cation pathway[37,38] for the formation of HBCs from unsubstituted hexaphenylbenzene. Herein, we present an experimental and computational study to examine the steric and substituent effects (particularly alkoxy) on the formation of HBC core through Scholl reaction. By this study, we have provided insights into the geometrical preferences of the Scholl reaction for the

formation of dodecylalkoxy substituted HBC core. We have also shown that why a number of electron rich precursors do not undergo complete cyclodehydrogenation reaction on exposure to oxidants. In this perspective, a deeper understanding of the regioselectivities of Scholl reaction on the formation of HBC can contribute to the efficient synthesis of large polycyclic benzenoid aromatic hydrocarbons. Density functional theory (DFT) calculations with the hybrid functional B3LYP and the 6-31G (d) basis set have been performed to analyze the nature of products formed and the reaction mechanism. The proton affinities of the intermediates and reactants involved have been understood in terms of the electrostatic potential calculations. The details of these findings are discussed in the context of arenium cation mechanism for the formation of HBC core.

Past reports[37,38] also suggested the contiguous formation of C-C bonds in the arenium cation pathway. However, this mechanism may not be applicable if substituent effects are taken into consideration. When complete oxidation does not occur, the order of C-C bond formation cannot be well defined. In this work, we have focused on the arenium cation route (owing to the presence of acids among the reactants) as the barriers for the arenium cation pathway were found to be lower than the radical cation pathway for unsubstituted HBCs. To the best of our knowledge, this is the first combined experimental and theoretical report describing the role of alkoxy substituents in the formation of hexa-*peri*-hexabenzocoronene core *via* Scholl reaction.

4.1.3 Results and Discussion

4.1.3.1 Synthesis of various HBC precursors

All the HBC precursors (Chart 4.1) employed in this study were synthesized using the standard synthetic procedures. King and co-workers[39] have shown that electronic directing groups can be used to control the Scholl reaction in case of triphenylene. In this framework, we plan to synthesize hexaphenylbenzenes with two alkoxy groups on each ring. We thought that because of the higher electron density due to two alkoxy groups compared to the HBC precursors reported in earlier studies, complete cyclodehydrogenation can be achieved.[31,32] For example, the synthesis of HBC precursor **5a** started from the alkylation of commercially available 4-bromocatechol **6a** with 1-bromooctane to give compound **7a** in quantitative yield.

The Stille-type coupling of **7a** with bis-(tributylstannyl)acetylene and $Pd(PPh_3)_4$ in toluene gave the corresponding symmetrical diphenylacetylenes **8a** in 55 % yield (Scheme 4.1). Subsequent cyclotrimerization of the diphenylacetylene **8a** with $[Co_2(CO)_8]$ in 1,4-dioxane yielded the hexaphenylbenzene precursor molecule **5a**. The synthetic details of various Scholl precursors in Chart 4.1 and the ^{1}H NMR, ^{13}C NMR, IR and MALDI-MS are presented in the experimental section and appendix III (Figures A1-A4, A9-A10).

Chart 4.1 Structures of various Scholl precursors used in this study.

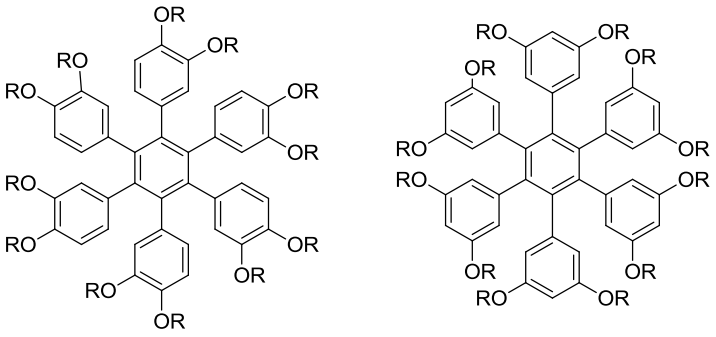

5a; R = C_8H_{17}
5b; R = C_5H_{11}
5c; R = CH_3

5d; R = C_5H_{11}
5e; R = CH_3

4.1.3.2 Oxidative cyclodehydrogenation of various HBC precursors

Scholl reaction was performed by treatment of HBC precursors say **5a** with 6 equiv. of dichlorodicyano-*p*-benzoquinone (DDQ)[40,41] in dichloromethane and methylsulfonic acid (10 % v/v) under an argon atmosphere at 0 ^{0}C (Scheme 4.2). After 2 h, the reaction was quenched with sodium carbonate (TLC monitoring) followed by a standard aqueous workup. From the complex reaction mixture, we were able to isolate the major product in 27 % yield. To our surprise, the ^{1}H NMR spectra of this product was very complex and resonances in the aromatic range showed five sharp singlet signals (Figure 4.1) which clearly indicated that some unexpected product has formed. MALDI-MS analysis revealed that the molecular weight of the product formed was corresponding to four newly formed C-C bonds. The regiochemistry of bond formation was unambiguously characterized by NMR spectroscopy and the product was assigned the structure **9a** using ^{1}H NMR, ^{13}C NMR, ^{1}H-^{1}H COSY, ^{1}H-

^{1}H NOESY and MALDI-MS experiments (appendix III, Figures A1, 2, 9, 15, 16), the only qualified structure that possess a C_2 symmetry axis (see Chart A1 for all possible structures).

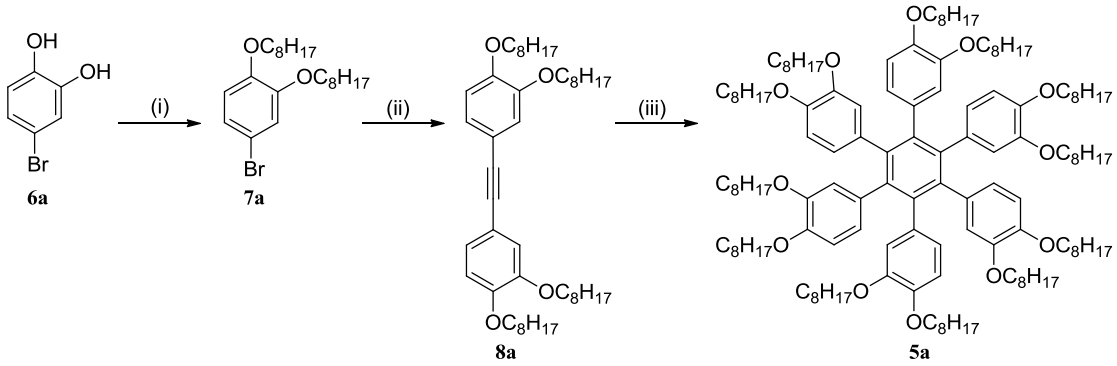

Scheme 4.1 Synthesis of HBC precursor **5a**. *Reagents and Conditions*: (i) $C_8H_{17}Br$, K_2CO_3, 2-Butanone, KI, reflux, 18 h, quantitative; (ii) Bis-(tributylstannyl)acetylene, $Pd(PPh_3)_4$, Toluene, reflux, 12 h, 55 %; (iii) $[Co_2(CO)_8]$, 1,4-Dioxane, reflux, 7 h, 49 %.

^{1}H-^{1}H COSY experiments (see appendix) revealed that there is no interaction as such in the bonded protons and from the ^{1}H-^{1}H NOESY experiments (see appendix), it was established that there is only a single interaction occurring between the non-bonded protons.

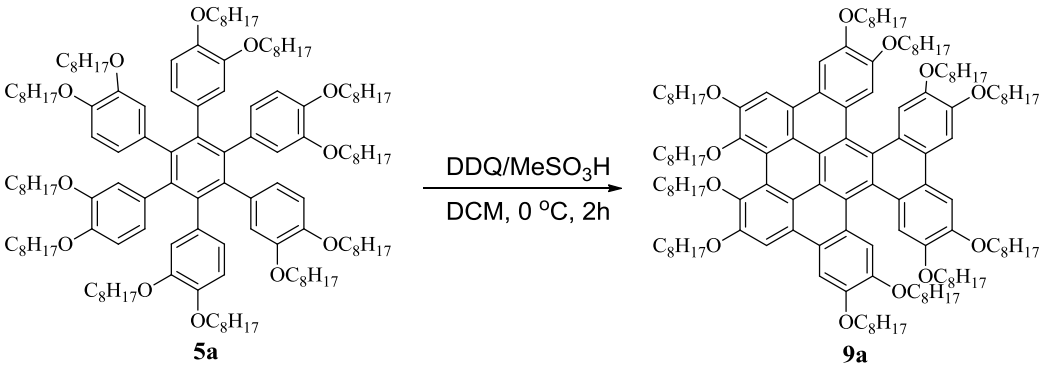

Scheme 4.2 Scholl reaction of HBC precursor **5a**.

The single isotopic envelop of **9a** at m/z 2064.6074 compared to m/z of fully fused HBC revealed a mass difference of four which is in agreement with dehydrogenation of eight protons due to four C-C bonds formation. The proposed C_2 symmetry was further confirmed by the observation of two sets of alkoxy signals for the chains as shown in Figure 4.1.

We next analyzed the reaction mixture of Scholl oxidation of compound **5a** as a function of reaction time. The reaction time was extended from 2 h to 24 h. Interestingly, final two C−C bonds did not form even at extended reaction times. Prolonged exposure of the partially cyclodehydrogenated mixture to an excess of DDQ also didn't lead to formation of other bonds. The reaction temperature was also varied from 0 °C to R.T. to refluxing in DCM. However, the final product remained invaried (Table 4.1).

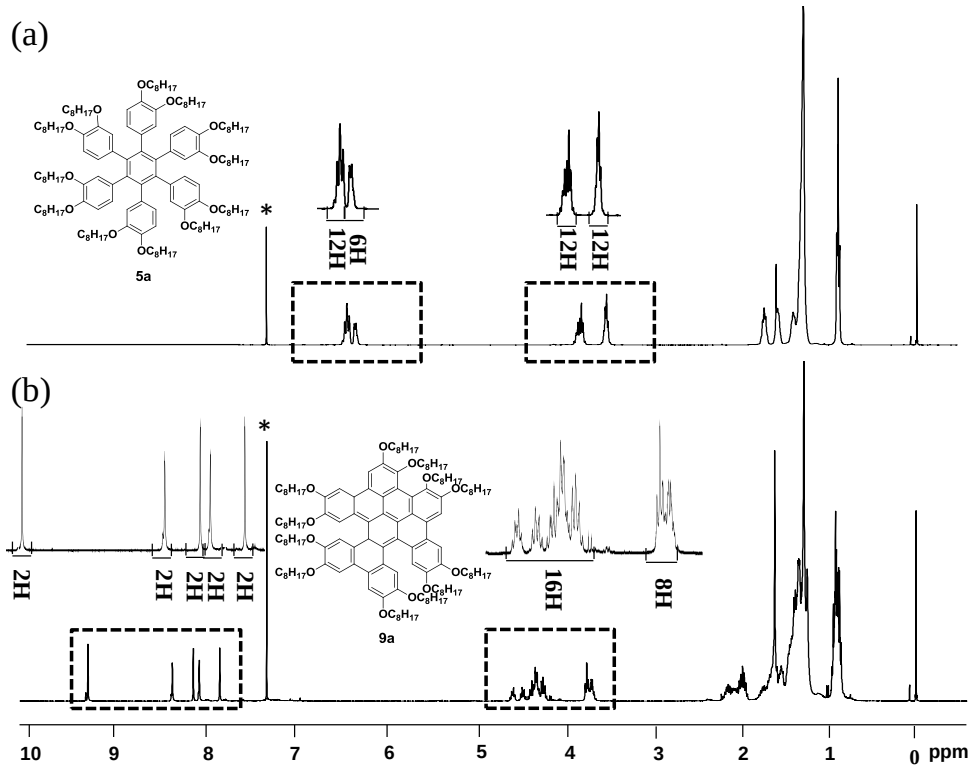

Figure 4.1 (a) ^{1}H NMR (400 MHz) of **5a** in $CDCl_3$ at r.t. and (b) ^{1}H NMR (400 MHz) of **9a** in $CDCl_3$ at r.t. The signals labeled with * are assigned to the resonances of $CDCl_3$.

We then decided to use the strong acids along with DDQ in the Scholl reaction. Interestingly, the use of strong acids like trifluoroacetic acid and trifluoromethane sulfonic acid also did not lead to complete cyclodehydrogenation. Interestingly, the use of powerful oxidizing agents like $FeCl_3$ and $VOCl_3$ as summarized in Table 4.1 was also in vain as same product formed irrespective of the conditions used. Thus we concluded that **9a** is indeed a product of Scholl reaction and not an intermediate. It is quite possible that steric hindrance is playing an

immense role in partial fusion of **5a**. Firstly, we hypothesized that steric hindrance associated with alkoxy groups is preventing these final two C-C bonds from forming.

4.1.3.3 Steric hindrance *vs.* electronic effect

In order to understand exactly whether steric hindrance of alkoxy groups is the reason for the unexpectedly formed partially fused product in this oxidative cyclodehydrogenation, we turned our attention to two substrates, one containing the pentyloxy chains 1,2,3,4,5,6-Hexakis((3,4-dipentyloxy)phen-1-yl)benzene **5b**, and the much simpler substrate 1,2,3,4,5,6-Hexakis((3,4-dimethoxy)phen-1-yl)benzene **5c** which were prepared according to the similar route as described for **5a**.

Table 4.1 Scholl reaction and product obtained under various conditions.

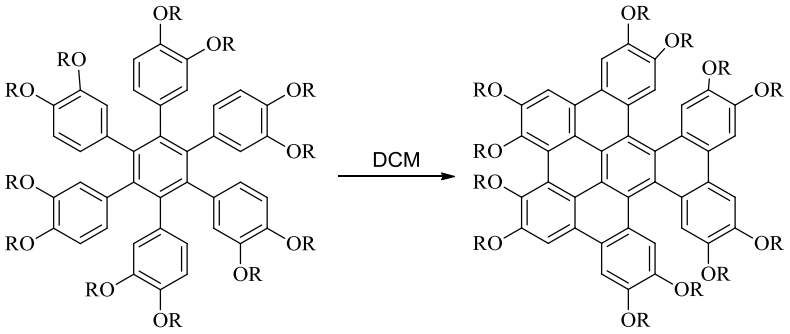

5a; R = C_8H_{17} **9a;** R = C_8H_{17}

Entry	Reagent	Temperature (°C)	Time (h)[a]
1	DDQ (6 equiv.)/CH_3COOH	0	2
2	DDQ (6 equiv.)/CF_3COOH	0	2
3	DDQ (6 equiv.)/CF_3SO_3H	0	2
4	DDQ (6 equiv.)/CH_3COOH	0	24[b]
5	DDQ (6 equiv.)/CH_3COOH	22	2
6	DDQ (12 equiv.)/CH_3COOH	0	2
7	$FeCl_3$ (12 equiv.)/CH_3NO_2	22	2
8	$FeCl_3$ (20 equiv.)/CH_3NO_2	22	2
9	$VOCl_3$ (5 equiv.)	22	2
10	DDQ (6 equiv.)/CH_3COOH	Reflux	2

[a]TLC monitoring till completion of reactant. [b]Extended reaction time after completion of reactant

Interestingly, in both these cases, we obtained the partially oxidized product only and MALDI-MS of these products exhibits it's most intense peak eight mass units lower,

corresponding to the formation of four new C-C bonds, clearly indicating that here electronic effects are dominating than the steric effects. However, while synthesizing compound **5d** from the respective diacetylene precursor, we failed to obtain the same.

On the other hand, we succeeded in obtaining 1,2,3,4,5,6-Hexakis((3,5-dimethoxy)phen-1-yl)benzene (**5e**) precursor but, in low yields compared to **5a**, **5b** and **5c**. **5e** was then cyclodehydrogenated with DDQ under the same conditions as described above for **5a** as shown in Scheme 4.3. MALDI-MS of the reaction mixture indicated a loss of 12 amu, corresponding to the formation of 6 C-C bonds resulted in completely fused HBC core.

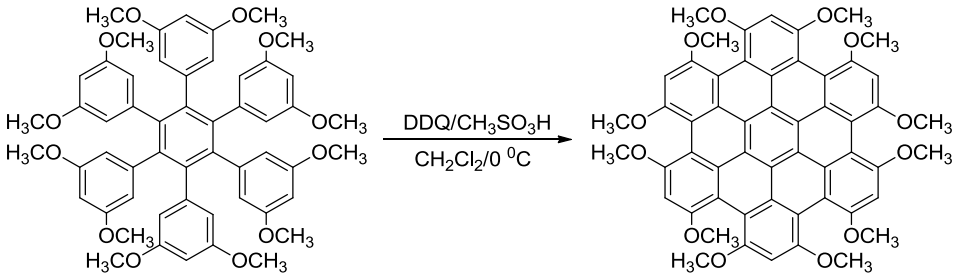

5e **9e**

Scheme 4.3 Scholl reaction of HBC precursor **5e**.

A comparison of these results suggests that the course of the Scholl oxidation is highly sensitive to changes in the structure of the hexaphenylbenzene precursor. A change in the position of the alkoxy substituent can lead to formation of completely fused product.

With this compound **5e** in hand, we examined its optical characteristics in chloroform at room temperature and compared its properties with partially fused compound **5a**. The absorption spectra of **5a** showed many peaks with significant absorption band in the 450-550 nm range as observed previously by Dichtel and co-workers for the semi-fused HBCs.[42]

On the other hand, the spectra of **5e** showed only two peaks, one for the β band at 334 nm and one for the α-band at 400-475 nm as shown in Figure 4.2, similar to those observed for alkyl substituted HBC derivatives.[43] Hence, the features of the UV-vis spectra were in correspondence with the literature studies.

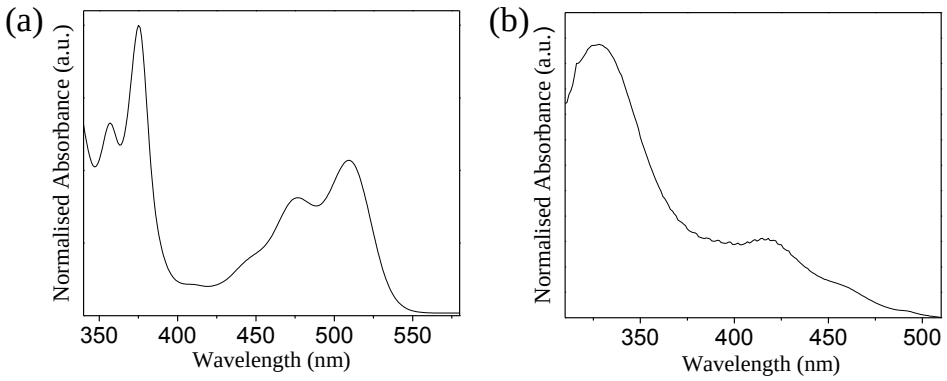

Figure 4.2 UV-vis absorption spectra of (a) **5a** and (b) **5e**. Solutions were prepared in $CHCl_3$ at concentrations of approximately 15×10^{-6} M.

4.1.3.4 Theoretical calculations and mechanistic consideration for the formation of 9a and 9e by oxidative dehydrogenation

To provide more information on this, we investigated the mechanistic scenario of this reaction. Several works in the literature have debated on the existence of two kinds of mechanisms for the Scholl reaction for the formation of HBCs, one involving an arenium cation mechanism[37,38] and the other involving a radical cation.[36] The presence of acids supports an arenium cation mechanism whereas the presence of oxidizing agents favors a radical cation mechanism.

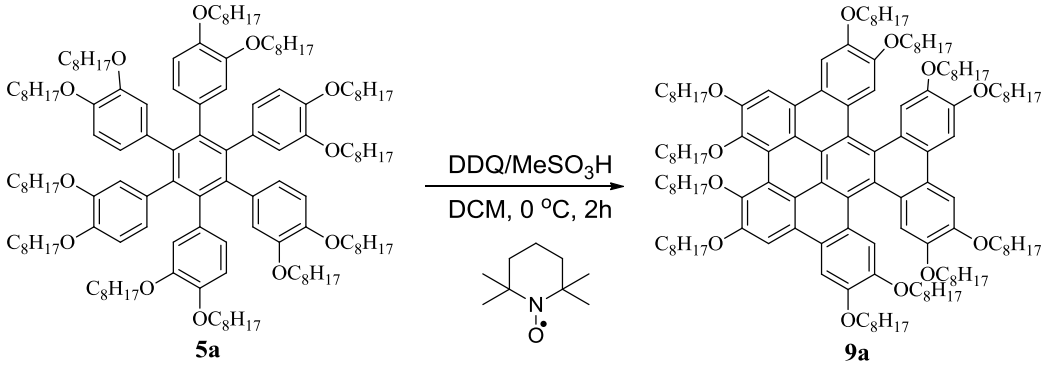

Scheme 4.4 Scholl reaction of HBC precursor **5a** in the presence of radical scavenger.

In order to see which mechanism is being followed in our case, we performed Scholl reaction of precursor **5a** in the presence of a radical scavenger TEMPO.[44] It is well known that when radicals are being generated in the reaction, this radical scavenger binds with them and quench the reaction. Keeping this in the mind, we added this compound during the progress of the reaction (Scheme 4.4). However, we didn't get any product corresponding to the addition of this radical binder with the starting material or any other intermediate. This led us to conclude that in our case reaction is taking place *via* arenium cation mechanism and not *via* radical cation mechanism. So, this work has its focus on an arenium cation mechanism. It is clearly evident from the experiments that changing the position of the methoxy substituents with respect to each other has an influence on the reactivity of these hexaphenylbenzene **5a**, **5b**, **5c** and **5e** systems towards an electrophile.

In order to understand how the position of alkoxy substituent affects the bond formation, the real systems with methoxy substituents as given by the structures **5c**, **5e**, **9c** and **9e** have been modelled to analyze the electronic effects in the reaction. The theoretical calculations were carried out with Gaussian 09[45] suite of packages. A full optimization was carried out using the hybrid functional, Becke's three parameter exchange and the LYP Correlation Functional (B3LYP)[46] at a split valence basis set 6-31G(d).[47] This basis set and level of theory have been found to be acceptable, since the previous Scholl reactions[37-39] have been successfully analyzed and reported at this model chemistry and basis set. All the structures were confirmed to be minima on the potential energy surface *via* a frequency calculation.

Table 4.2 Calculated protonation energies of structures [$\Delta E = E(IH^+) - E(I)$] at B3LYP/6-31G(d), where I is unprotonated species.

Structures	$\mathbf{I_1}$	**9c**	$\mathbf{I_6}$	$\mathbf{I_{15}}$	$\mathbf{I_{18}}$	$\mathbf{I_{21}}$
ΔE (kcal/mol) *o*-phenyl protonation	-223.83	-230.81	-235.35	-216.07	-243.40	-237.85
ΔE (kcal/mol) *p*-phenyl protonation	-228.74	-237.51	-240.04	-242.57	-248.45	-244.29

The transition state structures have been characterized by negative eigenvalues of the Hessian matrix. The arenium cation mechanism involves the formation of an arenium cation, its electrophilic attack on an arene, deprotonation and oxidative dehydrogenation to restore aromaticity. The first step in the reaction i.e., proton addition to one of the aromatic carbons in the presence of an acid to form the arenium cation has been quantified by calculating the energy difference between protonated (IH^+) and unprotonated species (I), $\Delta E = E(IH^+) - E(I)$ which has been given in Table 4.2 for the site specific proton affinity of both *o*-phenyl and *p*-phenyl sites. It is clearly inferred from Table 4.2 that *p*-phenyl protonation always takes precedence over the *o*-phenyl protonation, the energetic stabilization being more for the *p*-pathway. Further, a comparison of the energies of intermediates of the Scholl reaction of **5c** and **5e** suggested that the energies are more negative for the formation of **9e** which indicated that the attack of acid is more facile in **5e** than **5c**.

At this point, it is worthwhile to address the question why the *p*-phenyl protonation takes precedence over the *o*- case. Such an explanation is found by analyzing the electrostatic potentials (ESP)[48-50] of the unprotonated PAH's. The ESP is classically defined to be the work done in order to bring a unit positive test charge from infinity to a point of reference near the molecule. The ESP has been calculated for the unprotonated PAH's using the Gaussian'09 package and has been visualized using Jmol.[51] In Figure 4.3, the ESP-textured van der Waals surfaces of the PAH's are portrayed. The red regions indicate the most negative regions of the electrostatic potential. A further analysis was done to find the most negative critical point of the region using iso-surfaces. In case of methoxy substituted PAH's, the most negative region of the ESP is near the oxygen lone pair region of the methoxy substituent. This region of stabilization is where the proton is mostly likely to bind. In the next step, the proton gets strongly bound to the carbon atom of the phenyl ring to which the substituent is attached.

A semi-quantitative comparison given in Figure 4.3 of the most negative ESP regions clearly falls in line with the site specific proton affinities of the PAH's.

The energetics of bond formation has been investigated computationally in both *o*-phenyl and *p*-phenyl protonation pathways. It is believed that the reaction barrier obtained for the

transition state corresponding to protonated intermediate will drive the further steps of the reaction mechanism. The mechanistic schemes for the formation of **9c** *via* both ortho and para protonation pathway are illustrated in Schemes 4.5 and 4.6. The potential energy curves for the *o*-phenyl and *p*-phenyl protonation pathway along the bond formation reaction coordinate in the case of arenium cation mechanism are shown schematically in Figure 4.4.

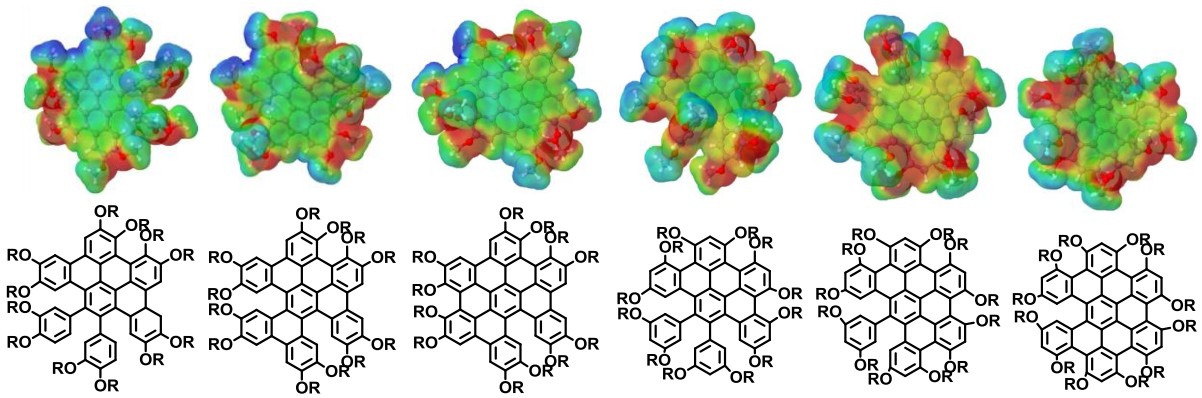

Figure 4.3 Electrostatic potenial textured van der Waals surfaces of the polycyclic aromatic hydrocarbons $\mathbf{I_1}$, **9c**, $\mathbf{I_6}$, $\mathbf{I_{15}}$, $\mathbf{I_{18}}$ and $\mathbf{I_{21}}$. The red regions indicate the most negative regions. See text for details.

The next step in the analysis would be to check the energetics involved in the bond formation to give the fused rings starting from the protonated PAH system. For this a transition state has been identified in all the cases corresponding to carbon-carbon bond formation. A reaction pathway analysis was done using an intrinsic reaction coordinate (IRC) calculation and it was confirmed that the transition state is indeed the one connecting the protonated PAH with the fused intermediate.

For the precursor **5c**, the lowest energy barrier (8.53 kcal/mol) is obtained for the protonated intermediate $\mathbf{I_2}$. In the next step ($\mathbf{I_4}$-$\mathbf{I_5}$), there is an increase in the energy barrier. The high energy barrier (18.98 kcal/mol) in the case of protonated intermediate $\mathbf{I_4}$ prevents the further bond formation and hence, **9c** has been isolated as the final product.

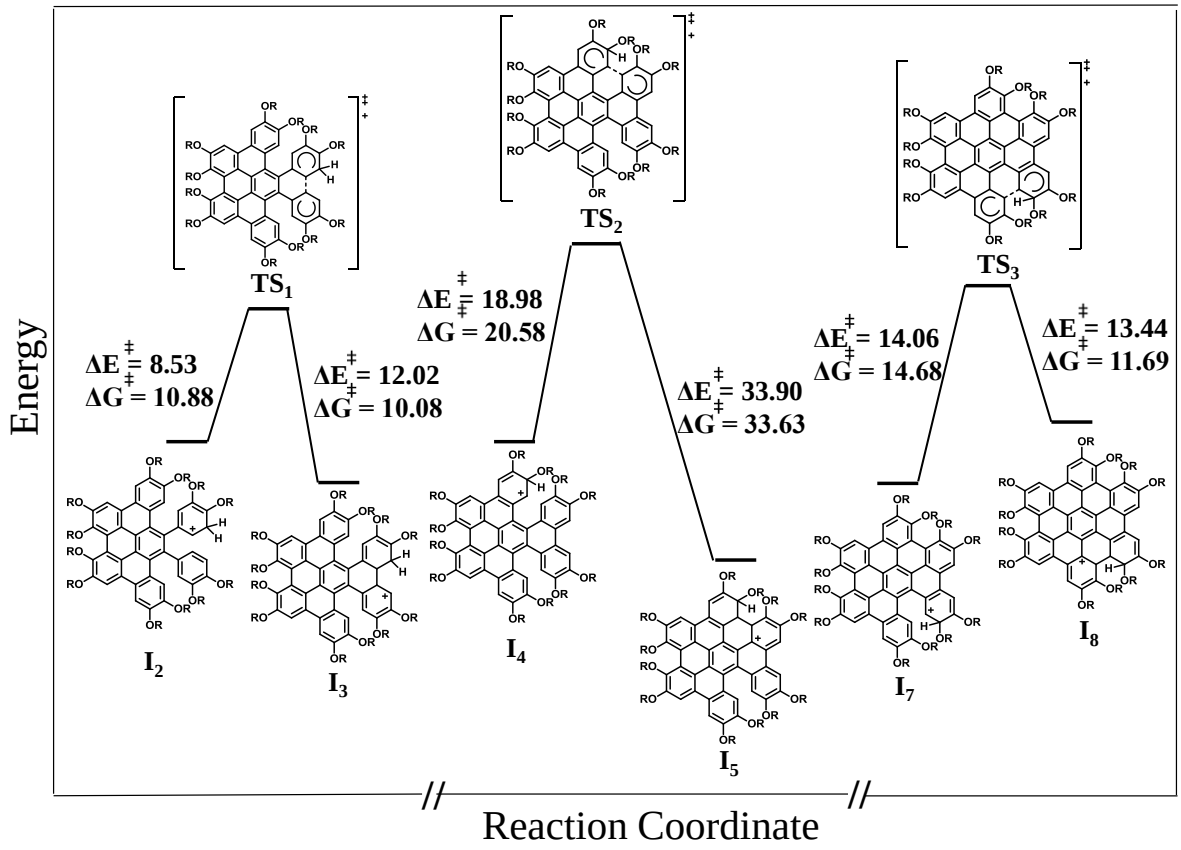

Figure 4.4 *o*-phenyl protonation pathway reaction coordinate profile for the protonated intermediates involved in the bond formation of **9c**. All the energies are in kcalmol^{-1}.

A comparison of the computational results for the formation of **9c** *via* both *o*-phenyl and *p*-phenyl pathways suggests that in both the pathways, the energetics of formation of **9c** is comparable. For ortho protonation pathway, formation of **9c** requires overcoming a free energy barrier of 10.88 kcal/mol in going from $\mathbf{I_2}$ to $\mathbf{I_3}$. For para protonation, free energy barrier is 9.43 kcal/mol in going from $\mathbf{I_9}$ to $\mathbf{I_{10}}$ for the formation of **9c**. It is thus clear that the free energy barrier for the para protonation pathway is 1.45 kcal/mol lower than the barrier for analogous ortho protonation pathway indicating that the fourth bond is formed by para protonation pathway only. Experimentally, the reaction does not proceed further from this point. The formation of the fifth bond i.e., $\mathbf{I_6}$ requires overcoming a free energy barrier of 20.58 kcal/mol for ortho protonation pathway ($\mathbf{I_4}$ to $\mathbf{I_5}$) and 9.93 kcal/mol for para protonation pathway ($\mathbf{I_{11}}$ to $\mathbf{I_{12}}$).

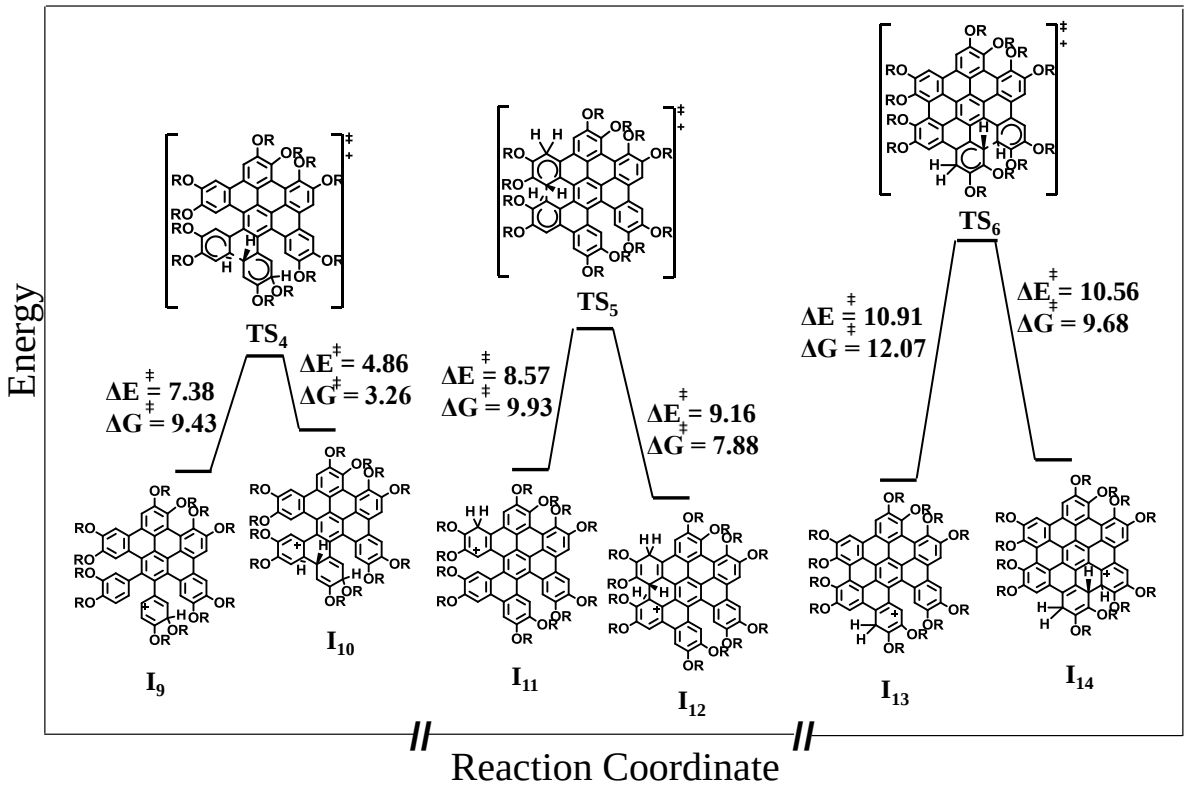

Figure 4.5 *p*-phenyl protonation pathway reaction coordinate profile for the protonated intermediates involved in the bond formation of **9c**. All the energies are in kcalmol^{-1}.

If para protonation was chosen, as it results in a lower barrier compared to ortho protonation, then the fifth bond should form, as its barrier is comparable to the barrier of formation of fourth bond. This suggests that probably, for the fifth bond formation from **9c**, protonation is taking place through the ortho pathway and the high energy barrier through this pathway prevents the further bond formation.

Rates of forward reaction for *o*-phenyl and *p*-phenyl protonation pathway have also been calculated[52] (Table 4.3). In *o*-phenyl protonation pathway, the low reaction rate for the formation of $\mathbf{I_6}$ also confirms that more driving force is required for the bond formation process from partially fused product **9c** to fully fused system **10**. This is also found in support of experimental result where the bond formation process stops at **9c** with two missed bond. Thus, both the rates of forward reaction and computed activation barriers show why the reaction does not proceed further from compound **9c.**

Table 4.3 Reaction rate constant (in s^{-1}) calculated at B3LYP/6-31G(d) for *o*-phenyl and *p*-phenyl protonation pathways for the formation of product **9c** and **9e**.

o-phenyl protonation pathway	For **9c**	**I_2**	**I_4**	**I_7**
		6.566×10^{4}	5.087×10^{-3}	1.075×10^{2}
	For **9e**	**I_{16}**	**I_{19}**	**I_{22}**
		7.614×10^{7}	8.259×10^{5}	7.598
p-phenyl protonation pathway	For **9c**	**I_9**	**I_{11}**	**I_{13}**
		7.590×10^{5}	3.264×10^{5}	8.810×10^{3}
	For **9e**	**I_{24}**	**I_{26}**	**I_{28}**
		2.119×10^{4}	2.236×10^{6}	6.367×10^{6}

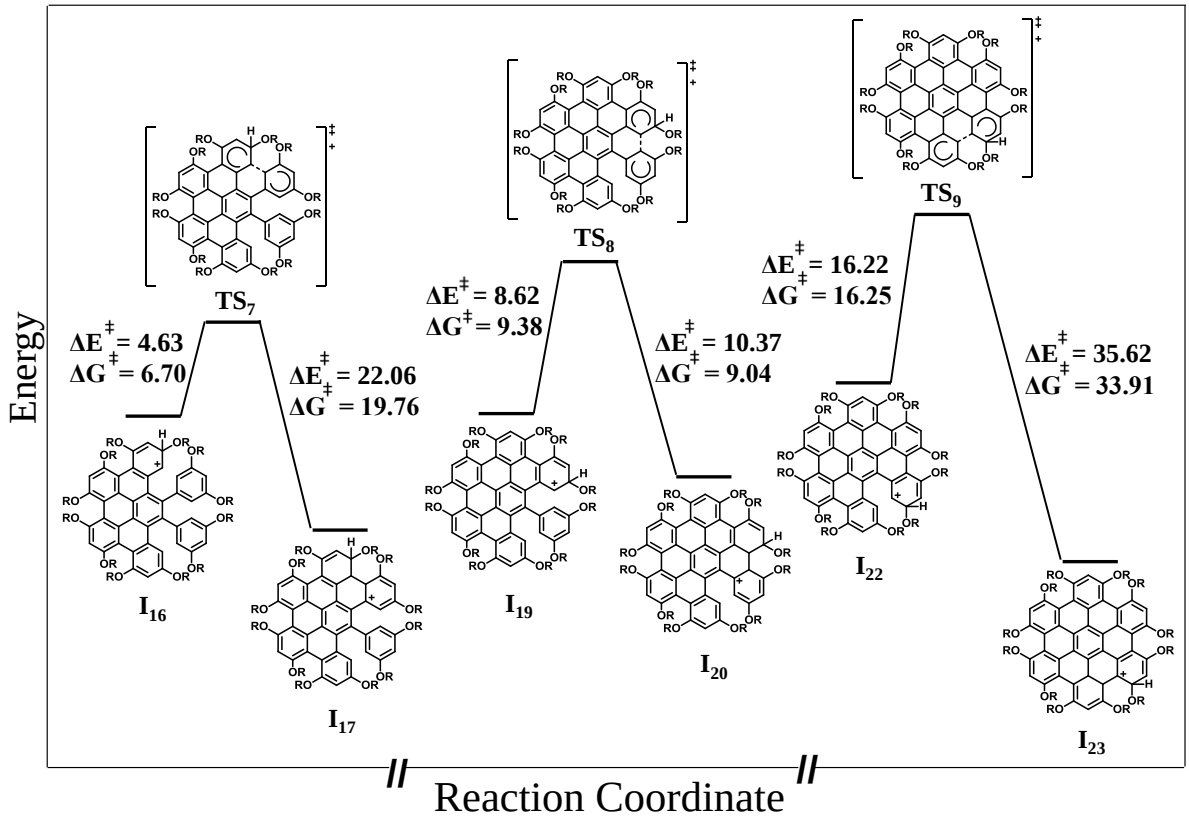

Figure 4.6 *o*-phenyl protonation pathway reaction coordinate profile for the protonated intermediates involved in the bond formation of **9e**. All the energies are in $kcalmol^{-1}$.

The mechanistic schemes for the formation of **9e** *via* both ortho and para protonation pathway are illustrated in Schemes 4.7 and 4.8. The analysis of energetics in the *p*-phenyl protonation pathway for the formation of **9e** from **5e** reveals some priority over *o*-phenyl protonation pathway. The gradual increase in the energy barrier for the formation of **9e** through protonated intermediates $\mathbf{I_{16}}$ to intermediate $\mathbf{I_{23}}$ made the *o*-phenyl pathway less viable than the *p*-phenyl pathway in which decrease in energy barrier from intermediate $\mathbf{I_{24}}$ to intermediate $\mathbf{I_{29}}$ for the formation of **9e** has been observed.

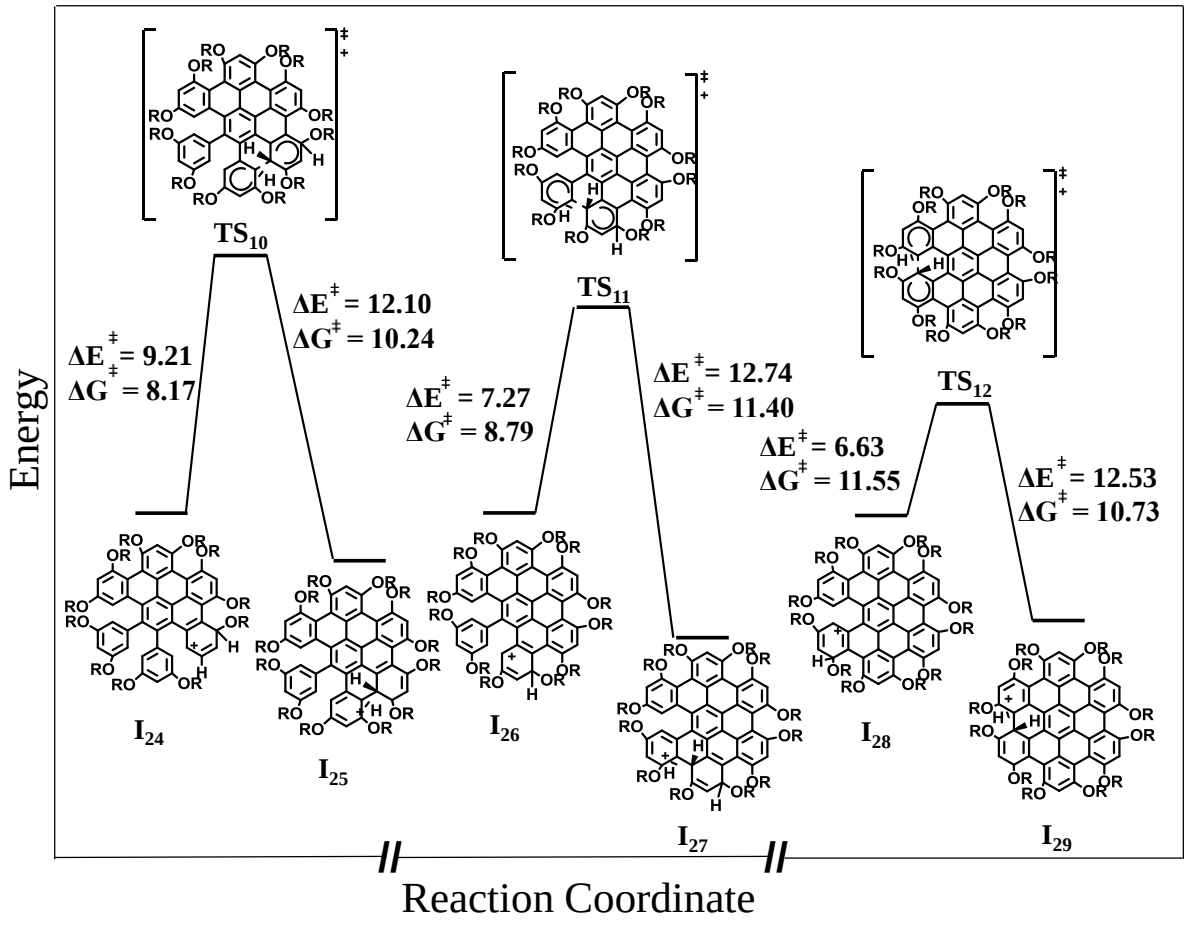

Figure 4.7 *p*-phenyl protonation pathway reaction coordinate profile for the protonated intermediates involved in the bond formation of **9e**. All the energies are in kcalmol^{-1}.

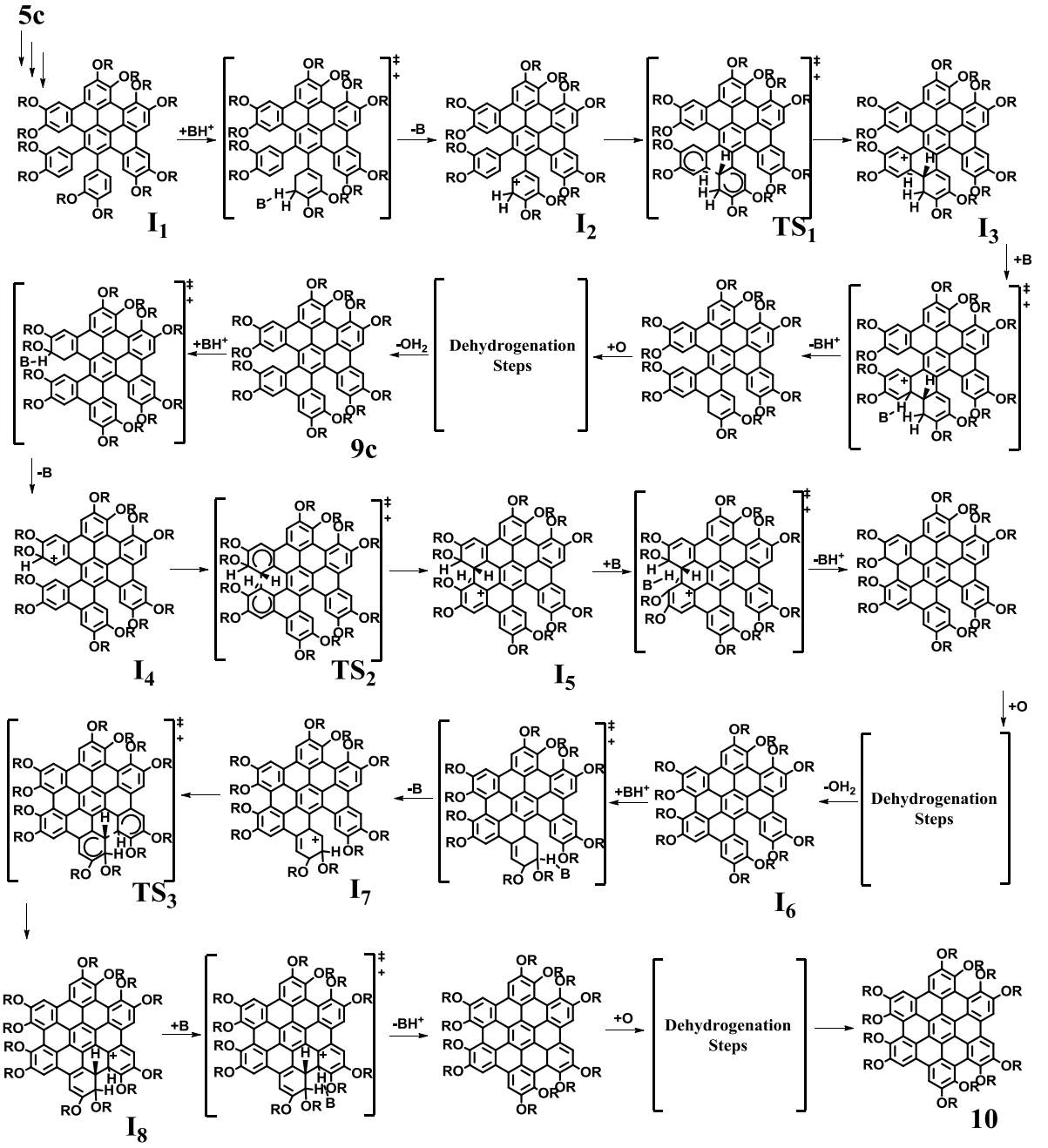

Scheme 4.5 Arenium cation mechanism for the formation of **9c** *via o*-phenyl protonation pathway.

On the basis of the discussion above, it can be said that formation of **9c** is taking place *via p*-phenyl protonation pathways but, the further steps i.e., formation of **10** from **9c** is taking place *via o*-phenyl protonation pathway. On the other hand, the formation of **9e** involves *p*-protonation pathway only. A question that needs to be answered at this point is why are the

barriers higher for the case in which the methoxy substituents are adjacent to each other. The effect is majorly an electronic effect and this can be explained in terms of the *o*, *p*- directing nature of the methoxy substituents.

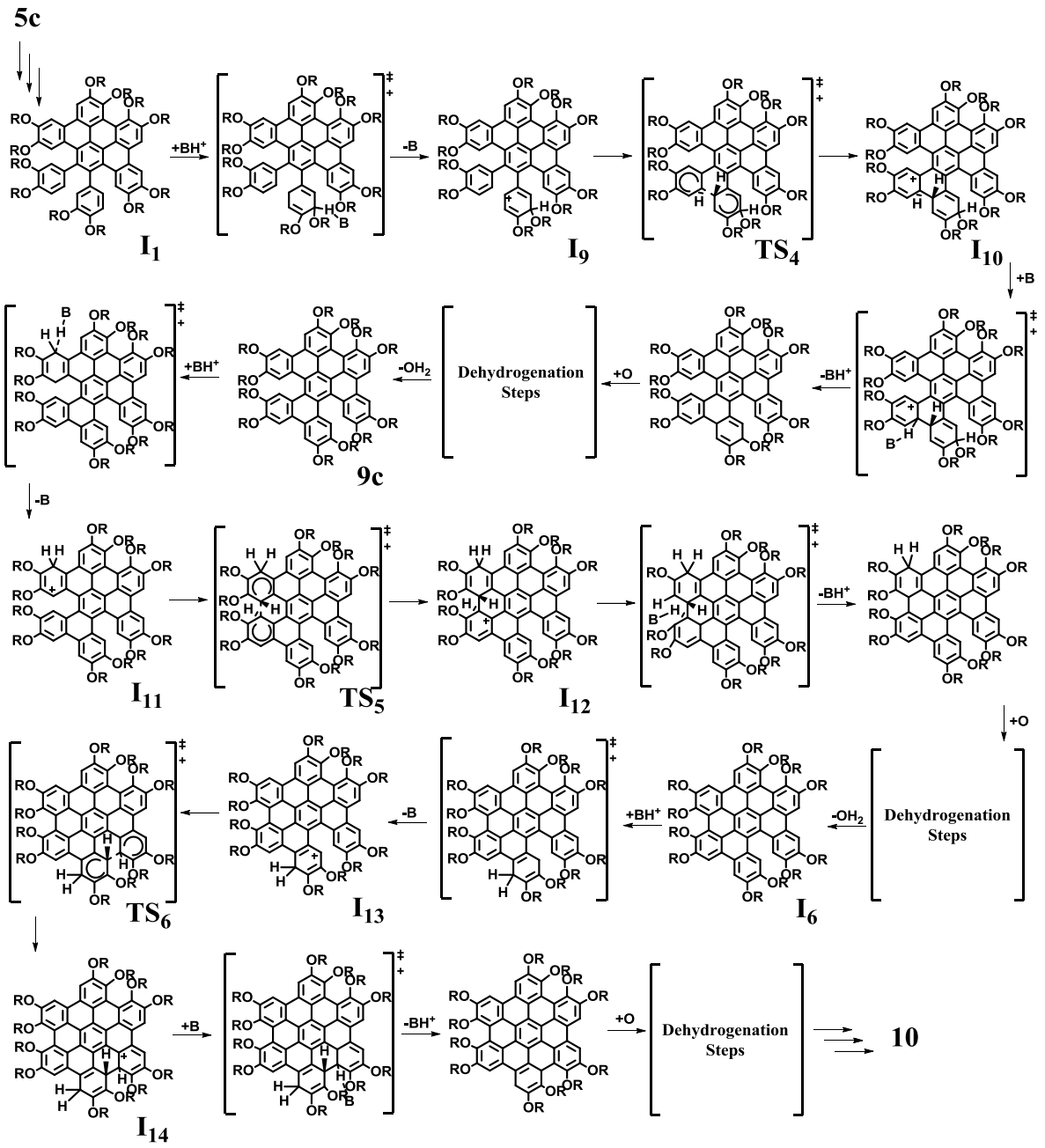

Scheme 4.6 Arenium cation mechanism for the formation of **9c** *via p*-phenyl protonation pathway.

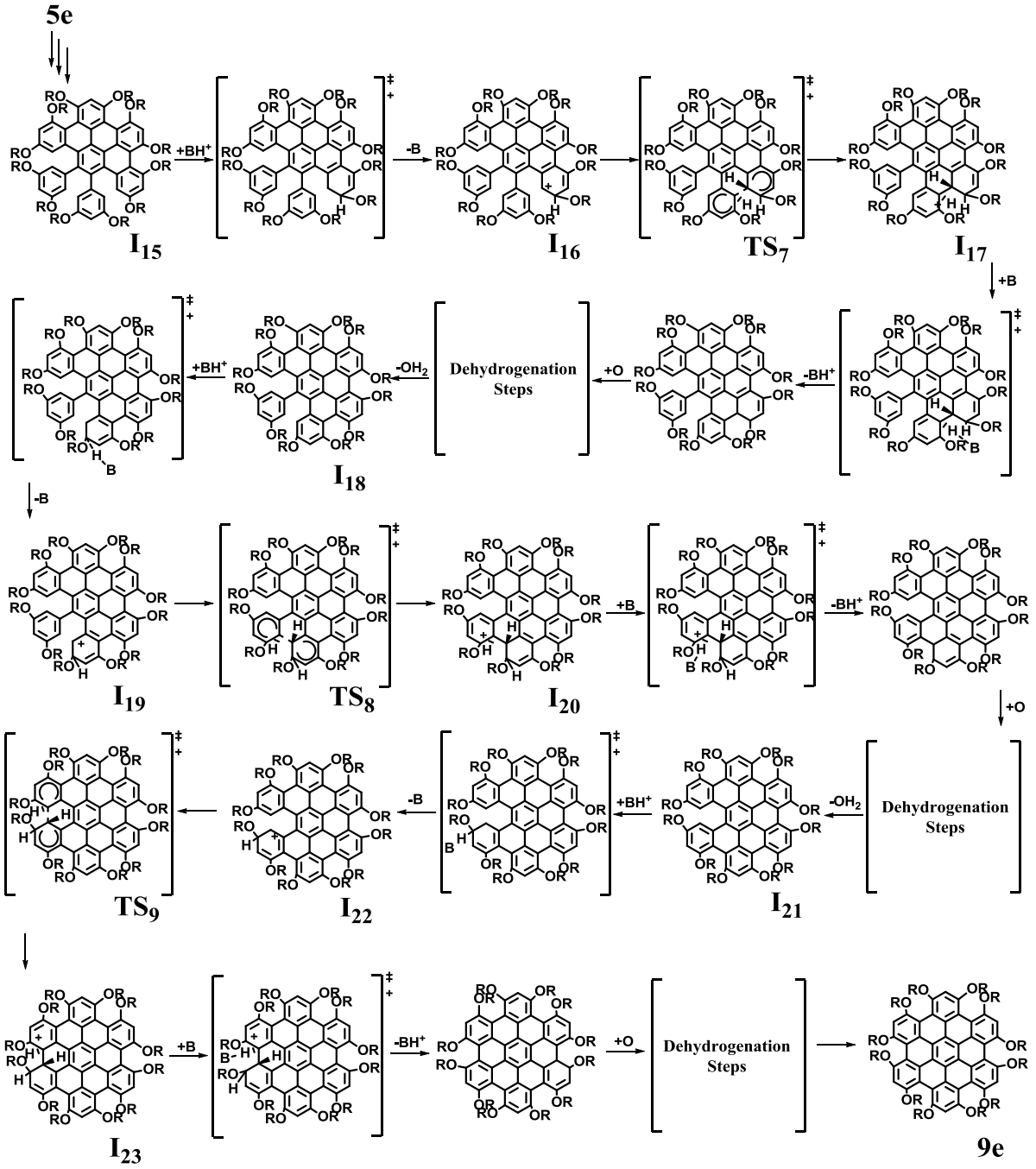

Scheme 4.7 Arenium cation mechanism for the formation of **9e** *via o*-phenyl protonation pathway.

From the calculated charges (Natural and Mulliken charges, Table 4.4) and orbital densities, it is evident that the electron density is increased at the carbon positions which are *o*- and *p*-

to each of the methoxy substituents. This indicates that ring closing of **5e** undergoes *via p*-phenyl protonation pathway.

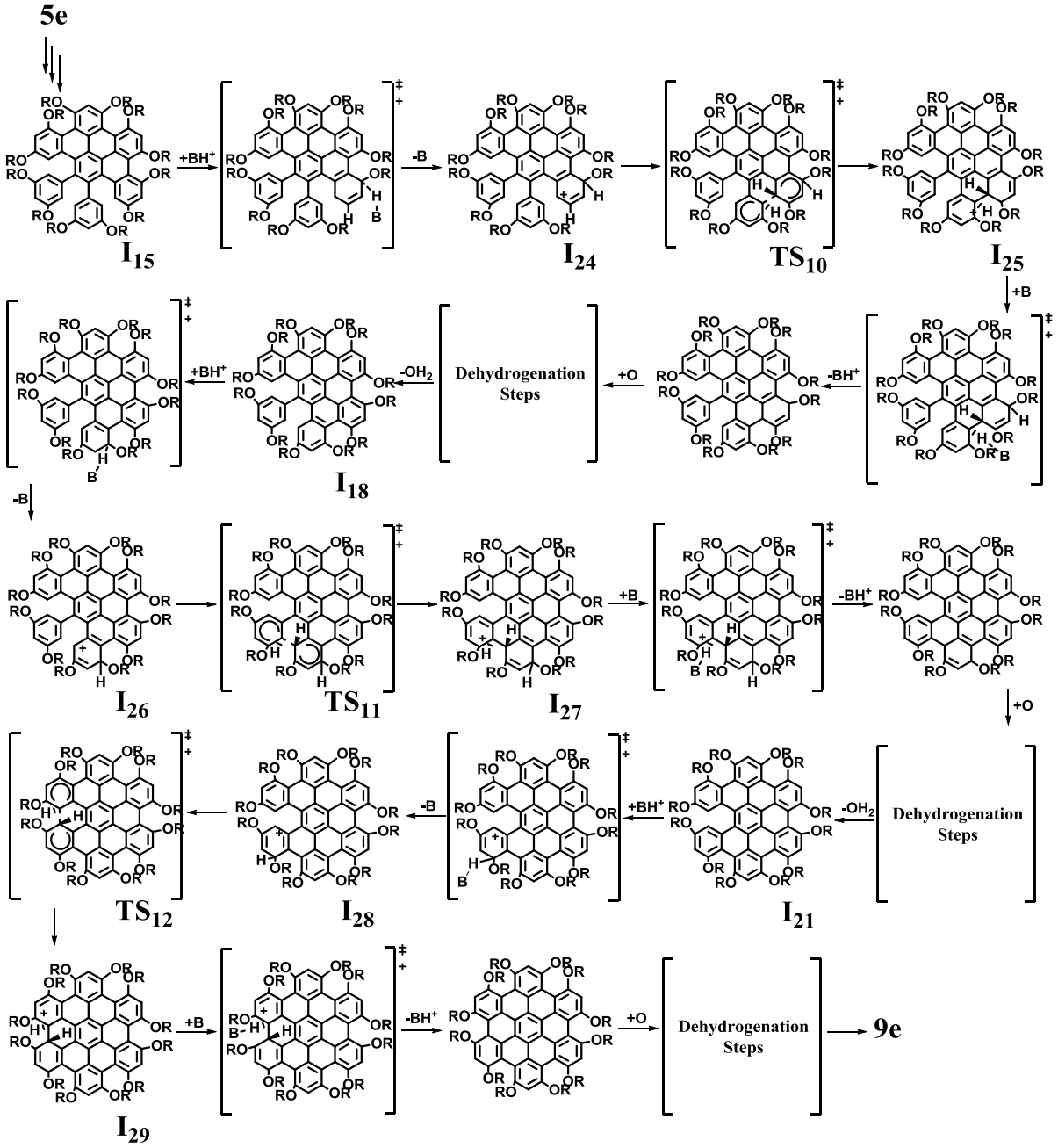

Scheme 4.8 Arenium cation mechanism for the formation of **9e** *via p*-phenyl protonation pathway.

The high reaction rates obtained for the bond forming steps in *p*-phenyl protonation pathway for the formation of **9e** making it kinetically more favorable than the *o*-phenyl protonation pathway as shown in Table 4.3. When the methoxy substituents are adjacent to each other, the ring activating increased density is distributed on two different sets of carbon atoms B or A/C (Figure 4.8). But, when the methoxy substituents are on alternating positions, the *o*, *p*-directing nature results in an increased electron density on three carbon atoms, one of them gets highest density which enables an increased overlap between the orbitals situated on the carbon atoms to be bonded. This ensures that the barrier is decreased *via* a stabilization of the transition state.

Table 4.4 Natural and Mulliken charges on the carbon atoms which are actively participating in the *o*-phenyl and *p*-phenyl protonation pathways (see Figure 4.8 and appendix III, Table A1).

Structures	Natural Charge	Mulliken Charge	Structures	Natural Charge	Mulliken Charge
I_4			**I_{19}**		
$C^{B}{}_{12}$	-0.237	-0.271	$C^{D}{}_{20}$	-0.285	-0.248
$C^{C}{}_{43}$	-0.235	-0.269	$C^{F}{}_{21}$	-0.292	-0.209
[a]$C^{o}{}_{44}$	+0.277	+0.333	[a]$C^{o}{}_{34}$	+0.334	+0.385

[a]ortho to B, C or D, F carbon atoms

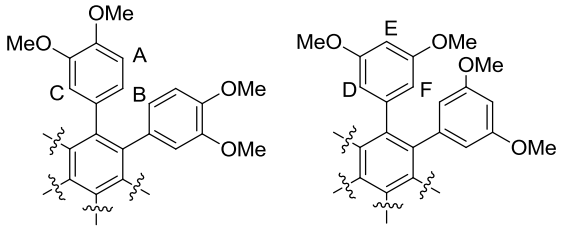

Figure 4.8 Different sets of carbon atoms corresponding to ring activating density. The atoms labelled A, B, C, D, E and F are the ones to check for activation/deactivation. See Table 4.4 for details.

A comparison of charges of the bond forming carbon atoms in structures **I_4** and **I_{19}** reveals that further bond formation would be easier in case of **I_{19}** compared to **I_4**. It follows that

position of the alkoxy substituents plays an immense role in determining the product of Scholl reaction and these findings can be very useful for the design and synthesis of a variety of alkoxy functionalized oligoarenes *via* Scholl reaction.

4.1.4 Conclusions

We have presented the results of an experimental and computational study to examine the steric and substituent effects (particularly alkoxy) on the formation of HBC core *via* Scholl reaction. Experimentally, it has been found that precursor **5e** leads to completely cyclized system and precursors **5a**, **5b** and **5c** escort partially cyclized products. i.e., when the alkoxy substituents are ortho to each other, then the Scholl reaction resulted in partially cyclized products irrespective of the alkyl chain length but, when the alkoxy groups are meta to each other, then cyclodehydrogenation resulted in the formation of completely fused product. Under different sets of conditions, formation of same partially fused product has been observed. Ab-initio calculations with the hybrid functional B3LYP at 6-31G (d) basis set have been performed to understand the reaction mechanism and the nature of products formed based on arenium cation mechanism. The first step in the reaction i.e., proton addition to one of the aromatic carbons in the presence of an acid to form the arenium cation has been quantified in terms of proton affinity for both *o*-phenyl and *p*-phenyl sites. A semi-quantitative comparison of the most negative ESP regions falls in line with the site specific proton affinities of the intermediates and reactants involved in the mechanism. The thermodynamic calculations and reaction rate analysis based on the arenium cation mechanism *via* both *o*-phenyl and *p*-phenyl protonation pathways suggest that it is the high free energy barrier which is preventing further bond formation from the partially fused structure. Computational results indicate that cyclodehydrogenation of **5e** takes place *via* the *p*-phenyl protonation pathway. But, for **5c**, oxidative C-C bond formation occurs *via* a combination of *o*-phenyl and *p*-phenyl protonation pathways. The regioselectivity of Scholl reaction is highly dependent on the position of all the electron donating groups on the ring with respect to each other. This can be attributed to the electronic effects in accordance with the natural and mulliken charge calculations. These findings can also be applied for the synthesis of large polycyclic aromatic systems.

4.2 Part B: Unsymmetrically substituted room temperature discotic liquid crystals based on hexa–*peri*–hexabenzocoronene core

4.2.1 Introduction

In recent years, graphene has motivated many researchers to investigate polycyclic benzenoid aromatic hydrocarbons (PAHs) as graphene model systems due to their exceptional electronic properties, such as high mobility and near-ballistic transport.[53] In addition, the optical and mechanical properties associated with graphene are ideal for micro- and nano-mechanical systems, thin-film transistors, transparent and conductive electrodes, flexible electronics, photonics and so on.[54-58] Since planarity is the key geometric trait for graphene, a variety of planar molecules ranging from flat triangular molecules ($C_{60}H_{24}$) to giant discotic molecules ($C_{222}H_{42}$) have been prepared which are expected to lead to regions of local graphene structure.[59,60] Among them, hexa-*peri*-hexabenzocoronenes (HBCs), the smallest member of PAH series, are particularly interesting as they often exhibit strong π-π interactions that endorse supramolecular self-assembly in solution as well in films leading to excellent electronic and optoelectronic properties.[29,61-63] Previous studies comprised the use of HBCs as electron donors in organic photovoltaic devices and as *p*-type semiconductors in organic field effect transistors due to their electron-rich nature.[17] However, very few reports are there in the literature for their use in organic light emitting diodes (OLEDs).[64] It is a significant challenge to modify this core to achieve room temperature phase as this is associated with high melting point. The advantage of room temperature phase[65,66] is that one anticipates the problems of trapping of charge carriers at grain boundaries will be removed. Additionally, the visible emission can be achieved in the columnar phase at room temperature making the processing easier. Past reports suggested that the saturated red light emission from OLEDs is less common than the blue and green light emission.[67] Noticeably, organic red light emitting devices are mostly based on rare earth complexes and amorphous conjugated polymers.[68-73] Only a few reports are there in the literature showing columnar discotics exhibiting red light emission. However, these derivatives showed columnar mesophases at very high temperature.[74] Dehydrogenative coupling reaction of aromatic compounds is a key step in the synthesis of giant graphene-like molecules with different sizes and shapes.[75] While alkyl substituted polyphenylenes can be cyclized rapidly,

cyclodehydrogenation of their heteroatom-containing counterparts is a more complex endeavor as both partially and fully fused species tend to be generated in a single reaction.[76,77] King and co-workers[39] have shown that electronic directing groups can be used to control cyclodehydrogenation reaction in case of triphenylenes. In our laboratory, we have established that strategic positioning of electron-donating groups with respect to each other plays a crucial role in the C-C bond formation under oxidative cyclodehydrogenation conditions.[78]

4.2.2 Objective

Despite the large number of HBC mesogens with different substitutional symmetries and peripheral decorations, alkoxy substituted HBC discotics are among less investigated species in nanographene systems.[79-81] Herein, we present two new HBC derivatives **11** and **12** incorporating alkoxy chains in the core.

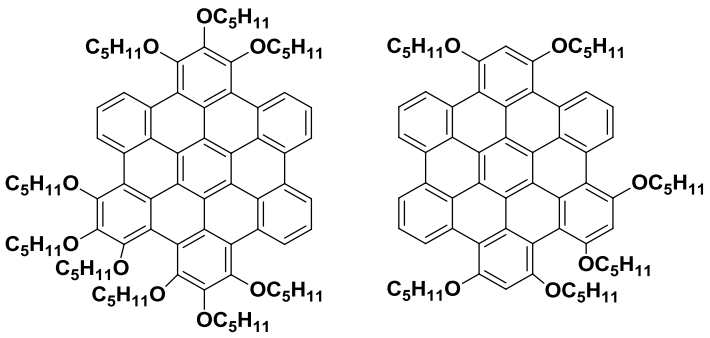

11 **12**

The key feature of implemented chain is the introduction of heteroatom closer to aromatic core which dramatically influences self-organization behavior. Noticeably, cyclodehydrogenation reactions of corresponding symmetrical hexaphenylbenzene gave unusually these two rearranged products. These molecules exhibit red (**11**) and yellowish-green (**12**) light emission in solution as well as in solid states. Hence, these materials perfectly fulfil the described demands: room temperature mesophase, high purity, facile processing from the isotropic state due to their low isotropization temperature and visible emission in the solution and solid states. This series of molecules are the first report on HBC discotics exhibiting red and yellowish-green emission.

4.2.3 Results and Discussion

4.2.3.1 Synthesis and characterization

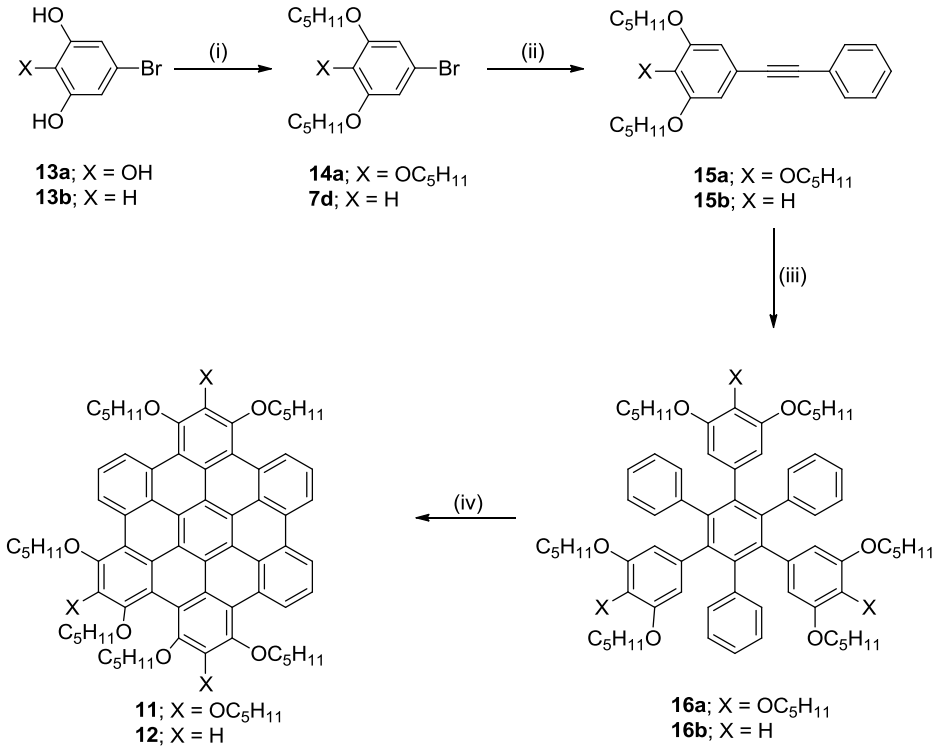

Scheme 4.9 Synthesis of HBC **11** and **12**. *Reagents and Conditions:* (i) K_2CO_3, 2-Butanone, $C_5H_{11}Br$, KI, quantitative; (ii) Phenylacetylene, $Pd(PPh_3)_2Cl_2$, CuI, PPh_3, Toluene, Diisopropylamine, 82 % (**15a**) and 78 % (**15b**); (iii) Co_2CO_8, 1,4-Dioxane, reflux, 7 h, 59 % (**16a**) and 57 % (**16b**); (iv) DDQ, $MeSO_3H$, DCM, 15 % (**11**) and 17 % (**12**).

The synthetic protocol for the preparation of HBC **11** and **12** is outlined in Scheme 4.9. The synthesis started from alkylation of 5-bromobenzene-1,2,3-triol and 5-bromobenzene-1,3-diol with 1-bromopentane to give the respective compounds **14a** and **7d** in quantitative yield. The Sonogashira coupling of **14a** and **7d** with phenylacetylene gave the corresponding unsymmetrical diphenylacetylenes **15a** and **15b** in 82 and 78 % yield, respectively. Subsequent cyclotrimerization of the diphenylacetylene **15a** and **15b** with $Co_2(CO)_8$ yielded the hexaphenylbenzene precursor molecules **16a** and **16b**. It has been reported that 2,3-Dichloro-5,6-dicyano-1,4-benzoquinone (DDQ) in the presence of some acid is an effective system for oxidative C-C bond formation. DDQ reactions are generally clean and also

obviate side reactions such as chlorination and dealkylation.[40,41] Keeping this in mind, the crucial final cyclodehydrogenation step was carried out by treating **16a** and **16b** with DDQ/methylsulphonic acid in pure dichloromethane. After 2 h, the reaction was quenched with saturated solution of sodium carbonate and crude product was purified by column chromatography. Details of the synthesis are provided in experimental section. The chemical structures of these compounds were determined using spectroscopic techniques (^{1}H NMR, ^{1}H-^{1}H COSY NMR, ^{13}C NMR and FTIR) as detailed in the experimental section and appendix III (Figures A5-8, 11, 12, 17, 18). Further, MALDI-MS data were also found to be consistent with molecular structure. It should be noted that final product of cyclodehydrogenation reaction is not symmetrical one, instead phenyl group migration has occurred leading to formation of unsymmetrical alkoxy substituted HBCs from symmetrical hexaphenylbenzenes. This kind of rearrangement has previously been reported by Mullen and co-workers[82] but, in our case system is more hindered compared to them. This further indicated that outcome of Scholl reaction is highly unpredictable as indicated by Bock also.[34,35]

4.2.3.2 Thermal behavior

The thermal behavior of **11** and **12** was monitored by a combination of differential scanning calorimetry (DSC) and polarizing optical microscopy (POM). Their thermal transition temperatures along with the associated enthalpies as obtained from the DSC studies are summarized in Table 4.5. Compound **11** in DSC showed only one phase transition from a liquid crystalline phase (LC) to the isotropic melt at 60.1 °C (ΔH = 14.14 kJ/mol). On cooling, an exothermic transition appeared at 57.2 °C, which corresponds to the formation of LC phase (appendix III, Figure A13). However, on further cooling up to -90 °C, no signature of crystallization appeared. LC morphology of both these compounds was checked under polarizing optical microscope (POM) with a hot stage. Fresh samples were kept between a glass slide and a cover slip. The images were captured under cross polars on cooling from the isotropic phase in the LC window using a high resolution camera. When observed under POM, compound **11** exhibited an undefined mobile texture at room temperature. On cooling from isotropic liquid, under microscope, typical broken fan shaped texture of the columnar phase is displayed, as shown in Figure 4.9. This broken fan shaped texture is characteristic

texture for the columnar rectangular phase.[83] In DSC, compound **12** exhibited a transition from LC phase to the isotropic phase (appendix III, Figure A14) at 131.40 °C (ΔH = 15.95 kJ/mol). However, no phase transition was observed on cooling to room temperature in DSC.

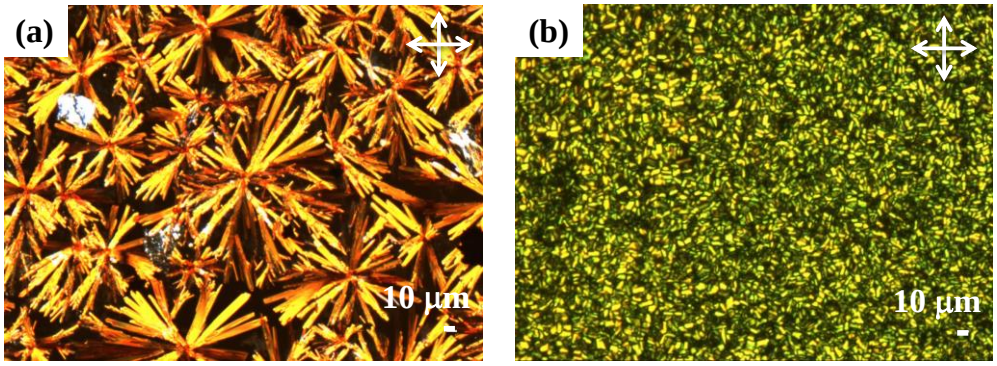

Figure 4.9 POM images of discogens (a) **11** on slow cooling from isotropic phase at 42.6 °C and (b) **12** on slow cooling from isotropic phase at 109.1 °C kept between glass slide and cover-slip observed under two crossed polarizers.

Table 4.5 Mesophase behavior of HBCs **11** and **12.**[a]

Mesogen	Heating Cycle	Cooling Cycle
11	LC 60.1 (14.1) I	I 57.2 (13.8) LC
12	LC 131.40 (15.9) I	[b]I 129.9 LC

[a]transition temperatures in °C and the respective enthalpy changes in brackets in kJ/mol. [b]From POM.

Under POM, compound **12** goes to isotropic phase at around 130 °C on heating. Upon slow cooling from the isotropic phase, a mosaic texture appeared that is typical for columnar LCs (Figure 4.9). The transition to LC phase was not observed in DSC which might be because of the small enthalpy change associated with the formation of these phases.[84] Surprisingly, compared to other *n*-alkyl-substituted HBCs, the isotropization temperature was shifted considerably from ~420 °C[85] (above decomposition) to ~60 °C and 130 °C for derivatives **11** and **12,** respectively making these derivatives potentially viable for processing.

4.2.3.3 X-ray scattering studies

In order to further investigate the molecular stacking behaviors of the compounds **11** and **12** in the mesophase, samples were filled in a glass capillary and wide- and small angle X-ray analyses (WAXS and SAXS, respectively) were performed at room temperature and higher temperatures.

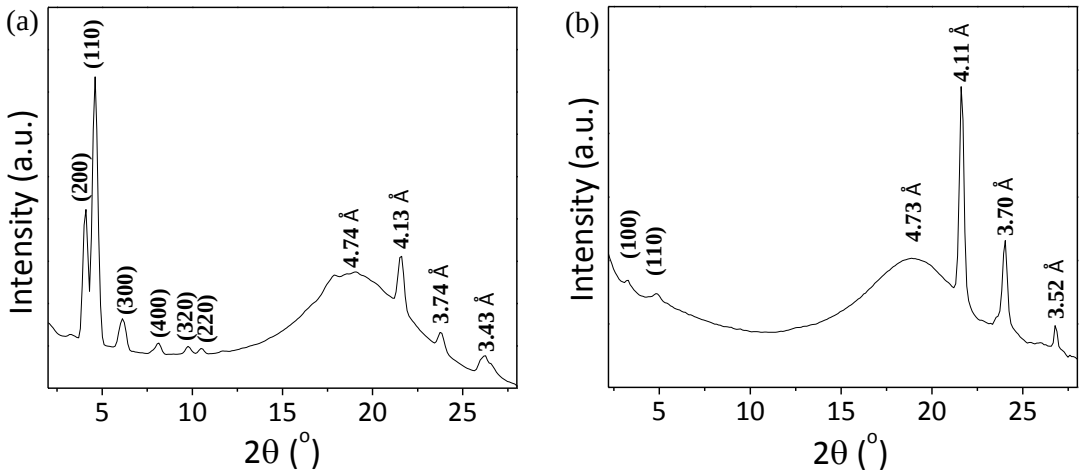

Figure 4.10 An intensity *vs.* 2θ graph derived from the X-ray scattering pattern of (a) compound **11** at 50 °C and (b) compound **12** at r.t. after cooling from the isotropic phase.

The X-ray pattern (Figure 4.10) confirms the identity of columnar rectangular mesophase between room temperature to the temperature of transition to the isotropic liquid for compound **11**. At room temperature, the scattering profile shows six sharp reflections (Figure 4.10) in the small angle region that can be assigned to a two-dimensional rectangular lattice in which molecules stack one on top of another and the columns generated adopt a rectangular packing with rectangular lattice constants: a = 43.14 and b = 21.43 Å.[86-88] The proposed indexing, lattice constants and parameters, and the observed and calculated spacings are gathered in Table 4.6. The symmetry of the phase was assigned as *p2gm* owing to the presence of 300 reflection. The missing 01 or 10 and 12 or 31 reflections allow us to exclude *p2mm* and *p2gg* symmetries. In this case, *c2mm* symmetry can also be excluded because the reflection with an odd sum of h+k was also observed which is forbidden in this

symmetry group. The sublattice compression ratio q_{hex}, which expresses the distortion of the Col_r lattice relative to the hexagonal lattice, equals 1.2 corresponding to a compression of the lattice along the b direction and the tilt angle θ (θ = $\cos^{-1}$(b/a), where a and b are the lattice constants) along this direction takes value of ≈ 60°.[89]

For compound **12**, in the small angle region, two reflections are seen whose *d*-spacings are indexed to the 10 and 11 planes respectively, consistent with a two-dimensional hexagonal lattice of *p6mm* symmetry and lattice parameter *a* = 31.28 Å. The weak small angle reflections and lack of higher order scattering intensities indicate low supramolecular ordering in the sample. The demonstration of different kinds of mesophases in these compounds indicates that shape of the mesogen (core and aliphatic chains) plays an important role for the self-assembly and hence self-organization of the columns.

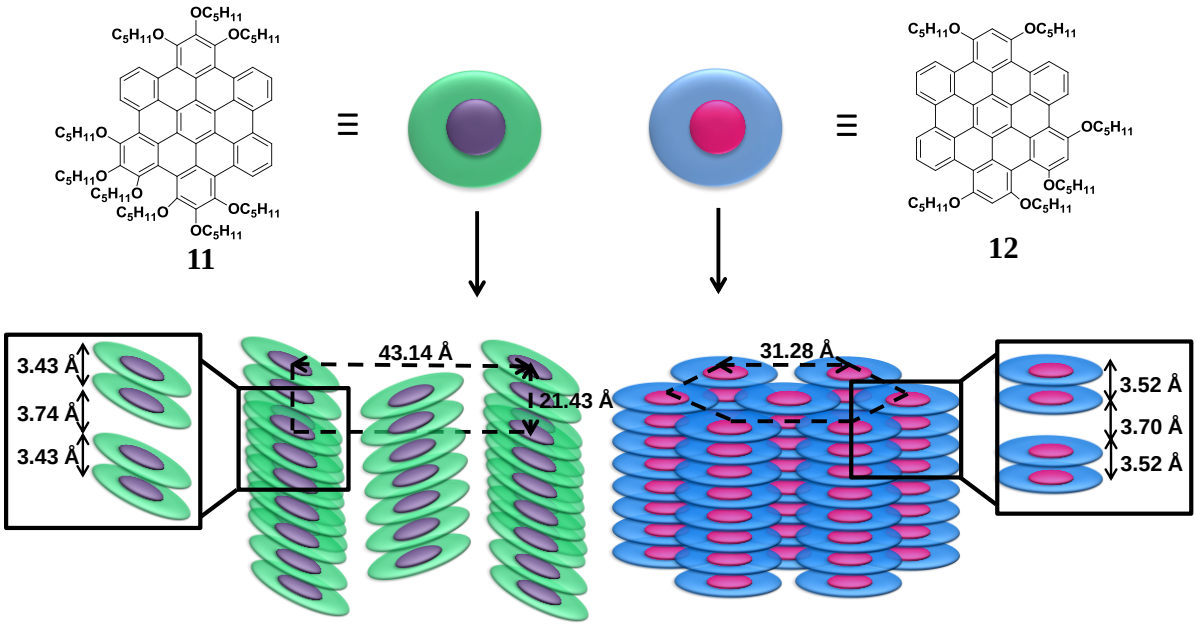

Figure 4.11 Model for the supramolecular arrangement of mesogens **11** and **12** in the mesophase.

The wide angle region of both the compounds consisted of four signals: (i) a large diffuse halo associated with molten aliphatic chains at 4.74 and 4.73 Å for compounds **11** and **12**, respectively (ii) one sharp signal at 4.13 and 4.11 Å for compounds **11** and **12**, respectively (iii) another sharp signal at 3.74 and 3.70 Å for compounds **11** and **12**, respectively and (iv)

an additional reflection at 3.43 and 3.52 Å for compounds **11** and **12**, respectively. We attributed this phenomena based on two different types of π-π stacking arrangements of the discotic molecules in the columnar phase as shown in Figure 4.11.

Table 4.6 The proposed indexing, lattice constants and parameters, and the observed and calculated spacings for compounds **11** and **12** obtained from XRD.

Compound	d_{obs} (Å)[a]	d_{calc} (Å)[a]	hkl[b]	Lattice Constants (Å)[c]	Lattice parameters[d]
11	21.57	21.57	200	a = 43.14	T = 50 °C; Col_r, *P2gm*;
	19.19	19.19	110	b = 21.43	q_{hex} = 1.2; S = 924.5 Å^2;
	14.45	14.38	300		S_{col} = 462.3 Å^2;
	10.86	10.79	400		V_m = 2198.7 Å^3(d = 1 gcm^{-3});
	9.06	9.60	320		Z = 1.5; h_m = 3.43 Å
	8.43	8.58	220		
	4.74 (br)				
	4.13				
	3.74				
	3.43				
12	27.09	27.09	100	a = 31.28	T = 22 °C; Col_h, *P6mm*;
	18.27	15.64	110		q_{hex} = 1; S = 847.3 Å^2;
	4.73 (br)				S_{col} = 423.7 Å^2;
	4.11				V_m = 1725.7 Å^3(d = 1 gcm^{-3});
	3.70				Z = 1.7; h_m = 3.52 Å
	3.52				

[a]d_{obs} and d_{cal} are the measured and theoretical scattering spacings; d_{cal} is calculated from the following mathematical expression for the rectangular phase: $1/d_{hk} = \sqrt{(h^2/a^2 + k^2/b^2)}$; hk are the indices of the reflections corresponding to the rectangular symmetry, and a and b are the lattice parameters of the Col_r phase and for the hexagonal phase: $1/d_{hk} = \sqrt{(1/ d_{100})(h^2 + k^2 + hk)}$; hk are the indices of the reflections corresponding to the hexagonal symmetry, and a is the lattice parameter of the Col_h phase. [b]Proposed indexing. [c]For Col_h phase; $a = d_{100}*2/\sqrt{3}$. [d]q_{hex}, the ratio $a/(b\sqrt{3})$ (q_{hex}) measures the deformation of the columnar lattice (by using rectangular coordinates) from the special case of hexagonally packed cylinders ($a=b\sqrt{3}$). S is the lattice area, for the Col_r, S = $a \times b$ and for the Col_h, S = $a^2*\sqrt{3}/2$. S_{col} is the columnar cross-section, S_{col} = S/2. V_m is Molecular volume, $V_m = M/\lambda d N_A$, where M is the molecular weight of the compound, N_A is Avogadro number, d is the volume mass density (1 g cm^{-3} for organic compounds), and λ(T) is the temperature correction coefficient at the temperature of the experiment (T), $\lambda = V_{CH2}(T_0)/V_{CH2}(T)$, where T_0 = 25 °C, $V_{CH2}(T) = 26.5616 + 0.02023T$. Z is the number of molecules per columnar slice of thickness h_m: $h_m S = ZV_m$.

Based on the X-ray scattering results we claim that discs are arranged in a dimeric fashion (Z ≈ 2, Table 4.6) and the intra-dimer distances are lesser (3.43 and 3.52 Å for **11** and **12**, respectively) compared to the inter-dimer distances (3.74 and 3.70 Å for compounds **11** and **12**, respectively) as observed also in past studies.[90] It is also quite possible that in the columnar mesophase, molecules stack in an anti-parallel fashion so as to minimize any sort of steric interactions between the alkyl chains. However, due to the lack of single crystal data, this can-not be confirmed. Another sharp signal at ~ 4.1 Å points to some kind of additional order. This peak can be correlated to the distance between the alkyl chains by Van der Waals interactions.[91] Such additional order (as can be seen in the wide angle region) generally occurs in the crystalline state of molecules. However, in these molecules, this order is present itself in the LC state. Based on the aforesaid data, we concluded that compound **11** exists in a highly ordered Col_r phase and compound **12** exists in the Col_h phase. Compound **11** exhibits long range intra- and inter-columnar order. However, for compound **12**, the intracolumnar order is much higher compared to the intercolumnar order due to the low intensity of small angle reflections. Since such an arrangement basically generates from the stacking of shape anisotropic molecules, so changing the anisotropic molecule have an enormous effect on the columnar organization.

4.2.3.4 Photophysical characterization

The UV-vis absorption and photoluminescence spectra of compounds **11** and **12** have been determined both in solution as well as in solid state. The spectra were recorded over a range of wavelengths (λ) in chloroform solution at concentrations of approximately 10^{-6} M. Figures 4.12, 4.13 and Table 4.7 compares absorption and photoluminescence spectra of mesogens **11** and **12**. As can be seen, pronounced maxima corresponding to β bands of HBC core as described by Clar[92] are displayed at 359 nm and 376 nm for **11** and **12**, respectively. The lowest energy absorptions observed in these compounds are purely electronic, symmetry forbidden α(0-0) bands at λ ≈ 400 nm which resulted due to low symmetry of these compounds. Overall, the absorption was broader for HBC **12** than for HBC **11**, indicating that intermolecular π-π interactions are stronger in case of **12** than that of **11** in solution state. This might be because of more number of bulky pentyloxy groups in **11** than in **12**, resulted in efficient packing in **12** as compared to **11**.

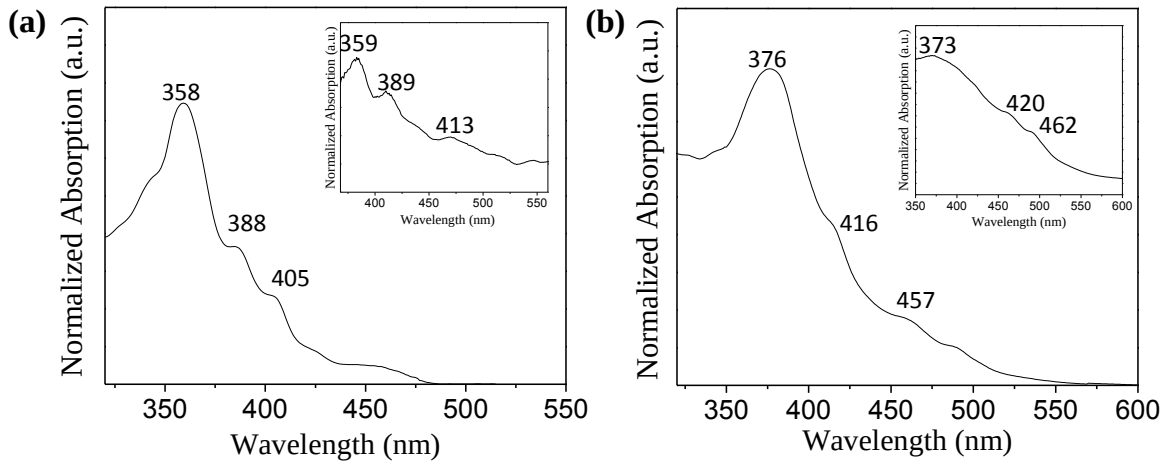

Figure 4.12 UV-vis absorption spectra of (a) HBC **11** and (b) HBC **12**. The insets show the corresponding absorption spectra in the thin film state.

Photoluminescence (PL) spectroscopy revealed a blue-shifted emission when going from **11** (570 nm) to **12** (509 nm) due to greater inherent dipole moment in **11** compared to **12**.[93] A stokes shift of 211 and 133 nm has been observed for compounds **11** and **12**, respectively. Compound **11** exhibited reddish fluorescence on irradiation with long wavelength UV light. On the other hand, compound **12** showed yellowish-green fluorescence on irradiation with 365 nm UV light (Figure 4.13c and 4.13d).

The measured life-time was found to be longer for **12** than for **11** (Table 4.7). The observed decrease in fluorescence life time could be due to higher non-radiative rate involved in the processes due to a change of size and shape of the molecules.[84,93] These observations suggested that number of alkyl chains has a tremendous effect on the photo-physical properties.

Thin film of compounds **11** and **12** were prepared by drop casting milli-molar solutions of compounds in $CHCl_3$ on a glass substrate and then evaporating solvent at room temperature. The absorption spectra recorded for both the compounds showed spectra similar to solution state with some broadening. Only a little red shift has been observed in the absorption maxima of compound **11**, while for compound **12** blue shift has been observed (Table 4.7). However, the emission showed two peaks and the emission maxima was bathochromically

shifted in solid state compared to solution state for both compounds. This red-shifted emission in thin film state can be due to close overlap of cores in thin film state resulting in aggregated state.[94] Two kinds of aggregated states have been observed in past reports. H-aggregates result from stacking of molecules one on top of another and J aggregates are formed when molecules are arranged in slip disk manner in aggregated state. Since, J-aggregates lead to transition to lower level and hence, red shifted absorption, so, in compound **11,** energy levels are getting lowered and compound **12** is undergoing H- type of aggregation.[95-97] Further, thin film of compound **11** showed reddish fluorescence and compound **12** exhibited yellowish-green fluorescence in 365 nm UV light (Figure 4.13). This clearly indicates the emissive nature of both these compounds in the LC state at room temperature.

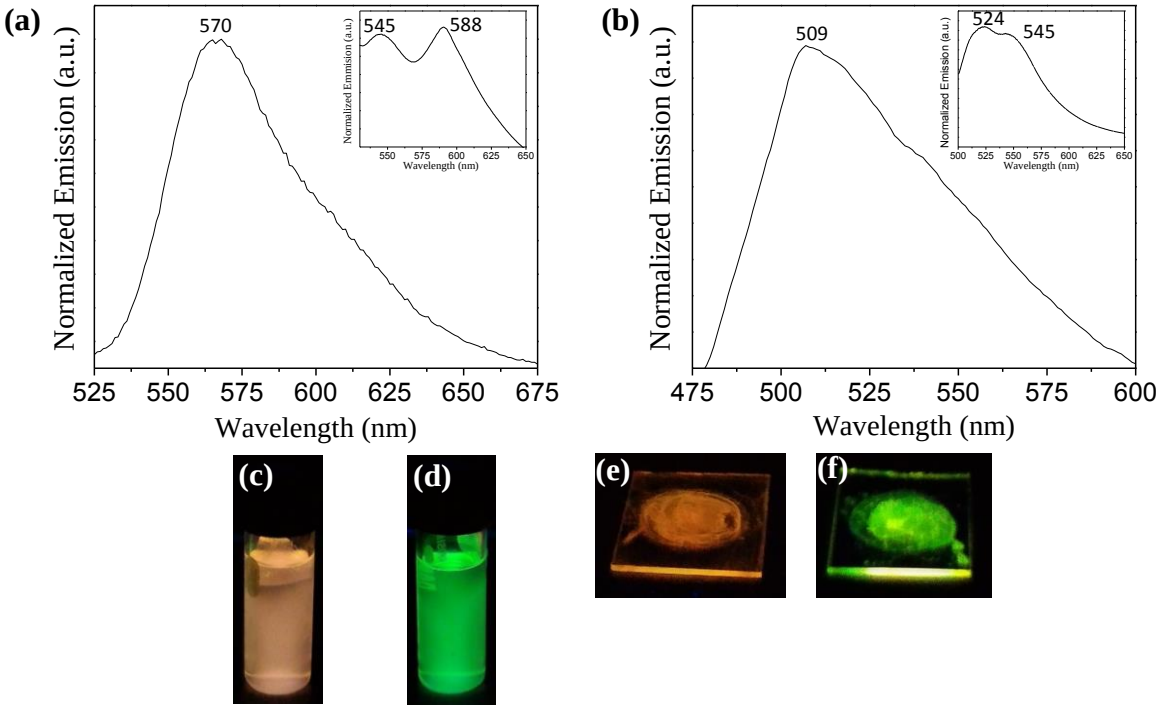

Figure 4.13 Photoluminscence spectra of (a) HBC **11** and (b) HBC **12** recorded at excitation at λ_{max}. The insets show the corresponding emission profiles in the thin film state. Pictures of micromolar chloroform solutions and thin film of compound **12** (c), (e) and of compound **12** (d), (f) as observed under the UV illumination of 365 nm light.

The optical energy gap was calculated from the onset of absorption in $CHCl_3$ as 2.71 eV (for **11**) and 2.42 eV (for **12**). The observed band gap value is also much lesser compared to the literature-known alkyl-substituted HBCs having energy gap of approximately 2.90 eV.[98] The thin films for the photo-physical properties were prepared from the highly concentrated solutions which lead to the aggregated state of the molecules. However, irrespective of aggregation, molecules in thin films exhibited reddish and yellowish-green emission similar to solution state on irradiation with 365 nm UV light and band gap was found to be much lesser in both solution and solid states. Overall, in this study we have obtained stable red light and yellowish-green light emitting HBCs with highly ordered mesophases at room temperature.

Table 4.7 Photophysical properties of compounds **11** and **12**.

	Solution State[a]							Thin Film[e]			
Mesogen	Absorption (nm)		Emission[b] (nm)	Stokes shift (nm)	Band Gap[c] (eV)	r_1[d] (ns)	r_2[d] (ns)	Absorption (nm)		Emission[f] (nm)	Stokes shift (nm)
11	358, 405	388,	570	212	2.71	3.11	3.83	359, 413	383,	545, 588	235
12	376, 457	416,	509	133	2.42	3.16	6.20	373, 462	420,	524, 547	174

[a]Measurements done in chloroform solutions of micromolar concentrations. [b]Corresponding to excitation wavelength 358 nm for **11** and 376 nm for **12**. [c]Calculated from the absorption onset, 457 nm for **11** and 514 nm for **12**. [d]Fluorescence life-time. [e]Prepared by solution processing from millimolar chloroform solutions. [f]Corresponding to excitation wavelength 359 nm for **11** and 373 nm for **12**.

4.2.4 Conclusions

In summary, a new set of alkoxy substituted have been synthesized. Cyclodehydrogenation of the corresponding symmetrical hexaphenylbenzenes lead to the formation of unsymmetrical HBCs which is very uncommon. The formation of these properly stacked or highly ordered columnar mesophases have been observed at room temperature. Compound **11** exhibited Col_r phase with *p2gm* lattice symmetry, whereas compound **12** exhibited Col_h phase with *p6mm* symmetry. Compound **11** showed reddish fluorescence in the solution as well as in the thin film state, while compound **12** showed yellowish green fluorescence in the

solution and thin films. HOMO-LUMO gap has been found to be much smaller in these molecules compared to alkyl substituted HBCs. Since band gap and room temperature mesophase are exceedingly important for the technological applications of such supramolecular systems such as in OLEDs, therefore, these molecules can be considered as powerful entry to the toolbox of molecular engineering of graphene nanostructures.

4.3 Experimental Section

4.3.1 Measurements

All the reactions were performed under N_2 atmosphere. Chemicals and solvents (AR quality) were used as received without any further purification. Column chromatographic separations were performed on silica gel (100-200 & 230-400 mesh). Thin layer chromatography (TLC) was performed on aluminium sheets pre-coated with silica gel (Merck, Kieselgel 60, F254). Structural characterization of the compounds was carried out through a combination of ^{1}H NMR and ^{13}C NMR (Bruker Biospin Switzerland Avance-iii 400 MHz and 100 MHz spectrometers, respectively), UV-vis-NIR spectrophotometers (Agitech Technologies, Cary Series), Infrared spectroscopy (Perkin Elmer Spectrum Two), and MALDI-MS spectrometry (WATERS Synapt G-2-S QTOF with MALDI as ion source and α-cyano-4-hydroxycinnamic acid as matrix). IR spectra were recorded in neat form for intermediate and target compounds. ^{1}H NMR spectra were recorded using deuterated chloroform ($CDCl_3$) as solvent and tetramethylsilane (TMS) as an internal standard. Fluorescence experiments were performed on Horiba Scientific Fluoromax Spectrofluorometer 4. Time resolved lifetime measurements were done on Time Correlated Single Photon Counter from Horiba Jobin Yvon. All the fluorescence and UV-vis experiments were performed in 15 μM $CHCl_3$ solutions. For Time resolved experiments excitation was done by 375 nm Laser Diode, emission wavelength was 570 nm for **11** and 510 nm for **12**. Thin film fluorescence studies were performed on Shimadzu spectrofluorophotometer –RF-5301PC. The transition temperatures and associated enthalpy values were determined using a differential scanning calorimeter (Perkin Elmer DSC 8000 coupled to a controlled liquid nitrogen accessory (CLN 2)) which was operated at a scanning rate of 5 °C min^{-1} both on heating and cooling. Textural observations of the mesophase were performed with Nikon Eclipse LV100POL polarizing

microscope provided with a Linkam heating stage (LTS 420). All images were captured using a Q-imaging camera. X-ray scattering was carried out on powder samples filled in glass capillaries using Cu-Kα (λ = 1.5418 Å) radiation from Xeuss (Model C HP100 fm) X-ray diffractometer from Xenocs equipped with GeniX3D source operating at 50 kV and 0.6 mA in conjunction with a multilayer mirror and Pilatus 200 hybrid pixel detector from Dectris.

4.3.2 Synthesis of 4-bromo-1,2-bis(octyloxy)benzene (7a) In a two-necked flask, a mixture of 4-bromo-1,2-dihydroxybenzene (1 g, 5.29 mmol), K_2CO_3 (8.17 g, 31.64 mmol), KI (catalyst) and 1-bromooctane (3.2 g, 26.45 mmol) was refluxed in 2-butanone (70 mL) for 18 h with stirring under a nitrogen atmosphere. After cooling to room temperature, reaction mixture was filtered. The filtrate was then evaporated under vacuum and the residue was purified by column chromatography (silica gel, hexane/ethylacetate) to give the product as colourless oil in quantitative yield. ^{1}H NMR (400 MHz, $CDCl_3$, δ ppm): 7.00-6.98 (m, 2H), 6.76-6.73 (m, 1H), 4.99-3.95 (m, 4H), 1.85-1.78 (m, 4H), 1.50-1.45 (m, 4H), 1.37-1.32 (m, 16H), 0.93-0.90 (m, 6H). ^{13}C NMR (100 MHz, $CDCl_3$, δ ppm): 150.04, 148.37, 123.43, 116.87, 115.07, 112.80, 69.46, 69.33, 31.86, 31.83, 29.41, 29.38, 29.32, 29.27, 29.23, 29.19, 26.04, 26.03, 25.95, 22.71, 22.68, 14.13. IR (Neat, KBr, ν_{max}/cm^{-1}): 2926.40, 2855.78, 1586.86, 1503.33, 1468.26, 1403.57, 1390.47, 1324.50, 1293.35, 1252.09, 1221.65, 1133.60, 1022.42, 915.24, 870.55, 836.00, 795.77, 722.89, 640.19, 578.02.

4.3.3 Synthesis of 4-bromo-1,2-bis(pentyloxy)benzene (7b) Compound **7b** was synthesized according to a similar procedure to **7a**. It was purified by column chromatography (silica gel, hexane/ethylacetate) to give the product as colourless oil in quantitative yield. ^{1}H NMR (400 MHz, $CDCl_3$, δ ppm): 7.02-6.99 (m, 2H), 6.77-6.75 (m, 1H), 4.00-3.96 (m, 4H), 1.88-1.79 (m, 4H), 1.49-1.38 (m, 8H), 0.97-0.93 (m, 6H). ^{13}C NMR (100 MHz, $CDCl_3$, δ ppm): 149.99, 148.32, 123.40, 116.78, 115.00, 112.77, 69.45, 69.31, 29.09, 28.92, 28.84, 28.19, 28.18, 22.70, 22.65, 22.49, 22.47, 14.08. IR (Neat, KBr, ν_{max}/cm^{-1}): 2955.48, 2871.45, 1586.72, 1504.83, 1469.26, 1403.73, 1390.75, 1324.69, 1293.57, 1251.61, 1222.01, 1134.07, 1073.92, 1049.57, 1003.58, 989.97, 922.39, 862.20, 835.62, 796.33, 639.95, 578.15.

4.3.4 Synthesis of 5-bromo-1,3-bis(pentyloxy)benzene (7d) Compound **7d** was synthesized according to a similar procedure to **7a**. It was purified by column chromatography (silica gel, hexane/ethylacetate) to give the product as colourless oil in quantitative yield. ^{1}H NMR (400 MHz, $CDCl_3$, δ ppm): 6.66 (d, 2H, J = 2.20 Hz), 6.39 (t, 1H, J = 2.20 Hz), 3.92 (t, 4H, J = 6.56 Hz), 1.80-1.75 (m, 4H), 1.47-1.37 (m, 8H), 0.97-0.94 (t, 6H, J = 7.16 Hz). ^{13}C NMR (100 MHz, $CDCl_3$, δ ppm): 160.75, 122.83, 110.19, 100.55, 68.28, 28.84, 28.15, 22.44, 19.21, 14.04. IR (Neat, KBr, ν_{max}/cm^{-1}): 2956.51, 2933.80, 2872.06, 1598.39, 1575.40, 1454.97, 1428.90, 1386.41, 1330.25, 1278.14, 1169.51, 1054.35, 831.61, 676.04.

4.3.5 Synthesis of 3,3',4,4'-tetraoctyloxydiphenylacetylene (8a) In a two-necked round bottom flask, 4-bromo-1,2-bis(octyloxy) benzene **7a** (1.64 g, 3.97 mmol) was dissolved in anhydrous toluene (30 mL) under an argon atmosphere. A constant stream of argon was then passed through the reaction mixture for half an hour and then palladium(0)tetrakis(triphenylphosphine) (91.83 mg, 0.08 mmol) was added. Bis(tributylstannyl)acetylene (1.1 mL, 1.98 mmol) was added dropwise and the mixture was refluxed for 18 h. The solvent was then removed under vacuum. The residue was purified by column chromatography (silica gel, hexane/ethylacetate) to give **8a** as a white crystalline solid in 45 % yield (1.2 g). ^{1}H NMR (400 MHz, $CDCl_3$, δ ppm): 7.09 (dd, 2H, J = 1.9 Hz), 7.05 (d, 2H, J = 1.9 Hz), 6.84 (d, 2H, J = 8.3 Hz), 4.02 (t, 8H, J = 6.7 Hz), 1.88-1.81 (m, 8H), 1.50-1.31 (m, 40H), 0.93-0.89 (m, 12H). ^{13}C NMR (100 MHz, $CDCl_3$, δ ppm): 149.41, 148.67, 124.72, 116.46, 115.60, 113.21, 112.96, 87.97, 69.18, 69.13, 31.85, 29.73, 29.40, 29.37, 29.30, 29.22, 29.14, 26.03, 26.00, 22.70, 14.14. IR (Neat, KBr, ν_{max}/cm^{-1}): 2953.84, 2923.95, 2853.05, 1595.85, 1514.97, 1468.84, 1335.89, 1247.52, 1202.15, 1138.40, 1066.30, 1020.22, 961.09, 842.73, 805.40, 722.53. MALDI-MS m/z calcd for $C_{46}H_{74}O_4^+$: 690.5587; found: 690.5574.

4.3.6 Synthesis of 3,3',4,4'-tetrapentyloxydiphenylacetylene (8b) Compound **8b** was synthesized according to a similar procedure to **8a**. It was purified by column chromatography (silica gel, hexane/ethylacetate) to give the product as white crystalline solid in 47 % yield (330 mg). ^{1}H NMR (400 MHz, $CDCl_3$, δ ppm): 7.09 (dd, 2H, J = 1.9 Hz), 7.06 (d, 2H, J = 1.9 Hz), 6.84 (d, 2H, J = 8.3 Hz), 4.03 (t, 8H, J = 6.7 Hz), 1.89-1.82 (m, 8H), 1.50-1.41 (m, 16H), 0.97-0.94 (m, 12H). ^{13}C NMR (100 MHz, $CDCl_3$, δ ppm): 149.40,

148.86, 124.71, 116.43, 115.59, 113.17, 87.97, 69.16, 69.10, 28.91, 28.90, 28.21, 28.20, 22.49, 14.09, 13.91. IR (Neat, KBr, ν_{max}/cm^{-1}): 2958.24, 2930.85, 2852.74, 1598.90, 1519.66, 1467.39, 1331.50, 1247.90, 1203.69, 1135.97, 1055.34, 998.35, 980.82, 847.12, 807.67, 727.76. MALDI-MS m/z calcd for $C_{34}H_{50}O_4^+$: 522.3709; found: 522.3723.

4.3.7 Synthesis of 3,3',4,4'-tetramethoxydiphenylacetylene (8c) Compound **8c** was synthesized according to a similar procedure to **8a**. It was purified by column chromatography (silica gel, hexane/ethylacetate) to give the product as white solid in 54 % yield (450 mg). ^{1}H NMR (400 MHz, $CDCl_3$, δ ppm): 7.14 (dd, 2H, J = 1.9 Hz), 7.05 (d, 2H, J = 1.9 Hz), 6.86 (d, 2H, J = 8.3 Hz), 3.93 (s, 12H). ^{13}C NMR (100 MHz, $CDCl_3$, δ ppm): 149.30, 148.60, 124.71, 115.60, 114.13, 111.00, 87.99, 55.91. IR (Neat, KBr, ν_{max}/cm^{-1}): 2923.07, 2835.16, 1589.16, 1518.92, 1460.82, 1416.98, 1366.57, 1331.50, 1247.52, 1210.54, 1134.24, 1059.72, 1020.27, 961.09, 851.50, 829.58, 807.67, 681.92. MALDI-MS m/z calcd for $C_{18}H_{18}O_4^+$: 298.1205; found: 298.1202.

4.3.8 Synthesis of 3,3',5,5'-tetrapentyloxydiphenylacetylene (8d) Compound **8d** was synthesized according to a similar procedure to **8a**. It was purified by column chromatography (silica gel, hexane/ethylacetate) to give the product as white crystalline solid in 49 % yield (50 mg). ^{1}H NMR (400 MHz, $CDCl_3$, δ ppm): 6.68 (d, 4H, J = 2.2 Hz), 6.43 (t, 2H, J = 2.2 Hz), 4.00 (t, 8H, J = 6.5 Hz), 1.85-1.80 (m, 8H), 1.42-1.39 (m, 16H), 0.92-0.91 (m, 12H). ^{13}C NMR (100 MHz, $CDCl_3$, δ ppm): 160.73, 139.25, 129.19, 105.03, 101.00, 68.11, 28.52, 28.17, 22.82, 22.39, 14.43, 14.19. IR (Neat, KBr, ν_{max}/cm^{-1}): 2928.26, 2838.46, 1591.18, 1516.81, 1459.80, 1418.91, 1367.51, 1332.56, 1246.51, 1208.08, 1133.21, 1057.76, 1024.25, 959.07, 849.55, 827.55, 806.67, 682.92. MALDI-MS m/zcalcd for $C_{34}H_{50}O_4^+$: 522.3709; found: 522.3732.

4.3.9 Synthesis of 3,3',5,5'-tetramethoxydiphenylacetylene (8e) Compound **8e** was synthesized according to a similar procedure to **8a**. It was purified by column chromatography (silica gel, hexane/ethylacetate) to give the product as white solid in 61 % yield (650 mg). ^{1}H NMR (400 MHz, $CDCl_3$, δ ppm): 6.72 (d, 4H, J = 1.9 Hz), 6.49 (t, 2H, J = 2.4 Hz), 3.83 (s, 12H). ^{13}C NMR (100 MHz, $CDCl_3$, δ ppm): 160.55, 148.67, 124.36, 109.39, 101.94, 88.94, 55.46. IR (Neat, KBr, ν_{max}/cm^{-1}): 2923.07, 2839.56, 1588.26, 1455.39,

1418.43, 1368.07, 1331.50, 1248.39, 1209.97, 1158.77, 1062.72, 1020.27, 927.27, 850.26, 831.77, 681.75. MALDI-MS m/zcalcd for $C_{18}H_{19}O_4^+$: 299.1283; found: 299.1279.

4.3.10 Synthesis of 1,2,3,4,5,6-Hexakis((3,4-dioctyloxy)phen-1-yl)benzene (5a) In a two-necked round bottom flask, 3,3',4,4'-tetraoctyloxydiphenylacetylene (303 mg, 0.44 mmol) was dissolved in 1,4-dioxane (30 mL) under an argon atmosphere and dicobaltooctacarbonyl (29.99 mg, 0.088 mmol) was added. The resulting mixture was refluxed for 7 h and then the solvent was removed under vacuum. The residue was purified by column chromatography (silica gel, hexane/ethylacetate) to give **5a** as a light brown solid in 49 % yield (446 mg). ^{1}H NMR (400 MHz, $CDCl_3$, δ ppm): 6.41-6.36 (m, 12H), 6.30-6.28 (m, 6H), 3.82-3.75 (m, 12H), 3.52-3.47 (m, 12H), 1.74-1.71 (m, 12H), 1.59-1.57 (m, 12H), 1.40-1.29 (m, 120H), 0.92-0.88 (m, 36H). ^{13}C NMR (100 MHz, $CDCl_3$, δ ppm): 147.57, 147.39, 146.50, 140.15, 133.85, 133.74, 124.20, 118.26, 117.96, 112.24, 111.80, 69.24, 68.96, 31.90, 31.85, 29.48, 29.40, 29.31, 29.17, 26.05, 22.73, 22.69, 14.11. IR (Neat, KBr, ν_{max}/cm^{-1}): 2949.45, 2918.68, 2855.09, 1603.28, 1580.27, 1514.94, 1469.78, 1432.32, 1416.98, 1378.95, 1255.04, 1222.02, 1140.41, 1121.09, 1024.11, 992.77, 870.47, 803.51, 722.93. MALDI-MS m/z calcd for $C_{138}H_{222}O_{12}^+$: 2072.6795; found: 2072.6768.

4.3.11 Synthesis of 1,2,3,4,5,6-Hexakis((3,4-dipentyloxy)phen-1-yl)benzene (5b) Compound **5b** was synthesized according to a similar procedure to **5a**. It was purified by column chromatography (silica gel, hexane/ethylacetate) to give the product as light brown solid in 47 % yield (257 mg). ^{1}H NMR (400 MHz, $CDCl_3$, δ ppm): 6.44-6.36 (m, 12H), 6.31-6.29 (m, 6H), 3.85-3.74 (m, 12H), 3.50-3.48 (m, 12H), 1.75-1.72 (m, 12H), 1.60-1.57 (m, 12H), 1.39-1.31 (m, 48H), 0.94-0.91 (m, 36H). ^{13}C NMR (100 MHz, $CDCl_3$, δ ppm): 147.55, 147.38, 146.48, 140.16, 133.83, 133.73, 124.21, 118.16, 117.89, 112.18, 111.77, 69.13, 68.68, 28.97, 28.83, 28.19, 22.52, 22.46, 14.10, 14.06. IR (Neat, KBr, ν_{max}/cm^{-1}): 2957.53, 2932.47, 2860.23, 1603.10, 1579.28, 1516.57, 1470.16, 1433.32, 1415.89, 1379.19, 1255.26, 1222.29, 1140.67, 1050.97, 992.77, 870.47, 803.51, 764.62, 642.22. MALDI-MS m/z calcd for $C_{102}H_{150}O_{12}^+$: 1568.1161; found: 1568.1189.

4.3.12 Synthesis of 1,2,3,4,5,6-Hexakis((3,4-dimethoxy)phen-1-yl)benzene (5c) Compound **5c** was synthesized according to a similar procedure to **5a**. It was purified by

column chromatography (silica gel, hexane/ethylacetate) to give the product as light brown solid in 48 % yield (279 mg). ^{1}H NMR (400 MHz, $CDCl_3$, δ ppm): 6.46-6.35 (m, 18H), 3.74 (s, 18H), 3.45 (s, 18H). ^{13}C NMR (100 MHz, $CDCl_3$, δ ppm): 147.55, 147.49, 146.54, 140.34, 140.24, 133.52, 124.29, 123.97, 123.71, 115.60, 115.30, 115.09, 109.85, 109.71, 109.58, 55.72, 55.64, 55.55. IR (Neat, KBr, ν_{max}/cm^{-1}): 2997.80, 2932.89, 2830.76, 1601.09, 1583.59, 1518.69, 1463.94, 1409.49, 1313.97, 1253.90, 1230.69, 1138.75, 1027.95, 915.06, 851.50, 807.02, 768.33, 732.55. MALDI-MS m/z calcd for $C_{54}H_{54}O_{12}^{+}$: 894.3615; found: 894.3644.

4.3.13 Synthesis of 1,2,3,4,5,6-Hexakis((3,5-dimethoxy)phen-1-yl)benzene (5e) Compound **5e** was synthesized according to a similar procedure to **5a**. It was purified by column chromatography (silica gel, hexane/ethylacetate) to give the product as light brown solid in 17 % yield (21 mg). ^{1}H NMR (400 MHz, $CDCl_3$, δ ppm): 7.08 (d, 12H, J = 2.4 Hz), 6.75 (t, 6H, J = 2.4 Hz), 3.85 (s, 36H). ^{13}C NMR (100 MHz, $CDCl_3$, δ ppm): 159.03, 122.89, 111.56, 101.56, 56.10. IR (Neat, KBr, ν_{max}/cm^{-1}): 2968.83, 2923.85, 2845.40, 1596.18, 1455.10, 1423.60, 1365.15, 1275.57, 1204.59, 1157.13, 1060.63, 990.13, 943.16, 931.42, 833.50, 749.94. MALDI-MS m/z calcd for $C_{54}H_{55}O_{12}^{+}$: 895.3649; found: 895.3668.

4.3.14 Synthesis of 1,2,6,7,10,11,12,13,16,17,21,22- dodecaoctyloxydibenzo [*fg*,*ij*] triphenyleno [1,2,3,4-rst]pentaphene (9a) In a two-necked round bottom flask, 1,2,3,4,5,6-Hexakis((3,4-dioctyloxy)phen-1-yl)benzene (100 mg, 0.048 mmol) was dissolved in dichloromethane (5 mL) under an argon atmosphere. Throughout the whole reaction, a constant stream of argon was bubbled through the reaction mixture. The reaction mixture was then cooled to 0 ºC and methylsulfonic acid (0.5 mL) was added dropwise. After this 2,3-Dichloro-5,6-dicyano-1,4-benzoquinone (65.38 mg, 0.288 mmol) was added and the mixture was stirred for 40-45 min at 0 ºC. TLC monitoring was done after every 10 min and reaction was stopped until completion of reactant. Saturated solution of Na_2CO_3 was added to quench the reaction. The mixture was then extracted with dichloromethane, concentrated and the residue was purified by column chromatography (silica gel, hexane/ethyl acetate) to afford **9a** in 27 % yield (28 mg). ^{1}H NMR (400 MHz, $CDCl_3$, δ ppm): 9.28 (s, 2H), 8.34 (s, 2H), 8.11 (s, 2H), 8.04 (s, 2H), 7.81 (s, 2H), 4.52-4.17 (m, 16H), 3.72-3.64 (m, 8H), 2.14-1.93 (m, 16H), 1.74-1.51 (m, 8H), 1.49-1.24 (m, 120H), 1.02-0.86 (m, 36H). ^{13}C NMR (100 MHz,

$CDCl_3$, δ ppm): 151.53, 148.80, 148.10, 148.06, 147.89, 145.23, 127.07, 126.31, 125.07, 124.39, 123.96, 123.71, 123.23, 122.90, 121.45, 117.36, 114.14, 113.96, 111.23, 105.44, 74.21, 70.01, 69.40, 69.21, 68.54, 68.39, 31.98, 31.94, 31.90, 31.85, 31.81, 30.85, 29.82, 29.78, 29.72, 29.62, 29.55, 29.44, 29.38, 29.22, 28.90, 26.47, 26.20, 25.94, 25.88, 22.74, 22.25, 14.08. IR (Neat, KBr, ν_{max}/cm^{-1}): 2954.9, 2925.8, 2854.8, 1590.8, 1504.5, 1467.9, 1431.3, 1364.9, 1246.08, 1118.4, 1106.5, 1021.3, 809.0, 765.4, 747.5, 617.4. MALDI-MS (m/z): M^+ calcd for $C_{138}H_{215}O_{12}^+$: 2064.6169; found: 2064.6138.

4.3.15 Synthesis of 1,2,6,7,10,11,12,13,16,17,21,22- dodecapentyloxydibenzo [*fg*,*ij*] triphenyleno [1,2,3,4-rst]pentaphene (9b) Compound **9b** was synthesized according to a similar procedure to **9a**. It was purified by column chromatography (silica gel, hexane/ethylacetate) to give the product in 29 % yield (29 mg). ^1H NMR (400 MHz, $CDCl_3$, δ ppm): 9.29 (s, 2H), 8.35 (s, 2H), 8.12 (s, 2H), 8.04 (s, 2H), 7.82 (s, 2H), 4.32-4.21 (m, 16H), 3.73-3.65 (m, 8H), 2.02-1.96 (m, 24H), 1.73-1.31 (m, 48H), 0.97-0.86 (m, 36H). ^{13}C NMR (100 MHz, $CDCl_3$, δ ppm): 151.54, 148.83, 148.10, 148.07, 147.90, 145.27, 127.07, 126.32, 125.03, 124.41, 123.99, 123.73, 123.25, 122.92, 122.41, 121.46, 117.40, 114.15, 113.89, 111.21, 107.44, 105.52, 74.17, 69.89, 69.43, 69.15, 68.50, 68.30, 30.46, 29.71, 29.44, 29.11, 29.08, 28.58, 28.48, 28.36, 28.10, 28.04, 22.75, 22.68, 22.60, 22.56, 22.28, 22.25, 14.17, 14.14, 14.09. IR (Neat, KBr, ν_{max}/cm^{-1}): 2931.21, 2958.9, 2861, 1596.80, 1502.90, 1468.19, 1432.40, 1369.80, 1260.56, 1117.04, 1045, 1021.4, 990.13, 749.82. MALDI-MS m/z calcd for $C_{102}H_{143}O_{12}^+$: 1560.0535; found: 1560.0557.

4.3.16 Synthesis of 1,2,6,7,10,11,12,13,16,17,21,22- dodecamethoxydibenzo [*fg*,*ij*] triphenyleno [1,2,3,4-rst]pentaphene (9c). Compound **9c** was synthesized according to a similar procedure to **9a**. It was purified by column chromatography (silica gel, hexane/ethylacetate) to give the product in 31 % yield (31 mg). ^1H NMR (400 MHz, $CDCl_3$, δ ppm): 9.33 (s, 2H), 8.42 (s, 2H), 8.16 (s, 2H), 8.05 (s, 2H), 7.91 (s, 2H), 4.37 (s, 9H), 4.22 (s, 9H), 4.19 (s, 9H), 4.13 (s, 9H). ^{13}C NMR (100 MHz, $CDCl_3$, δ ppm): 152.05, 149.16, 148.28, 147.86, 147.77, 146.07, 126.85, 126.55, 124.67, 124.07, 123.88, 123.59, 123.50, 123.37, 122.93, 121.60, 117.61, 115.90, 114.07, 112.81, 112.61, 108.97, 61.05, 56.67, 56.09, 55.88, 55.64, 55.48, 53.43. IR (Neat, KBr, ν_{max}/cm^{-1}): 2951, 2923.62, 2852.85, 1572.85,

1506.08, 1464.18, 1373.85, 1261.02, 1119.15, 1009.7, 750.03. MALDI-MS m/z calcd for $C_{54}H_{46}O_{12}^{+}$: 886.2989; found: 886.2975.

4.3.17 Synthesis of 1,3,4,6,7,9,10,12,13,15,16,18-dodecamethoxyhexa-*peri*-hexabenzocoronene (9e) Compound **9e** was synthesized according to a similar procedure to **9a**. It was purified by column chromatography (silica gel, hexane/ethylacetate) to give the product **9e** in 4 % yield (4 mg). ^{1}H NMR (400 MHz, $CDCl_3$, δ ppm): 6.52 (s, 6H), 3.73 (s, 36H). ^{13}C NMR (100 MHz, $CDCl_3$, δ ppm): 161.12, 161.02, 160.58, 160.10, 159.93, 134.67, 107.56, 107.40, 107.04, 55.70, 55.33. IR (Neat, KBr, ν_{max}/cm^{-1}): 2971.8, 2924.8, 2863.2, 1603.1, 1461.0, 1402.8, 1399.5, 1270.6, 1200.6, 1093.8, 813.4, 764.9, 750.2, 676.8, 641.5, 617.3, 559.2. MALDI-MS m/z calcd for $C_{54}H_{42}O_{12}^{+}$: 882.2676; found: 882.2661.

4.3.18 Synthesis of 5-bromo-1,2,3-trihydroxybenzene (13a) In a schlenck flask, a solution of dichloromethane (40 mL) and 5-bromo-1,2,3-trimethoxybenzene (5 g, 20.24 mmol) was prepared and cooled to -78 ^{o}C under N_2 atmosphere. To this was then added a dichloromethane solution of BBr_3 (60 mL, 1M) at -78 ^{o}C. After the addition the mixture was allowed to warm to room temperature. After 16 h, the mixture was poured into ice-water (100 mL) and extracted with ethylacetate. This extract was then dried with Na_2SO_4 and solvent was evaporated to give off-white product in quantitative yield. ^{1}H NMR (400 MHz, DMSO-d6, δ ppm): 6.41 (s, 2H). ^{13}C NMR (100 MHz, DMSO-d6, δ ppm): 147.77, 133.17, 110.30, 109.56. IR (Neat, KBr, ν_{max}/cm^{-1}): 3341, 2933.80, 2872.06, 1609.2, 1519.5, 1443.6, 1374.6, 1178, 1005.4, 822.6, 657.

4.3.19 Synthesis of 5-bromo-1,2,3-tris(pentyloxy)benzene (14a) In a two-necked flask, a mixture of 5-bromo-1,2,3-trihydroxybenzene (**13a**) (1.5 g, 7.31 mmol), K_2CO_3 (15.17 g, 109.75 mmol), KI (catalytic amount) and 1-bromopentane (7.30 mL, 58.52 mmol) was refluxed in 2-butanone (90 mL) for 18 h with stirring under a nitrogen atmosphere. After cooling to room temperature, reaction mixture was filtered. The filtrate was then evaporated under vacuum and the residue was purified by column chromatography (silica gel, hexane/ethylacetate) to give the product as colourless oil in quantitative yield. ^{1}H NMR (400 MHz, $CDCl_3$, δ ppm): 6.69 (s, 2H), 3.97-3.91 (m, 6H), 1.84-1.73 (m, 6H), 1.50-1.37 (m, 12H), 0.97-0.92 (m, 9H). ^{13}C NMR (100 MHz, $CDCl_3$, δ ppm): 153.80, 137.31, 115.59,

110.02, 73.40, 69.24, 29.92, 28.94, 28.22, 28.19, 22.56, 22.4214.10, 14.04. IR (Neat, KBr, ν_{max}/cm^{-1}): 2956.51, 2933.80, 2872.06, 1598.39, 1575.40, 1454.97, 1428.90, 1386.41, 1330.25, 1278.14, 1169.51, 1054.35, 831.61, 676.04.

4.3.20 Synthesis of 1-(2-(3,4,5-tris(pentyloxy)phenyl)ethynyl)benzene (15a) In a two-necked round bottom flask, dry toluene (21 mL), 5-bromo-1,2,3-tris(pentyloxy)benzene (0.64 g, 1.54 mmol), $Pd(PPh_3)_2Cl_2$ (47.56 mg, 0.068 mmol), CuI (12.95 mg, 0.068 mmol), PPh_3 (10.10 mg, 0.039 mmol) and diisopropylamine (10 mL) were placed and degassed with Ar at 0 ^oC. Phenyl acetylene (0.2 mL, 1.87 mmol) was then added and the mixture was stirred at 80 ^oC overnight. The solvent was then removed under reduced pressure and the residue was purified by column chromatography (silica gel, hexane/ethylacetate) to give the product as bright orange viscous liquid in 78 % yield. ^1H NMR (400 MHz, $CDCl_3$, δ ppm): 7.57-7.55 (m, 2H), 7.38-7.36 (m, 3H), 6.78 (s, 2H), 4.02 (t, 6H, *J* = 6.52 Hz), 1.84-1.78 (m, 6H), 1.54-1.42 (m, 12H), 0.99-0.96 (m, 9H). ^{13}C NMR (100 MHz, $CDCl_3$, δ ppm): 153.02, 139.00, 131.54, 128.36, 128.15, 123.35, 117.67, 110.06, 89.77, 88.11, 73.40, 69.09, 30.00, 29.75, 29.04, 28.27, 22.60, 22.48, 14.17, 14.14, 14.09. IR (Neat, KBr, ν_{max}/cm^{-1}): 2930.43, 2861.53, 1592.57, 1485.96, 1250.16, 1215.34, 1132.05, 1022.46, 915.81, 755.75, 686.93, 525.03. MALDI-MS m/z calcd for $C_{29}H_{40}O_3^+$: 436.30; found: 436.28.

4.3.21 Synthesis of 1-(2-(3,5-bis(pentyloxy)phenyl)ethynyl)benzene (15b) Compound was synthesized according to a similar procedure to **15a**. It was purified by column chromatography (silica gel, hexane/ethylacetate) to give the product as bright orange viscous liquid in 82 % yield. ^1H NMR (400 MHz, $CDCl_3$, δ ppm): 7.56-7.53 (m, 2H), 7.37-7.36 (m, 3H), 6.69 (d, 2H, *J* = 2.41 Hz), 6.48 (t, 1H, *J* = 2.41 Hz), 3.97 (t, 4H, *J* = 6.42 Hz), 1.82-1.79 (m, 4H), 1.47-1.39 (m, 8H), 0.97-0.94 (t, 6H, *J* = 6.80 Hz). ^{13}C NMR (100 MHz, $CDCl_3$, δ ppm): 160.06, 131.66, 128.35, 128.33, 109.84, 102.75, 94.22, 88.71, 82.59, 75.61, 75.32, 68.17, 28.92, 28.20, 22.60, 22.43, 14.17, 14.14, 14.06. IR (Neat, KBr, ν_{max}/cm^{-1}): 2956.07, 2930.02, 2859.38, 1744.34, 1688.31, 1583.66, 1501.10, 1467.06, 1424.03, 1380.86, 1319.34, 1231.29, 1110.78, 1047.94, 1026.66, 992.75, 838.68, 758.56, 719.00, 698.94. MALDI-MS m/z calcd for $C_{24}H_{30}O_2^+$: 350.22; found: 350.16.

4.3.22 Synthesis of 1,3,5-tris(3,4,5-dipentyloxyphenyl)-2,4,6-triphenylbenzene (16a) In a two-necked round bottom flask, 1-(2-(3,4,5-bis(pentyloxy)phenyl)ethynyl)benzene (500 mg, 1.15 mmol) was dissolved in 1,4-dioxane (50 mL) under an argon atmosphere and dicobaltooctacarbonyl (78.65 mg, 0.23 mmol) was added. The resulting mixture was refluxed for 7 h and then the solvent was removed under vacuum. The residue was purified by column chromatography (silica gel, hexane/ethylacetate) to give **16a** as a light brown viscous liquid in 59 % yield. ^{1}H NMR (400 MHz, $CDCl_3$, δ ppm): 7.89-7.83 (m, 15H), 6.05-5.97 (dd, 6H, *J* = 6.88 Hz), 3.78-3.74 (m, 6H), 3.46-3.39 (m, 12H), 1.64-1.50 (m, 18H), 1.40-1.27 (m, 36H), 0.94-0.89 (m, 27H). ^{13}C NMR (100 MHz, $CDCl_3$, δ ppm): 150.04, 148.60, 125.49, 117.00, 114.00, 113.00, 83.99, 75.45, 69.22, 69.09, 31.84, 29.38, 29.29, 29.18, 29.16, 26.00, 22.69, 14.14. IR (Neat, KBr, ν_{max}/cm^{-1}): 2956.55, 2932.92, 2857.14, 1583.81, 1500.27, 1421.36, 1382.13, 1320.54, 1231.38, 1161.60, 1056.53, 845.45, 756.87, 699.09. MALDI-MS m/z cald. for $C_{87}H_{120}O_9^+$: 1308.89; found: 1308.90.

4.3.23 Synthesis of 1,3,5-tris(3,5-dipentyloxyphenyl)-2,4,6-triphenylbenzene (16b) Compound **16b** was synthesized according to a similar procedure to **16a**. It was purified by column chromatography (silica gel, hexane/ethylacetate) to give the product as light brown viscous liquid in 57 % yield. ^{1}H NMR (400 MHz, $CDCl_3$, δ ppm): 6.94-6.87 (m, 15H), 6.06-5.98 (m, 9H), 3.56-3.50 (m, 12H), 1.57-1.52 (m, 12H), 1.34-1.25 (m, 24H), 0.93-0.88 (m, 18H). ^{13}C NMR (100 MHz, $CDCl_3$, δ ppm): 158.69, 140.15, 131.27, 131.01, , 126.78, 110.98, 110.52, 68.07, 28.72, 28.65, 28.09, 28.05, 22.36, 22.35, 14.07. IR (Neat, KBr, ν_{max}/cm^{-1}): 2955.69, 2932.23, 2871.34, 1594.40, 1465.20, 1434.19, 1386.10, 1287.34, 1160.61, 1056.53, 844.15, 757.67, 698.29. MALDI-MS m/z calcd for $C_{72}H_{90}O_6^+$: 1051.69; found: 1051.68.

4.3.24 Synthesis of 1,2,3,7,8,9,13,14,15-nonapentyloxyhexa-*peri*-hexabenzocoronene (11) In a two-necked round bottom flask, **16a** (220 mg, 0.17 mmol) was dissolved in dichloromethane (20 mL) under an argon atmosphere. Throughout the whole reaction, a constant stream of argon was bubbled through the reaction mixture. The reaction mixture was then cooled to 0 ºC and methylsulfonic acid (2.0 mL) was added dropwise. After this 2,3-Dichloro-5,6-dicyano-1,4-benzoquinone (228.82 mg, 1.01 mmol) was added and the mixture stirred for 2 h at 0 ºC. TLC monitoring was done after every 10 min and reaction was stopped

until completion of reactant. Saturated solution of Na_2CO_3 was added to quench the reaction. The mixture was then extracted with dichloromethane, concentrated and the residue was purified by column chromatography (silica gel, hexane/ethyl acetate) to afford **11** (15% yield). ^{1}H NMR (400 MHz, $CDCl_3$, δ ppm): 10.45 (d, 2H, J = 8.04 Hz), 10.03 (d, 2H, *J* = 8.12 Hz), 9.13 (d, 2H, *J* = 7.60 Hz), 8.16 (t, 2H, *J* = 7.90 Hz), 8.03 (t, 1H, *J* = 7.62 Hz), 4.58 (t, 6H, *J* = 6.76 Hz), 4.19-4.13 (m, 12H), 2.33-2.20 (m, 6H), 2.15-2.10 (m, 12H), 2.09-1.98 (m, 18H), 1.76-1.70 (m, 18H), 1.08-0.98 (m, 18H). ^{13}C NMR (400 MHz, $CDCl_3$, δ ppm): 157.10, 156.98, 156.64, 156.53, 156.20, 131.79, 130.17, 129.59, 129.48, 129.00, 128.19, 127.20, 112.49, 98.84, 70.56, 70.40, 69.99, 69.67, 69.60, 30.07, 29.80, 29.74, 29.23, 29.12, 29.06, 29.03, 28.80, 28.63, 23.00, 14.53, 14.30. IR (Neat, KBr, ν_{max}/cm^{-1}): 2955.9, 2920.2, 2850.2, 1608.2, 1463.8, 1402.6, 1384.6, 1260.9, 1092.7, 803.5, 748.9, 765.2, 719.4, 616.5. MALDI-MS m/z calcd for $C_{87}H_{108}O_9^+$: 1296.7993; found: 1296.7986.

4.3.25 Synthesis of 1,3,7,9,13,15-hexapentyloxyhexa-*peri*-hexabenzocoronene (12) Compound **12** was synthesized according to a similar procedure to **11**. It was purified by column chromatography (silica gel, hexane/ethylacetate) Yield 17%. ^{1}H NMR (400 MHz, $CDCl_3$, δ ppm): 9.96 (d, 1H, *J* = 8.00 Hz), 9.72 (d, 1H, *J* = 8.00 Hz), 9.38 (d, 2H, *J* = 8.40 Hz), 8.27 (s, 1H), 7.99 (t, 1H, *J* = 8.00 Hz), 7.49-7.41 (m, 2H), 7.39 (s, 1H), 7.24 (s, 1H), 7.19-7.12 (m, 2H), 4.57-4.10 (m, 12H), 1.91-1.89 (m, 4H), 1.80-1.71 (m, 8H), 1.57-1.42 (m, 12H), 1.11-1.07 (m, 12H), 0.94-0.88 (m, 18H). ^{13}C NMR (400 MHz, $CDCl_3$, δ ppm): 156.76, 156.29, 155.94, 155.85, 155.59, 131.44, 129.24, 129.13, 128.65, 127.08, 126.85, 122.03, 121.02, 113.81, 112.14, 96.04, 93.37, 70.14, 69.88, 69.71, 69.65, 69.43, 69.27, 29.73, 29.52, 29.45, 29.39, 29.36, 29.32, 28.78, 28.72, 28.68, 28.67, 28.29, 22.66, 22.63, 22.61, 14.19, 14.16, 14.13. IR (Neat, KBr, ν_{max}/cm^{-1}): 2956.8, 2950.7, 2920.3, 1698.1, 1612.6, 1598.9, 1462.8, 1401.4, 1384.0, 1261.1, 1092.9, 803.9, 705.6, 704.4, 696.9, 660.8. MALDI-MS m/z calcd for $C_{72}H_{78}O_6^+$: 1038.5798; found: 1038.5768.

References

(1) Zeni, G.; Larock, R. C. *Chem. Rev.* **2006**, *106*, 4644-4680.

(2) Beccalli, E. M.; Broggini, G.; Martinelli, M.; Sottocornola, S. *Chem. Rev.* **2007**, *107*, 5318-5365.

(3) Grzybowski, M.; Skonieczny, K.; Butenschön, H.; Gryko, D. T. *Angew. Chem. Int. Ed.* **2013**, *52*, 9900-9930.

(4) Imrie, C. T.; Lu, Z.; Picken, S. J.; Yildirim, Z. *Chem. Commun.* **2007**, 1245-1247.

(5) Allen, M. T.; Diele, S.; Harris, K. D. M.; Hegmann, T.; Kariuki, B. M.; Lose, D.; Preece, J. A.; Tschierske, C. *J. Mater. Chem.* **2001**, *11*, 302-311.

(6) Wu, J.; Watson, M. D.; Zhang, L.; Wang, Z.; Müllen, K. *J. Am. Chem. Soc.* **2004**, *126*, 177-186.

(7) Ito, S.; Wehmeier, M.; Brand, J. D.; Kubel, C.; Epsch, R.; Rabe, J. P.; Mullen, K. *Chem. Eur. J.* **2000**, *6*, 4327-4342.

(8) Watson, M. D.; Jäckel, F.; Severin, N.; Rabe, J. P.; Müllen, K. *J. Am. Chem. Soc.* **2004**, *126,* 1402-1407.

(9) Thünemann, A. F.; Kubowicz, S.; Burger, C.; Watson, M. D.; Tchebotareva, N.; Müllen, K. *J. Am. Chem. Soc.* **2003**, *125*, 352-356.

(10) Pisula, W.; Kastler, M.; Wasserfallen, D.; Pakula, T.; Müllen, K. *J. Am. Chem. Soc.* **2004**, *126*, 8074-8075.

(11) van de Craats, A. M.; Warman, J. M.; Müllen, K.; Geerts, Y.; Brand, J. D. *Adv. Mater.* **1998**, *10*, 36-38.

(12) Wu, J.; Fechtenkötter, A.; Gauss, J.; Watson, M. D.; Kastler, M.; Fechtenkötter, C.; Wagner, M.; Müllen, K. *J. Am. Chem. Soc.* **2004**, *126*, 11311-11321.

(13) Bushby, R. J.; Lozman, O. R. *Curr. Opin. Colloid Interface Sci.* **2002**, 7, 343-354.

(14) Self-Organized Organic Semiconductors: From Materials to Device Applications Li, Q., Ed.; John Wiley & Sons: New Jersey, 2010.

(15) Kafer, D.; Bashir, A.; Dou, X.; Witte, G.; Mullen K.; Woll, C. *Adv. Mater.* **2010**, *22*, 384-388.

(16) Pisula, W.; Menon, A.; Stepputat, M.; Lieberwirth, I.; Kolb, U.; Tracz, A.; Sirringhaus, H.; Pakula T.; Müllen, K. *Adv. Mater.* **2005**, *17*, 684-689.

(17) Seyler, H.; Purushothaman, B.; Jones, D. J.; Holmes, A. B.; Wong, W. W. H. *Pure Appl. Chem.* **2012**, *84*, 1047-1067.

(18) Schmidt-Mende, L.; Fechtenkotter, A.; Mullen, K.; Moons, E.; Friend, R. H.; MacKenzie, J. D. *Science* **2001**, *293*, 1119-1122.

(19) Watson, M. D.; Fechtenkotter, A.; Mullen, K. *Chem. Rev.* **2001**, *101*, 1267-1300.

(20) Liquid Crystals Beyond Displays: Chemistry, Physics, and Applications, Li, Q., Ed.; John Wiley & Sons: New Jersey, 2012.

(21) Grimsdale, A. C.; Mullen, K. *Angew. Chem. Int. Ed.* **2005**, *44*, 5592-5629.

(22) Kato, T.; Yasuda, T.; Kamikawa, Y.; Yoshio, M. *Chem. Commun.* **2009**, 729-739.

(23) Li, C.; Liu, M.; Pschirer, N. G.; Baumgarten, M.; Mullen, K. *Chem. Rev.* **2010**, *110*, 6817-6855.

(24) Sergeyev, S.; Pisula, W.; Geerts, Y. H. *Chem. Soc. Rev.* **2007**, *36*, 1902-1929.

(25) O'Neill, M.; Kelly, S. M. *Adv. Mater.* **2003**, *15*, 1135-1146.

(26) O'Neill, M.; Kelly, S. M. *Adv. Mater.* **2011**, *23*, 566-584.

(27) Kaafarani, B. R. *Chem. Mater.* **2011**, *23*, 378-396.

(28) Kumar, S. *Chem. Soc. Rev.* **2006**, *35*, 83-109.

(29) Bushby, R. J.; Kawata, K. *Liq. Cryst.* **2011**, *38*, 1415-1426.

(30) Wasserfallen, D.; Kastler, M.; Pisula, W.; Hofer, W. A.; Fogel, Y.; Wang, Z.; Müllen, K. *J. Am. Chem. Soc.* **2006**, *128*, 1334-1339.

(31) Weiss, K.; Beernink, G.; Dötz, F.; Birkner, A.; Müllen, K.; Wöll, C. H. *Angew. Chem. Int. Ed.* **1999**, *38*, 3748-3752.

(32) Wadumethrige, S. H.; Rathore, R. *Org. Lett.* **2008**, *10*, 5139-5142.

(33) Feng, X.; Wu, J.; Enkelmann, V.; Müllen, K. *Org. Lett.* **2006**, *8*, 1145-1148.

(34) Pradhan, A.; Dechambenoit, P.; Bock, H.; Durola, F. *J. Org. Chem.* **2013**, *78*, 2266-2274.

(35) Pradhan, A.; Dechambenoit, P.; Bock, H.; Durola, F. *Angew. Chem. Int. Ed.* **2011**, *50*, 12582-12585.

(36) Stefano, M. D.; Negri, F.; Carbone, P., Mullen, K. *Chem. Phys.* **2005**, *314*, 85-99.

(37) Rempala, P.; Kroulík, J.; King, B. T. *J. Am. Chem. Soc.* **2004**, *126*, 15002-15003.

(38) Rempala, P.; Kroulík, J.; King, B. T. *J. Org. Chem.* **2006**, *71*, 5067-5081.

(39) King, B. T.; Kroulík, J.; Robertson, C. R.; Rempala, P.; Hilton, C. L.; Korinek, J. D.; Gortari, L. M. *J. Org. Chem.* **2007**, *72*, 2279-2288.

(40) Zhai, L.; Shukla, R.; Rathore, R. *Org. Lett.* **2009**, *11*, 3474-3477.

(41) Zhai, L.; Shukla, R.; Wadumethrige, S. H.; Rathore, R. *J. Org. Chem.* **2010**, *75*, 4748-4760.

(42) Arslan, H.; Uribe-Romo, F. J.; Smitha, B. J.; Dichtel, W. R. *Chem. Sci.* **2013**, *4*, 3973-3978.

(43) Clar, E.; Ironside, C. T.; Zander, M. *J. Chem. Soc.* **1959**, 142-147.

(44) Liu, W.; Li, L.; Li, C.-J. *Nat. Commun.* **2015**, DOI: 10.1038/ncomms7526.

(45) Gaussian 09, Revision D.01, Frisch, M. J.; Trucks, G. W.; Schlegel, H. B.; Scuseria, G. E.; Robb, M. A.; Cheeseman, J. R.; Scalmani, G.; Barone, V.; Mennucci, B.; Petersson, G. A.; Nakatsuji, H.; Caricato, M.; Li, X.; Hratchian, H. P.; Izmaylov, A. F.; Bloino, J.; Zheng, G.; Sonnenberg, J. L.; Hada, M.; Ehara, M.; Toyota, K.; Fukuda, R.; Hasegawa, J.; Ishida, M.; Nakajima, T.; Honda, Y.; Kitao, O.; Nakai, H.; Vreven, T.; Montgomery, J. A., Jr.; Peralta, J. E.; Ogliaro, F.; Bearpark, M.; Heyd, J. J.; Brothers, E.; Kudin, K. N.; Staroverov, V. N.; Kobayashi, R.; Normand, J.; Raghavachari, K.; Rendell, A.; Burant, J. C.; Iyengar, S. S.; Tomasi, J.; Cossi, M.; Rega, N.; Millam, M. J.; Klene, M.; Knox, J. E.; Cross, J. B.; Bakken, V.; Adamo, C.; Jaramillo, J.; Gomperts, R.; Stratmann, R. E.; Yazyev, O.; Austin, A. J.; Cammi, R.; Pomelli, C.; Ochterski, J. W.; Martin, R. L.; Morokuma, K.; Zakrzewski, V. G.; Voth, G. A.; Salvador, P.; Dannenberg, J. J.; Dapprich, S.; Daniels, A. D.; Farkas, Ö.; Foresman, J. B.; Ortiz, J. V.; Cioslowski, J.; Fox, D. J. Gaussian, Inc., Wallingford CT, 2009.

(46) Becke, A. D. *J. Chem. Phys.* **1993**, *98*, 5648-5652.

(47) Ditchfield, R.; Hehre, W. J.; Pople, J. A. *J. Chem. Phys.* **1971**, *54*, 724-728.

(48) Suresh, C. H.; Gadre, S. R. *J. Am. Chem. Soc.* **1998**, *120*, 7049-7055.

(49) Gadre, S. R.; Shirsat, R. N. in Electrostatics of atoms and molecules, Universities Press: Hyderabad, 2000.

(50) Gadre, S. R.; S. A. Kulkarni; Shrivastava, I. H. *J. Chem. Phys.* **1992**, *96*, 5253-5260.

(51) Jmol: an open-source Java viewer for chemical structures in 3D. http://www.jmol.org/

(52) Truhlar, D. G.; Hase, W. L.; Hynes, J. T. *J. Phys. Chem.* **1983**, *87*, 2664-2682.

(53) Lin, Y. M.; Dimitrakopoulos, C.; Jenkins, K. A.; Farmer, D. B.; Chiu, H. Y.; Grill, A.; Avouris, Ph. *Science* **2010**, *327*, 662.

(54) Geim, A. K.; Novoselov, K. S. *Nature Mater.* **2007**, *6*, 183-191.

(55) Charlier, J. C.; Eklund, P. C.; Zhu, J.; Ferrari, A. C. *Topics Appl. Phys.* **2008**, *111*, 673-709.

(56) Bonaccorso, F.; Sun, Z.; Hasan, T.; Ferrari, A. C. *Nature Photon.* **2010**, *4*, 611-622.

(57) Torrisi, F.; Hasan, T.; Wu, W.; Sun, Z.; Lombardo, A.; Kulmala, T. S.; Hsieh, G. W.; Jung, S.; Bonaccorso, F.; Paul, P. J.; Chu, D.; Ferrari, A. C. *ACS Nano* **2012**, *6*, 2992-3006.

(58) Sun, Z.; Hasan, T.; Torrisi, F.; Popa, D.; Privitera, G.; Wang, F.; Bonaccorso, F.; Basko, D. M.; Ferrari, A. C. *ACS Nano* **2010**, *4*, 803-810.

(59) Simpson, C. D.; Brand, J. D.; Berresheim, A. J.; Przybilla, L.; Räder, H. J.; Müllen, K. *Chem. Eur. J.* **2002**, *8*, 1424-1429.

(60) Rouhanipour, A.; Roy, M.; Feng, X.; Räder, H. J.; Mullen, K. *Angew. Chem. Int. Ed.* **2009**, *48*, 4602-4604.

(61) Hill, J. P.; Jin, W.; Kosaka, A.; Fukushima, T.; Ichihara, H.; Shimomura, T.; Ito, K.; Hashizume, T.; Ishii, N.; Aida, T. *Science* **2004**, *304*, 1481-1483.

(62) Schmidt-Mende, L.; Fechtenkötter, A.; Mullen, K.; Moons, E.; Friend, R. H.; MacKenzie, J. D. *Science* **2001**, *293*, 1119-1122.

(63) Crispin, X.; Cornil, J.; Friedlein, R.; Okudaira, K. K.; Lemaur, V.; Crispin, A.; Kestemont, G.; Lehmann, M.; Fahlman, M.; Lazzaroni, R.; Geerts, Y.; Wendin, G.; Ueno, N.; Brédas, J. L.; Salaneck, W. R. *J. Am. Chem. Soc.* **2004**, *126*, 11889-11899.

(64) Cao, X.-Y.; Zi, H.; Zhang, W.; Lu, H.; Pei, J. *J. Org. Chem.* **2005**, *70*, 3645-3653.

(65) Setia, S., Sidiq, S., Pal, S. K. *Tetrahedron Lett.* **2012**, *53*, 6446-6450.

(66) Setia, S.; Soni, A.; Gupta, M.; Sidiq, S.; Pal, S. K. *Liq. Cryst.* **2013**, *40*, 1364-1372.

(67) Sergeyev, S.; Pisula, W.; Geerts, Y. H. *Chem. Soc. Rev.* **2007**, *36*, 1902-1929.

(68) Deun, R. V.; Fias, P.; Nockemann, P.; Schepers, A.; Parac-Vogt, T. N.; Hecke, K. V.; Meervelt, L. V.; Binnemans, K. *Inorg. Chem.* **2004**, *43*, 8461-8469.

(69) Thomas, K. R. J.; Velusamy, M.; Lin, J. T.; Chien, C.-H.; Tao, Y.-T.; Wen, Y. S.; Hu, Y.-H.; Chou, P.-T. *Inorg. Chem.* **2005**, *44*, 5677-5685.

(70) Zhao, Q.; Liu, S.; Shi, M.; Wang, C.; Yu, M.; Li, L.; Li, F.; Yi, T.; Huang, C. *Inorg. Chem.* **2006**, *45*, 6152-6160.

(71) Wong, W.-Y.; Ho, C.-L. *J. Mater. Chem.* **2009**, *19*, 4457-4482.

(72) Tessler, N.; Medvedev, V.; Kazes, M.; Kan, S.-H.; Banin, U. *Science* **2002**, *295*, 1506-1508.

(73) Yuan, Y.-F.; Cardinaels, T.; Lunstroot, K.; Hecke, K. V.; Meervelt, L. V.; Gorller-Walrand, C.; Binnemans, K.; Nockemann, P. *Inorg. Chem.* **2007**, *46*, 5302-5309.

(74) Seguy, I.; Jolinat, P.; Destruel, P.; Farenc, J.; Mamy, R.; Bock, H.; Ip, J.; Nguyen, T. P. *J. Appl. Phys.* **2001**, *89*, 5442-5448.

(75) Grzybowski, M.; Skonieczny, K.; Butenschön, H.; Gryko, D. T. *Angew. Chem. Int. Ed.* **2013**, *52*, 9900-9930.

(76) Lu, Y.; Moore, J. S. *Tetrahedron Lett.* **2009**, *50*, 4071-4077.

(77) Arslan, H.; Uribe-Romo, F. J.; Smith, B. J.; Dichtel, W. R. *Chem. Sci.* **2013**, *4*, 3973-3978.

(78) Setia, S.; Singh, S. P.; Kumar, S.; Balanarayan, P.; Pal, S. K. Communicated.

(79) Zhang, Q.; Prins, P.; Jones, S. C.; Barlow, S.; Kondo, T.; An, Z.; Siebbeles, L. D. A.; Marder, S. R. *Org. Lett.* **2005**, *7*, 5019-5022.

(80) Wang, Z.; Watson, M. D.; Wu, J.; Mullen, K. *Chem. Commun.* **2004**, 336-337.

(81) Feng, X.; Pisula, W.; Takase, M.; Dou, X.; Enkelmann, V.; Wagner, M.; Ding, N.; Mullen, K. *Chem. Mater.* **2008**, *20*, 2872-2874.

(82) Dou, X.; Yang, X.; Bodwell, G. J.; Wagner, M.; Enkelmann, V.; Mullen, K. *Org. Lett.* **2007**, *9*, 2485-2488.

(83) Kumar, S. in Chemistry Of Discotic Liquid Crystals: From Monomers to Polymers; Percec, V., Ed., CRS Press, Taylor & Francis Group: Boca Raton, FL, 2011.

(84) Gupta, S. K.; Setia, S.; Sidiq, S.; Gupta, M.; Kumar, S.; Pal, S. K. *RSC Adv.* **2013**, *3*, 12060-12065.

(85) Gherghel, L.; Kubel, C.; Lieser, G.; Rader, H. J.; Mullen, K. *J. Am. Chem. Soc.* **2002**, *124*, 13130-13138.

(86) Ban, K.; Nishizawa, K.; Ohta, K.; van de Craats, A. M.; Warman, J. M.; Yamamoto, I.; Shirai, H. *J. Mater. Chem.* **2001**, *11*, 321-331.

(87) Hatsusaka, K.; Ohta, K.; Yamamoto, I.; Shirai, H. *J. Mater. Chem.* **2001**, *11*, 423-433.

(88) Kim, D.; Jon, S.; Lee, H.-K.; Baek, K.; Oh, N.-K.; Zin, W.-C.;Kim, K. *Chem. Commun.* **2005**, 5509-5511.

(89) Myśliwiec, D.; Donnio, B.; Chmielewski, P. J.; Heinrich, B.; Stępień, M. *J. Am. Chem. Soc.* **2012**, *134*, 4822-4833.

(90) Wijesinghe, L. P.; Lankage, B. S.; Maille, G. M. O.; Perera, S. D.; Nolan, D.; Wangab, L.; Draper, S. M. *Chem. Commun.* **2014**, *15*, 10637-10640.

(91) Zhao, B.; Liu, B.; Png, R. Q.; Zhang, K.; Lim, K. A.; Luo, J.; Shao, J.; Ho, P. K. H.; Chi, C.; Wu, J. *Chem. Mater.* **2010**, *22*, 435-449.

(92) Clar, E. in Polycyclic Hydrocarbons, Springer, Berlin Heidelberg, 1964.

(93) Lakowicz, J. R. in Principles of Fluorescence Spectroscopy, Springer: US, 2006.

(94) Achalkumar, A. S.; Hiremath, U. S.; Rao, D. S. S.; Prasad, S. K.; Yelamaggad, C. V. *J. Org. Chem.* **2013**, *78*, 527-544.

(95) Kasha, M.; Rawls, H. R.; El-Bayoumi, M. A. *Pure Appl. Chem.* **1965**, *11*, 371-392.

(96) Prabhu, D. D.; Sivadas, A. P.; Das, S. *J. Mater. Chem. C* **2014**, *2*, 7039-7046.

(97) Spano, F. C. *Acc. Chem. Res.* **2010**, *43*, 429-439.

(98) Emrick, T.; Pentzer, E. *NPG Asia Mater.* **2013**, *5*, e43/1-15.

Appendix III

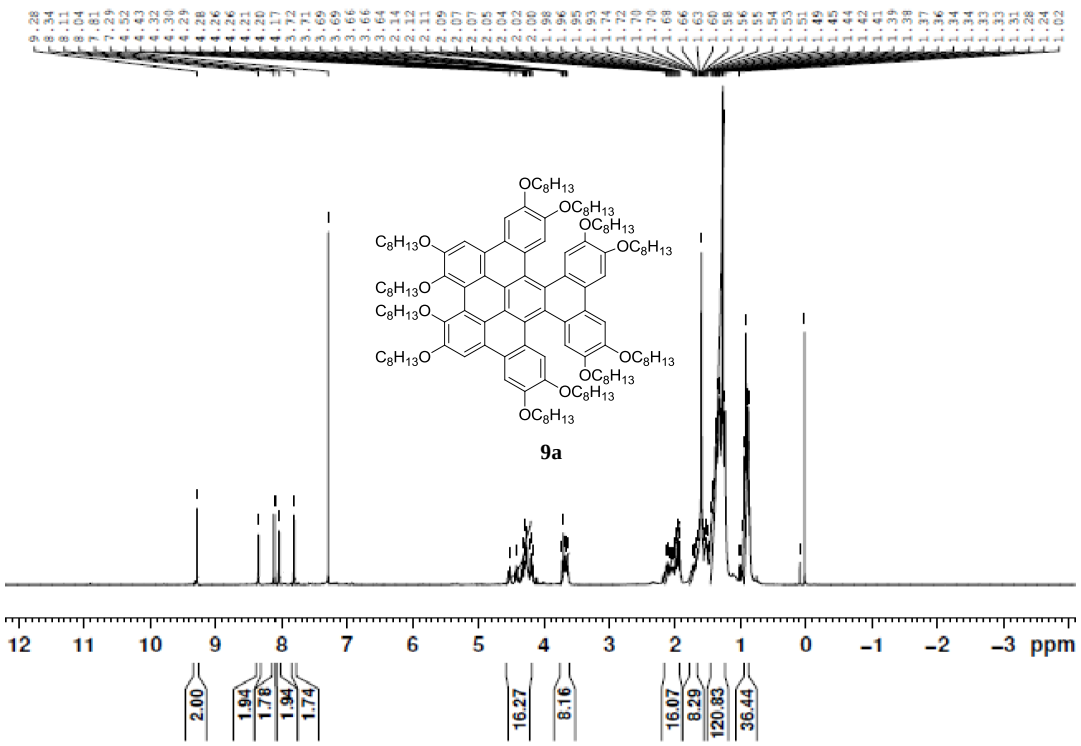

Figure A1 ^{1}H NMR of compound **9a.**

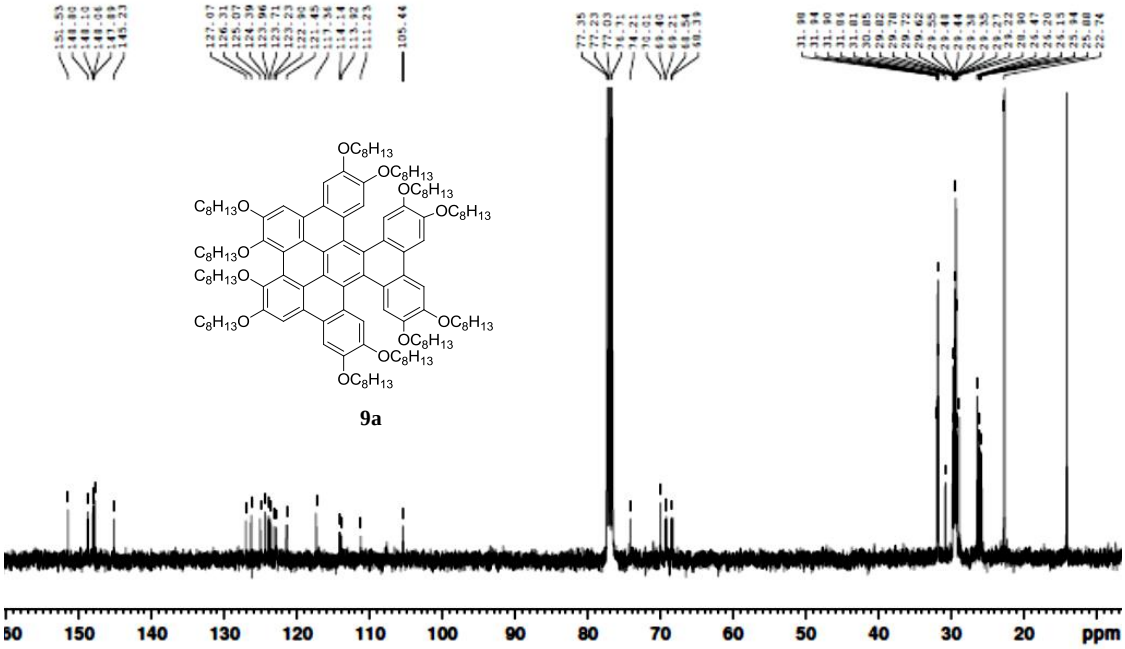

Figure A2 ^{13}C NMR of compound **9a.**

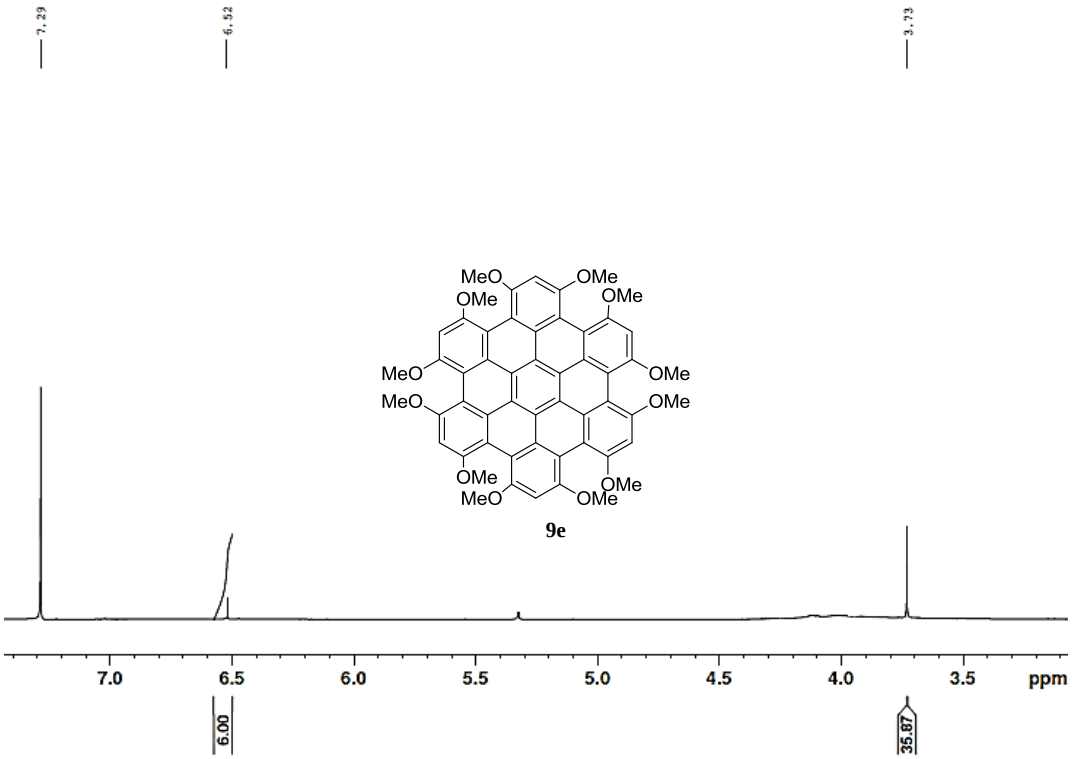

Figure A3 ^{1}H NMR of compound **9e.**

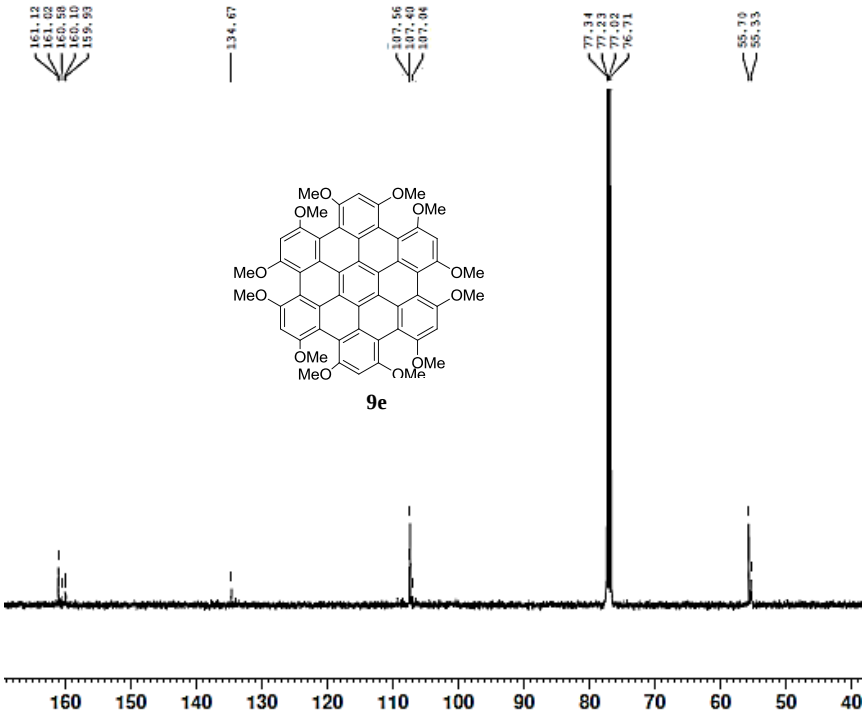

Figure A4 ^{13}C NMR of compound **9e.**

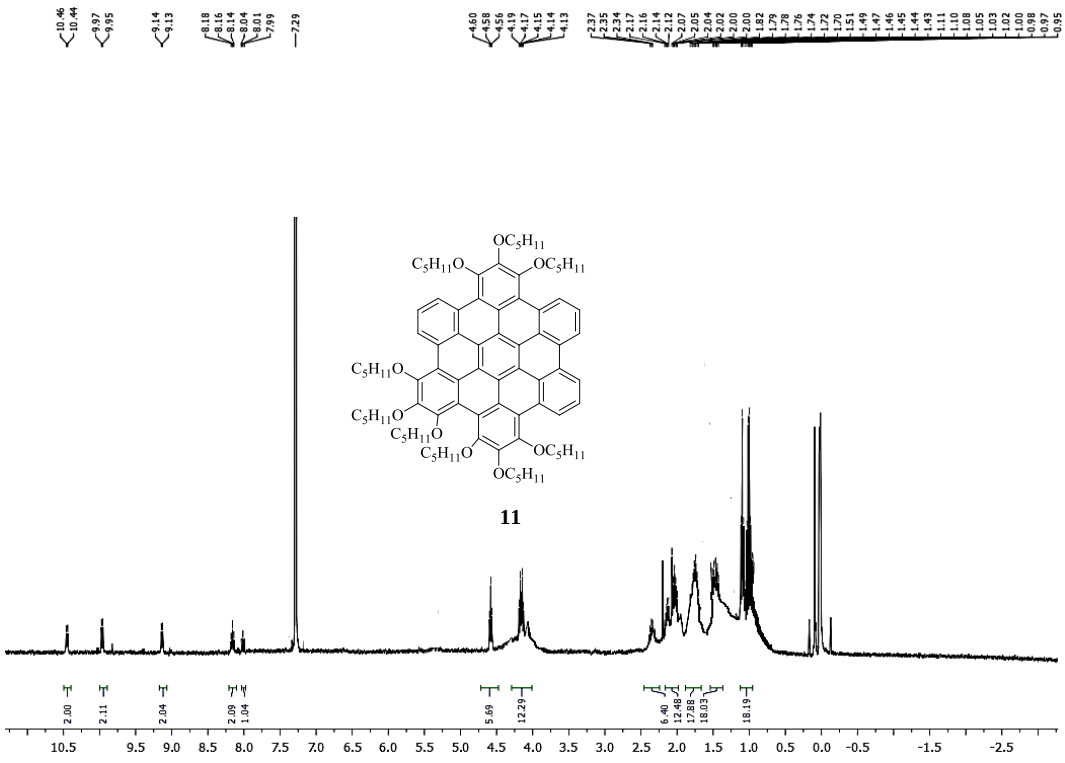

Figure A5 ^{1}H NMR of compound **11.**

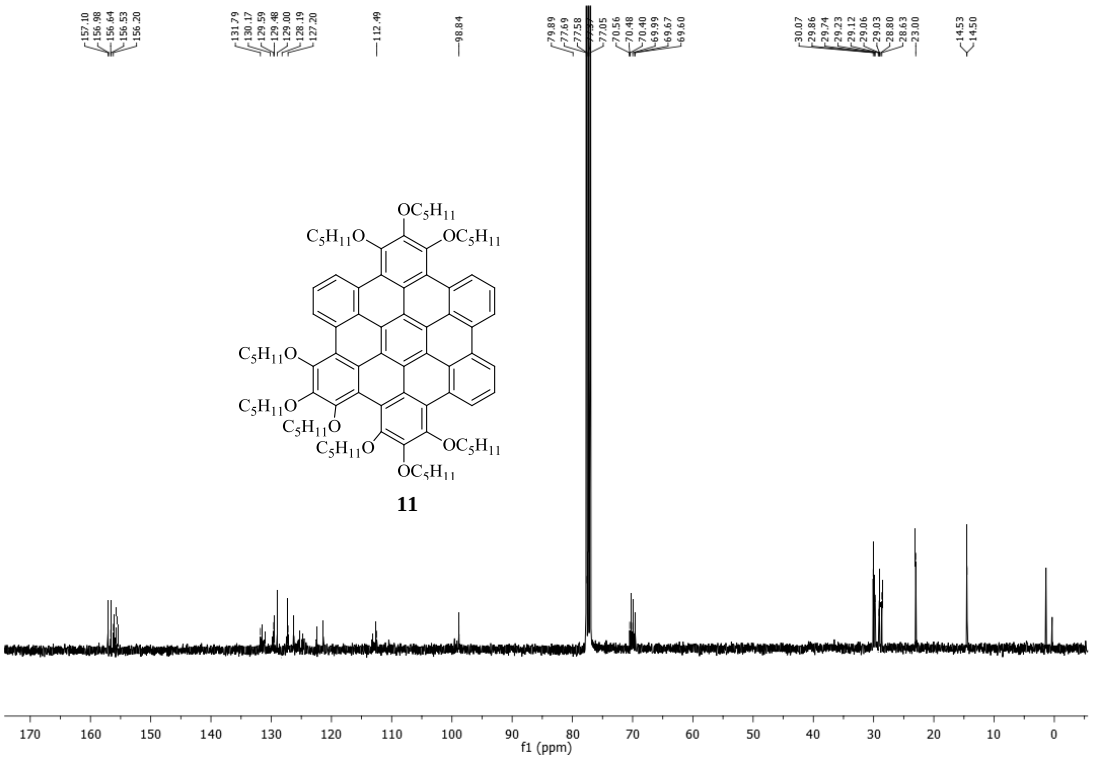

Figure A6 ^{13}C NMR of compound **11.**

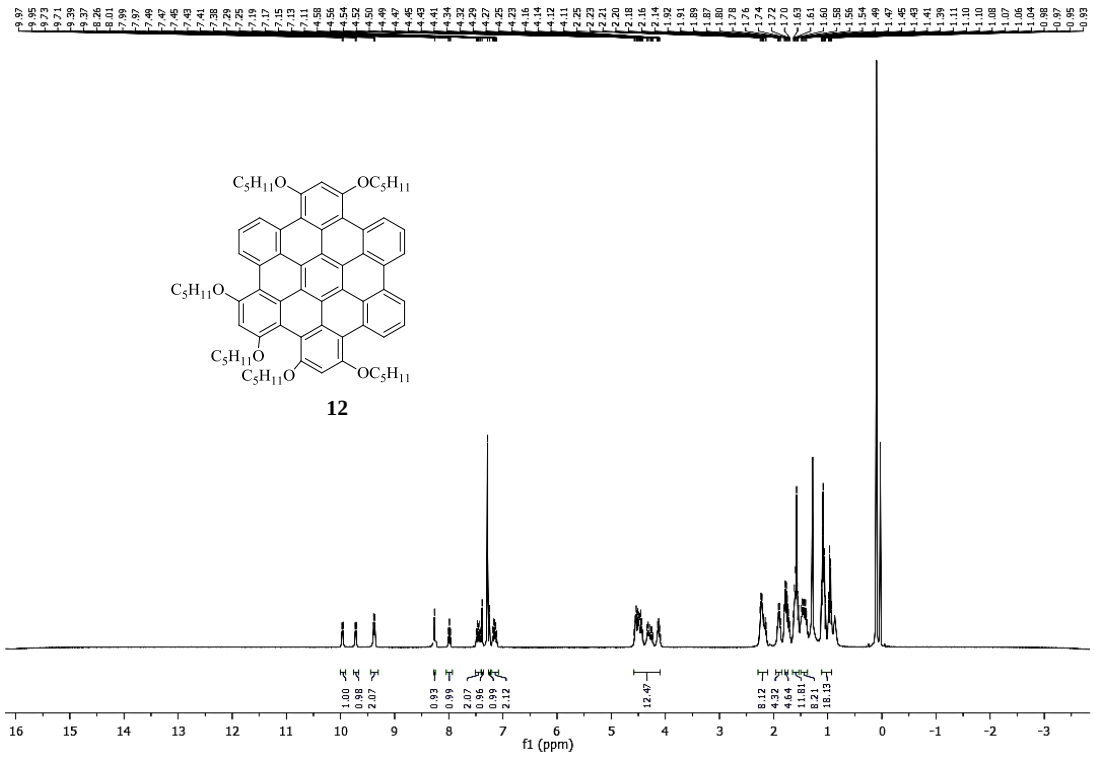

Figure A7 ^{1}H NMR of compound **12.**

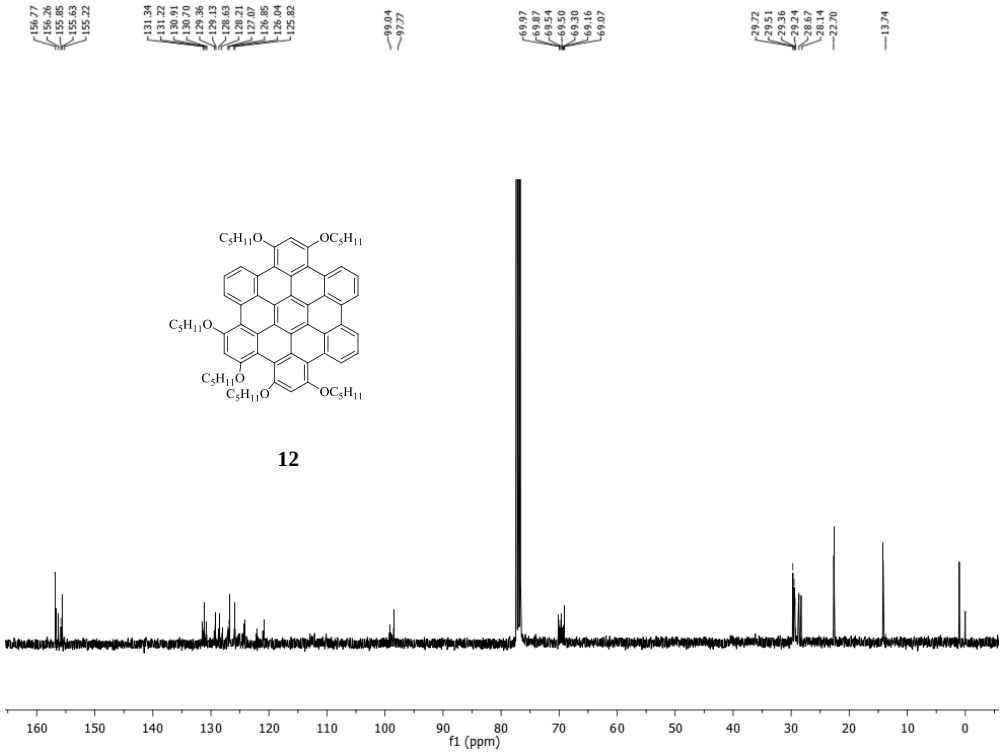

Figure A8 ^{13}C NMR of compound **12.**

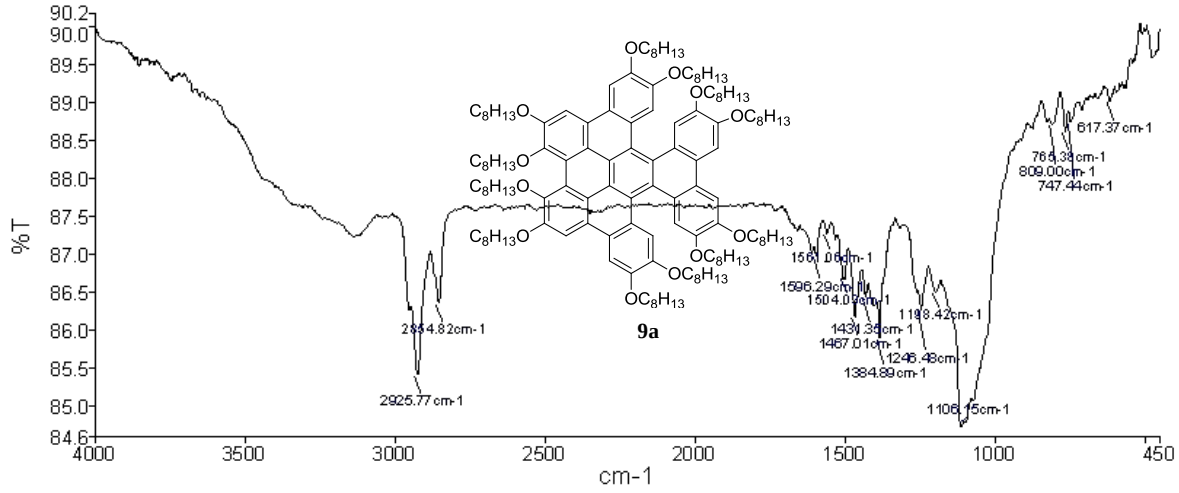

Figure A9 IR of compound **9a.**

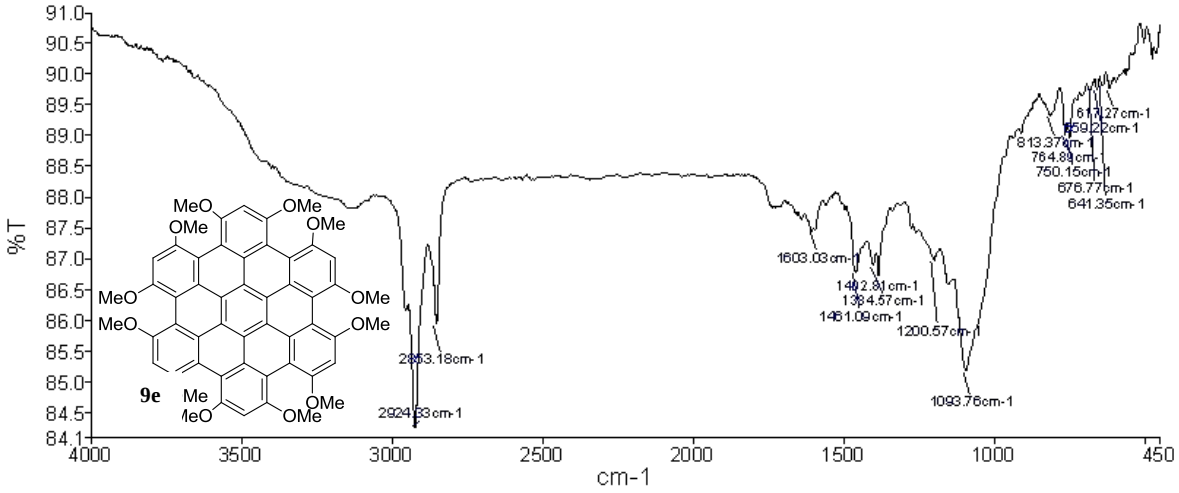

Figure A10 IR of compound **9e.**

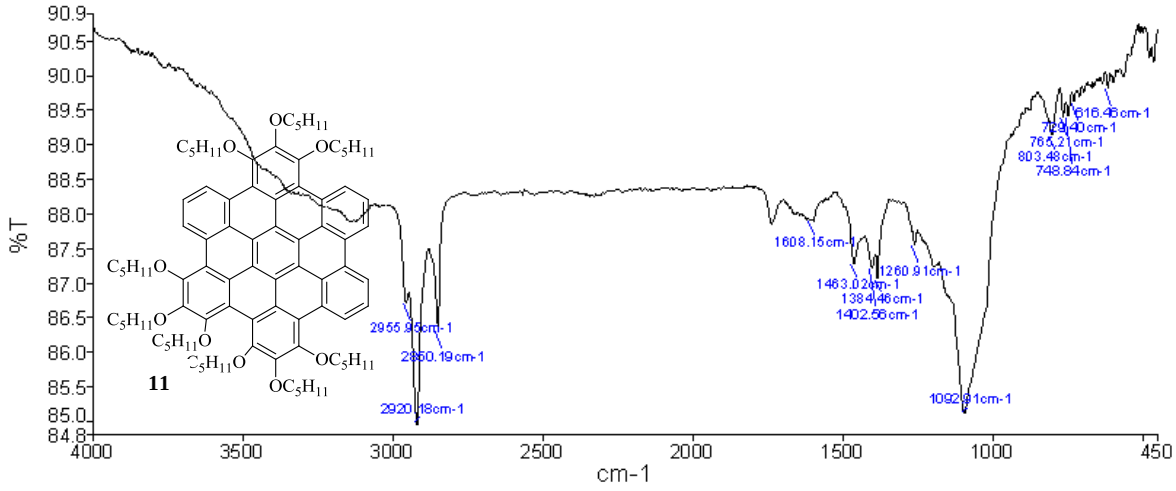

Figure A11 IR of compound **11.**

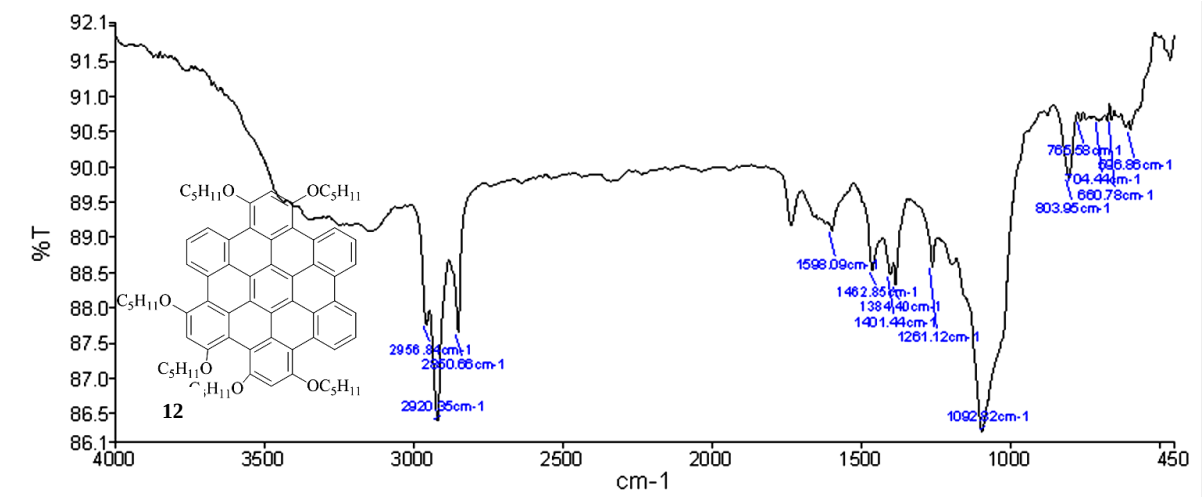

Figure A12 IR of compound **12.**

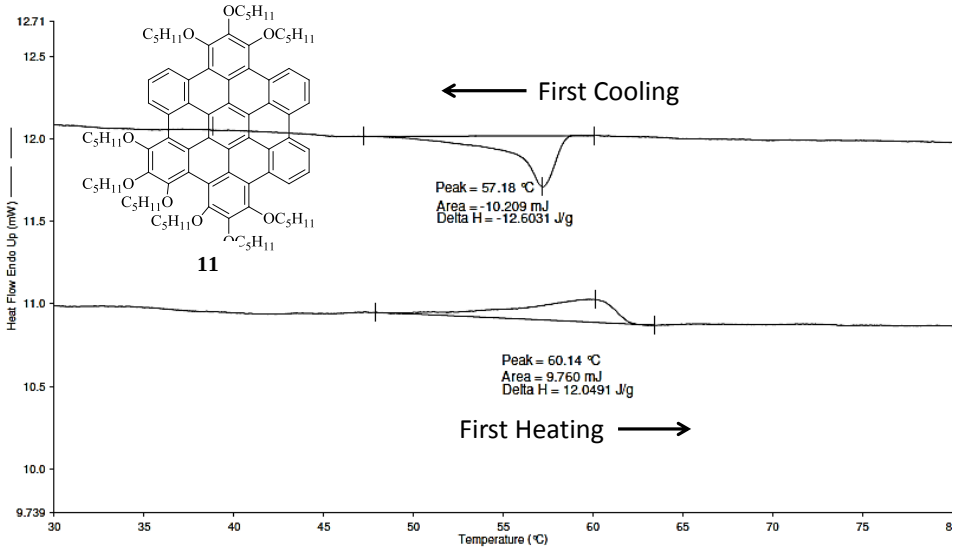

11

Figure A13 DSC thermogram of compound **11.**

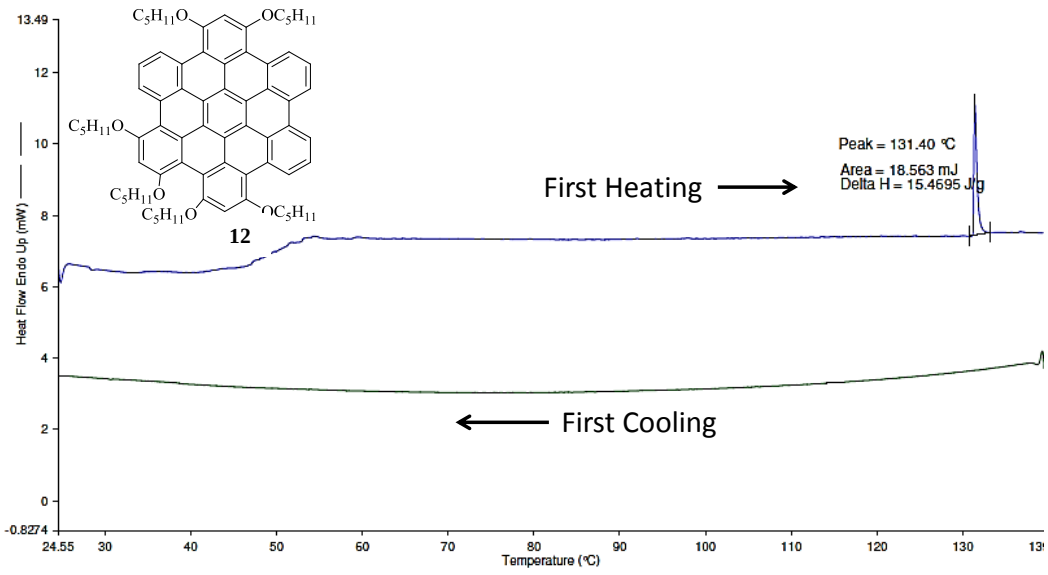

12

Figure A14 DSC thermogram of compound **12.**

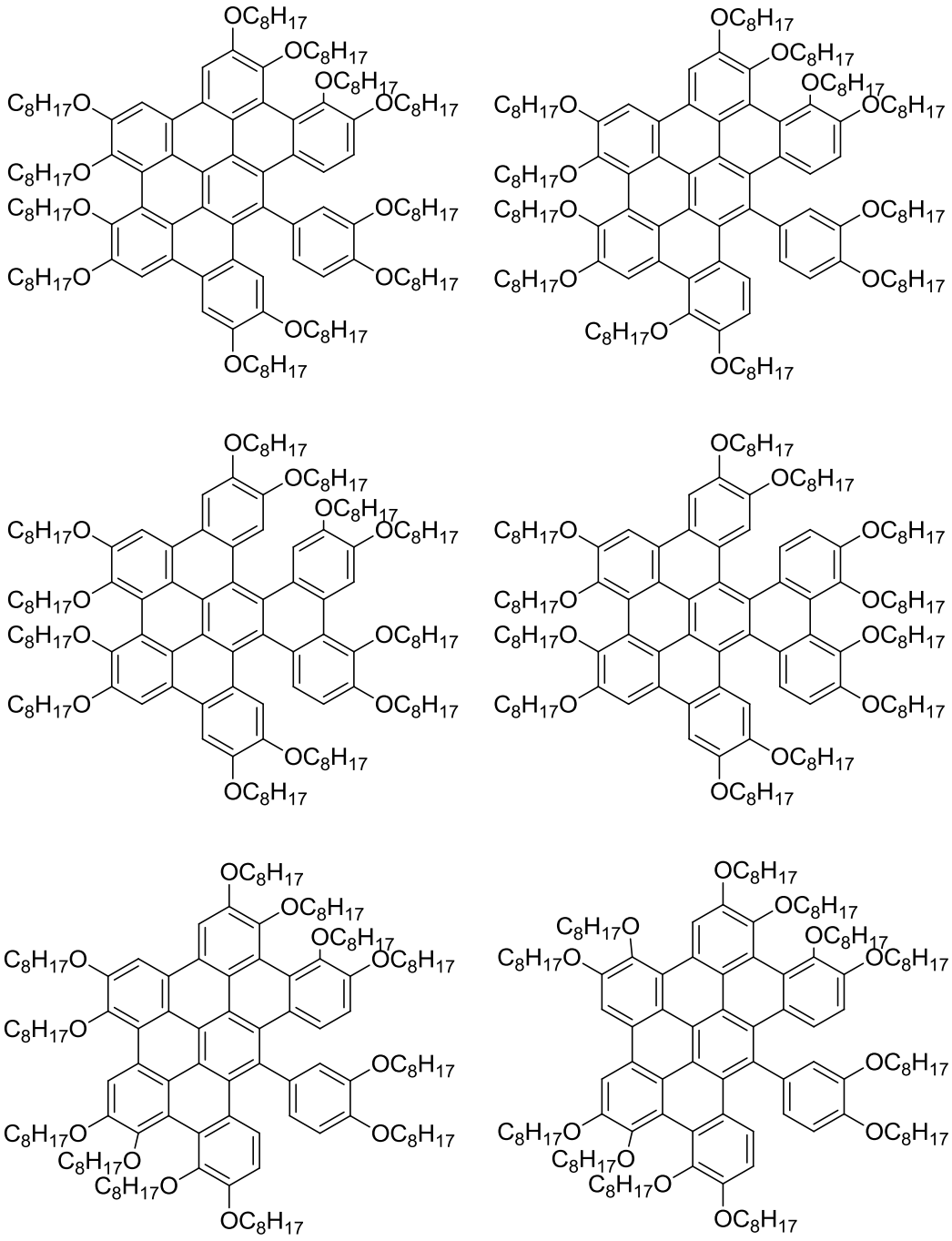

Chart A1. The alternative possible structures for compound **9a** as discussed in chapter 4 (part A).

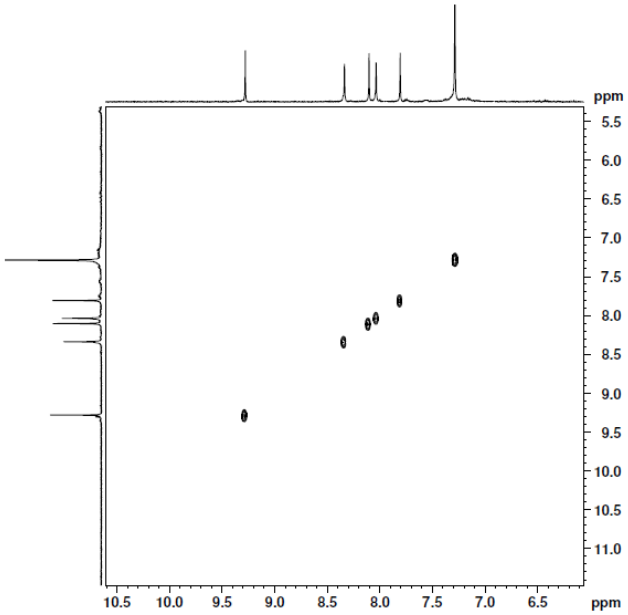

Figure A15 ^{1}H-^{1}H COSY spectra of compound **9a** indicating no interaction between the bonded protons, which further confirms the assigned structure as discussed in chapter 4 (part A).

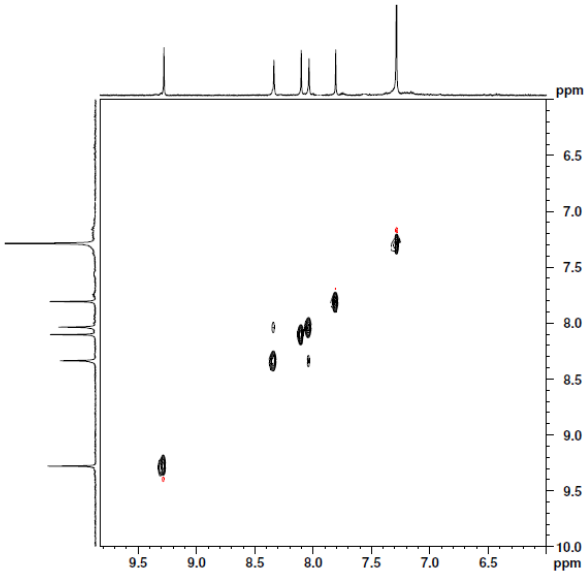

Figure A16 ^{1}H-^{1}H NOESY spectra of compound **9a** indicating only a single spatial interaction between the non-bonded protons, which further confirms the assigned structure as discussed in chapter 4 (part A).

Structural Assignment of Compound 11 (Chapter 4, Part B)

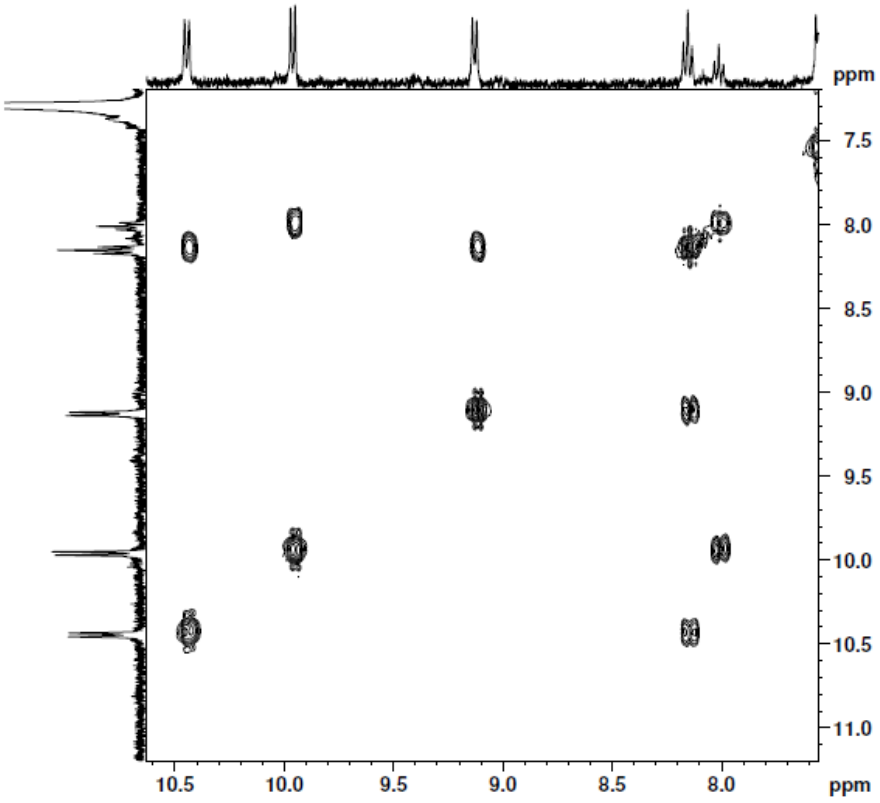

Figure A17 ^{1}H-^{1}H COSY NMR of compound **11** as discussed in chapter 4 (part B).

In the one dimensional proton nmr spectrum, the five different aromatic proton signals and one triplet corresponding to four protons and multiplet corresponding to fourteen protons of the alkoxy chain indicated that the compound is unsymmetric and not the symmetric one as in that case it would have exhibited only two aromatic signals ideally. This was further supported by ^{13}C NMR spectroscopy, whereby many peaks were present in the aromatic region. The structure was further confirmed by ^{1}H-^{1}H COSY experiments. In the ^{1}H-^{1}H COSY experiments, doublets of protons at 10.45 ppm and 9.13 ppm showed coupling signals with triplet of protons at 8.16 ppm. Further, doublet of protons at 10.03 ppm showed coupling signal with triplet of proton at 8.03 ppm. This confirmed the existence of two different sets of protons in the structure. Further, since in one set of protons, all the peaks

correspond to two protons each, so there must be two benzene rings of almost the same environment and third one with different environment. Thus we assigned the structure as compound **11**. Protons at 10.45 ppm were assigned as H_a, protons at 9.13 ppm as H_c and protons at 8.16 ppm as H_b corresponding to two equal benzene rings. Then, protons at 10.03 ppm were assigned as H_d, and proton at 8.03 ppm as H_e corresponding to third benzene ring.

Structural Assignment of Compound 12 (Chapter 4, Part B)

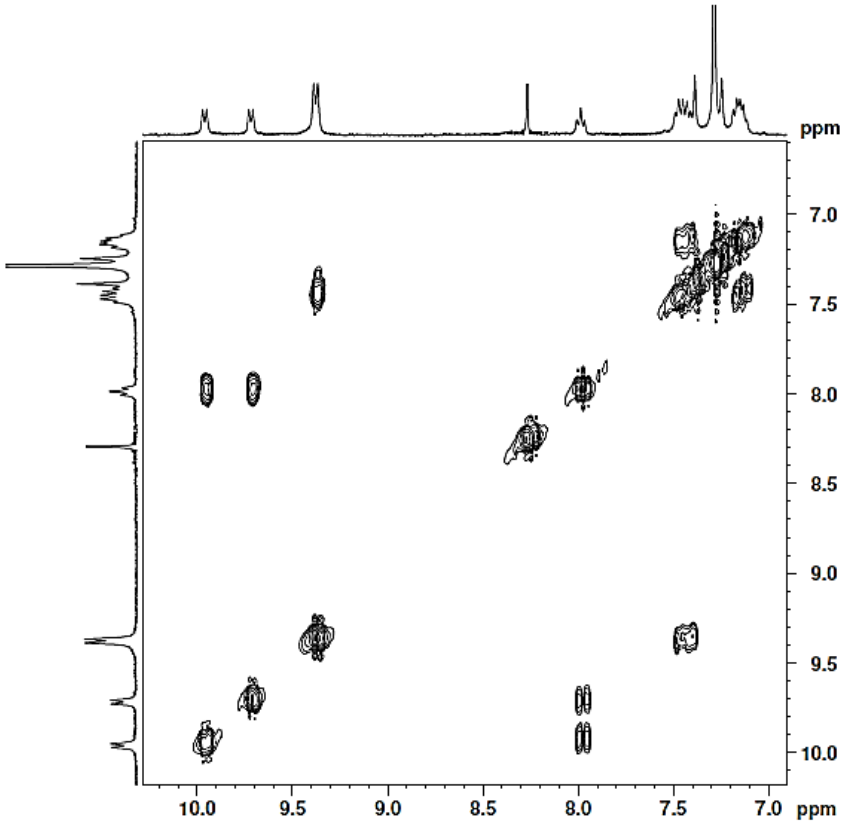

Figure A18 ^{1}H-^{1}H COSY NMR of compound **12** as discussed in chapter 4 (part B).

In the one dimensional proton nmr spectrum, the nine different aromatic proton signals and multiplet corresponding to twelve protons indicated that the compound is unsymmetric and not the symmetric one as in that case it would have exhibited only three aromatic signals ideally. This was further supported by ^{13}C NMR spectroscopy, whereby many peaks were present in the aromatic region. The structure was further confirmed by ^{1}H-^{1}H COSY experiments. In the ^{1}H-^{1}H COSY experiments, doublets of protons at 9.96 ppm and 9.72 ppm

showed coupling signals with triplet of protons at 7.99 ppm. This implies that this corresponds to three protons of the same ring, which indicated that this benzene ring is different from other two benzene rings. In the COSY nmr, doublet of protons at 9.38 ppm showed coupling with multiplet at 7.12-7.19 and multiplet of protons at 7.12-7.19 ppm showed coupling with multiplet at 7.41-7.49 ppm. Further, since in this set of protons, all the peaks correspond to two protons each, so there must be two benzene rings of almost the same environment and third one with different environment. Thus we assigned the structure as compound **12**. Protons at 9.96 ppm were assigned as H_d, protons at 9.72 ppm as $H_{d'}$ and protons at 7.99 ppm as H_e corresponding to two equal benzene rings. Then, protons at 9.38 ppm as H_a, 7.12-7.19 ppm were assigned as H_c, and proton at 7.41-7.49 ppm as H_b corresponding to third benzene ring.

Table A1 Natural and Mulliken charges on the carbon atoms which are actively participating in the *o*-phenyl and *p*-phenyl protonation pathways.[a,b]

Structures	Natural Charge	Mulliken Charge	Structures	Natural Charge	Mulliken Charge
I_2			**I_{16}**		
C_{22}	-0.285	-0.293	C_9	-0.319	-0.226
C_{34}	-0.293	-0.219	**C_{12}**	-0.254	-0.244
C_{30}	-0.243	-0.166	C_{11}	-0.330	-0.233
C_{43}	-0.247	-0.202	C_{39}	-0.317	-0.212
C_{39}	-0.211	-0.144	C_{38}	-0.280	-0.246
C_{52}	-0.231	-0.258	C_{39}	-0.317	-0.212
C_{31}	-0.257	-0.174	C_{26}	+0.324	+0.380
C_4	+0.276	+0.321	**C_{23}**	+0.334	+0.385
I_4			**I_{19}**		
C_{29}	-0.237	-0.259	**C_{20}**	-0.285	-0.248
C_{40}	-0.236	-0.275	**C_{21}**	-0.292	-0.209
C_{12}	-0.237	-0.271	C_{38}	-0.283	-0.197
C_{43}	-0.235	-0.269	C_{39}	-0.316	-0.256
C_{11}	+0.260	+0.343	**C_{34}**	+0.334	+0.385

C_{44}	+0.277	+0.333	C_{35}	+0.336	+0.395
C_{30}	+0.268	+0.336	C_{37}	+0.343	+0.392
C_{39}	+0.270	+0.337	C_{40}	+0.334	+0.374
I_7			**I_{22}**		
C_{29}	-0.235	-0.261	**C_{38}**	-0.259	-0.237
C_{40}	-0.235	-0.275	**C_{39}**	-0.319	-0.264
C_{30}	+0.266	+0.335	**C_{37}**	+0.319	+0.381
C_{39}	+0.270	+0.336	C_{40}	+0.339	+0.390
I_9			**I_{24}**		
C_{33}	+0.285	+0.353	**C_{28}**	+0.344	+0.271
C_{40}	-0.306	-0.208	C_{35}	+0.362	+0.307
I_{11}			**I_{26}**		
C_{32}	-0.246	-0.273	**C_{32}**	+0.363	+0.307
C_{37}	-0.298	-0.304	C_{37}	+0.343	+0.392
I_{13}			**I_{28}**		
C_{32}	-0.247	-0.272	**C_{35}**	+0.342	+0.281
C_{37}	-0.299	-0.311	C_{42}	+0.349	+0.330

[a]Red colored shows the possible bond formation between two carbon atoms. [b]Blue colored carbon shows the possible site for protonation in unprotonated species.

Chapter 5

Summary

The work presented in this thesis was performed with the view to explore the synthesis, characterization and self-assembly of novel functionalized discotic molecules for optoelectronic and display applications. The results obtained in the present work are summarized below.

1. A series of rod-disc oligomers based on anthraquinone and perylene core have been synthesized and characterized in the hunt of elusive biaxial nematic phase. In the design of molecules for the existence of this phase, one approach is to covalently attach rod and disc shaped moieties. In this direction, we have reported for the first time the synthesis of anthraquinone based mesogens in which one disc was joined to eight rod like cyanobiphenyl moieties.

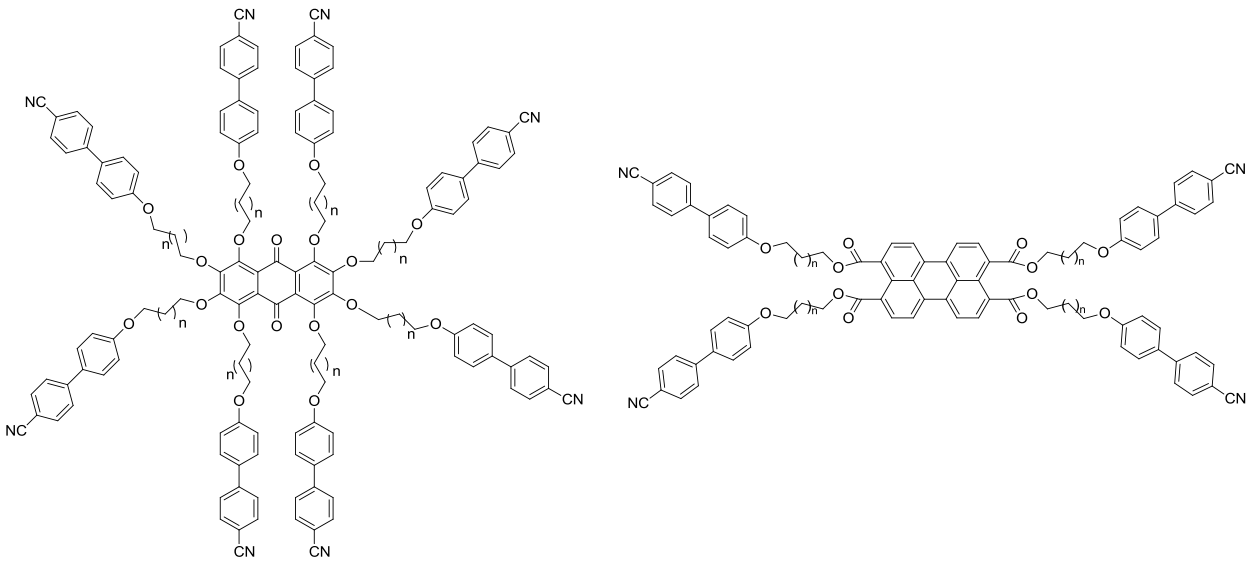

Perylene owing to its board shape is also a potential candidate for showing biaxial nematic phase. We have explored this possibility by attaching four cyanobiphenyls to this core. We have demonstrated that in both the cases, molecular shape has sufficiently been disturbed to achieve nematic mesophases.

2. We have prepared several mesogens based on rufigallol and perylene core in order to show the effect of various branched chains on the mesomorphic properties. We have demonstrated that the type, chain length and substituent position have large effect on the thermotropic behavior. By the introduction of branched chains to these cores, we have been able to synthesize some discotic liquid crystals (LCs) stabilizing columnar hexagonal mesophases upto room temperature. Compounds with perylene core exhibited yellowish green luminescence which can be seen with naked eyes. Some of the compounds also showed homeotropic alignment in the mesophase.

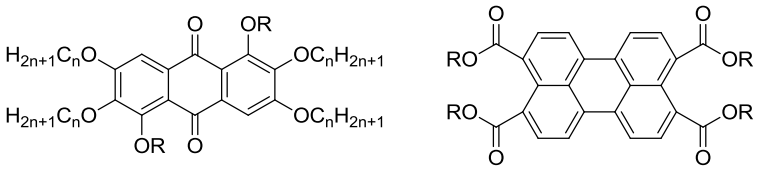

R = Branched Chain

3. The straightforward synthesis of mesogenic oligomers consisting of perylene core joined to four triphenylene units has been achieved. All these hybrids were isolated in the columnar hexagonal mesophases at room temperature and exhibited excellent photophysical properties in the solution and thin film states.

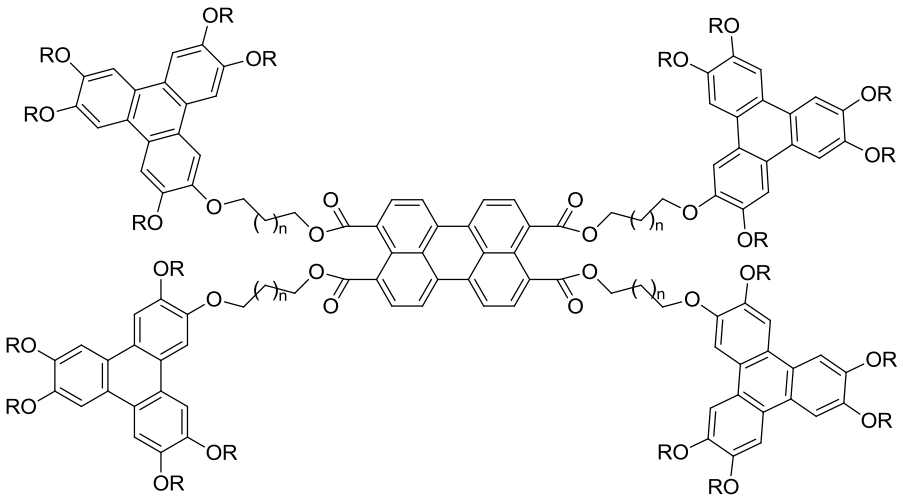

The aggregation of these compounds has also been studied in THF/water mixture. TGA studies have shown that these molecules are stabilized upto atleast 300 °C. These are low band gap molecules, with a band gap of 2.45 eV as calculated from the absorption spectra. These molecules can be potentially suited for various organic electronics.

4. Given the importance of hexa-*peri*-hexabenzocoronene (HBC) as a discotic core due to its high conductivity and π-π stacking, in the present work, we have demonstrated the factors which effect the formation of dodecyl alkoxy substituted HBC core both experimentally and computationally. Through this study, we have established that this reaction is taking place *via* arenium cation mechanism. We have established that the regioselectivity of Scholl reaction in the formation of dodecyl alkoxy substituted HBC is highly dependent on position of all the electron donating groups on the ring with respect to each other. These findings are expected to serve as guidelines for the synthesis of large polycyclic aromatic systems.

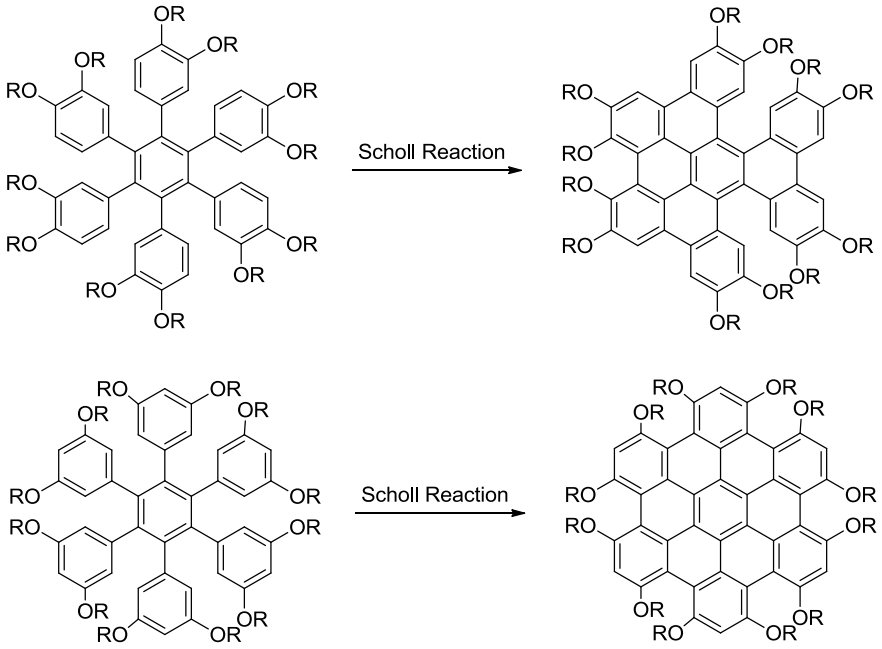

5. The synthesis of two alkoxy substituted unsymmetrical HBC derivatives has been achieved.

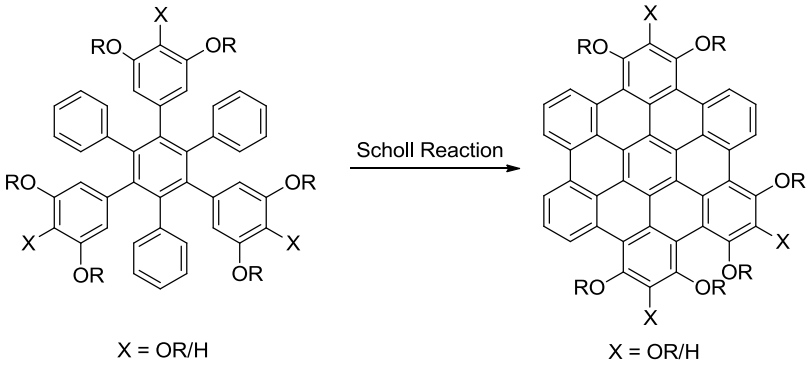

An unexpected rearrangement has been observed in the synthesis of both the derivatives. Both these derivatives were found to assemble into room temperature LC mesophases. One mesogen showed columnar rectangular mesophase and the other showed columnar hexagonal mesophase. They also possessed reddish and yellowish green luminescence in the solution and thin film state.

6. The present work has demonstrated the synthesis and characterization of a library of new discotic mesogenic molecules based on anthraquinone, perylene and hexa-*peri*-hexabenzocoronene discotic cores by using simple starting materials in an efficient manner. Given the importance of discotic LCs in optoelectronics and display technologies, the discotic mesogens reported in this work are expected to serve as valuable scaffolds for various organic electronics.

List of Publications

(1) **Setia, S.**; Sidiq, S.; Pal, S. K. Microwave-assisted synthesis of novel oligomeric rod-disc hybrids. *Tetrahedron Lett.* **2012**, *53*, 6446-6450.

(2) **Setia, S.**; Soni, A.; Gupta, M.; Sidiq, S.; Pal, S. K. Microwave-assisted synthesis of novel mixed tail rufigallol derivatives. *Liq. Cryst.* **2013**, *40*, 1364-1372.

(3) Gupta, S. K.;‡ **Setia, S.**;‡ Sidiq, S.; Gupta, M.; Kumar, S.; Pal, S. K. New perylene-based non-conventional discotic liquid crystals. *RSC Adv.* **2013**, *3*, 12060-12065. (‡*Joint first authors*).

(4) **Setia, S.**; Pal, S. K. Unsymmetrically substituted room temperature discotic liquid crystals based on hexa-*peri*-hexabenzocoronene. *ChemistrySelect* **2016**, *1*, 880-885.

(5) De, J.;‡ **Setia, S.**;‡ Pal, S. K. Unconventional mesophase behavior in a new class of anthracene based discotics (‡*Joint first authors*) *Communicated.*

(6) **Setia, S.**; Singh, S. P.; Kumar, S.; Balanarayan, P.; Pal, S. K. An expedient access towards alkoxy substituted hexa-*peri*-hexabenzocoronene core *via* regioselective Scholl reaction: Experimental and computational insights. *Communicated.*

(7) **Setia, S.**; Pal, S. K. Perylene based Discotic Liquid Crystals: Synthesis and Applications. *Manuscript under preparation.*

(8) Ghosh, S.; **Setia, S.**; Sidiq, S.; Pal, S. K. A new visual test for p-quinone and its relevance to the biodiesel industry. *Analytical Methods* **2012**, *4*, 3542-3544.

(9) Agarwal, A.; Sidiq, S.; **Setia, S.**; Bukusoglu, E.; de Pablo, J. J.; Pal, S. K.; Abbott, N. L. Colloid-in-Liquid Crystal Gels that Respond to Biomolecular Interactions. *Small* **2013**, *9*, 2785-2792.

Book Chapters

(1) **Setia, S.**; Kumar, S.; Pal, S. K. *Discotic Liquid Crystalline Dimers: Chemistry and Applications.* in Advanced Functional Materials, Tiwari, A.; Uzan, L. Ed., Scrivener Publishing LLC, 2015, Chapter 7.

Honors, awards and recognitions

(1) "*Unsymmetrically substituted room temperature discotic liquid crystals based on hexa-peri-hexabenzocoronene*" was featured as the Cover Picture in ChemistrySelect.

(2) "Dendritic texture of columnar mesophase of perylene mesogen" was selected for Artist of the month (December, 2014) and featured in the International Liquid Crystal Society (ILCS) art gallery. See the following link:

http://www.lcinet.kent.edu/ILCS/main/page137/page214/page24/page24.html

(3) The Dewan Jawahar Lal Nayar Memorial prize for best poster at 20th National Conference on Liquid Crystals (NCLC-20) in December 2013 at the Manipal Institute of Technology, Manipal University, Manipal, India.

(4) "*Colloid-in-Liquid Crystal Gels that Respond to Biomolecular Interactions*" was featured as the Front Cover in Small.

(5) "*Colloid-in-Liquid Crystal Gels that Respond to Biomolecular Interactions*" This work was selected for Press Release, see the following link in The Indian Express.

http://indianexpress.com/article/cities/chandigarh/liquid-crystal-gel-could-replace-horse-shoe-crabs-in-tests/

(6) "*A new visual test for p-quinone and its relevance to the biodiesel industry*" was selected as Key Scientific Article in Renewable Energy Global Innovations. This article was also featured in the Front End of Biodiesel Magazine.

Review

(1) Pal, S. K.; **Setia, S.**; Avinash, B. S.; Kumar, S. Triphenylene-based discotic liquid crystals: recent advances. *Liq. Cryst.* **2013**, *40*, 1769-1816.

Conferences

(1) Oral presentation entitled "*Development of alkoxy substituted hexa-peri-hexabenzocoronene discotics with higher ordered columnar mesophases at room temperature*" **Setia, S.**; Pal, S. K. at the *22nd National Conference on Liquid Crystals (NCLC-22)* held at the DIT University, Dehradun, India (21st-23rd December, 2015).

(2) Oral presentation entitled "*Effect of substituent on controlling the formation of dodecylalkoxy Hexa-peri-hexabenzocoronenediscotics*" **Setia, S**.; Pal, S. K. at the *21st National Conference on Liquid Crystals (NCLC-21)* held at the Vikramajit Singh Sanatan Dharm (VSSD) College, Chhatrapati Shahu Ji Maharaj University, Kanpur, India (10th-12th November, 2014).

(3) Participated in *National Seminar on Crystallography 43A* held at the Indian Institute of Science Education and Research Mohali (IISERM), S.A.S. Nagar Mohali, India (13th-17th October, 2014).

(4) Poster presentation entiltled "*Synthesis and Characterization of Novel Perylene-based Liquid Crystals*" **Setia, S**.; Pal, S. K. held at the *25th International Liquid Crystal Conference (ILCC-2014)* held at the Trinity College, Dublin, Ireland (29th June to 2nd July, 2014).

(5) Poster presentation entiltled "*Perylene-based non-conventional liquid crystals: synthesis and characterization*" **Setia, S.**; Pal, S. K. at the *20th National Conference on Liquid Crystals (NCLC-20)* held at the Manipal Institute of Technology, Manipal University, Manipal, India (16th-18th December, 2013).

(6) Poster presentation entiltled "*Microwave-assisted* synthesis of novel oligomeric rod-disc hybrids" **Setia, S.;** Sidiq, S.; Pal, S. K. at the *19th National Conference on Liquid Crystals (NCLC-19)* held at the Thapar University, Patiala, India (21st-23rd November, 2012).

(7) Participated in *7th Junior Organic Symposium (JNOST)* held at the Indian Institute of Science Education and Research Mohali (IISERM), S.A.S. Nagar Mohali, India (14th-17th December, 2011).

Chemistry SELECT

A journal of ChemPubSoc Europe

www.chemistryselect.org

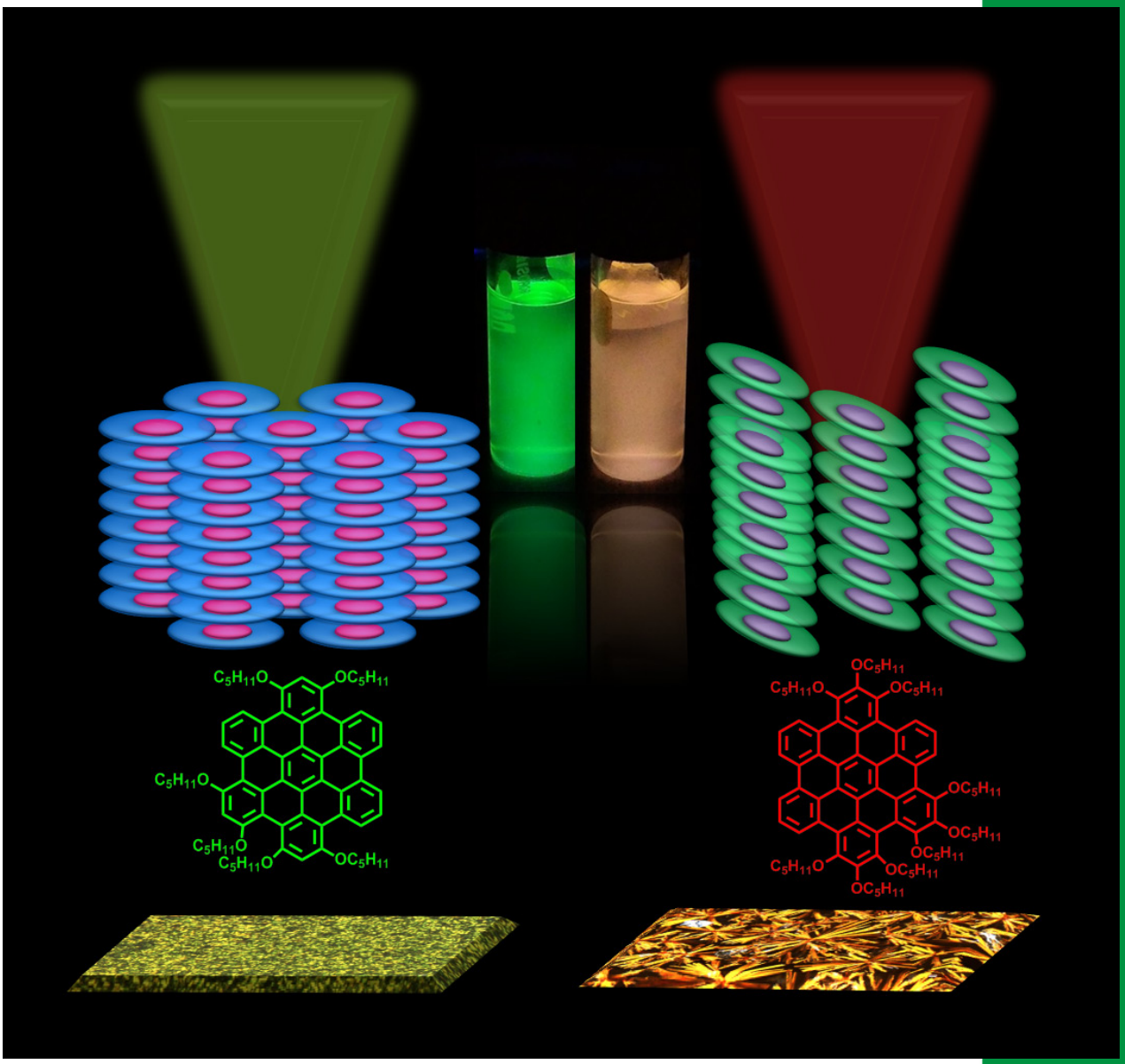

2016-01/05

The cover picture shows an artist's representation of a new class of luminescent discotic liquid crystals based on alkoxy-substituted unsymmetrical hexa-peri-hexabenzocoronene cores that self-organize into room-temperature columnar superstructures. This system is a promising candidate as an active component of organic light-emitting devices, due to its facile processability, low-band-gap, luminescence, and exceptionally higher ordered self-organization behavior in the mesophase derived from X-ray scattering studies. More information can be found in the Full Paper by Pal et al. at the IISER Mohali (DOI: 10.1002/slct.201600107).

WILEY-VCH